BIOGEOCHEMICAL INTERACTIONS OF NATURAL ORGANIC MATTER WITH ARSENIC IN GROUNDWATER

By

HARSHAD VIJAY KULKARNI

B.E., SHIVAJI UNIVERSITY, 2009

M.S., COLORADO STATE UNIVERSITY, 2012

AN ABSTRACT OF A DISSERTATION

Submitted in partial fulfillment of the requirements for the degree

DOCTOR OF PHILOSOPHY

Department of Civil Engineering

College of Engineering

KANSAS STATE UNIVERSITY

Manhattan, Kansas

2016

Abstract

Groundwater contamination with arsenic (As), a naturally occurring metalloid, is a worldwide problem. Over 100 million people are at health risk due to arsenic contaminated groundwater, especially in the Bengal Basin in south-east Asia. Dissolved organic matter (DOM), geology and geomicrobiology are important factors affecting arsenic mobility. This study focuses on interactions of different aspects of natural organic matter in arsenic-contaminated environments. A literature review specifically includes past studies done on fundamentals of arsenic geology, geomicrobiology, DOM characterization and relevant analytical methods and tools. Based on background information already collected, this research is focused on specific research questions and corresponding hypotheses.

The overarching goal of this investigation is to better understand the mechanisms by which DOM influences arsenic mobilization. The specific goals of this research are: 1) to evaluate role of oxidized humic quinones in reductive dissolution of Fe-As minerals and subsequent arsenic mobilization via electron shuttling, 2) to quantify the rate of microbially mediated reductive dissolution in the presence of oxidized humic quinones, 3) to evaluate DOM-Fe-As ternary complex formation and its influence on arsenic mobility and 4) to characterize DOM in the arsenic-contaminated aquifers of West Bengal, India and evaluate its role in arsenic mobilization using groundwater flow and contaminant transport modeling approach.

Results of this study revealed that oxidized quinone like moieties (such as fulvic acids) serve as an electron shuttle and enhance the reductive dissolution process under reducing conditions, hence mobilize the arsenic in groundwater. Another key result from this study suggested that arsenic binds with non-aromatic portion of the humic-like DOM under reducing conditions and increases its solution concentration. A field study conducted in West Bengal, India revealed that the mechanisms studied in the laboratory exists in reducing aquifer. A groundwater flow and reactive transport model was created to explain multiple interactions of DOM and arsenic spatial scales. Broader impacts of this study include significant addition to scientific knowledge about subsurface biogeochemistry and the role of DOM in biogeochemical reactions in the subsurface.

BIOGEOCHEMICAL INTERACTIONS OF NATURAL ORGANIC MATTER WITH ARSENIC IN GROUNDWATER

By

HARSHAD VIJAY KULKARNI

B.E., SHIVAJI UNIVERSITY, 2009

M.S., COLORADO STATE UNIVERSITY, 2012

A DISSERTATION

Submitted in partial fulfillment of the requirements for the degree

DOCTOR OF PHILOSOPHY

Department of Civil Engineering

College of Engineering

KANSAS STATE UNIVERSITY

Manhattan, Kansas

2016

Approved by:

Major Professor
David R. Steward

Abstract

Groundwater contamination with arsenic (As), a naturally occurring metalloid, is a worldwide problem. Over 100 million people are at health risk due to arsenic contaminated groundwater, especially in the Bengal Basin in south-east Asia. Dissolved organic matter (DOM), geology and geomicrobiology are important factors affecting arsenic mobility. This study focuses on interactions of different aspects of natural organic matter in arsenic-contaminated environments. A literature review specifically includes past studies done on fundamentals of arsenic geology, geomicrobiology, DOM characterization and relevant analytical methods and tools. Based on background information already collected, this research is focused on specific research questions and corresponding hypotheses.

The overarching goal of this investigation is to better understand the mechanisms by which DOM influences arsenic mobilization. The specific goals of this research are: 1) to evaluate role of oxidized humic quinones in reductive dissolution of Fe-As minerals and subsequent arsenic mobilization via electron shuttling, 2) to quantify the rate of microbially mediated reductive dissolution in the presence of oxidized humic quinones, 3) to evaluate DOM-Fe-As ternary complex formation and its influence on arsenic mobility and 4) to characterize DOM in the arsenic-contaminated aquifers of West Bengal, India and evaluate its role in arsenic mobilization using groundwater flow and contaminant transport modeling approach.

Results of this study revealed that oxidized quinone like moieties (such as fulvic acids) serve as an electron shuttle and enhance the reductive dissolution process under reducing conditions, hence mobilize the arsenic in groundwater. Another key result from this study suggested that arsenic binds with non-aromatic portion of the humic-like DOM under reducing conditions and increases its solution concentration. A field study conducted in West Bengal, India revealed that the mechanisms studied in the laboratory exists in reducing aquifer. A groundwater flow and reactive transport model was created to explain multiple interactions of DOM and arsenic spatial scales. Broader impacts of this study include significant addition to scientific knowledge about subsurface biogeochemistry and the role of DOM in biogeochemical reactions in the subsurface.

Table of Contents

List of Figures

List of Tables

Acknowledgements

I would like to thank all the individuals whose encouragement and support has made the completion of this dissertation possible. I am most grateful to Natalie Mladenov for the immense support and believing in my abilities since 2013. Her expert guidance on dissolved organic matter quality was very important being the major portion of this dissertation. I am indebted by her guidance in developing research projects, experimental designs and most importantly presenting the research findings to the scientific community. She has truly inspired me to become a better environmental scientist.

I am very thankful to David Steward, without his advice and support this work wouldn't have been successful. His expert advice with groundwater modeling greatly enhanced the quality of my research. I would like to thank Matthew Kirk (Geology Department, K-State) who introduced me to geomicrobiology and biogeochemical modeling, which substantially improved the quality of this dissertation. Special thanks must go to Saugata Datta (Geology Department, K-State) who provided great insight on hydro-geochemistry of the study area (Bengal Basin) and guided me to develop an international field research proposal which greatly improved this work. I am also grateful to Om Prakash and Alvaro Herrera for their help with ^{1}H NMR spectroscopy work. I am very thankful to Diane McKnight (INSTAAR, Boulder, CO) who gave her expert opinions on dissolved organic matter quality aspect of my research. I also would like to thank David Lipson and his students at SDSU for their great help with lab analyses. I also would like to thank Robert Stokes who believed in teaching capabilities and provided me an opportunity to teach environmental engineering laboratory during the course of study. Many thanks Prathap Parameswaran for introducing me to new research questions and his support. I also would like to thank many undergraduate and graduate students namely Hersy Enriquez, Kaley Oldani, Jose

Dedication

Every challenging work is inspired by a problem ! I would like to

dedicate my dissertation to those millions of people in India,

Bangladesh and worldwide who are fighting against the groundwater

arsenic problem in various capacities.

Chapter 1 - Introduction

Groundwater is an important source of drinking water in south and south-east Asia. Generally, groundwater is considered to be cleaner and safer to drink than the surface water since anthropogenic activities have polluted surface water sources over the last few decades. In Bengal Basin, the presence of geogenic arsenic (As) had led to high dissolved As concentrations and caused detrimental health effects to over 100 million people in India, Bangladesh, China, Myanmar, Pakistan, Vietnam, Nepal and Cambodia (*Fendorf et al., 2010, Figure 1*). Bio-geochemical transport processes in the aquifer have potential to also impact the quality of groundwater and these processes are studied.
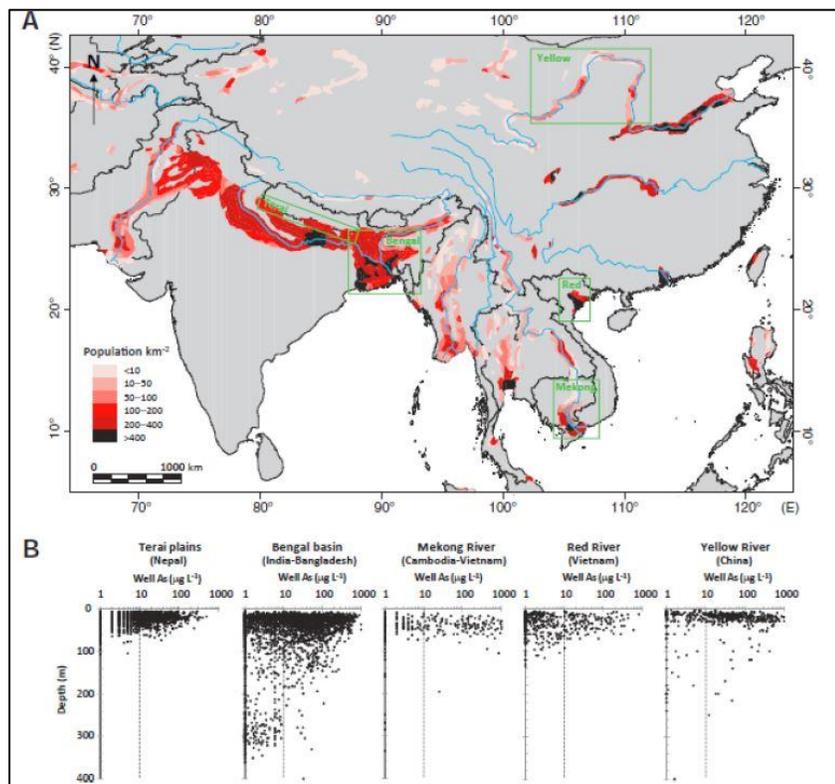
Figure 1 Distribution of As in South and South-East Asia (adopted from *Van Geen et al., 2011*)

An overview of existing scientific information about As contamination in reducing aquifers is presented that identifies the key research questions related to bio-geochemical transport processes that lead to arsenic mobilization. Chapter 1 provides an introduction to the As contamination problem in Bengal Basin, characteristics of As, and an overview of hypotheses proposed to explain mechanisms causing As contamination. In Chapter 2, a detailed account of prior relevant research is discussed. This review of literature is used as a basis for research questions addressed in this dissertation. The Chapter 3 discusses the methodologies used in laboratory experiments, field investigations and for mathematical modeling. The Chapter 4 explains the influence of the geochemical and organic matter characteristics on As mobility in the Murshidabad district of West Bengal, India. In Chapter 5, arsenic mobility due to formation of aqueous complexes between aromatic dissolved organic matter (DOM), As and iron (Fe) is discussed. Chapter 6 describes the electron shuttling abilities of aromatic DOM which enhance the process of microbial reductive dissolution of Fe and As minerals. In Chapter 7, bio-geochemical transport processes in the two geologically distinct (varying As concentrations) aquifers in Nadia and Hooghly districts of West Bengal, India are described. The summary of results, conclusions and prospects for future work is discussed in Chapter 8.

Characteristics of Arsenic

Arsenic is denoted as 3rd member of VA group in the periodic table. The atomic number of As is 33 and its atomic mass is 74.9216 gmol^{-1}. Four oxidation states of As are known as As^{-3}, zero valent As, As^{3+} and As^{5+}, however, arsenite As^{3+} and arsenate As^{5+} are the most common oxidation states found in the nature. The background As concentration in natural water has been reported to be 1-2 μgL^{-1} (WHO, 2011). There are about 200 known minerals with arsenic as the major

constituent. Arsenopyrite (FeAsS), realgar (As_4S_4) and orpiment (As_2S_3) have been considered as major ore minerals of the arsenic (*Smedley and Kinniburgh, 2002*).

In aquifers, the native form of arsenic has been considered to be As^{5+} as $H_xAsO_4^{x-3}$, often adsorbed to wide range of minerals such as hydroxides and oxyhydroxides of iron and aluminum (*Ying et al., 2012*). As^{3+} on the contrary, occurs as natural H_3AsO_3 species in non-sulfide environments and tend to adsorb on hydroxides, oxides and oxyhydroxides of iron (*Gupta and Chen, 1978; Masue et al., 2007; Raven et al., 1998; Dixit and Hering, 2003; Herbel and Fendorf, 2006; Ying et al., 2012*). As^{3+} has been considered to be more soluble and hence more bio-available, as it forms weak complexes and upon changes in the hydrochemistry; the weak bonds break easily resulting in mobilization of As^{3+} in solution (*Tufano and Fendorf, 2008*).
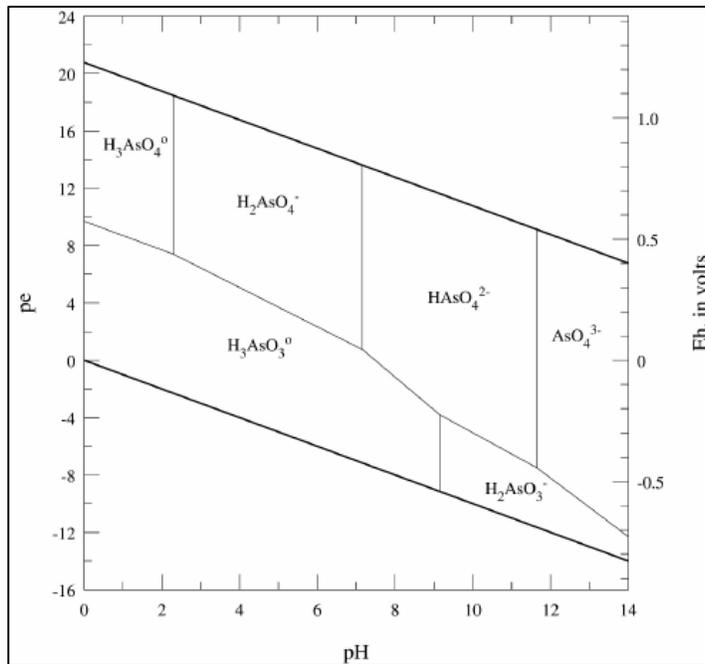
Figure 2 pe-pH diagram for predominant aqueous species of arsenic at equilibrium and 25^0C and 1 atm pressure (*Nordstrom and Archer, 2003*)

Arsenic has also been known as a redox sensitive element (Figure 2). Typically, $H_2AsO_4^-$ and $HAs_2O_4^{2-}$ species occur under oxidizing conditions (E_h>100 mV and pH 6-7.5) while under reducing conditions (E_h

3

< 100 mV and pH 6-7.5) $H_3AsO_3^0$ is the dominant species. Under very reducing conditions ($E_h <$ 250 mV), arsenic has often been found to form the mineral orpiment (As_2S_3) where the sulfide (HS^-, S^{2-} and H_2S) species are predominant. However, both As^{3+} and As^{5+} species occur in nature as the rate of redox transformation is slow (*Smedley and Kinniburgh, 2002; Mukherjee et al., 2009*). In general, the redox conditions strongly governs the ratio of As^{3+} to As^{5+} species.

Occurrence of Arsenic

Arsenic contamination in Bengal basin is designated (*Smith et al., 2000*) as "*The largest poisoning of a population in history*". In late 1980s, surface water used to be the main source of drinking water, which was severely polluted by pathogens (*Smith et al., 2000*). With the support from UNICEF, governments of India and Bangladesh installed about 4 million tube wells for obtaining drinking water. Unfortunately, a huge population was diagnosed with hyperpigmentation, peripheral neuropathy, bladder and lung cancer, skin cancer and peripheral vascular diseases (*Zaloga et al., 1985; Pierce et al., 2012).* Elevated levels of dissolved As are known to be responsible for severe health risks to about 60 million people in India and Bangladesh alone. Now, the World Health Organization (2011) has set maximum allowable As in drinking water as 10 ugL^{-1}.

The presence of sedimentary As in Bengal basin aquifers is termed as "geogenic" i.e., of natural origin since it is present in the aquifer sediments. The major rivers transported As rich Himalayan sediments to the Bengal Basin and deposited that during the quaternary period. Multiple bio-geochemical processes and redox conditions lead to mobilization of As. In other parts of the world as well, various sources of As are reported to contaminate the groundwater. Sulfide mineral deposits in British Columbia in Canada and in northern Bavaria in Germany leach As into the groundwater (*Smedley and Kinniburgh, 2002*). Aquifers in California, Nevada, Idaho and

South Dakota in the USA, China, Taiwan and Mongolia also hold significant sedimentary As that contaminates the groundwater. Arsenic contamination in Northern Chile, Mexico and Argentina (*Mukherjee et al., 2006*) is attributed to deposition of volcanic ash. Mining activities (Fairbanks, Alaska, USA; Moira Lake, Ontario, Canada; Brazil; Australia; Thailand) and geothermal activities (New Zealand, Russia, USA, Chile and France) also trigger As contamination.

Figure 3 Map depicting global arsenic occurrence (*Smedley and Kinniburgh, 2002*)

Contributions

Hydro-geochemical controls in Bengal Basin aquifers have been widely studied. Most studies reported groundwater quality and emphasize the varying distribution of dissolved As. Earlier, many studies examined the (1) nature of sediments, (2) adsorption of As onto the oxidized iron minerals and (3) potential of excessive pumping in mobilizing As. Recent studies examined the role of anoxic microorganisms and sedimentary carbon in mediating the process of reductive dissolution. This is concisely the status of existing research relevant to this study.

In this study, detailed analyses of DOM revealed that the characteristics of DOM were drastically different in high and low As sites in the Murshidabad district of West Bengal, India. Laboratory experiments showed that the aromatic DOM forms aqueous complexes with As and maintains an elevated dissolved As concentration. Another experiment showed that aromatic DOM accelerates the rate of microbial reductive dissolution of iron minerals by shuttling an electron from microorganisms to the mineral surface abiotically. An in-situ study with data collected in the field and subsequent model investigations demonstrated the geochemical processes and projected future transport conditions

Chapter 2 - Review of literature
Arsenic Contamination in Bengal Basin

Several studies have reported the arsenic contamination in Bengal basin as the greatest natural mass poisoning in human history (*Bhattacharya et al., 1997; Nickson et al., 1998; Smith et al., 2000; McArthur et al., 2001; Dowling et al., 2002; Paul, 2004; Ravenscroft et al., 2005, Routh et al., 2005; Acharya and Shah, 2007; Datta et al., 2011; Sankar et al., 2014 and references therein*). Groundwater in seven districts in the state of West Bengal, India and most parts of Bangladesh has been reported to be contaminated with As. In West Bengal, the affected districts are namely Malda, Murshidabad, Burdwan, Howrah, and Hooghly, Nadia, North 24-Paraganas and South 24-Paraganas. Typically, As contaminated aquifers have been located at a depth of 60 m in these areas (*McArthur, et al., 2001 and 2004; Dowling et al., 2002; Datta et al., 2011*). Younger alluvial deposition by Ganga-Meghana-Brahmaputra Rivers during the Holocene age covers most of these areas. These alluvial deposits have been known to be enriched in As. Older deposits below alluvial deposits designated as the Suja formation during Pleistocene age have been reported to arsenic free. Arsenic-rich Himalayan rocks eroded and transported to the Bengal basin formed in the foreland basin of the Himalayan mountain chain have been postulated as sedimentary As in fluvial deposits (*Nickson et al., 2000*). Earlier it was also postulated that the base metal deposits in the upstream areas of Bengal basin could be possible source of As contamination (Nickson et al., 1998); however this idea was rejected as the quantities were so low. Nickson (2000) also described the presence of coal seams and basalts of Rajmahal basin and isolated sulfide minerals containing about 0.8 % As in Darjeeling Himalayas and Gondwana coal seams as possible sources of As. In general, arsenic adsorbed on the oxides, hydroxides and oxyhydroxides of iron (*Nickson et al., 2000; McArthur et al., 2001; BGS, 2001; Dowling et al., 2002; Ravenscroft et al.,*

2005; Datta et al., 2011; Sankar, 2013 and references therein). These references document the sources of As contamination in Bengal basin.

Geology of Bengal Basin

The Bengal basin was formed as a result of India-Asia collision as the flexural subsidence of the Indian lithosphere created Ganges Plain foreland basin in front of the Himalayan mountain ranges during late Quaternary period (*Singh, 2004; Sinha et al., 2005*). The basin was named as GBM delta as it formed due to sediment deposition by meandering of three major rivers Ganges, Meghana and Brahmaputra (*Morgan and McIntyre, 1959; McArthur et al., 2011; Mukherjee et al., 2008; Hoque et al., 2011*). The basin ranges between the Himalayan mountain ranges on the north to the Precambrian, Peninsular Indian craton in the south. The basin has been chrono-stratigraphically classified to hold two major types of sedimentary units as the older Pleistocene and the younger Holocene unit (*Morgan and McIntyre, 1959; Mukherjee et al., 2008; Datta et al., 2011; McArthur et al., 2008 and 2011*). McArthur (2008) reported that the current paleo-inter-fluvial areas (highlands) in the basin were exposed, and a thin layer of paleosol was deposited during the last glacial maximum (~20 ka before present) when sea level was substantially lower. The low-stand of sea level caused deep erosion in paleo-channels (current low-lying areas) in the basin by paleo-rivers followed by weathering due to heavy rainfall during the warmer climate regime and developed a widespread paleosol of impermeable clay that has been found widely today across the basin (*McArthur et al., 2008; Hozque et al., 2011*). The Rajmahal hills to West and north-west boundaries of the basin are basalt lava traps of lower Jurassic age and are upper part of Gondwana system. Shillong plateau or Garo or Khasi or Jaintia hills composed of Archean quartzite, slates and schists with massive granitic intrusions with interbedded basaltic traps and overlain by Eocene sandstones and limestones beds, mark the northeastern boundary of the Bengal

basin. The Tripura hills and Chittagong marks the northeastern and southeastern boundary of the basin, while the western boundary is marked by Chottonagpur plateau which is composed of granites, amphibolite, carbonates and quartzities of Precambrian age (*Morgan and McIntyre, 1959*). The River Ganges from the northwest and the River Brahmaputra from northeast transports sediments from Himalayas, while the River Meghana brings sediments from Shillong Plateau (*Morgan and McIntyre, 1959*).

Hydrological Controls

Hydrological controls in the Bengal basin have been discussed in Mukherjee (2007) and several other studies. Briefly, the Bengal basin groundwater system is influenced by the rainfall due to the southeast monsoon winds. October/November to May/June is considered to be the dry season while June/July to September/October is considered to be the wet season. CGWB (1994) reported the annual rainfall ranges from 1200 mm to 2000 mm. In the delta region, precipitation exceeds annual potential evapotranspiration (*Allison, 1998*), and frequent floods occur in the lowlands of the basin due to heavy rainfall during monsoon period together with snow melt from the Himalayas. Considering the topography, the northern part of the Bengal basin has hydraulic gradient of 1 m/km while the southern part near the delta region has lower hydraulic gradient of 0.01 m/km in its alluvial aquifers. These alluvial aquifers in this area have been found to be highly productive with the water table mostly within 15 m of ground level. Although there are some seasonal variations based on irrigation pumping, the average yearly water table remains the same, suggesting that there is sufficient recharge replenishing the groundwater systems (*BGS/DPHE, 2001*). The estimated transmissivity (T) values vary from 3300 to 7000 m^2/day in the northern district of Murshidabad, 5000 to 8800 m^2/day in the North 24-Paraganas and 500 to 3000 m^2/day in the South 24-Paraganas with average storativity (S) of 0.03 (*Mukherjee et al., 2007*). The

porosity of the alluvial aquifers has been reported to be 0.2 (*Harvey, 2002*). The hydraulic conductivity (K) has been reported to vary from 10 to 100 m/day (*BGS/DPHE, 2001*). The natural groundwater flux to the Bay of Bengal from the Bengal basin was estimated to be 2E11 m^3/year, which was 19% of the total surface water flux (*Basu et al., 2001*) and 15% of the Ganges-Brahmaputra river flux (*Dowling et al., 2003*). The river Bhagirathi – Hooghly has been considered to be a losing stream along most of its length and recharges the shallow aquifers (*Ghosh and Mukherjee, 2002*).

Mechanisms of Arsenic Release

The scientific agreement on sedimentary As to be the primary and main source of As contamination in groundwater in Bengal basin led to further questions such as why As was mobilized in the fluvial alluvium in Bengal basin deposited during the Holocene. One of the earlier proposed mechanisms was that the drawdown in aquifers permitted atmospheric oxygen to invade the aquifer and resulted into oxidation of arsenopyrite minerals in alluvial sediments (*Mallick and Rajagopal, 1996; Mandal et al., 1998; Roy Chowdhury et al., 1999*). Acharya (1999) proposed that the over application of phosphorous fertilizers leached significant amounts of phosphates into the groundwater, which displaced the arsenic anions adsorbed to iron minerals by competitive anion exchange and released As into the groundwater. Although it was found that pyrite was present in the aquifer sediments (*Nickson et al., 1998 and 2000*), the presence of pyrite indicated that it has not been oxidized and is potentially a sink for and not a source of arsenic in the Bengal basin (*McArthur et al., 2001*). It was also shown that even in case of pyrite oxidation, the released arsenic would re-adsorb onto oxyhydroxides of iron rather than being in solution (*Mok and Wai, 1994; Savage et al., 2000*). The mechanism of pyrite oxidation was not strongly supported by anoxic conditions in groundwater and lower sulfate concentrations in high arsenic groundwater

(*DPHE, 1999 and 2000; McArthur et al., 2001*). Finally, a more likely mechanism for anoxic conditions in Bengal basin aquifer was proposed and it was widely accepted that arsenic was released by reductive dissolution of iron oxyhydroxides (*Bhattacharya et al., 2997; Nickson et al., 1998 and 2000*). This mechanism was previously used to explain presence of arsenic in anoxic surface waters (*Aggett and O'Brien, 1985; Cullen and Reimer, 1989; Belzile and Tessier, 1990; Ahmann et al., 1997)* and in anoxic groundwaters *(Matisoff et al., 1982; Cullen and Reimer, 1989; Korte, 1991; Korte and Fernando, 1991; Bhattacharya et al., 1997; Nickson et al., 1998 and 2000, McArthur et al., 2001*).

Microbially Mediated Reductive Dissolution

It was determined that the reduction of iron minerals was driven by microbial metabolism of organic matter (*Chapelle and Lovley, 1992; Nealson, 1997; Lovley, 1997; Banfield et al., 1998; Chapelle, 2000*). This was supported by several studies that reported high concentrations of dissolved iron (*DPHE, 2000; Nickson et al., 1998 and 2000; Safiullah, 1998*) and high concentrations of bicarbonates (*McArthur et al., 2001*) in the groundwater of Bengal basin aquifers. Many recent studies have found hydrochemical data in strong agreement with this mechanism (*Dowling et al., 2002; Hasan et al., 2007; Sankar et al., 2014*). The labile organic carbon required in the microbially mediated reductive dissolution mechanism was thought to be drawn to depth from ponds and other surface water laden with sewage (*Harvey et al., 2006; Neumann et al., 2010*), however, dispersed sedimentary organic matter has also been implicated as a major source (*McArthur et al., 2004; Sengupta et al., 2008; Datta et al., 2011*). Harvey (2002) and Saunders (2008) showed the increase in dissolved As concentration upon injection of labile carbon into the aquifer, supporting the role of labile carbon in arsenic release by stimulating microbially-mediated reductive dissolution of iron minerals.

The Role of Dissolved Organic Matter

Recently, additional roles have been proposed for DOM in aquifers in the Bengal Basin that may have important consequences for iron and arsenic mobilization (*Wang et al., 2006; Mladenov et al., 2010*). Dissolved organic carbon (DOC) has been considered to be the largest pool of organic carbon in most aquatic ecosystems (*Cole et al., 1999, 2007*). The term DOM has been considered to include DOC as well as other organic compounds expected to be involved in most ecological processes (*Zsolnay, 2003*). Mladenov (2010) characterized DOM in Holocene aquifers in central Bangladesh and provided valuable information on the role of DOM in arsenic mobility. Terrestrially-derived and microbially-derived components of DOM were observed at different depths where As concentration was considerably high. Determination of the redox state of DOM suggested that fluorescent quinone-like moieties were more reduced in the deeper, older groundwater of the Holocene aquifer (*Mladenov et al., 2010*).

Different mechanisms have been hypothesized by which the DOM could mobilize the arsenic. For instance, humic substances, a biologically refractory class of DOM, are involved in complexation reactions with Fe and As (*Liu et al., 2011; Sharma, 2010*), competition with As for sorption sites (*Bauer and Blodau, 2006*), and electron shuttling reactions (*Lovley et al., 1996, 1998 and 1999; Scott et al., 1998; Klapper et al., 2002; Kappler et al., 2004; Jiang et al., 2008; Wolf et al., 2009; Mladenov et al., 2010, 2015*). Therefore, DOM of both labile and recalcitrant quality may enhance the process of arsenic release by several mechanisms, including by serving as an electron donor (i.e., as direct source of energy) and by more chemically reactive mechanisms involving humic substances (*Mladenov et al., 2015*). Characterization of biologically labile as well as humic and chemically reactive fractions of DOM provides the potential to develop insights into the sources of DOM and, therefore, its influence on arsenic mobility.

Chapter 3 - Hypotheses and objectives

Several geochemical and hydrological processes are important for arsenic mobility in aquifers. This study is focused on interactions of these different processes in the reducing aquifers contaminated with natural or geogenic arsenic. The overarching goal is to better understand the mechanisms by which DOM influences arsenic mobilization. The specific goals are: (1) to explore the key characteristics of DOM in aquifers that are distinct in dissolved arsenic concentrations, (2) to evaluate the role of oxidized humic substances in reductive dissolution of Fe minerals and subsequent arsenic mobilization via electron shuttling, (3) to evaluate binary or ternary complex formation of DOM with As and Fe, (4) to understand biogeochemical transport processes with the flow of groundwater.

To achieve these goals, laboratory experiments, analyses of samples collected in field and groundwater flow and transport modeling were performed.

Hypothesis # 1: Higher arsenic concentrations in Holocene aquifers and lower concentrations in Pleistocene aquifers are linked with the contrasting quality of DOM in the aquifers.

In order to test this hypothesis, groundwater samples from high arsenic wells (aquifer with younger or Holocene period sediment deposition) and low arsenic wells (aquifer with older or Pleistocene period sediment deposition) in Murshidabad district, West Bengal, India were analyzed for water chemistry and characteristics of DOM.

Hypothesis 2 Humic substances act as intermediate electron shuttles and the rate of microbial iron/arsenic reduction is accelerated by the presence of humic substances.

This hypothesis was tested by conducting two separate laboratory experiments. The first experiment was set up to find out whether microbially reduced humic substances isolated from

high arsenic groundwater shuttles the electron(s) and reduce the iron minerals independent of microbial metabolism. In the second experiment, iron reducing bacteria were grown in the presence of humic substances to determine whether the rate of iron reduction is accelerated.

Hypothesis 3 Arsenic and iron forms aqueous complexes with dissolved organic matter.

To test this hypothesis, fluorescence titrations were carried out between DOM-Fe, DOM-As and DOM-Fe-As. Quenching of fluorescence was quantified to be linked with aqueous complex formation. Further, structural information about the DOM molecule during the reaction was obtained by nuclear magnetic resonance spectroscopic analysis.

Hypothesis 4 Groundwater flow and biogeochemical transport results in spatially discontinuous arsenic concentrations.

In order to test this hypothesis, hydrogeological models of two aquifers (1) the Bengal basin aquifer, West Bengal, India and (2) the Mahomet Bedrock Valley (MBV) aquifer, IL, USA were developed. Different hydro geochemical scenarios were simulated to understand flow and transport processes in the aquifers.

Hypothesis 5 Monsoonal recharge influences the quality of dissolved organic matter in shallow alluvial aquifer and subsequently the arsenic mobility.

This hypothesis was tested by collecting the groundwater samples from a shallow aquifer (high arsenic site in Nadia district) and a deeper aquifer (low arsenic site in Hooghly district) in West Bengal before and after the monsoon. A detailed examination of DOM quality by absorbance and fluorescence spectroscopy, along with hydrochemical analyses of groundwater was conducted.

Chapter 4 - Methodology

Field Investigations

Three months of fieldwork in Nadia, West Bengal was conducted for the current research work during May – August 2015. During the fieldwork, intensive groundwater sampling was done with focus to study DOM in groundwater in relation to Arsenic concentrations. The selection of sites was done in consultation with host Prof. Chatterjee at University of Kalyani. This institute maintains five multi-level piezometers at two sites (Chakudanga (23°4'57.42"N, 88°38'9.96"E) and Shahispur (23° 4'18.47"N, 88°36'34.96"E)), located east of the River Hooghly by about 12 kilometers, near the town of Chakdah. This area typically exhibits reduced aquifers characterized by Holocene sediments and elevated dissolved arsenic. These two sites were selected primarily because of access to piezometers.

Groundwater samples were collected from piezometers as well as drinking tube-wells surrounding piezometers within 500 m distance. In order to study DOM in groundwater where arsenic is in low concentrations, two sites were selected 12 kilometers west of River Hooghly, near the town of Naksha. This area typically exhibits relatively lower concentrations of dissolved arsenic, and the aquifer is characterized by Pleistocene sediments. There are no pre-installed piezometers in this study area; hence groundwater samples from two villages Bele (23° 3'40.55"N, 88°21'7.81"E) and Radhanagar (23° 3'18.22"N, 88°20'41.10"E) were collected. Surface water samples were also collected from the ponds in nearby areas with significantly large surface areas. During sample collection, information about the tube-well (i.e., depth), the method of installation, the age of well etc. was collected from the head of household. Geographic coordinates of all tube-wells were recorded using a handheld GPS device.

Monsoons impact groundwater flux and may influence the characteristics of DOM and mechanism of their transport or their functions. To understand the impact of the monsoon on DOM quality, a sampling strategy to collect samples before (in dry season) and after (in wet season) monsoon was used. The monsoon started around 15th June 2015 in the study area. Samples collected during 4th – 11th June 2015 were representative of the pre-monsoon season while those collected during 20th July – 13th August 2015 were representative of the post-monsoon season.
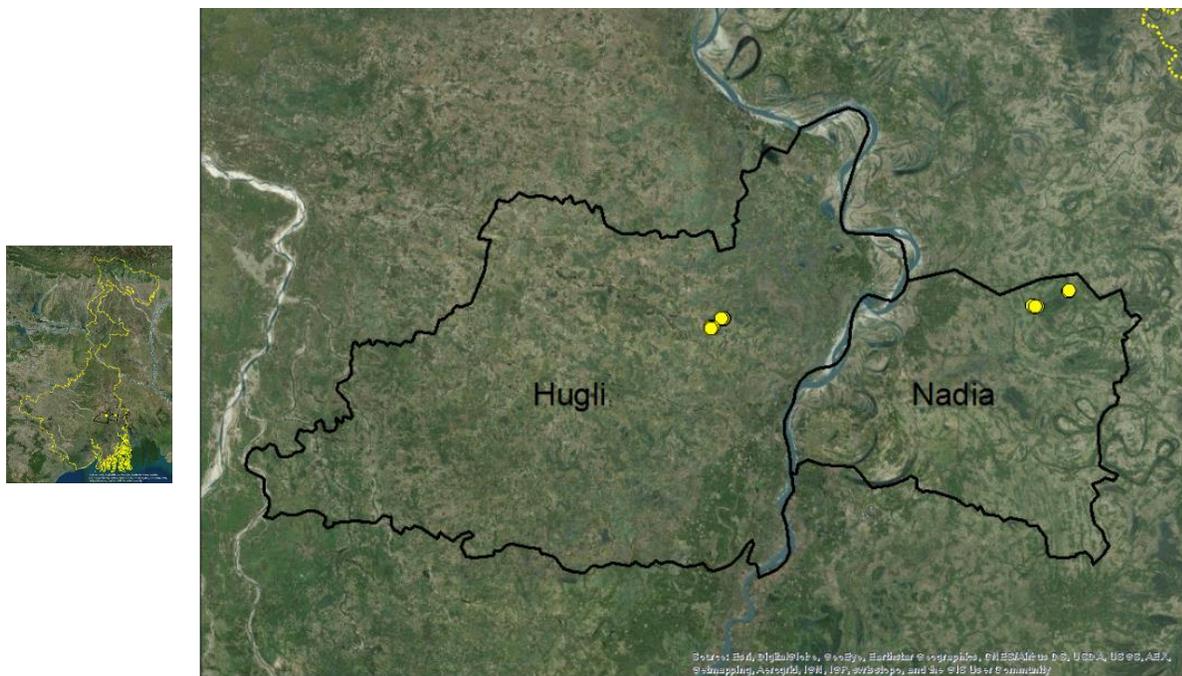
Figure 4 Google Earth Map showing the study area. Sampling sites are shown in Yellow. Inset shows the location map.

Figure 5 Enlarged view of four sampling sites and locations of sampled wells

Sample collection and storage

Tube-wells were pumped at a slow and steady rate manually for about 45 minutes to remove accumulated water, and then samples were filtered using a handheld vacuum pump device through a 0.7micron glass fiber filter. The filtered sample was collected in one 60 ml and two 125 ml clean HDPE bottles. For sample preservation, 200 microliters of 70% hydrochloric acid was added to one of 125 ml bottles, while 200 microliters of 70% nitric acid was added to another 125 ml bottle to maintain the pH of sample below 2. All the bottles were appropriately labeled and stored at 4°C in dark.

Figure 6 Typical drinking water tube well (Top Left), a surface water pond close to a tube well (Top Right), multilevel piezometers (Bottom Left) and the pre-rinsed bottles (125 mL and 250 mL) used to collect the samples (Bottom Right).

Field measurements

The dissolved oxygen was measured using a field probe in flowing water while the pump was running. The pH was measured using a pH probe in still water samples collected in clean and rinsed container. An additional filtered sample was used to measure chemical parameters using field test-kits. Alkalinity was measured using a field titration unit (Chemetrics K9810 and K9815). Arsenic was measured using color strip analysis kits (HACH 2800000 and HACH 2822800). The

total and ferrous iron was measured using field test kits (Chemetrics K6210 and K6210D) on filtered samples. Calibration of instruments, preparation of reagents and test kits was done in the chemistry lab at the University of Kalyani. Samples were shipped to US for further analysis at Kansas State University and San Diego State University. Three dimensional fluorescence spectroscopy analysis, total organic carbon, bulk protein analysis of anions and total arsenic was done at San Diego State University.

Figure 7 Field measurement of total and ferrous iron using Chemetrics K6210 and K6210D (Left). Field measurement of arsenic using HACH 2800000 and HACH 2822800 (Right).

Laboratory Analyses

Anions in the water samples were measured using a Ion Chromatograph (Dionex ion chromatography system) at the Biology Department, San Diego State University. A total of 40 tube wells and 10 pond water samples were analyzed, and all the samples were measured in triplicates for redundancy of the analyses. Standards were prepared for eight inorganic (chloride, bromide, fluoride, nitrate, nitrite, phosphate, sulfate and arsenate) and five organics (acetate,

citrate, formate, lactate and oxalate) anions. The samples for anion analysis were taken from 125 mL unfiltered unacidified plastic bottles. Later, 1.5 mL of the sample was transferred to an IC vial and placed in the auto-sampler of the IC unit.

Concentration of Fe^{2+} was measured by reacting the sample with Ferrozine reagent (5 mL Ferrozine reagent (*Stookey, 1970*) per 2 mL of sample). The presence of Fe^{2+} is indicated by a purple color upon reaction. This ferrous – Ferrozine complex absorbs at a λ_{max} of 562 nm. Standards were prepared using Fe $(NH_4)_2(SO_4)_2 \cdot 6H_2O$ ferrous ammonium sulfate hexahydrate (FW = 392.14). Blank was prepared using 2 mL of deionized water. All the reagents and standards were freshly prepared on the day of the analyses. Detailed procedures and preparation of reagents is provided in the Appendix. Filtered water samples (20 mL) acidified in the field using 70% hydrochloric acid were used for DOC and TN analyses. The analyses were carried out on a TOC-L Shimadzu Total Organic Carbon Analyzer. The standard operating procedure for TOC analyzer is included in the Appendix.

Bulk Protein Analysis

The method involves reaction of protein with cupric sulfate and tartrate in an alkaline solution, resulting in formation of tetradentate copper-protein complexes. When the Folin-Ciocalteu Reagent (*Miller, 1959; Hartree, 1972*) is added, it is effectively reduced in proportion to these chelated copper complexes, producing a water-soluble product whose blue color can be measured at 750 nm. Accordingly, protein concentrations generally are determined and reported with reference to standards of a common protein such as bovine serum albumin (BSA). This method has rarely been used to quantify protein content of water and groundwater samples, where the expected protein concentrations are low.

The 10 ml of groundwater sample was taken in a 50 ml polypropylene Falcon conical centrifuge tube (Fisher # 14-432-22). This sample was instantaneously frozen by inserting and swirling the centrifuge tube in a beaker containing a solution (slurry) of 99.5% tthyl alcohol (Sigma # 459844) and dry ice for about 15-20 minutes, making sure that the sample is frozen as a thin sheet of ice inside the centrifuge tube. The frozen samples were dried using a freeze-drying unit (combined of a freezer -150 °C and a vacuum pump) for 24 hours, allowing frozen samples to sublime completely. After freeze drying, 1 mL of 18.2 MOhm-cm ultrapure water was added to the centrifuge tube and vortex mixed. The solution was then transferred to a 1.5 ml polypropylene micro-centrifuge tube (Fisher # 05-408-130) and centrifuged at 10000 x G for 5 minutes. After centrifuging, the clear solution in the top layer was used for analyses, and the precipitate (white color precipitate of the Ca / Mg salts) was separated.

A modified Lowry Protein Assay Kit (Thermo Scientific 23240) was used to quantify the bulk proteins in pre-processed groundwater and surface water samples (*Hartree, 1972*). Aliquots of 40 uL were transferred to a 96 well polypropylene microplate. The modified Lowry Reagent (cupric sulfate, potassium iodide and sodium tartrate in an alkaline sodium carbonate buffer) was added (200 uL) to each well using a multi-channel pipettor. The microplate was covered and mixed for 30 seconds using the plate reader's vibration program. It was then allowed to stabilize for exactly 10 minutes at room temperature. Then, 20 uL of 1N Folin-Ciocalteu reagent (*Hartree, 1972*) (stock solution of 2N Folin-Ciocalteu reagent was diluted 50% in 18.2 MOhm-cm ultrapure water) was added to each well using a multi-channel pipettor. The microplate was covered and incubated for 30 minutes at room temperature. The absorbance at 750 nm was measured for all the wells. Ultrapure water (18.2 MOhm-cm) was used as blank, and standards were prepared using dilutions of Bovine Serum Albumin (BSA) in ultrapure water (1000, 500, 250, 125, 25, 5, 1 and 0

µg/ml). All the blanks and standards were analyzed in exactly same way as samples in the same microplate. All the samples, blanks and standards were analyzed in triplicates. The average value of the absorbance at 750 nm of the blank triplicates was subtracted from all other individual standards and unknown samples. A standard curve was prepared by plotting the blank corrected absorbance values for the standards vs. the known concentrations. This curve was used to determine the protein concentration for each unknown sample. Absorbance data for unknown samples was fitted to standard curve using a four-parameter curve-fitting algorithm for accurate estimation of protein concentrations. Detailed procedure of analysis and preparation of reagents is provided in the Appendix.

Spectroscopic Analyses of DOM

UV-visible absorbance and fluorescence spectroscopic techniques have been used to study DOM in a wide range of environments from marine waters (*Kalle, 1949; Duursma and Marchand, 1974) to* groundwater *(Mladenov et al, 2010, 2013, 2015*). Absorbance data was used for calculating absorbance at 254 nm (abs254) where molecules with specific bonding arrangement such as the conjugated systems in aromatic compounds exhibit greatest absorptivity (*Weishaar et al., 2003*). Specific UV absorbance (SUVA$_{254}$) indicating aromaticity of DOM was also calculated by normalizing the absorbance at 254 nm (abs$_{254}$) with DOC concentration. Two spectral slopes $S_{275-295}$ indicative of molecular weight and degree of photo-bleaching and $S_{350-400}$ indicative of colored DOM (CDOM) and contributions from terrestrially derived DOM (*Helms et al., 2008*) were determined. The spectral slope ratio S_R ($S_{275-295}$ / $S_{350-400}$) was calculated where $S_R > 1$ is indicative of low CDOM found in marine water samples, whereas $S_R < 1$ is characteristic of terrestrially dominated, high CDOM samples (*Helms et al., 2008*). An increase in the S_R value was observed due to reduced molecular weight of DOM and photo-bleaching, whereas a decrease in

the S_R value was observed due to microbial activities i.e. microbial production or preservation of long wavelength absorbing substances (*Helms et al., 2008; Moran et al., 2000; Vahatalo and Wetzel, 2004*). Fluorescence index (FI) that typically suggests the source of DOM, ~1.3 – 1.4 being terrestrially derived DOM and ~1.7 -1.9 being microbially derived DOM was calculated (*McKnight et al., 2001; Cory and McKnight, 2005*). Freshness index (β:α) (*Parlanti et al., 2000*) ranging from 0.4 – 0.6 represent recently derived DOM while that between 0.6 – 1 represent processed DOM (*Fellman et al., 2010*). Higher values of humification index (HIX) indicate higher degree of DOM humification (*Ohno, 2002*).

In the current study, the UV-visible absorbance and EEM spectra were measured simultaneously using a Jobin Yvon Aqualog Fluorometer with a clean quartz cuvette of 0.01 m path length. Integration time was set to 0.25 seconds, and an excitation range from 240 nm to 450 nm with 3 nm increments was used. Emission spectra were obtained from 212 nm to 619 nm with increments of 3.28 nm (according to instrument specifications). Fluorescence signals were collected in signal to reference (S:R) mode, and EEMs were corrected for the inner filter effect (*Ohno, 2002*), Raman normalized (using 18.3 MΩ cm Milli-Q ultra-pure water at ~350 nm), and blank subtracted. First and second order Rayleigh scattering bands also were excised (*Stedmon and Bro, 2008*). A quinine sulfate standard was also run, giving a value of 1 R.U. = 2.495 quinine sulfate units (QSU). Absorbance data was collected simultaneously on the same Aqualog Fluorometer between 240 nm to 450 nm wavelengths with a resolution of 3 nm. Absorption coefficients, *a*, were calculated as,

$$a = 2.303 * A/l$$

Where A = absorbance measured and l = path length (0.01m). Spectral slopes were calculated from the log transformed absorbance coefficients between 275 – 295 nm ($S_{275-295}$) and 350 – 400

nm ($S_{350-400}$). The FI is calculated as the ratio of fluorescence intensities at 470 nm and 520 nm emission and 370 nm excitation. The β:α was determined as the ratio of emission intensity at 380 nm with maximum intensity between 420-435 nm at excitation wavelength of 310 nm (*Parlanti et al., 2000*). The HIX was calculated as the ratio of peak area under the emission spectra at 435-480 nm to peak area from 300-345 nm obtained at an excitation wavelength of 254 nm (*Zsolnay, 2003*). Area under the curve was estimated by trapezoidal area calculation with increments of 1 nm for excitation and emission wavelengths. All corrections were performed using a computer program implemented in MATLAB (R2014a). Corrected three dimensional fluorescence excitation emission matrix (EEM) data was fitted to a four component PARAFAC model (*Harshman, 1970; Stedmon et al., 2003; Stedmon and Bro, 2008*).

PARAFAC Modeling using Fluorescence Data

DOM Fluor toolbox (*Stedmon and Bro, 2008*) was used to build a PARAFAC model for this sample dataset. The sample set included corrected EEMs from surface and groundwater with varying fluorescent intensities. In order to avoid false identification of extremely high or low concentration samples as outliers by PARAFAC, these EEMs were normalized using a modified method of Murphy (2013). In brief, each intensity value in the matrix was divided by the maximum intensity of that sample instead of dividing by the sum of squares of all intensities in that sample. This presets all the EEMs to a maximum intensity of 1, according to:

$$I(i,j)corrected = \frac{I(i,j)initial}{Imax}.$$

Outliers were removed from the PARAFAC model dataset if they met one of these conditions: negative spectral slope ratios, very high FI (> 2) that corresponded to a FI peak emission location > 470 nm, and, β:α values >1 indicating shift of peak in the 310 nm emission spectra. The dataset

was then fitted to a non-negativity constrained PARAFAC model according to *Stedmon et al., (2003)*. Additional outliers were identified by calculating the leverage of each sample and wavelength. Samples with leverages approaching 1 were examined to ensure that there was no analytical error before being considered as outliers (*Stedmon and Bro, 2008*). After removing outliers, a total of 60 samples were used. A four-component model was validated by split half analysis and random initialization techniques by running ten, four component models. For all the samples, the residual (difference between actual and modeled EEM) did not exceed 10% of the intensity in the original EEM (*Cawley et al., 2012*), which indicates an acceptable model fit (*Stedmon and Bro, 2008*). After complete validation, the actual intensities of each component were obtained by multiplying the intensity of each component by the maximum intensity (I_{max}) of the original EEM used in the normalization. Two indices based on PARAFAC components were developed to provide further insights into the nature of DOM. The humic:protein index was calculated as the ratio of the sum of humic-like DOM components to the sum of protein-like DOM components obtained from the PARAFAC model, according to:

$$humic:protein = \frac{\sum Humic - like\ DOM\ Components}{\sum Protein - like\ DOM\ Components}.$$

The (terr: microb) index was calculated as the ratio of the sum of terrestrially-derived to microbially-derived DOM components obtained from the PARAFAC model, according to:

$$terr:microb = \frac{\sum Terrestrially\ Derrived\ DOM\ Components}{\sum Microbially\ Derrived\ DOM\ Components}.$$

Statistical Analyses

Statistical analyses were carried out to determine descriptive parameters such as minimum, maximum, average and standard deviation of the data. Since the arsenic concentrations were not normally distributed, a non-parametric Mann – Whitney – Wilcoxon (MWW) U test was used to

compare the statistically significant variability among samples. Regression analyses was used to obtain R^2 and p statistics for correlation between two datasets. All statistical operations were performed using Microsoft Excel and MATLAB (R2014a).

Bio-geochemical Methods

Electron Shuttling Experiment

Geobacter metallireducens Lovley et al. (ATCC 53774) pure culture was used and initial cultures were propagated by incubating the cells at 30^0C in freshly prepared ferric citrate medium (ATCC 1768) for 7 days. The pH of the medium was maintained between $6.8 - 7.0$ after bubbling 80% N_2 and 20% CO_2. Suwanee River Fulvic Acid (SRFA) was used to study the growth rate of *G. metallireducens* and was obtained from International Humic Substances Society (IHSS # 2S101H). Ferric citrate (Fisher # 3388) and Goethite (*Schwertmann and Cornell, 2007*) were used as liquid and solid phase electron acceptor respectively. Dissolved Fe^{2+} was quantified by Ferrozine method (*Stookey, 1970, Appendix*) on a UV-Spectrophotometer. Bangladesh Fulvic Acid (BFA) samples were isolated from the groundwater ranging from $7 - 15$ m depths and <5 to >30 years old age. (*Mladenov et al., 2015*).

The study site was located in the Ganges Brahmaputra Delta (GBD) in central Bangladesh and underlay Holocene aquifers ($5 - 30$ m, elevated As) and deep Holocene aquifers ($40 - 90$ m, low As) separated by one or multiple layers of fine-grained sediment (*Zheng et al., 2005*). BFA samples were re-dissolved in 18.2 MΩ-cm Milli-Q ultra-pure water to obtain final concentration of 2 mg. mL^{-1}. Nutrients (as per ATCC 1768, except ferric citrate) were added and dissolved to BFA solutions in appropriate amounts. An industrial grade N_2 gas was bubbled through the BFA solutions for 1 hour in 18 x 150 mm glass anaerobic tubes and tubes were sealed under N_2 head

with 20 mm blue butyl rubber stopper and aluminum seal. 100 µL of each BFA sample was analyzed on Horiba Aqualog fluorometer to acquire fluorescence data.

As per ATCC 53774 propagation protocol, the frozen vials were thawed under anaerobic conditions and an aliquot of pure culture was transferred into previously prepared 10 ml of ferric citrate medium into sealed anaerobic test tube by a sterilized needle. After 7 days' incubation, 0.5 mL aliquot from the first test tube was transferred to second, three such transfers were made. Fe^{2+} concentration was measured at each stage to monitor the growth using Ferrozine method. In order to obtain, healthy bacterial cells possibly free from any dissolved iron trace, a successive filtration process was used. From the actively growing culture, 5 ml was filtered through 0.2-micron nylon sterilized syringe filter, pre-rinsed with 20 ml of anaerobic (N_2 purged) 18.2 MΩ-cm Milli-Q ultra-pure water. The filtrate contained the medium constituents, microbially produced Fe^{2+} and remainder ferric citrate while bacterial cells were retained on the filter. This filter was then backwashed using 2 mL of ultra-pure water to collect bacterial cells. To this, 3 mL of ultra-pure water was added and total 5 mL volume was again filtered through a new filter. This process was successively repeated four times to avoid any traces of culture medium and Fe^{2+}. At the end of 5th backwash, 400 µL of solution containing bacterial cells per 1 mL of the BFA medium was added for inoculation. After 7-day incubation under anaerobic conditions and room temperature, BFA sample was filtered through 0.2 µm sterile filter to separate bacterial cells. The filtrate aliquot of 1 mL was added to 1 mL of 55.93 mM freshly prepared ferric citrate solution in a 1.5 mL micro centrifuge tube. After allowing specific reaction times (0, 2, 4, 5, 6, 7 and 8 hours), an aliquot of the sample was tested for Fe^{2+} concentration using Ferrozine method.

Geobacter growth study and bio-geochemical modeling

Sodium acetate (2 mM) as primary electron donor and Goethite (10 mM) as primary electron acceptor were added to a 250 mL glass serum bottle containing 100 mL of ATCC 1768 medium. The medium was bubbled with 80% N_2 and 20% CO_2 to achieve final pH of 6.8 − 7. The bottles were sealed under N_2 head and sterilized in autoclave at liquid cycle. One sample was prepared with HS by adding 6 mgL^{-1} of SRFA while the other sample only had acetate. A 0.2 mL aliquot of *G. metallireducens* culture was injected into each sample. Blanks were prepared in similar way without adding the bacteria. Sample bottles were incubated at room temperature under anaerobic conditions for 18 days. Fe^{2+} concentrations were measured using Ferrozine method to monitor the bacterial growth in all the samples. An iterative algorithm (Geochemist's Workbench 10.0 Professional) was used to model theoretical growth of the bacteria using Monod kinetic equation (*Roden et al., 2006*) modified to include thermodynamic potential factor F_T (*Bethke et al., 2008*) and surface properties of Goethite to simulate environmentally relevant conditions. Fe^{2+} concentrations measured during the experiment were fitted to the modeled values to obtain kinetic rate constant.

$$r = k \ast [X] \ast \frac{mD}{mD + kD} \ast \frac{\left(\frac{[X]}{mA}\right)}{\left(\frac{[X]}{mA}\right) + kA} \ast FT$$

The rate of iron reaction (r) can be expressed by the above equation, where k is reaction rate constant, X is biomass concentration, mA and mD are molality of electron acceptor and donor respectively, kA and kD are half saturation constants for electron acceptor and donor respectively. Thermodynamic potential factor (F_T) is calculated by second equation $FT = 1 - \exp\left(\frac{dGR + n \ast dP}{x \ast R \ast T}\right)$,

where dG_R is the free energy change of the metabolic reaction in kJ/mol, *n* is the number of ATPs produced, dG_P is the free energy change of ATP synthesis in kJ/mol, *x* is the average number of times the rate determining step occurs, R is the gas constant and T is absolute temperature (*Jin et al., 2013*).

Groundwater Modeling

Groundwater flow in three dimensional domains was modeled by a finite difference equation given below,

$$\frac{\partial}{\partial x}\left(Kxx\frac{\partial h}{\partial X}\right) + \frac{\partial}{\partial y}\left(Kyy\frac{\partial h}{\partial y}\right) + \frac{\partial}{\partial X}\left(Kzz\frac{\partial h}{\partial z}\right) + W = Ss\frac{\partial h}{\partial t}$$

Where K_{XX}, K_{YY} and K_{ZZ} are values of hydraulic conductivity along the x, y and z coordinate axes; h is the potentiometric head; W is a volumetric flux per unit volume representing source and/or sinks of water, with W<0.0 for flow out of the groundwater system and W>0.0 for flow; Ss is the specific storage of the porous material and t is the time.

The model domain for West Bengal aquifer was defined using a shapefile of four districts of West Bengal (Murshidabad, Nadia, South 24 Parganas and North 24 Parganas). The major rivers (spatially varying head), the Bay of Bengal (constant head) and the net recharge rate were used to define the boundary conditions in the model domain. Stratigraphy of the model domain was defined by interpolating the horizons in 97 georeferenced borehole lithologs (*Mukherjee et al., 2007*). Mainly four types of sediments were observed within the 300 m depth of model domain as clay, sandy clay, sand and gravels. Horizontal hydraulic conductivities were defined for each material based on values estimated in previous studies ($K_{XX} = K_{YY} = 0.01$ m/d for Clay, 4 m/d for Sandy Clay, 42 m/d for Sand and 60 m/d for Gravel). Vertical hydraulic conductivities were defined by vertical anisotropy ($K_{XX}/K_{ZZ} = 10$) for each material.

Flow Model

Three dimensional flow in the complex stratigraphic model was modeled using USGS MODFLOW-NWT program which uses the Newton solution method and unstructured, asymmetric matrix solvers to calculate groundwater head (*Knoll and Keyes, 2004*). A three-dimensional grid of size 151.19 km x 404.62 km x 300 m was defined to completely include the model area with cell size of 1.5 km x 4 km x 30 m. The top elevations and starting heads were set to the elevations obtained from digital elevation model of the study area. Coverages of model area, boundary conditions were mapped to three-dimensional grid. The hydraulic conductivity values were assigned to each grid cell by mapping the stratigraphic model to this grid using overlay method. The head was computed using a steady state simulation.

In order to focus on the area where groundwater samples were collected during summer 2015 fieldwork, two stage telescopic grid refinement was used. A new model boundary of 10.33 km x 16.96 km x 300 m with a cell size of 103 m x 169 m x 30 m was created to cover completely the two field sites in Nadia district. The boundary conditions were defined by specifying the head to each boundary cell as computed in the regional model. No other boundary conditions were mapped to this local model except the stratigraphy for this area was cropped from the regional stratigraphic model. A new MODFLOW-NWT simulation was run to compute the heads. This local model was further refined by second stage grid refinement. A new model spanning 4.99 km x 2.24 km x 300 m with cell size of 50 m x 23 m x 30 m was developed. The boundary conditions and stratigraphy were assigned using heads computed in previous local model. Heads were computed again using MODFLOW-NWT and used for further analyses.

Transport model

Outputs from steady state MODFLOW simulation on the local model was used to track particles using the post-processing tool MODPATH to estimate the time of travel for particles moving through the system. Particles were created within the cells bounded by the field sites where the samples were collected. These particles were tracked backwards in time to the beginning to understand the flow direction. And to calculate the velocity of groundwater flow. Flow paths of the particles assigned in the lower layers in varying stratigraphic units were used to study the behavior of different materials and their hydraulic properties influencing the flow and transport processes.

Arsenic mobilization is a result of multiple biogeochemical reactions that take place in groundwater flow through the porous media, the geochemical reactions in the arsenic contaminated aquifer were modeled using a reactive multicomponent three-dimensional transport code RT3D incorporated in MT3DMS 5.3. In the local model computed heads from MODFLOW model were used in RT3D with a stress period of 10 years. Advection, dispersion, source/sink mixing and chemical reaction packages were activated in this model using porosity and longitudinal dispersivity values from the material properties. Equilibrium between aqueous Fe^{2+} and Fe^{3+} was considered as the background in the model, since in the reducing aquifers of West Bengal, mainly reductive dissolution of iron minerals has been reported to release arsenic in groundwater. Oxidized iron minerals were represented as Fe (OH)3 and the equilibrium reaction based on pH and pe is given by, Fe $(OH)_3$ + $3H^+$ → Fe3+ + $3H_2O$ and Fe^{3+} +e^- → Fe^{2+}. Initial concentrations of all the species, pH and pe values for all the cells in the grid were assigned and PHREEQC geochemical database was used to define thermodynamic parameters of the reactants and products.

Chapter 5 - Contrasting Dissolved Organic Matter Quality in Groundwater in Holocene and Pleistocene Aquifers and Implications for Influencing Arsenic Mobility

Highlights

- Dissolved organic matter in Holocene and Pleistocene aquifers was characterized.
- PARAFAC modeling identified 4 unique fluorescent components of DOM in groundwater.
- OM in groundwater in the Holocene aquifer was microbially-processed and humic-like.
- Humic DOM may be involved in promoting As mobilization in Holocene aquifer.
- Absence of humic-like DOM in Pleistocene aquifer reflects lack of microbial processing of DOM.
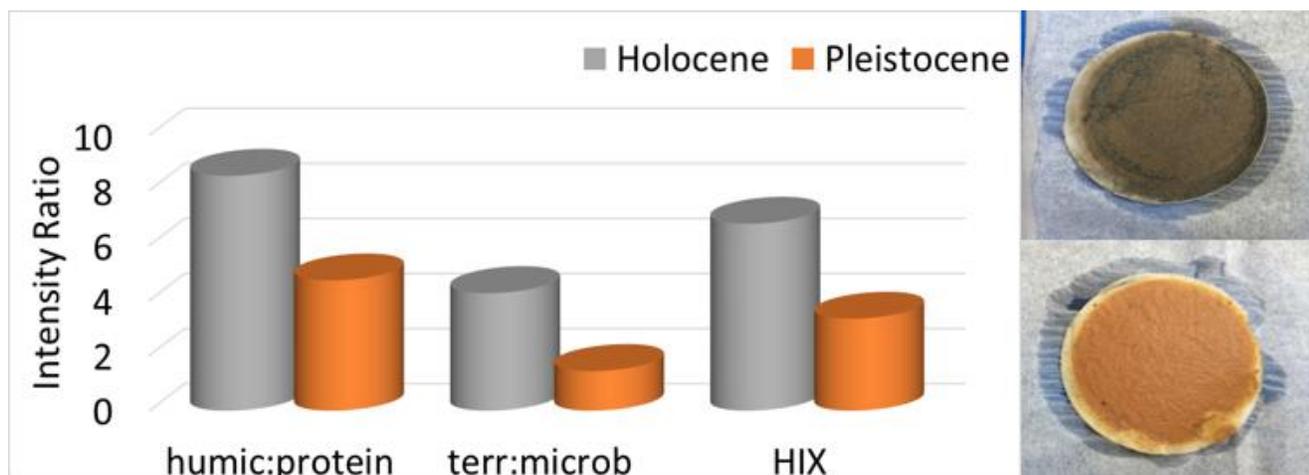
Figure 8 Contrasting DOM quality in groundwater in the Holocene and the Pleistocene aquifers (*Kulkarni H.V. et al., 2016*)

ABSTRACT

The discontinuous nature of elevated arsenic (As) in drinking water wells of West Bengal and other regions in the Bengal Basin has led to increased interest in the role that sediment-derived organic matter may play in enhancing reductive dissolution and AS mobilization. Higher As concentrations have been observed in groundwater in reduced Holocene (grey) aquifers when compared to oxidized Pleistocene (orange) aquifers. In order to evaluate if differences in the chemical character of dissolved organic matter (DOM) are present in groundwater in the Holocene and the Pleistocene aquifers that may influence dissolved As concentrations, shallow groundwater and surface water samples were collected from four study sites in Murshidabad district, West Bengal, India, and analyzed for water chemistry parameters and characteristics of DOM. For wells known to typically contain high As concentrations (in Holocene sediments) in Beldanga (10 – 4622 µg/L, at 35-45 m depth) and Hariharpara (5 – 695 µg/L, at 6-37, depth) sites, as well as wells characterized by low As concentrations (Pleistocene sediments) in Nabagram (0 – 16 µg/L, at 20-45 m depth) and Kandi (5 – 50 µg/L, at 20-55 m depth), detailed DOM characterization was carried out using fluorescence spectroscopy and parallel factor analysis (PARAFAC). Results from statistical analysis of a variety of optical (absorbance and fluorescence) DOM properties revealed that the DOM in groundwater in the Holocene aquifer had high humification index (HIX) and low freshness index (β:α) values, whereas groundwater in the Pleistocene aquifer comprised more labile and microbial DOM sources. Consistent with the more labile nature of DOM in groundwater in the Pleistocene aquifer, two ratios 1) humic-like to protein-like components (humic:protein) and 2) terrestrially-derived to microbially-derived components (terr:microb) obtained from a four-component PARAFAC model were 1.9 and 2.9 times greater, respectively, in groundwater in the

Holocene aquifer than that in Pleistocene aquifer, which suggests that the absence of humic-like DOM may be an important limitation to As mobility.

INTRODUCTION

Approximately 43 million people in West Bengal and 22 million in Bangladesh have been exposed to arsenic (As) concentrations greater than the World Health Organization guideline for drinking water (10 µg/L) (*Sankar et al., 2014; Datta et al., 2011; Bhattacharya et al., 1997; Nickson et al., 1998; Smith et al., 2000; McArthur et al., 2001; Dowling et al., 2002; Roychowdhury et al., 2002; Ravenscroft et al., 2005; Acharyya and Shah, 2006; Datta et al., 2009*). Microbially-mediated reductive dissolution of iron oxyhydroxides minerals has been invoked as one of the prominent mechanisms for the mobilization of sediment-bound As into reducing groundwater (*McArthur et al., 2001; Dowling et al., 2002; Hasan et al., 2007; Sankar et al., 2014*). The driver of this mechanism is labile dissolved organic matter (DOM). It has been hypothesized that labile DOM is drawn to depth from ponds and other surface waters laden with sewage (*Harvey et al., 2006; Neumann et al., 2010*), however, dispersed sedimentary organic matter has also been implicated as a source (*McArthur et al., 2004; Sengupta et al., 2008; Datta et al., 2011, Neumann et al., 2014*).

Recently, additional roles have been proposed for DOM in aquifers in the Bengal Basin that may have important consequences for iron and As mobilization (*Wang et al., 2006; Mladenov et al., 2010*). For instance, humic substances, a biologically refractory class of DOM, are involved in complexation reactions with Fe and As (*Liu et al., 2011; Sharma,2010*), competition with As for sorption sites (*Bauer and Blodau, 2006*) , and electron shuttling reactions (*Lovley et al., 1996, 1998 and 1999; Scott et al., 1998; Klapper et al., 2002; Kappler et al., 2004; Jiang et al., 2008; Wolf et*

al., 2009; Mladenov et al., 2010, 2015). Therefore, DOM of both labile and recalcitrant quality may enhance the process of As release by several mechanisms, including by serving as an electron donor (i.e. as direct source of energy) and by more chemically reactive mechanisms involving humic substances (*Mladenov et al., 2015*).

Characterization of biologically labile as well as humic and chemically reactive fractions of DOM provides insights into the sources of DOM and, therefore, its potential influence on As mobility. Absorbance and fluorescence spectroscopy techniques have opened a new window for the characterization of DOM (*Coble, 1996*) and have proven to be sensitive, reliable and rapid techniques for identifying DOM sources and transformations. For example, absorbance over the ultraviolet range of wavelengths provides a quantitative measure of source and molecular weight of DOM (*Helms et al., 2008*), while indices obtained from three dimensional fluorescence analysis provide insight into DOM source, age, freshness, and degree of processing in the environment. In addition, PARAFAC modeling of excitation-emission matrix (EEM) data allows quantification of humic-like, protein-like, terrestrially-derived and microbially-derived fluorescent components of DOM (*McKnight et al., 2001; Cory and McKnight, 2005; Mladenov et al., 2011; Mladenov et al., 2015*).

Shallow groundwater (< 40 m deep), the main source of drinking water for most communities within the Bengal Basin, is largely free of pathogenic bacteria. However, it has a wide range of As concentrations and its DOM sources may comprise both labile microbially-derived DOM transported to depth and terrestrially-derived DOM originating from dispersed sedimentary materials, subsurface peat deposits, or other lignaceous organic matter sources. In an investigation of the characteristics of the DOM in groundwater in the Holocene aquifer near Araihazar, Bangladesh, Mladenov et al. 2010 found through incubation experiments that, over time,

35

sediments released DOM with terrestrially-derived fluorescence properties. Results obtained from fluorescence spectroscopy of groundwater samples in the same aquifer found higher amino acid-like fluorescence in samples from young (~1.6 years), low As wells, whereas samples from 11 – 14 m depth with As concentration ~550 µg/l and age of ~ 19 years had lower amino acid-like fluorescence and more lignaceous dissolved organic matter (*Mladenov et al., 2010*). In groundwater samples in 12,300 – 48,500 years old (*Acharyya et al., 2000*) Pleistocene aquifers, more oxidized organic matter and microbial signatures were reported (*Sutton et al., 2009*).

The geochemistry of water and sediments in the Pleistocene aquifer in the region has also been studied, and the Pleistocene aquifer is known to contain much lower dissolved As concentrations than the Holocene aquifer as a result of more strongly oxidizing conditions that occurred when the sediments were deposited (*Fendorf et al., 2010*). Anaerobic incubation experiments with Pleistocene sediments, lactate as carbon source and metal reducing bacteria *Shewanella*, showed that phosphorous-extractable As increased even without addition of lactate (*Dhar et al., 2011*). Therefore, arsenic mobilization from the Pleistocene sediments may not have been caused by labile DOM. Much still remains to be understood about the similarities or differences in groundwater chemistry, particularly of the organic geochemistry that may influence As mobilization in Pleistocene and Holocene aquifers.

To our knowledge, the chemical and optical properties of DOM in groundwater in the Pleistocene aquifer have not yet been extensively studied. Therefore, this study evaluates the optical spectroscopic characteristics of DOM in groundwater in both the Pleistocene and Holocene aquifers in wells that are high and low in As. A unique feature of this study is that the sampling sites in Holocene and Pleistocene aquifers are located at similar depths, in close proximity to each other, on either side of a hydrologic divide that separates the two geologic formations, and are thus

subject to similar environmental and population pressures. Dissolved organic carbon (DOC) concentrations and UV-visible absorbance and fluorescence spectroscopy were employed to characterize the freshness and humification of groundwater DOM. This study further employs parallel factor analysis (PARAFAC) multivariate analysis modeling of fluorescence spectra from samples collected exclusively from the Bengal Basin. This first PARAFAC model of Bengal Basin groundwater fluorescence quantifies the relative amounts of protein-like and humic-like DOM components in groundwater in the Pleistocene and Holocene aquifers with different As concentrations.

MATERIALS AND METHODS
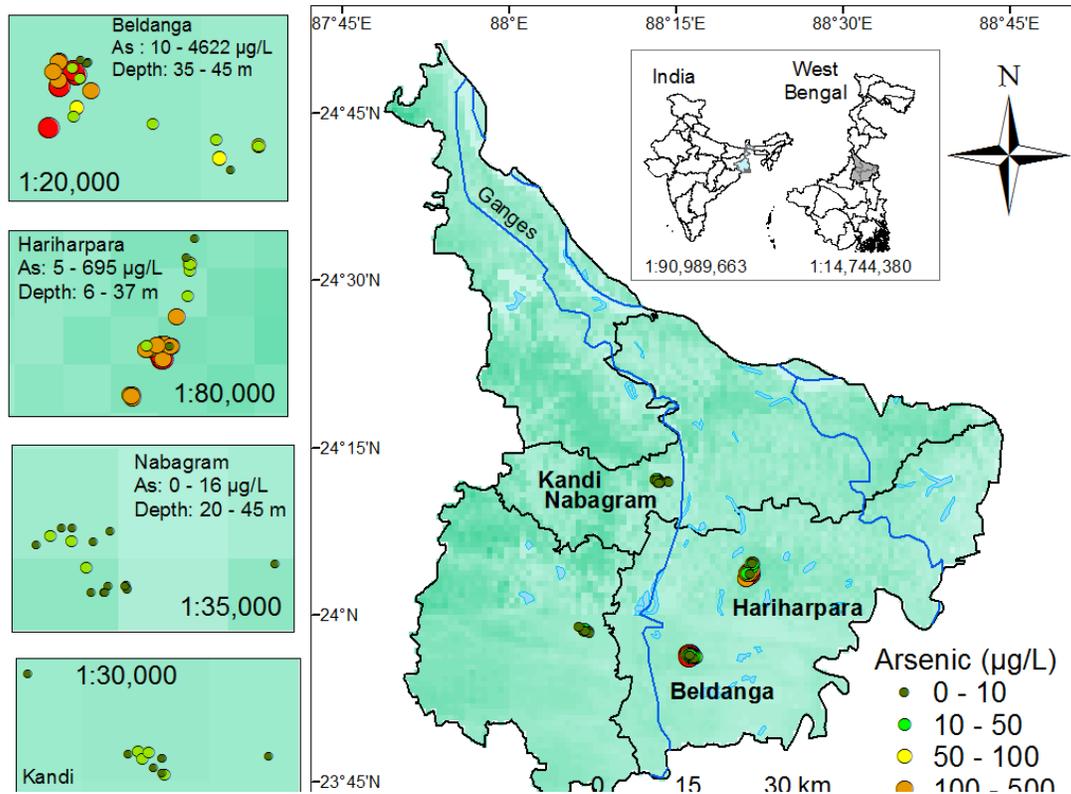
Study Site

Figure 9 Map of study area showing locations of samples collected. Insets to the left show concentrations of dissolved Arsenic at four study sites (*Kulkarni H.V. et al., 2016*)

To characterize DOM in groundwater in the Holocene aquifer, 32 wells were sampled covering a wide spatial extent (~623 km^2) in the Beldanga and Hariharpara blocks located to the east of River Bhagirathi (Figure S1) in which the geology is characterized by ~7000 years before present younger Holocene sediments (*Acharyya et al., 2000, Biwas and Roy, Mukherjee et al., 2007*). These sites to the east of the river are known to have a large proportion of high dissolved As wells (*Datta et al., 2011; Sankar et al., 2014*). To characterize DOM in groundwater in the Pleistocene areas, 23 wells covering a wide spatial extent (~544 km^2) in the Nabagram and Kandi blocks, located to the West of River Bhagirathi and characterized by 12,300 – 48,600 years before present (*Acharyya et al., 2000*) Pleistocene sediments, were sampled. These sites are known to have wells generally low in dissolved As (*Datta et al., 2011; Moran et al., 2000*). Lithological evidence suggests the presence of a clay layer at 100 m depth below the study area on both sides of the river (*Mukherjee et al., 2007*). Description of sediment type, total As, total iron and organic matter in sediments at all study sites is given in Table 1 (*Sankar, 2013*). In Beldanga, the maximum As concentration in older (Holocene) silty clay was 18.09 mg/kg, the total Fe concentration varied between 14.72 – 32.97 g/kg, and organic matter content was between 57.7 – 171.4 mg/kg at 15 m depth. In Hariharpara, the maximum As concentration was 15.54 mg/kg in older (Holocene) dark grey sticky clay while the concentration of total Fe was 26.22 – 31.73 g/kg and organic matter was 55.85 – 61.15 mg/kg at 6 m depth. Characterization of sedimentary organic matter in similar geological setting in Nadia district, West Bengal (*Rowland et al., 2006*) revealed the abundance of apolar compounds dominated by high molecular weight n-alkanes with small amounts of hopanes and steranes. Components of less abundant polar compounds were primarily the n-alkanols and small amounts of sterols. Rowland et al. (2006) also suggested that a significant fraction of organic

matter was presumably recalcitrant macromolecular material, which would be less available as a labile carbon source (electron donor) for microbial activities. In Nabagram, the highest sediment As concentration was 10.42 mg/kg with total Fe of 12.9 – 25.61 g/kg and organic matter content of 62.78 – 74.64 mg/kg at 3 m depth in reddish (Pleistocene) grey colored clay. In Kandi, the maximum sediment As was 15.67 mg/kg with total Fe of 25.39 – 36.12 g/kg and organic matter of 118.9 – 122.4 mg/kg at 12.2 m depth in reddish (Pleistocene) grey colored clay (*Sankar, 2013*).

The characteristics of sedimentary organic matter in Pleistocene age sediments have been reported in the literature. Ghosh et al. (2015) (a study conducted in Pleistocene brown sand aquifer of Nadia, West Bengal, a site just to the south of our study area) reported that the organic matter deposited during the Pleistocene was mainly from terrestrial, higher plant origin indicated by high molecular weight (HMW) n-alkanes and unsaturated alkanoic acids. However, low molecular weight (LMW) n-alkanes and n-alkanoic acids were also present and believed to be derived from microbial cells (*Ghosh et al., 2015*). Presence of terrestrially derived as well as microbially derived organic matter in Pleistocene sediments at other locations has also been reported by several other studies such as in aquifers of Red River Delta, Vietnam (*Lawati et al., 2012; Eiche et al., 2016*), in eastern Netherlands (*Hartog et al., 2004*) and Bangladesh (*Hossain et al. 2009*).

Mukherjee et al. (2007) reported the transmissivity of 3300 – 7000 m^2/day, permeability of 42 m/day for sand and 0.01 m/day for clay and porosity of 0.2 for the Holocene aquifer. Generally, the older (Pleistocene, typically yellow-reddish) sediments have a lower permeability than recent (Holocene, typically grey) sediments (*Mukherjee et al., 2007*). Ravenscroft et al. (2005) had reported the permeability of Pleistocene sands to be 20-30 m/day while that for Holocene sands to be 40-60 m/day for Pleistocene and Holocene sands with the same medium grain size. The lower permeability of Pleistocene sands was thus attributed to the presence of secondary clays and iron

oxides that partially clog the pore throats (*Ravenscroft et al., 2005*). The same study also reported that Pleistocene clays were thicker and more consolidated than Holocene aquitards, resulting in lower vertical permeability and lower specific yield in Pleistocene aquifer systems (*Ravenscroft et al., 2005*). Groundwater pumping for domestic and irrigation purposes was estimated as 3.32E-04, 8.84E-05 and 1.33E-04 $m^3/m^2/day$ during pre-monsoon, monsoon and post-monsoon seasons respectively. (*Mukherjee et al., 2007*).

Table 1 Description of sediment characteristics based on analyses of four sediment cores collected from study area (*Sankar, 2013 and Sankar et al., 2014*) and the characteristics of sedimentary organic matter obtained from sites in similar geologic settings (*Rowland et al., 2006 and Ghosh et al., 2015*).

Location	Depth (m)	As_T (mg/kg)	Fe_T (g/kg)	Organic Matter (mg/kg)	Sediment Description[#]	Age	Organic Matter Characteristics
Beldanga N 23 56.392 E 88 16.206	3	18.06	32.97	57.7	1	Holocene, ~7000 years before present	Abundant high molecular weight n-alkanes, hopanes and steranes; Less abundant n-alkanols and sterols (*Rowland et al., 2006*[*])
	15	18.09	21.56	171.4	1		
	27	16.52	24.6	55.3	1		
	30.5	9.71	11.91	53.2	2		
Hariharpara N 24 03.651 E 88 21.395	3	12.78	26.22	59.2	3		
	6	15.54	31.73	56.5	3		
	15	8.3	6.8	55.85	4		
	27.4	6.03	31.73	61.15	4		
Nabagram N 23 12.156 E 88 13.492	9.1	10.42	19.55	74.64	5	Pleistocene, 12,300 – 48,600 years before present	High molecular weight (HMW) n-alkanes; Low molecular weight (LMW) n-alkanes; Mono-unsaturated n-alkanoic acids; LMW n-alkanoic acids; Sterol and stanol monomers; Lipids (*Ghosh et al., 2015*[+])
	43	6.36	8.75	62.78	6		
Kandi N 23 58.570 E 88 06.814	3	7.4	6.46	-	7		
	12.2	15.67	25.39	118.9	5		
	21	11.04	36.12	-	5		
	27	5.6	5.29	121.8	8		
	30.5	9.51	31.74	-	3		
	33.5	9.92	35.5	122.4	3		

[#]Sediment Description from Sankar (2013): [1]Silty clay; [2]Sand; [3]Dark grey sticky clay; [4]Medium grained sand; [5]Reddish grey colored clay; [6]Grey colored medium grained sand; [7]Reddish color medium grained sand; [8]Dark grey colored fine-medium sand.

[*]Data obtained from analyses of Holocene sediments from Nadia district, West Bengal, India.

[+]Data obtained from Pleistocene sediments from Nadia district, West Bengal, India.

Sample Collection and Storage

For representative sampling of surface water and groundwater, samples were collected from 11 surface ponds (PW), 37 shallow depth tube wells (TW) (10 - 40 m), 3 deep tube wells (TW) (>40 m) and 11 irrigation wells (IW) (10-46 m). A total of 43 samples from the Holocene area (27 TW, 5 IW and 11 PW) and 29 from the Pleistocene area (20 TW, 3 IW and 6 PW) were analyzed. Samples were filtered through a 0.7 µm nominal pore size pre-combusted glass fiber filter in the field and stored at 4^0C until analysis. To avoid quenching effects from lowering pH, samples were not acidified either in field or in lab prior to fluorescence analysis.

Spectroscopic Analyses

UV-visible absorbance and fluorescence spectroscopic techniques have been used to study DOM in a wide range of environments from marine waters (*Kalle, 1949; Duursma and Marchand, 1974) to* groundwater *(Mladenov et al, 2010, 2013, 2015)*. Spectroscopic data was acquired using Jobin Yvon Aqualog Fluorometer. A filtered water sample was excited with range of wavelengths from 240 nm to 450 nm with 3 nm increments and integration time of 0.25 seconds. From absorbance data, absorption coefficient "a" was calculated as, a = 2.303*A/L, where A is the absorbance and L is the path length (0.01 m). Absorbance at 254 nm (abs_{254}) has been used to understand characteristics of organic molecules as the molecules with specific binding arrangements such as the conjugated systems in aromatic compounds exhibit greatest absorptivity at 254 nm (*Weishaar et al., 2013*). Log-transformed absorbance coefficients were used to calculate spectral slope between 275 nm to 295 nm ($S_{275-295}$) and between 350 nm to 400 nm ($S_{350-400}$). The former has been shown to be an indicator of molecular weight and degree of photo bleaching while the latter represents chromophoric DOM (CDOM) and contributions from terrestrially-derived

DOM (*Helms et al., 2008*). The spectral slope ratio (S_R) was calculated by taking the ratio of $S_{275-295}$ and $S_{350-400}$. A $S_R>1$ indicates marine-like DOM and $S_R<1$ is characteristics of terrestrially dominated high CDOM samples (*Helms et al., 2008*). An increase in S_R values has been attributed to reduced molecular weight of DOM and photo bleaching while microbial activities such as microbial production or preservation of long wavelength absorbing substances have been observed to decrease S_R (*Helms et al., 2008; Moran et al., 2000; Vahatalo and Wetzel, 2004*).

Emission spectra were collected in signal to reference (S:R) mode from 212 nm to 619 nm with 3.28 nm increment (instrument default). EEMs were corrected for the inner filter effect (*Ohno, 2002*), Raman normalized (using 18.3 MΩ cm Milli-Q ultra-pure water at ~350 nm), and blank subtracted. First and second order Rayleigh scattering bands were excised (*Stedmon and Bro, 2008*). A quinine sulfate standard was also run, giving a value of 1 R.U. = 2.495 quinine sulfate units (QSU). The fluorescence Index (FI) was calculated as the ratio of fluorescence intensities at 470 nm and 520 nm emission and 370 nm excitation. Lower values of FI (~1.3-1.4) indicate terrestrial sources of DOM while higher values (~1.7-1.9) indicate microbially-derived DOM (*McKnight et al., 2001; Cory and McKnight, 2005*). The freshness index (β:α) was calculated as the ratio of emission intensity at 380 nm to the maximum intensity between 420 nm to 435 nm at an excitation wavelength of 310 nm (*Parlanti et al., 2000*). More recently derived DOM is represented by β, while α represents highly decomposed DOM (*Wilson and Xenopoulos, 2008; Fellman et al., 2010*). The humification index (HIX) was calculated as the ratio of peak area under the emission spectra at 435 nm to 480 nm to peak area from 300 nm to 345 nm at an excitation wavelength of 254 nm (*Zsolnay, 2003*). Higher values of the HIX indicate a higher degree of DOM humification (*Ohno, 2002*). All the corrections, data processing and calculations of indices were performed using MATLAB R2014a (Figure S3 and Figure S4). Corrected three

dimensional fluorescence excitation emission matrix (EEM) data was fitted to a four component PARAFAC model (*Harshman, 1970; Stedmon et al., 2003; Stedmon and Bro, 2008*). Statistical analyses were performed for descriptive statistics parameters. Since the As concentrations were not normally distributed, a non-parametric Mann – Whitney – Wilcoxon (MWW) U test was used to compare the statistically significant variability among samples.
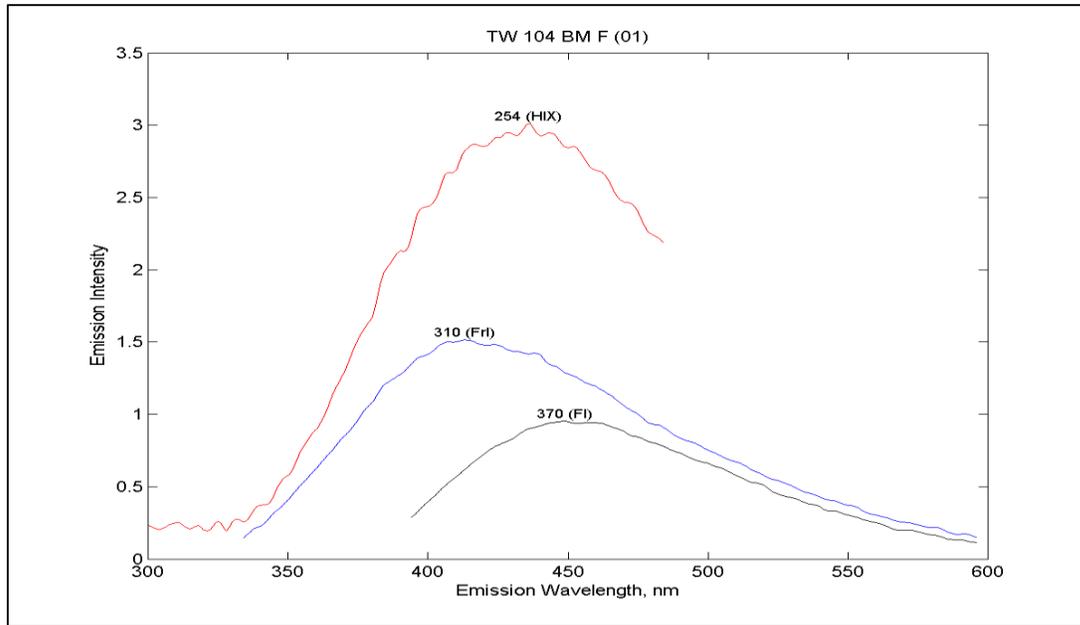
Figure 11 Representation of emission spectra used for fluorescence indices calculation
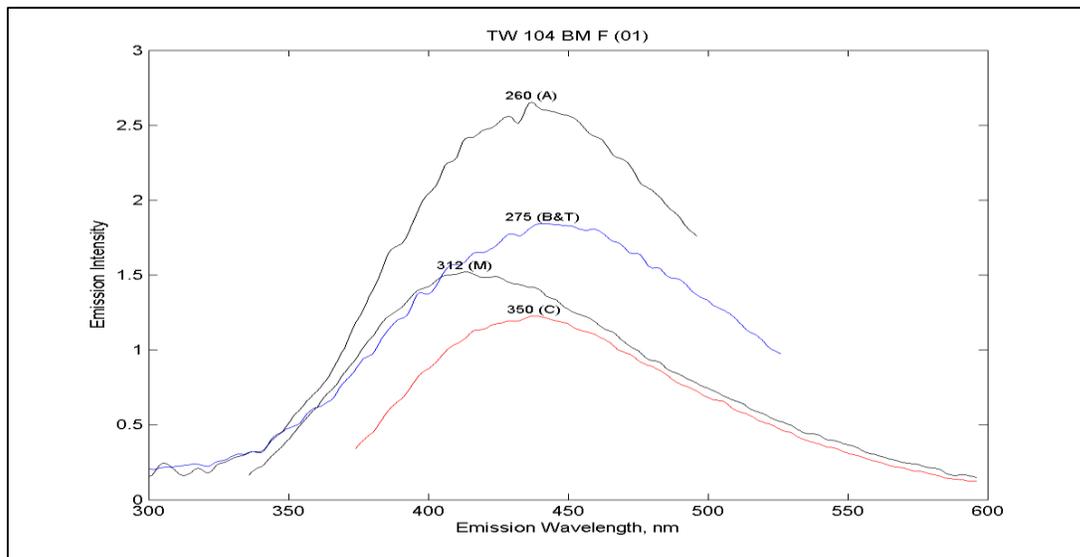
Figure 10 Representation of emission spectra used for fluorescence peaks calculation

PARAFAC Modeling

The DOM Fluor toolbox (*Stedmon and Bro, 2008*) was used to build a PARAFAC model for this sample dataset. The sample set included corrected EEMs from surface and groundwater with varying fluorescence intensities. In order to avoid false identification of extremely high or low concentration samples as outliers by PARAFAC, these EEMs were normalized using a modified method of Murphy et al. (2013). In brief, each intensity value in the matrix was divided by the maximum intensity of that sample instead of dividing by the sum of squares of all intensities in that sample. This presets all the EEMs to a maximum intensity of 1, according to:

$$I(i,j)corrected = \frac{I(i,j)initial}{Imax}.$$

Outliers were removed from the PARAFAC model dataset if they met one of these conditions: negative spectral slope ratios, very high FI (> 2) that corresponded to a FI peak emission location > 470 nm, and, β:α values >1 indicating shift of peak in the 310 nm emission spectra. The dataset was then fitted to a non-negativity constrained PARAFAC model according to Stedmon et al. (2003). Additional outliers were identified by calculating the leverage of each sample and wavelength. Samples with leverages approaching 1 were examined to ensure that there was no analytical error before being considered as outliers (*Stedmon and Bro, 2008*). After removing outliers, a total of 60 samples were used. A four-component model was validated by split half analysis (Figure 3) and random initialization techniques by running ten, four component models. For all the samples, the residual (difference between actual and modeled EEM) did not exceed 10% of the intensity in the original EEM (*Cawley et al., 2012*), which indicates an acceptable model fit (*Stedmon and Bro, 2008*). After complete validation, the actual intensities of each component were obtained by multiplying the intensity of each component by the maximum

intensity (I_{max}) of the original EEM used in the normalization. Two indices based on PARAFAC components were developed to provide further insights into the nature of DOM. The humic:protein index was calculated as the ratio of the sum of humic-like DOM components to the sum of protein-like DOM components obtained from the PARAFAC model, according to:

$$humic: protein = \frac{\sum Humic - like\ DOM\ Components}{\sum Protein - like\ DOM\ Components}.$$

The terrestrial:microbial (terr:microb) index was calculated as the ratio of the sum of terrestrially-derived to microbially-derived DOM components obtained from the PARAFAC model, according to:

$$terr: microb = \frac{\sum Terrestrially\ Derrived\ DOM\ Components}{\sum Microbially\ Derrived\ DOM\ Components}.$$
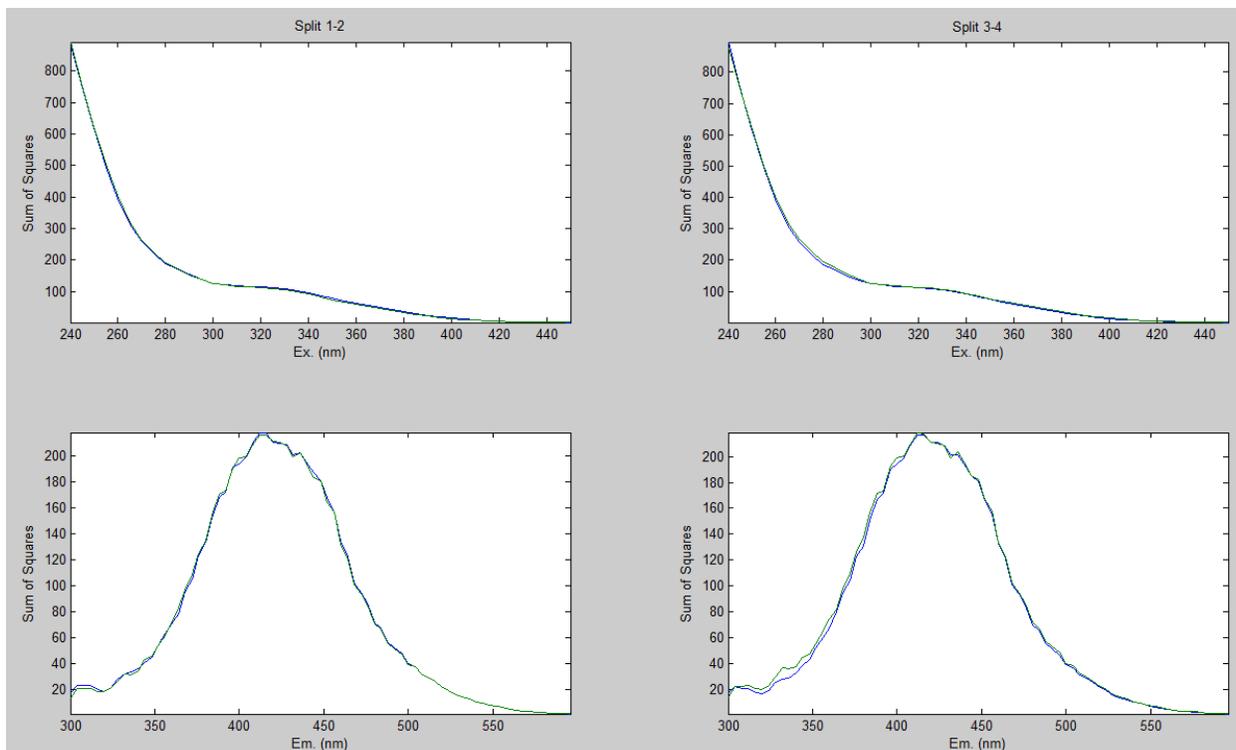
Figure 12 Split half analysis for four component PARAFAC model showing validation of the model

RESULTS

Comparison of chemical and DOM properties in groundwater in Holocene and the Pleistocene aquifers

Significantly higher dissolved As concentrations in the groundwater in Holocene aquifer than that in Pleistocene ($p < 0.05$, Table 3) were observed, where concentrations in the former ranged from 5 µg/L to 1264 µg/L (average = 261 µg/L), and those in the latter ranged from 0.4 µg/L to 50 µg/L (average = 14.5 µg/L) (Table 2). More than 70% of the groundwater samples in the Holocene aquifer contained As concentrations > 50 µg/L, which is the Indian drinking water standard (*Datta et al., 2011; IS 10500, 2012*). All of the groundwater samples in the Pleistocene aquifer contained As concentrations < 50 µg/L. Groundwater collected from the Holocene aquifer had higher average dissolved Fe concentrations (average = 3.19 mg/L), and was more reducing (average = -44.3 mV) than in Pleistocene sites. DOC concentrations were also significantly higher ($p < 0.05$) in groundwater in the Holocene aquifer (average = 2.94 mg/L) than in the Pleistocene aquifer (average = 1.79 mg/L) (Table 2).

Similar to the trends noted for DOC concentration, a_{254} values (Table 2) were significantly higher ($p < 0.05$; Table 3) in groundwater in the Holocene aquifer (average = 0.047 a.u.) compared to that in the Pleistocene aquifer (average =0.034 a.u.). However, $SUVA_{254}$ values did not show any statistically significant difference ($p>0.05$; Table 3) between groundwater in the Holocene (average = 2.26 $L.mg^{-1}.m^{-1}$) and Pleistocene (average = 2.35 $L.mg^{-1}.m^{-1}$) aquifer. S_R values (Table 2) were significantly lower ($p < 0.05$; Table 3) in groundwater in the Holocene aquifer (average =1.33) than that in the Pleistocene aquifer (average = 1.78). Groundwater in the Pleistocene aquifer had notably higher intensities 1.65 Raman Units (R.U.) in the protein-like region (PARAFAC

component C3), at 1.65 Raman Units (R.U.), compared to that in the Holocene aquifer, at, 0.38 R.U. (Figure 1a and 1b). The FI (Table 2) was similar for groundwater in both the Pleistocene (mean of 1.73) and Holocene (mean of 1.72) aquifers, and at the high end of the typical FI range (1.2 − 1.8). The β:α was statistically lower ($p < 0.05$; Table 3) in groundwater in the Holocene aquifer (average = 0.77) than that in the Pleistocene aquifer (average = 1.0; Table 2). The HIX was significantly higher ($p < 0.05$; Table 3) in groundwater in the Holocene aquifer (average = 6.79) than that in the Pleistocene (average = 3.34).
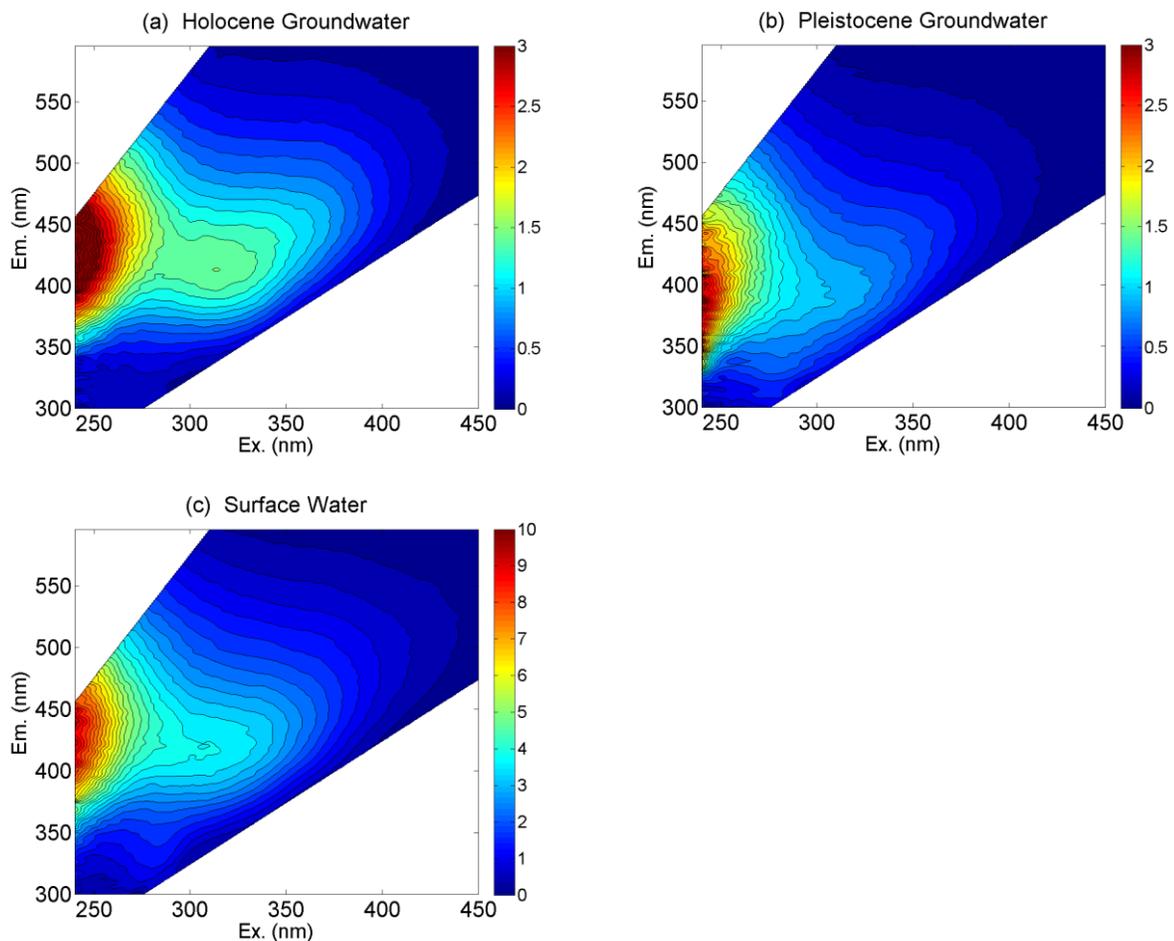
Figure 13 Representative EEM spectra (a) Groundwater in Holocene aquifer, (b) Groundwater in Pleistocene aquifer, (c) Surface water. Note different intensity scale on (c)

Table 2 Properties of groundwater (GW) in Holocene and Pleistocene aquifers and overlying surface water (SW)

Analysis type	Holocene SW	Pleistocene SW	Holocene GW	Pleistocene GW
[2]Water Chemistry				
Total Dissolved Arsenic (µg/L)	35.2 ± 38.1 (0 – 110.3)	3.13 ± 2.71 (0 – 4.69)	261 ± 285 (5 – 1263)	14.5 ± 10 (0.4 - 50)
Total Dissolved Iron (mg/L)	6.57 ± 21.3 (0 – 70.8)	0.06 ± 0.08 (0 – 0.15)	3.19 ± 3.86 (0 – 13.6)	0.52 ± 0.39 (0.07 – 1.03)
Dissolved Organic Carbon (mg/L)	7.28 ± 2.49 (2.64 – 9.62)	9.84 ± 1.90 (8.67 – 12.03)	2.94 ± 1.97 (1.25 – 6.76)	1.79 ± 1.48 (0.85 – 4.91)
ORP	NA	NA	-44.25 ± 49.08 (-108 – 69)	+74.48 ± 71.58 (-55 – 156.5)
Absorbance				
[3]Abs_{254} (a.u.)	0.23 ± 0.08 (0.08 – 0.38)	0.22 ± 0.11 (0.11 – 0.35)	0.047 ± 0.01 (0.02 – 0.08)	0.034 ± 0.01 (0.02 – 0.05)
[4]SUVA ($L.mg^{-1}.m^{-1}$)	2.65 ± 0.22 2.48 – 3.16	3.03 ± 0.17 2.92 – 3.23	2.26 ± 1.13 0.60 – 4.19	2.35 ± 1.20 0.93 – 4.65
[5]S_{275_295}	-0.02 ± 0 (-0.02 – -0.01)	-0.02 ± 0 (-0.02 – -0.01)	-0.02 ± 0.00 (-0.02 - -0.01)	-0.02 ± 0.00 (-0.02 - -0.01)
[6]S_{350_400}	-0.01 ± 0 (-0.02 – -0.01)	-0.01 ± 0 (-0.01 – -0.01)	-0.01 ± 0.01 (-0.03 - 0)	-0.01 ± 0.00 (-0.02 - -0.01)
[7]S_R	1.26 ± 0.22 (0.84 – 1.73)	1.27 ± 0.14 (1.08 – 1.42)	1.33 ± 0.47 (0.69 – 2.34)	1.78 ± 0.43 (1.10 – 2.54)
[8]Fluorescence Indices				
FI	1.60 ± 0.04 (1.55 – 1.70)	1.63 ± 0.03 (1.60 – 1.67)	1.73 ± 0.06 (1.59 – 1.83)	1.72 ± 0.10 (1.54 – 1.88)
β:α	0.85 ± 0.10 (0.77 – 1.12)	0.76 ± 0.04 (0.72 – 0.81)	0.77 ± 0.06 (0.68 – 0.96)	0.99 ± 0.14 (0.66 – 1.09)
HIX	5.39 ± 0.89 (3.38 – 6.31)	6.38 ± 2.21 (4.06 – 9.06)	6.79 ± 1.98 (3.48 – 10.45)	3.34 ± 1.38 (1.67 – 7.25)
[9]PARAFAC (R.U.)				
C1	3.57 ± 2.99 (1 – 11.48)	3.73 ± 2.54 (0.89 – 6.07)	1.87 ± 3.21 (0.23 – 17.13)	2.47 ± 3.37 (0.17 – 10.08)
C2	2.28 ± 1.41 (0.79 – 5.30)	2.56 ± 1.69 (0.66 – 4.07)	1.18 ± 1.56 (0.19 – 8.14)	2.18 ± 2.82 (0.19 – 8.15)
C3	1.24 ± 0.87 (0.38 – 3.21)	0.94 ± 0.47 (0.42 – 1.55)	0.38 ± 0.5 (0.05 – 2.59)	1.65 ± 2.26 (0.17 – 6.67)
C4	1.73 ± 2.60 (0.38 – 9.51)	1.27 ± 1.16 (0 – 2.30)	0.6 ± 1.76 (0 – 9.9)	3.93 ± 6.4 (0.03 – 20.02)

Analysis type	Holocene SW	Pleistocene SW	Holocene GW	Pleistocene GW
Calculated Parameters				
Total Fluorescence (R.U.)	8.84 ± 7.60 (2.74 – 29.50)	8.50 ± 5.84 (1.96 – 13.83)	4.03 ± 6.88 (0.53 – 37.02)	10.23 ± 14.77 (0.63 – 44.93)
% C1	40.45 ± 1.97 (36.56 – 43.77)	44.27 ± 0.81 (43.29 – 45.22)	46.25 ± 3.19 (40.25 – 51.43)	27.76 ± 8.59 (22.37 – 52.25)
% C2	28.14 ± 3.42 (17.96 – 30.33)	31.29 ± 2.35 (28.98 – 34.18)	33.40 ± 3.63 (22 – 39.06)	25.79 ± 4.77 (18.14 – 34.72)
% C3	14.96 ± 3.47 (10.87 – 20.67)	14.43 ± 6.19 (8.28 – 21.40)	11.81 ± 4.35 (4.98 – 23.19)	18.17 ± 4.08 (13.90 – 29.05)
% C4	16.46 ± 5.81 (11.01 – 32.24)	10.01 ± 9.17 (0 – 17.33)	8.53 ± 6.66 (0 – 26.75)	26.28 ± 13.10 (2.45 – 44.57)
[10]Humic:protein	5.98 ± 1.43 (3.84 – 8.20)	7.07 ± 3.21 (3.67 – 11.08)	8.53 ± 3.42 (3.31 – 19.10)	4.71 ± 1.03 (2.44 – 6.19)
[11]terr:microb	2.23 ± 0.38 (1.32 – 2.78)	3.15 ± 0.55 (2.61 – 3.80)	4.27 ± 1.52 (2.15 – 7.71)	1.44 ± 1.24 (0.68 – 5.11)

[1]All numbers are expressed as average value ± standard deviation, minimum – maximum range in parenthesis.
[2]Data source: Sankar et al., 2014, except oxidation reduction potential (ORP) data from 2014 field season.
[3]Absorbance at 254 nm.
[4]Specific ultra-violet absorbance.
[5]Spectral Slope between 275 nm and 295 nm.
[6]Spectral Slope between 400 nm and 350 nm
[7]Spectral Slope Ratio (S_{275_295} / S_{350_400})
[8]Fluorescence Index (FI), Freshness Index (β:α), Humification Index (HIX).
[9]C1 to C4 = Four components obtained by PARAFAC model.
[10]Ratio of humic like to protein like component obtained by PARAFAC model = (C1+C2+C4) / (C3).
[11]Ratio of terrestrially produced DOM to microbially produced DOM = (C1+C2) / (C3+C4).

Table 3 P statistics (non-parametric Mann-Whitney-Wilcoxon Test) * showing statistical variation among DOM properties in samples

Analysis type	Holocene – Pleistocene SW	Holocene – Pleistocene GW	GW – SW Holocene	GW – SW Pleistocene
Total Dissolved Arsenic (µg/l)	0.048	<0.001	0.012	0.014
DOC (mg/l)	0.121	0.003	0.00014	0.00275
Absorbance				
Abs 254 (a.u.)	0.5	0.01	<0.001	<0.001
SUVA (L.mg^{-1}.m^{-1})	0.024	0.303	0.197	0.146
S275-295	0.01	0.49	0.46	0.44
S350-400	0.19	0.02	0.47	0.02
S_R	0.33	<0.001	0.30	0.01
Fluorescence Indices				
FI	0.07	0.40	<0.001	0.04
β:α	<0.001	<0.001	<0.001	<0.001
HIX	0.22	<0.001	0.01	<0.001
PARAFAC (R.U.)				
C1	0.50	0.18	<0.001	0.12
C2	0.50	0.45	<0.001	0.19
C3	0.37	0.03	<0.001	0.25
C4	0.40	<0.001	<0.001	0.39
Calculated Parameters				
Humic: protein	0.33	<0.001	0.01	0.22
terr:microb	<0.001	<0.001	<0.001	<0.001

Values in shaded cells: P<0.05 indicate statistically different parameter
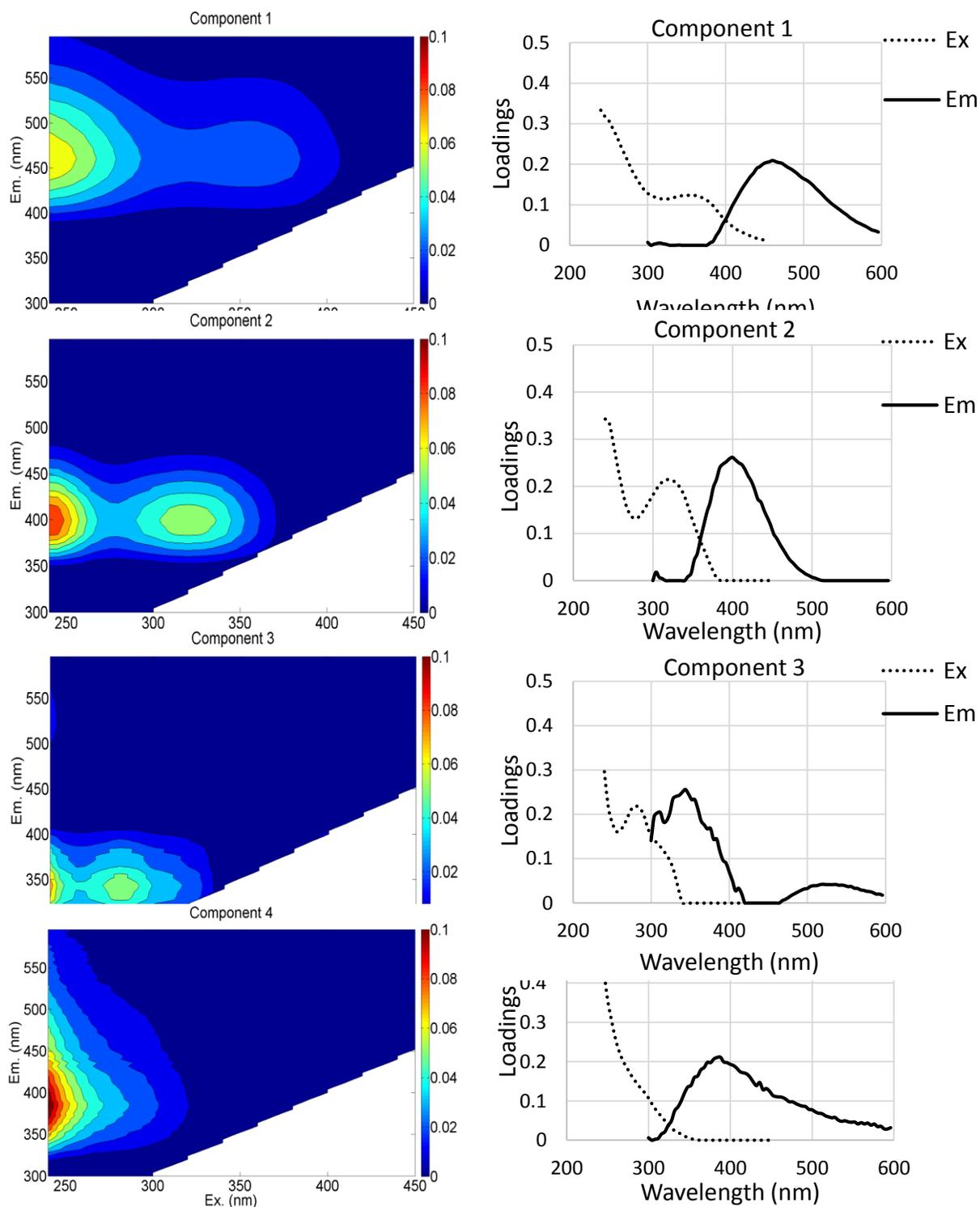
Figure 14 EEM spectra (left) and emission-excitation curve (right) showing loadings of four PARAFAC components identified in the model

Comparison of groundwater and surface water DOM properties

In both the high As (Holocene sediments) and low As (Pleistocene sediments) locations in our study area, DOC concentrations and optical spectroscopic properties related to DOC concentration (abs_{254}) were significantly different between groundwater and surface water samples (Tables 2 and 3). Overall, the EEMs of surface water samples had distinct fluorescence signatures when compared to groundwater samples, with very pronounced peaks in the protein-like region and elevated total fluorescence intensity (Figure 1c). Indeed, all fluorescence and PARAFAC parameters were significantly different in surface water and groundwater samples (Table 3). However, in the low As (Pleistocene sediments) areas, the optical properties of DOM in groundwater samples were statistically similar to surface water samples in most properties other than Abs_{254}, S_R, $\beta:\alpha$, HIX (Table 3).

Table 4 Fluorescence peaks in groundwater (GW) in Holocene and Pleistocene aquifers and overlying surface water (SW)

Analysis type	Holocene SW	Pleistocene SW	Holocene GW	Pleistocene GW
	[*]Fluorescence Peaks (R.U.)			
Peak A	3.97 ± 3.50 (1.13 – 13.57)	4.01 ± 2.78 (0.91 – 6.49)	1.99 ± 3.46 (0.27 – 18.81)	4.20 ± 6.01 (0.25 – 18.41)
Peak B	0.91 ± 0.69 (0.27 – 2.67)	0.60 ± 0.34 (0.25 – 1.08)	0.25 ± 0.32 (0.06 – 1.54)	1.08 ± 1.51 (0.11 – 4.61)
Peak T	1.20 ± 0.95 (0.37 – 3.63)	0.92 ± 0.55 (0.33 – 1.62)	0.35 ± 0.55 (0.06 – 2.62)	1.61 ± 2.37 (0.12 – 7.25)
Peak C	1.63 ± 1.12 (0.51 – 4.12)	1.80 ± 1.19 (0.47 – 2.98)	0.87 ± 1.20 (0.13 – 6.03)	1.47 ± 1.99 (0.10 – 6)
Peak M	2.24 ± 1.56 (0.72 – 6.06)	2.37 ± 1.63 (0.55 – 3.83)	1.08 ± 1.62 (0.16 – 8.58)	2.14 ± 2.89 (0.19 – 8.52)

*Peaks A, B, T, C and M are peaks defined by Coble, 1996.

The intensities of tyrosine-like Peak B, ranging from 0.11 Raman Units (R.U.) to 4.61 R.U. (average = 1.08), and tryptophan-like Peak T, ranging from 0.12 R.U. to 7.25 R.U. (average =

1.61) in groundwater in Pleistocene aquifer, were also significantly higher (p < 0.05; Table 5) than those in groundwater in Holocene aquifer (average of 0.25 and 0.35, respectively; Table 5).

Table 5 P statistics (non-parametric Mann – Whitney - Wilcoxon Test) * showing statistical variation between fluorescence peaks.

Analysis type	Holocene – Pleistocene SW	Holocene – Pleistocene GW	GW – SW Holocene	GW – SW Pleistocene
Fluorescence Peaks (R.U.)				
Peak A	0.41	0.29	<0.001	0.29
Peak B	0.22	0.03	<0.001	0.29
Peak T	0.33	0.02	<0.001	0.29
Peak C	0.46	0.28	<0.001	0.19
Peak M	0.50	0.37	<0.001	0.25

*Values in shaded cells: P<0.05 indicate statistically different parameter

PARAFAC model components

The PARAFAC model identified four components (Figure 2), which were similar to components identified in other studies (Table 4). C1, C2 and C4 had excitation and emission wavelength maxima consistent with humic-like components, whereas C3 was identified as a protein-like component, with a peak similar to that of tryptophan. C4 has been identified in other studies as a microbial humic-like peak, and C1 and C2 were found to be more commonly derived from terrestrial organic material (Table 3). Therefore C1 and C2 are considered to be the terrestrial components, and C3 and C4 are taken as the microbial components in this study. The humic:protein ratio showed a good correlation ($R^2 = 0.72$, Figure S2) with the ratio of intensities of traditional fluorescence peaks Peak B and Peak T to the intensities of Peak A, C and M described in Coble et al., 1998.

Table 6 Description of PARAFAC components from this study and similar components identified in other studies (not an exhaustive list)

Reference	Component 1 240 (360)/460	Component 2 240 (320) / 400	Component 3 240 (280) / 344	Component 4 240 (280) / 388
This Study	Terrestrial humic-like	humic-like, impacted by agriculture, marine humic	protein-like, tyrosine and tryptophan	microbial humic-like
Parlanti et al., (2000)	α' - humic like, 250-260/380-480 α- humic like, 330-350/420-480 Terrestrial source, HMW* and aromatic humic-like	α' - humic like, 250-260/380-480 β-marine humic like, 310-320/380-420 Terrestrial source associated with microbial, wastewater, agricultural activity, LMW* humic-like	δ- tryptophan like, 270-280/320-350 γ- tyrosine like, 270-280/300-320 amino acids, free or bound in proteins, free tryptophan and tyrosine, intact proteins, more or less degraded peptide material	-
Stedmon et al., (2003)	C1 – humic like, 240-320/428	C2 – marine humic like, impacted by agriculture, 315/384	C4 – tryptophan like, 278/348	-
Fellman et al., (2009)	UVC humic like 1, 320-360/420-460 UVC humic like 2, <260/448-480	UVA humic like, 290-325(<250)/370-430	tyrosine-like, 270-275/304-312 tryptophan like, 270-280/330-368	U – Unknown, 250(320)/370 HMW humic, widespread, but highest in wetlands and forested environments, very labile, associated with freshly produced DOM
Williams et al., (2013)	C1 – terrestrial humic, <250/440(468)	C2 – terrestrial humic, <250(310)/420(388)	C7 – protein like, 280/342 (318)	C6 – microbial humic, <250(285)/386
Coble, (1996)	A = UV humic, 260/400-460; C = humic like, 350/420-480	A = UV humic, 260/400-460; M = marine humic, 290-310/370-410	T = tryptophan like, 275/340 B = tyrosine like, 270/305	-
Coble et al., (1990)	A – UV humic like, 260/400-460 C – visible humic like, 320-360/420-460	A – UV humic like, 260/400-460, M – visible marine humic, 290-310/370-410	T – tryptophan like, 275/340, B – tyrosine like, 275/305	N – unknown, 280/370

*HMW = High Molecular Weight, LMW = Low Molecular Weight

The HIX, humic:protein ratio, and terr:microb ratio showed distinct differences between the fluorescent components in groundwater in the Holocene and Pleistocene aquifers (Tables 1 and 2). The average percentages of two of the microbial components, C3 and C4 were statistically lower ($p < 0.05$; Table 3) in groundwater in the Holocene aquifer (at 11.8% and 8.53%, respectively) than in groundwater in the Pleistocene aquifer (at 18.2% and 28.3%, respectively; Table 3). As a result, the terr:microb ratio (average = 4.27) of groundwater in the Holocene aquifer was significantly higher than in groundwater in the Pleistocene aquifer (average = 1.44; Table 2). Similarly, the humic:protein ratio was found to be 1.8 times higher in groundwater in the Holocene aquifer (average = 8.53) than in the Pleistocene aquifer (average = 4.71). Surface waters from the Hariharpara, Beldanga (underlying Holocene aquifer) and Nabagram, Kandi (underlying Pleistocene aquifer) were not statistically different with respect to all the parameters analyzed except for the terr:microb ratio, which was significantly lower (average = 2.23) in Hariharpara and Beldanga areas compared to the Nabagram and Kandi areas (average = 3.15) and β:α, which was significantly higher (average = 0.85) in Hariharpara and Beldanga areas compared to the Nabagram and Kandi areas (average = 0.76) (Table 2). Groundwater samples were statistically different from surface water samples with respect to all parameters except S_R for the Holocene sites (Table 3). In Pleistocene areas, groundwater samples were statistically different from surface water samples in S_R, β:α (average 0.99 and 0.77), HIX (average 3.34 and 6.79), humic:protein (average 4.71 and 8.53) and terr:microb (average 1.44 and 4.27) respectively (Table 3).

DISCUSSION

The difference in As concentration in groundwater in Holocene and Pleistocene aquifers is well documented, with Holocene aquifers generally having higher dissolved As concentrations than Pleistocene aquifers (*Fendorf et al., 2010*). Even though Pleistocene sediments can contain

substantial amounts of As, dissolved As concentrations were reported as insignificant in groundwater of the aquifer (*Eiche et al., 2008*). It has been suggested that the lower As concentrations result from Pleistocene aquifers experiencing more flushing than Holocene aquifers due to their older age of deposition (*Morgan and McIntire, 1959*). However, Ravenscroft et al. (2005) instead showed that flushing of Pleistocene sediments is limited because of their lower permeability than Holocene sands due to clogging by secondary clays and iron oxides. Even for sediments with low As content, Hering and Kneebone (2002) found that generally very low concentrations of sedimentary As (1.8 mg/kg) are sufficient to produce dissolved As concentration exceeding 10 μgL^{-1}. Sedimentary As found in all the sites in this study including those in the Pleistocene aquifer is > 1.8 mg/kg (Table 1), and sediment Fe_T and organic matter content are also present in both Holocene as well as Pleistocene aquifers in significant amounts (Table 1). Therefore, the limitation for As mobilization is more complicated, and consideration of microbial processing, redox state, and DOM chemical quality merit further investigation.

DOM characteristics in groundwaters in the Holocene and Pleistocene aquifer

Previous studies have shown that DOC concentrations tend to be substantially higher in groundwater of the Holocene aquifer than in groundwater of the Pleistocene aquifer (*Sutton et al., 2009*; *Datta et al., 2011; Sankar et al., 2014*). The lower DOC concentrations in groundwater of Pleistocene than Holocene aquifers may limit the release of As from those sediments (*Fendorf et al., 2010; Berg et al., 2008; Postma et al., 2007; Polizzotto et al., 2008; Harvey et al., 2002*). Similarly, our study found lower DOC concentrations in groundwater in Pleistocene sediments. Harvey et al. (2002) and Saunders et al. (2008) both showed that an increase in dissolved As

concentration occurs upon injection of labile carbon into the aquifer. However, even without labile carbon addition, DOC concentrations can increase under reducing conditions. Mladenov et al. (2010) found that DOC increased from 4.84 to 6.10 mgL^{-1} in sediment incubations with native groundwater in Bangladesh due to the release of DOM from the sediment. Neumann et al. (2014) also performed incubations with sediments in Vietnam high in As and found those sediments to release DOM that was easily biodegradable.

Our analyses shed light on the spectroscopic properties of CDOM and suggest that differences in the chemical character of CDOM in these two geologically distinct settings may have an influence on As release. Despite high FI values in both settings that reflect high amounts of microbial activity, several independent measures of DOM character indicate that DOM in groundwater in the Pleistocene aquifer was fresher, less biologically processed and less humified, than DOM in groundwater in the Holocene aquifer. First, the high S_R (~1.78) in groundwater in the Pleistocene aquifer was similar to values in systems with low-molecular-weight microbial contributions to the DOM pool (*Helms et al., 2008*). Second, PARAFAC modeling identified components that been previously reported in a variety of aquatic environments (Table 4). The ratios of terr:microb and humic:protein PARAFAC components in groundwater in the Pleistocene aquifer were ~1/2 and 1/3, respectively, of those in groundwater in the Holocene aquifer, indicating that CDOM in groundwater in the Pleistocene aquifer was more microbially-derived and less humic than in the Holocene aquifer.

The burial history and lack of microbial communities may help explain why these older sediments contain such seemingly young DOM. Paleo-sedimentary studies indicate that the Pleistocene sediments in the study area are floodplain deposits of the early Ganges-Brahmaputra river system (*Hasan et al., 2007; Stollenwerk et al., 2007; Acharyya et al., 2000*). In other river

systems as well, such as in the Gulf coast Pleistocene sediments in the United States, the Pleistocene sediments have been reported to be early river flood plain deposits (*Morgan and McIntire, 1959; Robert, 1997; Blum and Roberts, 2012*). The quantity of glacial ice on the continents caused fluctuation in the sea level during the Pleistocene time. Sea level dropped abruptly with each glacial advance causing an increase in the discharge of rivers into the sea. This caused rapid erosion, weathering and oxidation of the river sediments. At the end of the interglacial period, sea level rose with the waning of the glaciers, which lowered the flow gradient of rivers and filled the valleys with alluvial sediments (*Morgan and McIntire, 1959*). The highly weathered and oxidized Pleistocene sediments were then buried under recent alluvial deposition (*Morgan and McIntire, 1959*). The buried Pleistocene sediments have been reported to contain 0.13-0.17% TOC by weight in sand and 0.2-0.67% by weight in clay and comprise organic matter mainly derived from both terrestrial vegetation and microbial constituents *(Ghosh et al., 2015)*. These chemical characteristics are consistent with our findings of low HIX, terr:microb and humic:protein ratios, and high FI, S_R and β:α values, which are indicative of less-processed microbial DOM, in groundwater that is in contact with these Pleistocene sediments. Dissolved organic matter with such characteristics should be biologically labile and theoretically be able to drive microbial reduction of Fe and As in the sediments if reducing conditions predominate, Fe-reducing microorganisms are present, and other terminal electron acceptors (oxygen and nitrate) are depleted. Although reducing conditions have not explicitly been investigated at our sites, Sankar et al., (2014) did measure dissolved oxygen, nitrate, nitrite and sulfate, and did not find significant differences between the concentrations of these electron acceptors in the groundwater of the Holocene (high As) and Pleistocene (low As) aquifers. Along the same lines, an emerging area of research has shown that biologically-labile soil organic matter can persist over long periods of

time if conditions, such as physical disconnection between organic matter and microbial communities and energy or nutrient limitation, prevail (*Schmidt et al., 2012*). At least one study has investigated microbial communities in the Pleistocene sediments. Lawati et al. (2012) demonstrated that the Pleistocene sediments contain a very low abundance of microbial population, which they concluded could be responsible for lower As concentrations in the groundwater. This microbial limitation may explain why the organic matter in the groundwater seems, from our absorbance and fluorescence analyses, to be relatively fresh and unprocessed by microorganisms. However, the high FI values and low terr:microb ratios we measured in groundwater of the Pleistocene aquifer suggest that microbial constituents should be elevated rather than lacking in this setting. To gain more clarity on the presence and role of microbes in DOM processing and to better understand why the cascade of reductive dissolution is not underway in the Pleistocene aquifer, the composition of the microbial consortia and other factors that influence Fe reductive dissolution must be further explored.

In contrast to the labile character of CDOM in groundwater of the Pleistocene aquifer, groundwater of the Holocene aquifer was found to have CDOM with optical properties similar to humic substances. Based on previous studies showing release of Fe, humic DOM (*Mladenov et al., 2010*), and biodegradable DOM (*Neumann et al., 2015*) from sediments during incubations with native groundwater, we expect that sediments are a likely source of DOM in groundwater of the Holocene aquifer. A potential scenario, proposed by Mladenov et al. (2015), is that humic DOM, containing quinone-like moieties known to shuttle electrons to accelerate Fe reduction (*Lovley et al. 1996, 1998 and 1999*), could be enhancing the same reaction in groundwater leading to associated mobilization of As from sediments into groundwater.

The lower β:α and S_R values (Table 2), similar to those found in wetlands and swamps with large amounts of high molecular weight DOM (*Helms et al., 2008*), for groundwater in the Holocene aquifer further indicate more biologically-processed DOM (*Fellman et al., 2010*). Higher HIX values, representative of greater humification of DOM (*Zsolnay, 2003; Ohno, 2002*), also point to a less labile DOM source that may instead participate in humic DOM-stimulated reductive dissolution. In addition, DOM with this more chemically-reactive character participates in other reactions that may lead to As mobilization, such as complexation and competitive sorption, which have been described in other studies (*Wang and Mulligan, 2006*; *Mikutta and Kretzschmar, 2011*). The observation that CDOM in groundwater of the Pleistocene aquifer lacks the humic character found in CDOM in groundwater of the Holocene aquifer may reflect both the unprocessed nature of the DOM and an absence of humic moieties that could serve important functions related to As mobilization, as described above.

Comparison of DOM chemical character in surface and groundwater

Surface water samples from Hariharpara and Beldanga contained younger (higher β:α) and more microbial (lower terr:microb ratio) DOM than those in Nabagram and Kandi. Characteristics of DOM differed significantly between groundwater and surface water. Spectroscopic properties suggested that humic and more biologically-processed DOM was found in this order: groundwater in Holocene > surface water > groundwater in Pleistocene. The higher values of β:α and lower HIX in surface water in Hariharpara and Beldanga, than underlying groundwater in the Holocene aquifer may be attributed to mixing of groundwater and surface water, which has been known to contain more fresh, microbially-derived and less humified organic matter from sewage and other wastewater inputs (*Knappett et al., 2011; Mladenov et al., 2015*) and algae (*Parlanti et al., 2000*). In contrast, the surface water samples from Nabagram and Kandi were less fresh (lower β:α) and

more humified (higher HIX) than the underlying groundwater in the Pleistocene aquifer, thus eliminating the possibility of surface water mixing.

CONCLUSIONS

The factors affecting the variability in groundwater As concentration in Holocene as well as Pleistocene aquifers are still in question and are relevant for an improved understanding of As mobility throughout the Bengal Basin. The quality of DOM in these two geological settings in the context of As mobility has not been studied. In this study, for Pleistocene sediments located in close proximity to Holocene sediments, multiple lines of evidence, including S_R, HIX and β:α values and humic:protein and terr:microb ratios of PARAFAC components, indicate that the CDOM in groundwater in the Pleistocene aquifer contains a higher proportion of protein-like and microbially-derived constituents and may be less humified and less biologically-processed than DOM in groundwater in the Holocene aquifer, which had elevated As concentrations. The absence of humic DOM may indicate that microbial degradation of DOM did not proceed in the Pleistocene aquifer as it had in the Holocene. The more proteinaceous and less humic DOM in groundwater of the Pleistocene aquifer also would be less likely to participate in reactions, such as complexation, electron shuttling, and competition with As for sorption sites. The absence of humic-like DOM from groundwater in Pleistocene aquifer may, therefore, be an important limitation to As mobility.

On the other hand, our spectroscopic analyses indicate that the predominance of humic-like DOM in groundwater in the Holocene aquifer may result from mobilization of humic substances from the sediments as well as greater microbial processing of DOM. This more humic DOM may promote chemical reactions that mobilize or maintain As in solution, such as DOM-As binary or DOM-Fe-As ternary complex formation and humic DOM serving as an electron shuttle to

accelerate the process of reductive dissolution. Therefore, the results of this study are also relevant

to the understanding of As mobilization in Holocene aquifers

Chapter 6 - Detection of Aqueous Complexes of Arsenic, Iron and Dissolved Organic Matter using Fluorescence and ^{1}H NMR Spectroscopy.

ABSTRACT

Complexation of arsenic (As) with dissolved organic matter (DOM) in reducing aquifers is one of the mechanisms that controls As concentrations in aqueous solution. It has been shown that in the presence of dissolved iron (Fe), DOM may bind to As to form ternary complexes (As-Fe-DOM) or binary complexes (As-DOM) in absence of Fe. Fluorescence spectroscopy with excitation-emission matrix (EEM) analysis has been identified as an effective tool for characterization of DOM in aquatic environments. Fluorescence has also been used to identify some DOM-metal complexes but has not been applied toward identification of complexes of As, Fe, and DOM. Recent advances in solution nuclear magnetic resonance (NMR) spectroscopy have shed light on the structural characterization of DOM in environmental samples. In this study, we applied fluorescence and ^{1}H NMR spectroscopy to detect binary and ternary complex formation between As, Fe and Suwanee River Fulvic Acid (SRFA) as the DOM source. Fluorescence quenching experiments were designed using natural ranges of Fe, SRFA, and As concentrations and under oxic and oxygen-free conditions. SRFA solution was titrated with Fe only, As only, and As with Fe. Results showed clear evidence for the formation of Fe-DOM complexes. No fluorescence quenching was observed for As-DOM or Fe-As-DOM complexes, suggesting that these complexes do not form between As, Fe, and the aromatic, conjugated, multiple bonds that fluoresce in organic compounds. Solutions were further analyzed using ^{1}H NMR spectroscopy, and results indicated that a 9.6% change in chemical shifts and a 19.09% change in the ratio of ^{1}H NMR peak intensities did occur after addition of As. However, the changes occurred in non-

aromatic region protons and were negligible in the aromatic region of SRFA. These findings suggested that fluorescence quenching by As-DOM complexes was not detected because complexes did not form between As and fluorescence-active molecules of SRFA. The ^{1}H NMR detection of binary complex formation between As and non-aromatic region protons was found to be relevant for studies of arsenic mobility since such complexes could maintain high As concentrations in groundwater.

INTRODUCTION

Arsenic, a naturally occurring metalloid has caused severe health risk to over 43 million in West Bengal, India and over 22 million people in Bangladesh (*Sankar et al., 2014; Datta et al., 2011; Bhattacharya et al., 1997; Smith et al., 2000; McArthur et al., 2001; Dowling et al., 2002; Roychowdhury et al., 2002; Ravenscroft et al., 2005; Acharyya and Shah, 2007; Datta et al., 2009*). In most reducing aquifers, dissolved iron (ferric / ferrous) has been found abundantly and reductive dissolution of iron minerals has been considered as main mechanism of dissolved arsenic release (*Nickson et al., 2000*). Labile dissolved organic matter (DOM) is the driver for this process, stimulating microbial reduction of both Fe minerals and As (V). In addition, DOM influences arsenic mobility by forming stable complexes with mineral surfaces, effectively blocking arsenic from re-adsorption (*Bauer et al., 2006*). This ability to form complexes was particularly pronounced for reactive constituents of DOM, such as humic and fulvic acids. Humic acids have been shown to form Fe-bridged aqueous complexes with dissolved arsenic (*Liu et al., 2011*). Formation of arsenate – ferric – NOM complexes were also observed during dialysis experiments (*Ritter et al., 2006*). Binary and ternary colloidal and dissolved complexes of arsenate, Fe and DOM have been detected using ATR-FTIR and Mossbauer-spectroscopy (*Sharma et al., 2010*).

Fluorescence spectroscopy was successfully used to characterize DOM in an arsenic-contaminated aquifer of Araihazar, Bangladesh (*Mladenov et al., 2010*). Using a combination of fulvic acid isolation, ^{13}C-NMR spectroscopy, and fluorescence spectroscopy, Mladenov (2015) further showed that significant relationships existed between dissolved Fe, As, and fulvic acid molar concentrations. Fluorescence spectroscopy has also been utilized to directly measure the formation of complexes between fulvic acids and metals via quenching of DOM fluorescence by complexed metal cations. For example, complexation between copper and fulvic acid was explored using fluorescence quenching titration (*Ryan et al., 1982*) and interactions between Hg (II) and natural DOM (*Lu and Jaffe, 2001*) Metal ligand complexes of copper and aluminum with DOM were also detected and complexation parameters were determined by using fluorescence spectroscopy based on PARAFAC analysis (*Ohno et al., 2008*).

Optical methods such as fluorescence and absorption spectroscopy have limitations in exploring complex heterogeneous properties of DOM such as structure, state of aggregation, conformation and surface charge distribution. Solution state NMR has been used to investigate these properties of DOM in soil, sediments and water (*Earl et al., 1998; Cardoza et al., 2004; Simpson et al., 2001, 2011; Wang et al., 2003; Cook et al., 2003, 2004; Lam et al., 2007*). Solution state NMR spectroscopy provides useful information on structural interactions of molecules that are readily soluble after extraction, isolation and pre-concentration steps, such as fulvic acid (*Nebbioso et al., 2013; Cook et al., 2003; Lam et al., 2007*). It has been shown that a highly resolved one dimensional ^{1}H NMR spectra can be obtained for isolated and pre-concentrated fulvic acid solution because 1) fulvic acid is readily soluble at any pH, 2) high regional mobility occurs within macro-molecules and 3) the majority of molecules are small (*Cook et al., 2003*). Additional experiments such as proton correlation spectroscopy (COSY), total correlation spectroscopy

(TOCSY), nuclear overhauser effect spectroscopy (NOESY), and a combination of COSY and heteronuclear single quantum coherence (HSQC) have been used to obtain structural and functional information about protons and protonated carbons (*Haiber et al., 1999; Chien et al., 1998; Hertkorn et al., 1998, 2002; Morris et al., 1999; Fan et al., 2000; Simpson et al., 2001, 2011, 2012*).

To our knowledge, fluorescence spectroscopy has not been used to investigate As – DOM aqueous complex formation. In this study we used three dimensional EEM fluorescence spectroscopy to detect binary complexes of Fe – SRFA, As – SRFA and ternary complexes of Fe – As – SRFA under environmentally relevant conditions. Further, we used 1D – ^{1}H NMR spectroscopy to identify potential locations of complex formation within SRFA.

MATERIALS AND METHODS

Sample Preparation for Fluorescence spectroscopy

DOM stock solution was prepared by dissolving 9.5 mg of SRFA obtained from International Humic Substances Society (IHSS Catalog # 2S101H) in 100 mL of ultrapure water and stored at 4^0C in dark. Five different concentration solutions of SRFA were tested for dissolved organic carbon using Shimadzu TOC Analyzer which resulted in 52.44% of Total Carbon (data not shown). The stock solution of Fe (II) was prepared fresh using reagent grade ferrous sulfate. As (III) stock solution (10 mgL^{-1}) was prepared by dissolving appropriate mass of sodium meta-arsenite (98%, Aldrich). All the solutions were prepared using N_2 bubbled 18.3 MΩ cm Milli-Q ultra-pure water in the N_2 filled glovebox.

Two concentrations of SRFA 6.25 mgL^{-1} and 12.5 mgL^{-1} were used for the complexation titration experiment. These concentrations were chosen considering their environmental relevance and sensitivity to fluorescence and TOC analysis. For Fe – DOM titration, each SRFA solution

was titrated with Fe (II) stock solutions by making final concentration of 0, 0.1, 1, 5, 10 and 20 mgL^{-1}. For As – DOM titration, each SRFA solution was titrated with As (III) stock solution by making final concentrations of 0, 10, 50, 100, 500 and 1000 µgL^{-1}. For Fe – As – DOM ternary complex titration, a matrix of samples with combination of two SRFA concentrations (6.25 and 12.5 mgL^{-1}), three concentrations of ferrous (2, 10 and 20 mgL^{-1}), and five concentrations of As (10, 50,100,500 and 1000 µgL^{-1}) were prepared. Necessary blanks were prepared for all the samples. All the samples were prepared and analyzed in triplicates. Samples were prepared in 20 mL clear TOC free glass vials. Samples were mixed for 30 minutes using orbital shaker machine.

Spectroscopic Analyses

Samples were analyzed using Jobin Yvon Aqualog Fluorometer with a clean quartz cuvette of 0.01 m path length to acquire UV-Vis absorbance and 3D – EEM fluorescence data. Integration time was set to 0.25 seconds in S:R mode with a range of excitation wavelengths between 240 nm to 450 nm with increment of 3 nm. Absorbance intensities were acquired for the same range of excitation wavelengths. Blank data was acquired by running 18.3 MΩ cm Milli-Q ultra-pure water. Quinine sulfate standard was run and correlation of 1 Raman Unit = 2.495 Quinine Sulfate Unit (QSU) was found. Acquired fluorescence data was corrected for inner filter effect (*Ohno, 2002*), normalized by water Raman area and for first and second order Rayleigh scattering (*Stedmon and Bro, 2008*). After all corrections, fluorescence and absorbance data was spline interpolated to obtain 1 nm resolution, which was used to calculate all spectroscopic properties.

Absorbance coefficient (a) was calculated by following equation (*Weishaar et al., 2003*), where A is measure absorbance and l is path length of the cuvette,

$$a = 2.303 * A/l$$

Natural log-transformed absorption coefficients were used to calculate spectral slope between 275 nm to 295 nm ($S_{275-295}$) and between 350 nm to 400 nm ($S_{350-400}$). $S_{275-295}$ has been considered to be indicator of molecular weight and degree of photo-bleaching, while $S_{350-400}$ of colored DOM (CDOM) and contributions from terrestrially derived DOM (*Helms et al., 2008*). Spectral slope ratio ($S_R = S_{275-295} / S_{350-400}$) was also calculated where, $S_R > 1$ has been found in marine water samples with low CDOM, and $S_R < 1$ is characteristic of terrestrially dominated, high CDOM samples (*Helms et al., 2008*). An increase in the S_R value was observed due to reduced molecular weight of DOM and photo-bleaching, whereas a decrease in the S_R value was observed due to microbial activities i.e. microbial production or preservation of long wavelength absorbing substances (*Helms et al., 2008; Moran et al., 2000; Vahatalo and Wetzel, 2004*).

Fluorescence Index (FI) as an indicator for the source of DOM i.e. terrestrially-derived (FI ~ 1.3) or microbially-derived (FI ~ 1.8) was calculated as the ratio of fluorescence intensities at 470 nm and 520 nm emission and 370 nm excitation (McKnight et al., 2001; Cory and McKnight, 2005). Freshness Index (β:α) was calculated to distinguish between recently derived (β:α ~ 0.4 to 0.6) and processed (β:α ~ 0.8 -1) DOM by taking a ratio of emission intensity at 380 nm with maximum intensity between 420-435 nm at excitation wavelength of 310 nm (*Parlanti et al., 2000*). Degree of humification was estimated by humification index (HIX) calculated as the ratio of peak area under the emission spectra at 435-480 nm to peak area from 300-345 nm obtained at an excitation wavelength of 254 nm (Ohno, 2002; *Zsolnay, 2003*) were higher value of HIX indicates higher degree of humification. Fluorescence peaks (Coble, 1996) were also recorded as Peak A (260 nm / 380-460 nm) and Peak C (350 nm / 420-480 nm) indicating humic-like DOM, Peak M (312 nm / 380-420 nm) indicating marine humic-like DOM, Peak B (275 nm / 310 nm)

indicating tyrosine-like or protein-like DOM and Peak T (275 nm /340 nm) indicating tryptophan-like or protein-like DOM.

Complexation Modeling

A modified metal-ligand complexation model based on non-linear regression approach (Ryan and Webber, 1982; Luster et al., 1996) was employed to estimate conditional stability constant (K_C) and complexation capacity (L_T). The model shown in the equation inputs included measured Peak C intensity (I) at given Fe (II) concentration (Fe_T) and the intensity of Peak C of pure SRFA solution (I_0)

$$\frac{I}{I_{ref}} = 1 + \left(\frac{I_{FeL}}{I_{ref}} - 1\right)(\frac{1}{2K_cL_t})\{1 + K_cL_t + K_c[Fe]_t - \sqrt{(1 + K_cL_t + K_c[Fe]_t)^2 - 4K_c^2L_t[Fe]_t}\}$$

$$\left|\frac{I}{I_{ref}} - 1\right| = \left|\frac{I_{FeL}}{I_{ref}} - 1\right|(1 - e^{-\propto[Fe]_t})$$

Sample Preparation for Solution ^{1}H NMR

To avoid interference of paramagnetic cations (such as Fe), SRFA was dissolved in 18.3 MΩ cm Milli-Q ultra-pure water, excess sodium sulfide was added and incubated for 12 hours at room temperature. After incubation, solution was centrifuged at 5000 rpm for 30 minutes to remove the precipitate and the supernatant was freeze dried using a vacuum freeze drying unit at -150^{0}C. Freeze dried SRFA (10 mg) was re-dissolved into 1 mL of D_2O. In natural groundwater, maximum expected concentration of SRFA may be 6.25 mgL^{-1} and As concentrations vary from 0 to 5000 ugL^{-1}. Molar ratio of As to SRFA (MW of SRFA = 1000 Da, MW of As = 74.992) in natural groundwater was calculated as 0, 0.02, 0.22, 2.22 and 11.11 for 0, 10, 100, 1000 and 5000 ugL^{-1} of As. Since NMR analysis requires such a high and unrealistic concentration of

SRFA (10 mgmL^{-1}), respective As doses were calculated as 0, 0.07, 0.69, 6.93and 34.67 mgmL^{-1}. The volume of sample was 0.8 mL.

Experimental Conditions

The 1-D ^{1}H NMR experiments were performed at 25˚C on a Varian 500 NMR System (Varian Inc., now Agilent Technologies, Palo Alto, CA) equipped with a 5 mm triple-resonance inverse detection pulse field gradient cryogenic probe operating at 499.84 MHz for ^{1}H frequency. Briefly, samples had pH of 3.87 after dissolving in D_2O. The ^{1}H NMR spectra were acquired with presaturation of the HDO peak using 8000 Hz spectral width (SW), 25us pulse width (PW), 1.9 second acquisition time and 5 second pulse delay time respectively. Calibration of the HDO peak was set to 7.42 ppm referenced to sodium 3-trimethylsilyl-propionate-2, 2', 2, 3', d$_4$ (TSP). Peak area was measured with an integrator. When necessary, spectral resolution was enhanced by Lorenzian-Gaussian apotization. Data processing was done using the program VnmrJ 3.2 (Varian Inc., Palo Alto, CA). The ^{1}H NMR spectra were subdivided into 4 spectral regions (0.0-1.6, 1.6-3.3, 3.3-5.5, and 5.5-9.0 ppm).

RESULTS AND DISUCSSIONS

Fe-DOM Complexation

Our results indicated that quenching of fluorescence by Fe was the most pronounced in 6.25 mgL^{-1} than in 12.5 mgL^{-1} of SRFA. This may be attributed to the limited number of available binding sites. Decrease in overall intensities of Peak A, B, T, C and M (Figure 16) of SRFA was observed when titrated with Fe. This decrease in intensities of fluorescent peaks was an effect of fluorescence quenching due to metal binding as previously reported by Ohno (2008). However, effect of metal binding on other spectral properties of DOM have not been reported before. In this

study, absorbance and fluorescence data was acquired for Fe (II) to ensure that the changes in spectral properties were attributed to Fe-DOM complex and not due to mere absorption by free Fe (II) in the solution.

In this study, we found that absorbance at 254 nm (abs254) increased by 55.4 % and this increase was strongly correlated ($R^2 = 0.97$) and statistically significant (P = 0) with increase in Fe (II) concentration from 0, 0.1, 1, 5, 10 and 20 mgL^{-1}. This was found to be consistent with Yan (2013) that reported significant increase in the absorbance as the bound iron absorbs in the wavelength range of 220 nm to 440 nm. We observed a decrease by 21.63 % in S_R strongly correlated ($R^2 = -0.97$, P = 0) with increase in iron, which asserted that iron complexed with SRFA must have absorbed more in higher wavelengths (350 nm – 400 nm) than in lower wavelengths (275 nm to 295 nm) which was strongly in agreement with results described in Yan (2013). This phenomenon was also supported by 35.14% decrease in absolute value of $S_{275-295}$ ($R^2 = 0.82$, P = .01) suggesting decreased absorption between 275 nm to 295 nm than between 350 nm to 400 nm.
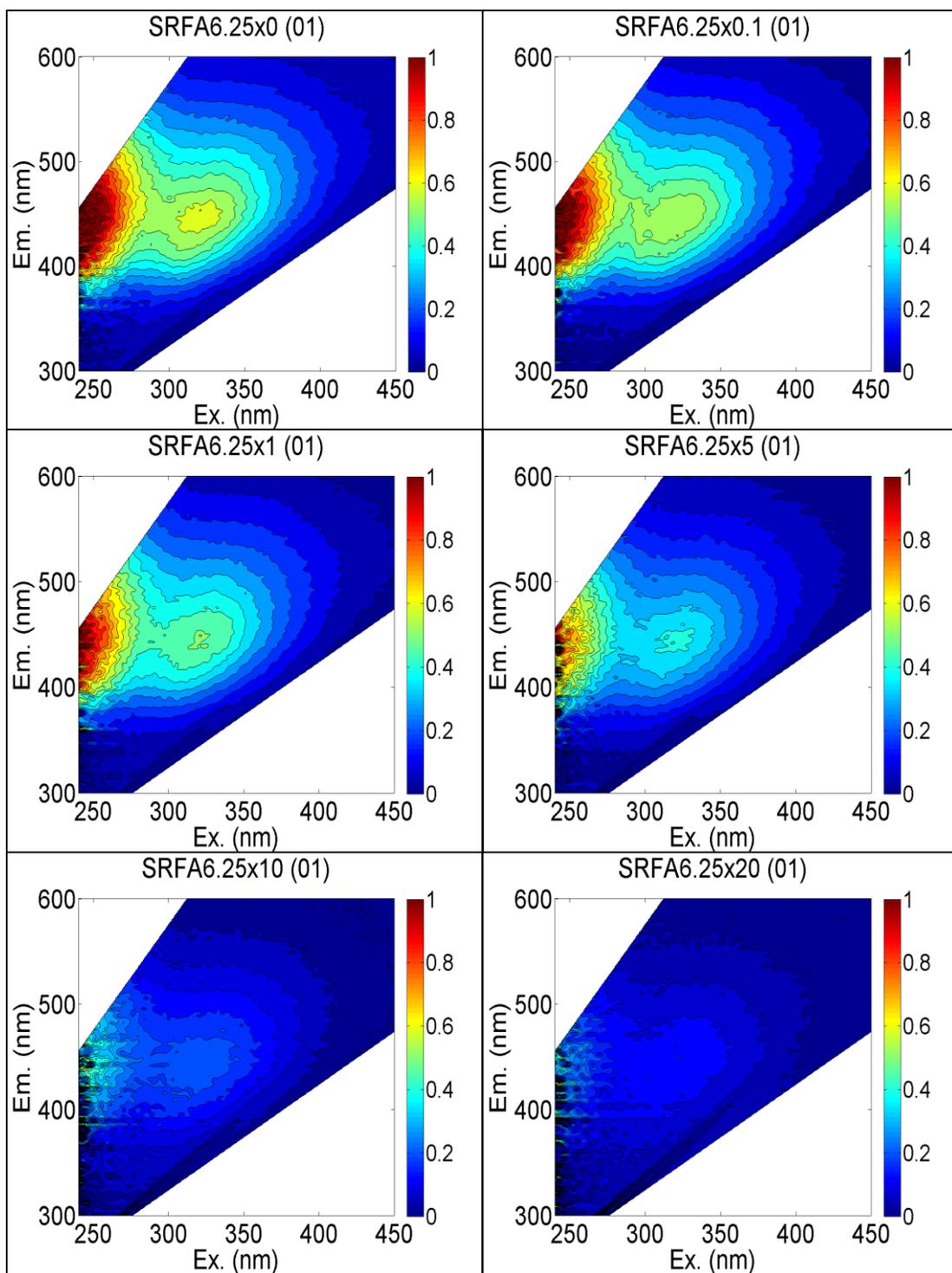
Figure 15 3D EEMs of 6.25 mgL-1 SRFA titrated with 0, 0.1, 1, 5, 10 and 20 mgL-1 of Fe

Table 7 Results of regression analysis of average (n = 3) spectral properties of Suwanee River Fulvic Acid upon titration with varying concentrations of Fe and As. P-value < 0.05 indicates statistically significant correlations with 95% confidence.

Experiment		Abs254	$S_{275-295}$	$S_{350-400}$	S_R	FI	FrI	HIX	A 260/380-460 nm	B 275/310 nm	T 275/340 nm	C 350/420-480 nm	M 312/380-420 nm
SRFA Calibration	R^2	0.99	-0.44	0.40	-0.30	0.01	0.21	0.95	0.99	-0.61	0.99	0.99	0.99
	P	0.00	0.22	0.25	0.34	0.90	0.43	0.00	0.00	0.12	0.00	0.00	0.00
Fe-DOM [2]	R^2	0.09	0.44	0.46	-0.20	0.56	0.44	-0.68	-0.94	-0.48	-0.39	-0.94	-0.95
	P	0.55	0.15	0.13	0.36	0.08	0.15	0.04	0.00	0.13	0.18	0.00	0.00
Fe-DOM [3]	R^2	0.97	0.82	0.58	-0.97	0.93	0.97	-0.80	-0.89	-0.27	-0.17	-0.89	-0.89
	P	0.00	0.01	0.08	0.00	0.00	0.00	0.02	0.00	0.29	0.40	0.00	0.00
As-DOM[4]	R^2	0.01	0.79	0.26	-0.64	0.73	0.85	-0.49	-0.71	0.01	0.37	-0.63	-0.84
	P	0.84	0.02	0.30	0.05	0.03	0.01	0.12	0.03	0.83	0.20	0.06	0.01
As-DOM[5]	R^2	0.73	0.65	0.27	-0.22	0.56	0.30	-0.48	0.11	-0.26	0.12	0.53	-0.18
	P	0.03	0.05	0.29	0.34	0.09	0.26	0.13	0.53	0.30	0.50	0.10	0.40
As-Fe-DOM[6]	R^2	0.51	0.87	-0.12	-0.80	0.30	-0.03	-0.54	-0.09	0.08	0.02	-0.57	-0.07
	P	0.11	0.01	0.48	0.02	0.25	0.72	0.09	0.55	0.86	0.98	0.41	0.60
As-Fe-DOM[7]	R^2	-0.37	0.94	0.36	-0.98	0.00	0.39	0.09	-0.28	-0.34	-0.35	-0.33	-0.27
	P	0.20	0.00	0.21	0.00	0.98	0.18	0.56	0.28	0.22	0.21	0.23	0.29
As-Fe-DOM[8]	R^2	0.07	0.00	-0.04	-0.85	0.01	-0.12	-0.08	0.67	0.03	0.24	0.37	0.27
	P	0.61	0.99	0.70	0.01	0.81	0.49	0.58	0.04	0.76	0.31	0.20	0.29

[1] SRFA concentrations 0, 6.25, 12.5, 25, 50 and 100 mg/l
[2] SRFA (12.5 mgL^{-1}) titrated with 0, 0.1, 1, 5, 10, 20 mg/l of dissolved Fe
[3] SRFA (6.25 mgL^{-1}) titrated with 0, 0.1, 1, 5, 10, 20 mg/l of dissolved Fe
[4] SRFA (12.5 mgL^{-1}) titrated with 0, 10, 50, 100, 500 and 1000 ug/l of dissolved As
[5] SRFA (6.25 mgL^{-1}) titrated with 0, 10, 50, 100, 500 and 1000 ug/l of dissolved As
[6] 6.25 mg/l SRFA + 2 mg/l Fe titrated with 0, 10, 50, 100, 500 and 1000 ug/l of dissolved As
[7] 6.25 mg/l SRFA + 10 mg/l Fe titrated with 0, 10, 50, 100, 500 and 1000 ug/l of dissolved As
[8] 6.25 mg/l SRFA + 20 mg/l Fe titrated with 0, 10, 50, 100, 500 and 1000 ug/l of dissolved As

Increase by 11.78 % of FI strongly correlated iron doses ($R^2 = 0.93$, P = 0) was observed. This is consistent with our previous observation of higher absorption at higher wavelengths due to iron binding. Increase in FI may be due to extra absorbance at 370 nm causing overall reduction in emission intensity and more importantly, absorbance of emitted intensity by the iron present. Iron has been shown to absorb more intensity at 520 nm than at 450 nm (*Yan et al., 2013*) which might have caused FI to increase. This observation has wide relevance in environmental samples, particularly groundwater samples with high concentrations of dissolved iron. The lower FI and higher FI values have been linked with terrestrially-derived and microbially-derived DOM respectively (*McKnight et al., 2001*) based on fulvic acids isolated from streams and rivers receiving predominantly terrestrial sources of organic material and from lakes with microbial sources of organic material. The groundwaters in reducing aquifers, such as in Bengal basin, typically have higher dissolved iron concentrations than the rivers, streams and lakes (*Harvey et al., 2002; Dowling et al., 2002; McArthur et al., 2001 and 2004; Ravenscroft et al., 2005; Zheng et al., 2005; Mukherjee et al., 2007; Datta et al., 2009; Sankar et al., 2014; Mladenov et al., 2015*). Few studies have reported FI ranging between 1.2 − 1.6 in groundwater beneath Okavango delta (*Mladenov et al., 2008 and 2013*) and 1.4 − 1.6 in groundwater in Bangladesh aquifer (*Mladenov et al., 2010 and 2015*) suggesting terrestrially-derived origin of DOM. In our study we observed FI increased from 1.29 ± 0.047 to 1.44 ± 0.028 at 0 mgL^{-1} to 20 mgL^{-1} Fe respectively. Although, elevated FI values are attributed to microbially-derived DOM sources, such as wastewater inputs (*Chen et al., 2009; Goldman et al., 2012*), in reducing groundwaters, it may also be linked to higher dissolved iron concentrations.

We also observed 29.15 % increase in β:α strongly correlated ($R^2 = 0.98$, P = 0) with increase in Fe (II) concentrations. This observation was also consistent with our previous

observation of increase in abs254, FI and decrease in S_R. Since β:α was the ratio of emission intensity at 380 nm to maximum emission intensity between 420 nm to 435 nm, this increase in β:α can be explained by higher absorption by iron at wavelengths between 420 nm to 435 nm than at 380 nm. Williams and Xenopoulos (2013) reported β:α ranging from 0.73 to 0.92 in a storm-water pond with continuous supply of fresh DOM. Interestingly, Mladenov (2013) reported β:α ranging from 0.5 to 0.6 in groundwater and slightly lower ~ 0.48 in surface water samples in Okavango delta. Although β:α has been used widely as a good indicator of fraction of recently derived DOM in various environmental scenarios, particularly in the groundwater, influence of dissolved iron that causes β:α to increase should be taken into the considerations.

Humification index (HIX) was observed to drop by 55.64 % with a significant correlation (R^2 = -0.80, P = 0.02) with Fe (II) concentrations. This can primarily be explained by absorption of emitted intensities rather than absorption of excitation intensity at 254 nm, as iron absorbs more at higher wavelengths. Hence, the area under the emission spectra between 435 nm to 480 nm might have decreased much more than that between 300 nm to 345 nm, decreasing the ratio i.e. HIX. Increase in HIX was attributed to increase in the degree of aromaticity of DOM (*Zsolnay et al., 1999; Huguet et al., 2009*) while the process of humification to be associated with increase in C/H ratio (*Stevenson, 1982*). The groundwaters have been shown to have higher HIX than surface water but lower than top soil pore water (*Kalbitz et al., 1999*). Results in this study indicated that the degree of humification of DOM may be underestimated by the decreased HIX due to presence of Fe-DOM binary complexes.
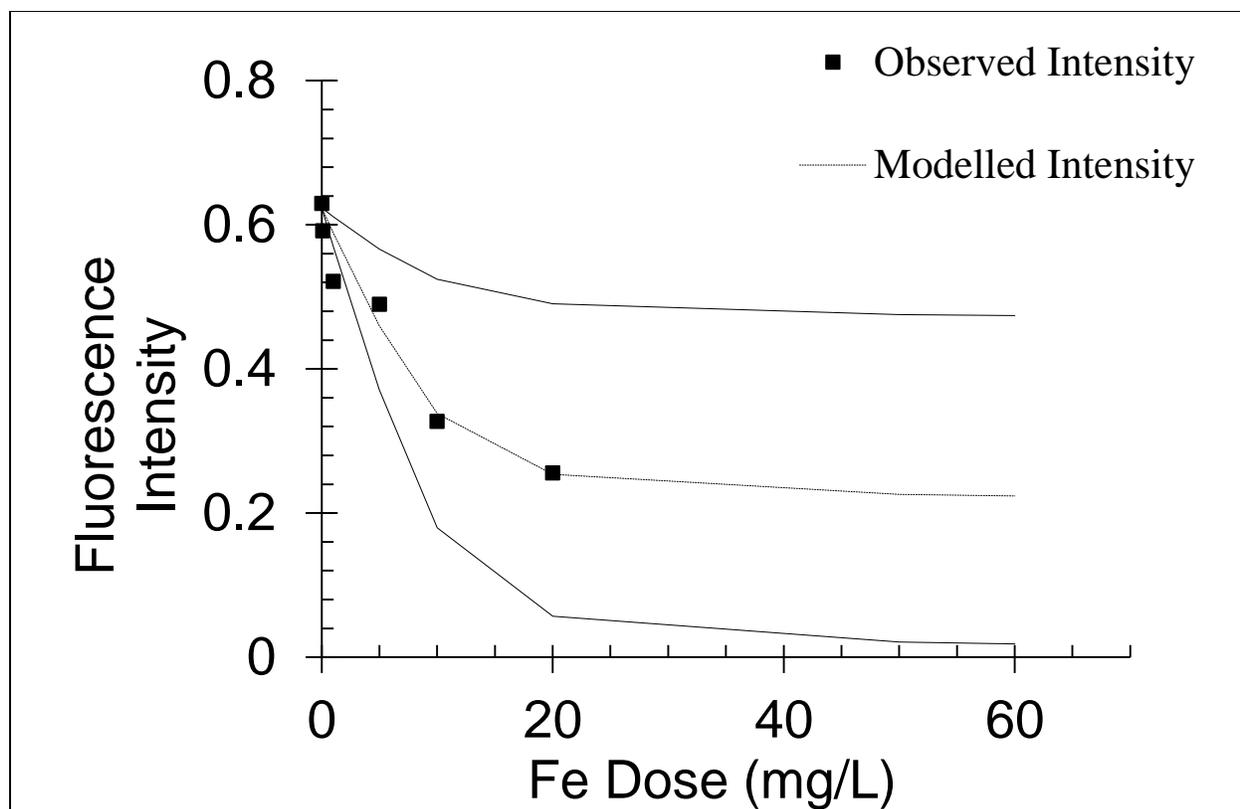
Figure 16 Figure 5: Graph showing complexation modeling (Ryan & Webber) using fluorescence intensity at peak C, for 6.25 mg/l SRFA titrated with 0, 0.1, 1, 5, 10 and 20 mg/l of Fe. Dotted line indicated modeled intensity, square filled dots indicate observed intensity, two solid lines indicate sensitivity of conditional stability constant (K).

As seen in Figure 16, intensities of humic-like peaks were also observed during titration with dissolved iron. Intensity of Peak A decreased by 74.54 % (R^2 = -0.89, P = 0), of Peak C by 73.99% (R^2 = -0.89, P = 0) and of Peak M by 75.88 % (R^2 = -0.89, P = 0). Approximately similar percentage of decrease in intensity of all three peaks can be explained by their common emission wavelength range from 380 nm to 480 nm. Intensities of Peak C were then used to determine complexation parameters by complexation model (*Ryan and Webber, 1982*). Model revealed the conditional stability constant for SRFA – Fe (II) aqueous complex to be $10^{4.71}$ and the binding capacity to be 191 µmol/kg (Figure 17). Log K of 4.71 was consistent with other studies showing iron binding with SRFA. For example, recent work using the PHREEQC-Model VI and linear free

energy relationship (LFER) method found the conditional log K for phenolic binding sites of SRFA (1000 mgL^{-1}) to be 4.46 (*Catrouillet et al., 2014; Rose and Waite, 2003*). In another study using a more environmentally representative SRFA concentration (10 mgL^{-1}) and a differential absorbance approach, the NICA-Donnan modeling parameter log K was found to be 6 (*Yan et al., 2013, 2014*). Using fluorescence titration and the Ryan and Webber model, similar to that used in this study, log K values of 4.91 and 4.85 were measured for Fe complexation of deciduous water-soluble organic matter (30 mgL^{-1}) and coniferous water soluble organic matter (30 mgL^{-1}), respectively (*Ohno et al., 2008*). Additionally, the ligand (SRFA) concentrations used in the present study are relevant to DOM concentrations typically found in arsenic contaminated reducing aquifers. Studies with much higher SRFA concentrations reported higher log K values for example log K of 11.04 for Fe binding with 10 gL^{-1} of SRFA (*Fujii et al., 2014*).

As – DOM Complexation
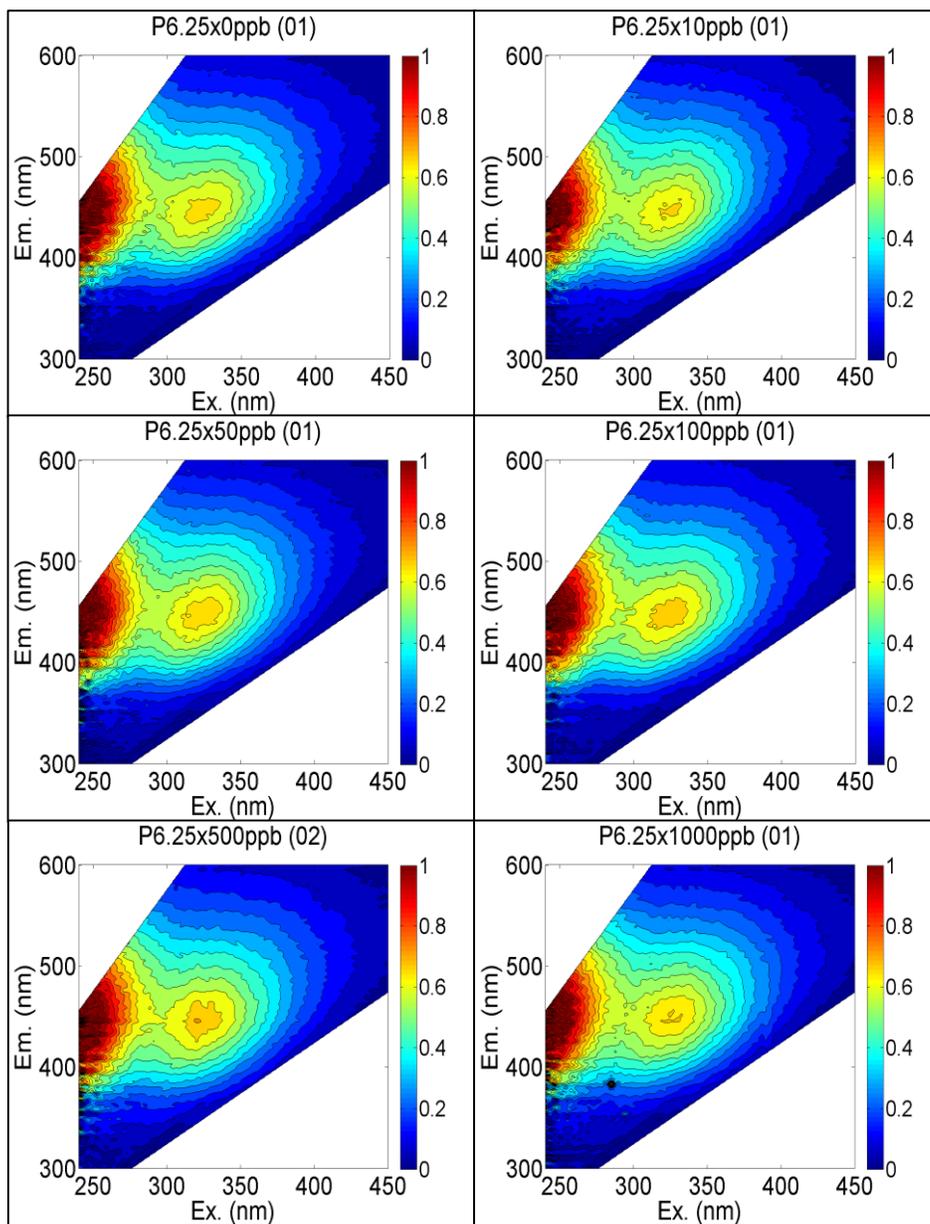
Figure 17 3D EEMs of 6.25 mgL-1 SRFA titrated with 0, 10, 50, 100, 500 and 1000 ugL-1 of As
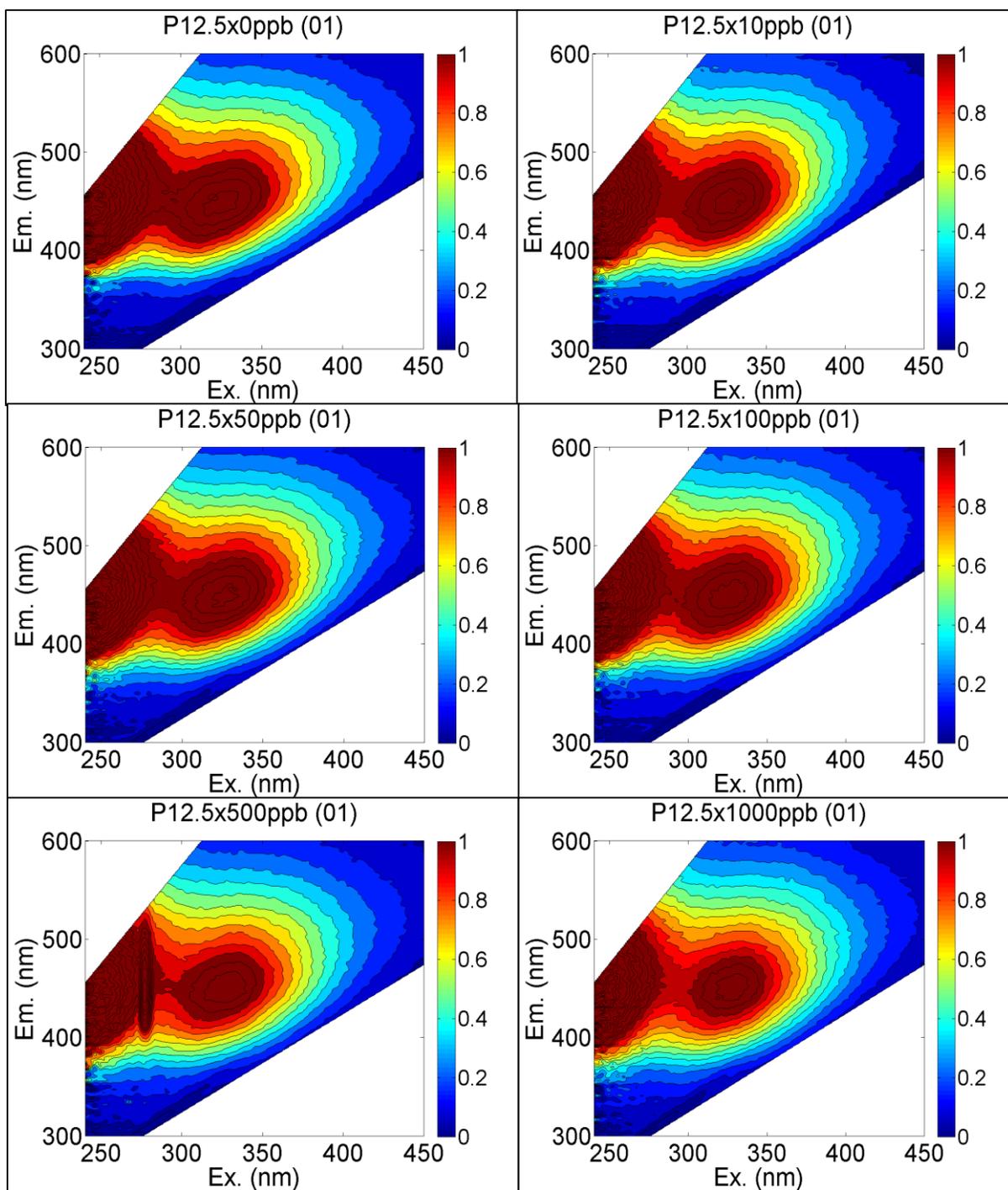
Figure 18 3D EEMs of 12.5 mgL-1 SRFA titrated with 0, 10, 50, 100, 500 and 1000 ugL-1 of As

In As (III) – SRFA titration experiment, any statistically significant correlations ($R^2 > 0.8$ and $P < 0.05$) were not observed with 6.25 mgL^{-1} SRFA concentration. In an experiment with 12.5 mgL^{-1} SRFA, a good and significant correlation between β:α ($R^2 = 0.85$, $P = 0.01$) and As (III) concentrations was observed. However, the increase in β:α in this experiment was not significant (7.65%) as compared to increase in β:α in Fe – SRFA titration experiment (29.15 %). Peak M intensity was also observed to be in good and significant correlation ($R^2 = -0.84$, $P = 0.01$) with As (III) concentrations. However, this decrease in intensity was again found to be insignificant (13.80 %) as compared to that in Fe – SRFA experiment (75.88 %). Further, these two changes in β:α and Peak M intensity during As – SRFA experiment were contradictory to known optical properties of dissolved As that it absorbs in the lowermost portion of the UV spectrum at 193.7 nm, and hence alterations in optical properties of SRFA due to As (III) binding were very unlikely (*Pellegrini, 2010*).
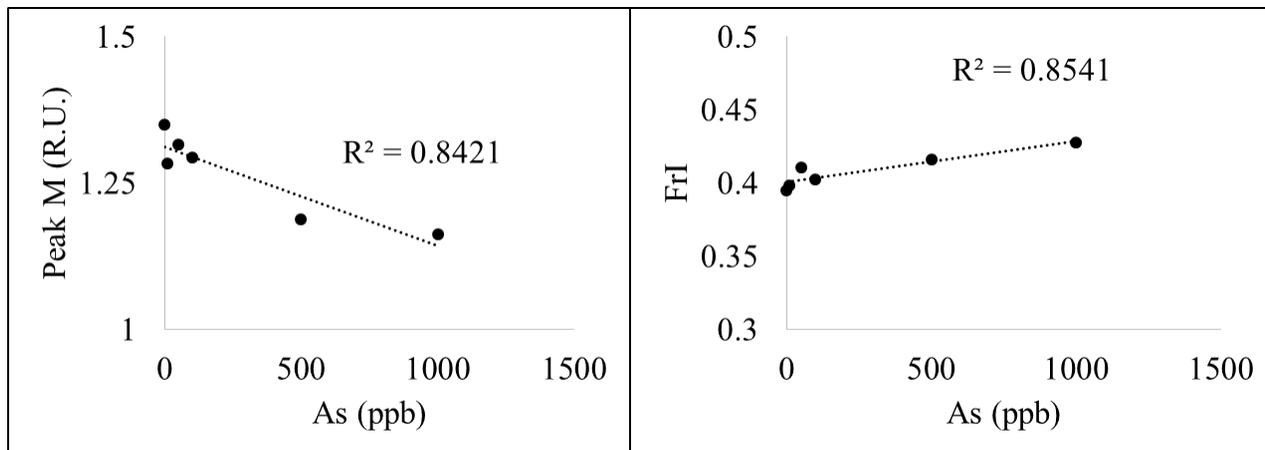
Figure 19 Correlation of Peak M intensity (left) and FrI (right) with As dosages.

Since, very small change in only two of the optical properties was observed, it was not attributed to As (III) – SRFA binding. Perhaps As – SRFA binary complex was not formed in this experiment or was not detected with fluorescence spectroscopy. However, such binary complexes have been reported to have formed and detected by ATR-FTIR and Mossbauer-spectroscopy

(*Sharma et al., 2010*). To further investigate, As –SRFA samples were analyzed with 1H solution NMR spectroscopy which has been discussed later.

As-Fe-DOM Complexation

In this experiment, concentration of SRFA was kept constant at 6.25 mgL^{-1}. Three concentrations of Fe (II) were used as 2, 10 and 20 mgL^{-1}. These combinations were titrated with six different concentrations of As (III) as 0, 10, 50, 100, 500 and 1000 μgL^{-1}. Results of titration revealed that with 2 mgL^{-1} Fe (II), absolute values of $S_{275-295}$ were found to decrease with a good and significant correlation ($R^2 = 0.87$, $P = 0.01$) with increase in As (III) concentrations. The decrease however was not significant (10.55 %) when compared to 54.19 % decrease in Fe – SRFA experiment. A good correlation was observed for S_R ($R_2 = -0.80$, $P = 0.02$) which was smaller magnitude of decrease (14.69 %) as compared to 21.63% in Fe –SRFA experiment. Similarly, with 10 mgL^{-1} of Fe (II), strong and significant correlation was observed for $S_{275-295}$ ($R^2 = 0.94$, $P = 0$) as well as for S_R ($R^2 = -0.98$, $P = 0$) with increase in As (III) concentrations. However, the increase of 8.32 % in S275-295 and decrease of 6.91 % in SR was not significant as compared to those in Fe –SRFA experiment, 54.19 % and 21.63 % respectively. In the experiment with 20 mgL^{-1} Fe (II) concentration, only good and significant correlation was observed for SR ($R^2 = -0.85$, $P = 0.01$). However, this decrease in SR was not significant as well (5.21 %) as compared to 21.63 % in Fe – SRFA experiment.
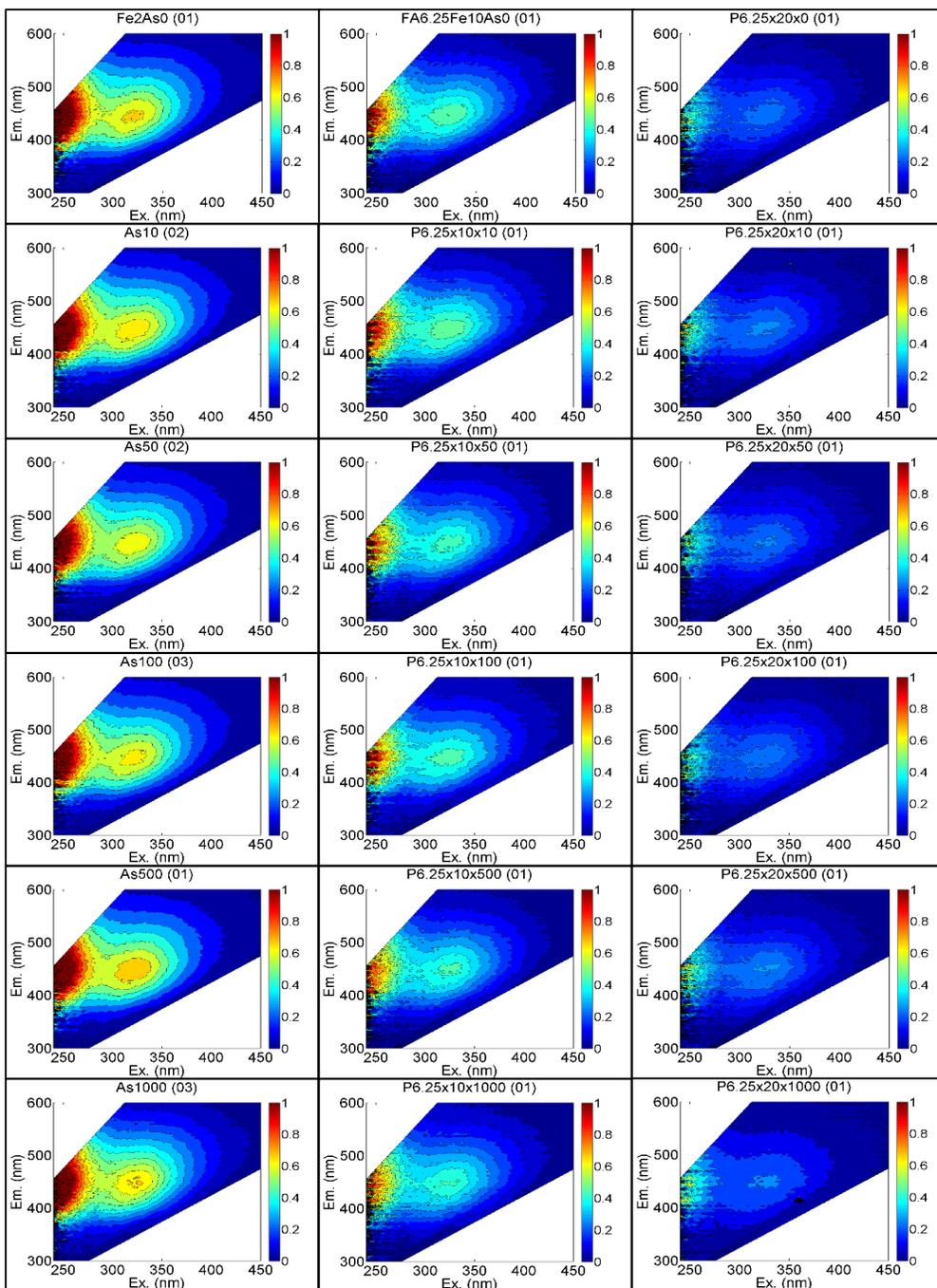
Figure 20 3D EEMs of (1) In column 1, solution of 6.25 mg/l SRFA and 2 mg/l Fe titrated with 0, 10, 50, 100, 500 and 1000 ug/l of As; ; (2) In column 2, solution of 6.25 mg/l SRFA and 10 mg/l Fe titrated with 0, 10, 50, 100, 500 and 1000 ug/l of As; (3) In column 3, solution of 6.25 mg/l SRFA and 20 mg/l Fe titrated with 0, 10, 50, 100, 500 and 1000 ug/l of As.

These results suggested that lack of very strong and significant correlations was consistent with lower wavelength absorption of As. However, there was a notable trend in % decrease of S_R values. Decrease was 14.69, 6.91 and 5.21 % for 2, 10 and 20 mgL^{-1} Fe (II) solution respectively. This trend was found to be consistent with the observation of Liu (2011) that the small presence of dissolved Fe enhances the process of Fe bridged As − DOM complex formation and as the concentration of Fe increased the number of binding sites available for As decreased and hence less As was bound. However, due to lack of strong and significant correlations and changes in other important optical properties, it was not possible to conclude whether ternary complex was formed.

^{1}H NMR SPECTROSCOPY

Changes in Proton Chemical Shift and Intensity Ratio

The formation of Fe-bridged ternary complexes of As and DOM has been considered to be an important mechanism for maintaining arsenic in circumneutral pH solutions under reducing conditions (*Sharma et al., 2010*). Mikutta and Kretzschmar (2011) identified inner-sphere binding of As (V) to Fe-DOM complexes as a way in which these ternary complexes form. Complexes directly between As and DOM also have been observed (*Liu et al., 2011; Sharma et al., 2010*), but the specific reaction sites are not known. In our study, we used proton NMR spectroscopy (paramagnetic cations such as Fe were removed by sulfide treatment) to obtain further insight into the specific As-DOM complexation sites. The NMR spectra resulting from the spin of ^{1}H of pre-treated SRFA in D$_2$O were comparable to previously collected data (*Thorn et al., 1989*). In our study, seven significant peaks were identified from the ^{1}H NMR analysis and divided into four regions for analysis (Figure 22). The peaks indicated the presence of a ^{1}H atom attached to a carbon atom in the DOM molecule. The consistent decrease (Figure 23) in chemical shifts (CS) and

intensity ratio at particular peaks can be considered to have effect of arsenic binding at that location due to arsenic addition (Figure 23). Shielding (upfield) in chemical shifts was observed in the ^{1}H NMR spectra upon addition of 1, 10, 100, 1000 and 5000 ppb of As to the SRFA solution in peak C (9.67%) and peak E (7.85%) in Region 2 (1.6 − 3.3 ppm, chemical shift region for aliphatic protons attached to carbonyl or carboxyl group) and peak I (3.1%) and peak H (3.5%) in Region 3 (3.3 − 5.5 ppm, chemical shift region for carbohydrate or polyether or amino acid alpha protons). The differences in CS (Δ CS >0.1 ppm) for peaks C and E (methyl and methylene on carboxyl and
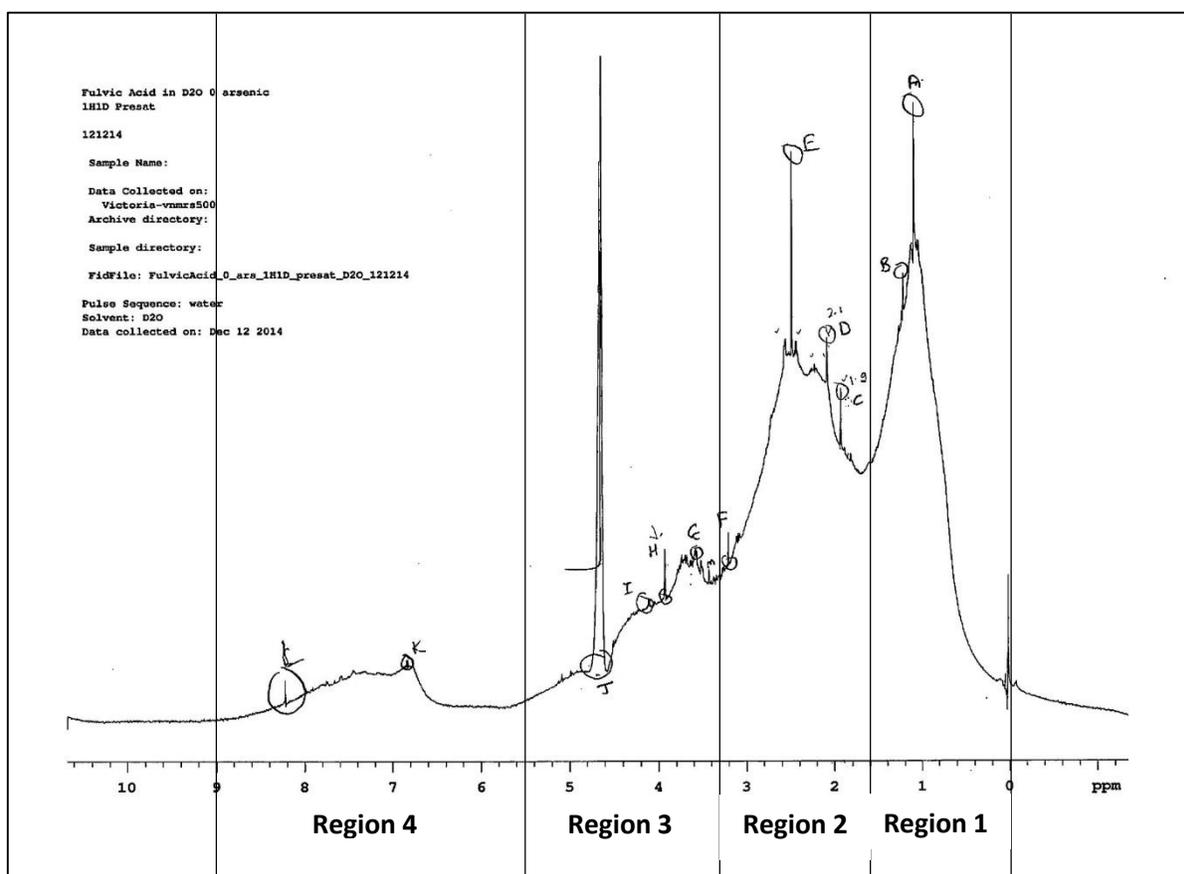
Figure 21 1D- ^{1}H NMR spectrum of 10 mg/ml SRFA solution after removal of paramagnetic cations by sulfide treatment, dissolved in D_2O. Peaks in the different regions indicate significantly different molecular structures of SRFA.
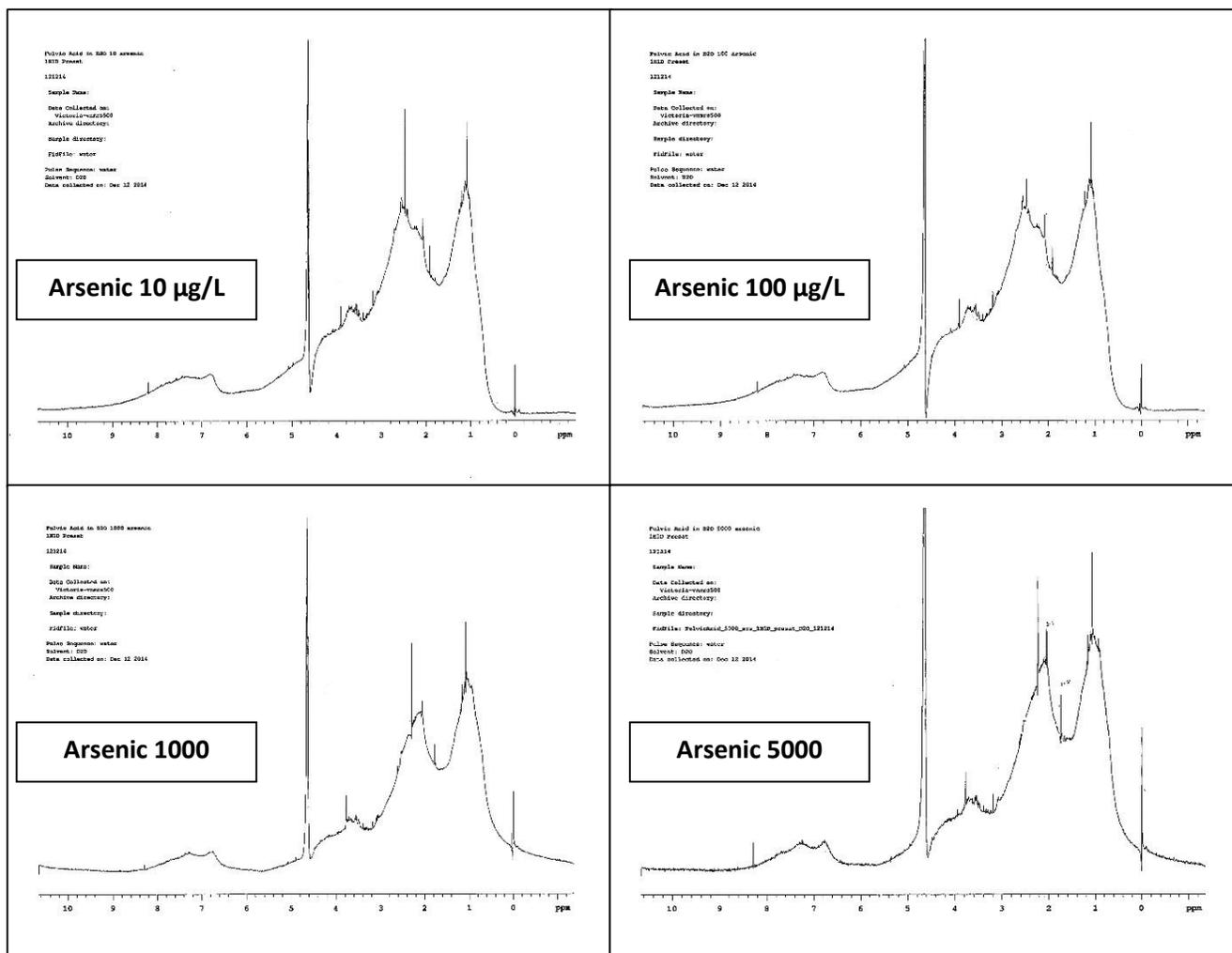
Figure 22 1D- ^{1}H NMR spectra of 10 mg/ml SRFA solution with different dosages of As.

Carbonyl groups), peaks I and H (methyl, methylene or methine attached to oxygen or nitrogen including carbohydrate and amino acid) may be attributed to the addition of electron density in neighboring atoms or functional groups (*Balci, 2005*), possibly due to binding of As.

NMR peaks in the aliphatic region showed decrease in the peak area while no significant differences in chemical shift or in the intensity ratio were observed in aromatic Region. This finding helps explain the lack of a quenching effect with the addition of As to the SRFA solution in our fluorescence titration experiments. Fluorescence of the DOM molecule is due in large part to the presence of aromatic functional groups, and structural changes (such as attachment of Fe or

87

As to aromatic functional groups) are detected by fluorescence spectroscopy, but structural changes to non-aromatic groups would not be detected. Our ^{1}H NMR results instead implicate As binding to non-fluorescent moieties such as, methyl groups, methylene on carboxyl and carbonyl groups, and/or methyl, methylene or methine attachment to oxygen or nitrogen.
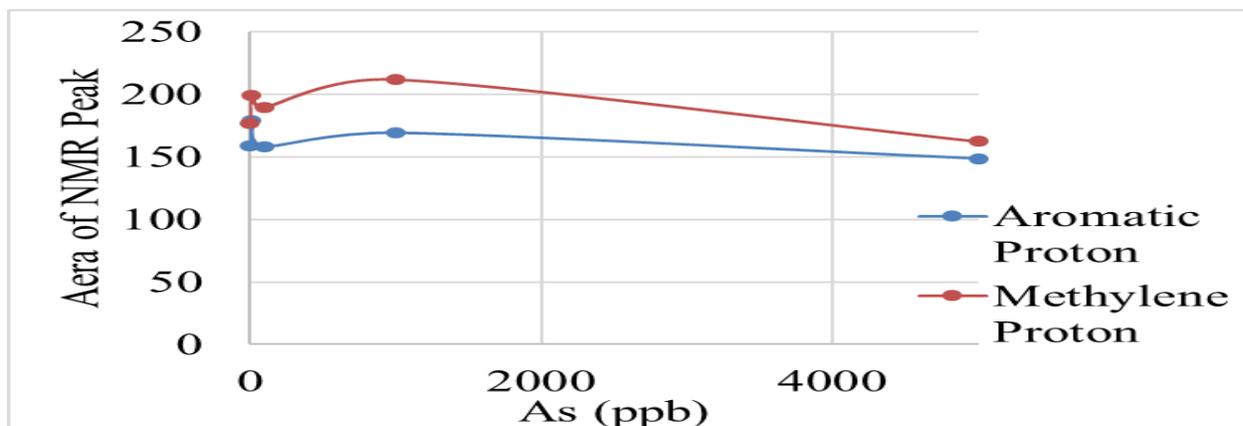
Figure 23 Scattered plot of ratio of peak areas obtained by ^{1}H NMR versus As concentration.

Results from ^{1}H NMR analyses provide additional information about the type of complex that is formed between As and DOM. Arsenic has been shown to form inner-sphere complexes directly via organic functional groups such as hydroxyl groups (*Sharma et al., 2010; Warwick et al., 2005; Goldberg et al., 2002*).

At the same time, arsenic has been shown to form coordination complexes with DOM via metal bridges (*Sharma et al., 2010; Redman et al., 2002; Bauer et al., 2006; Ritter et al., 2006; Wang et al., 2006; Buschmann et al., 2006; Lin et al., 2004*). Results of the S_R decrease in As – Fe – DOM samples with increasing in As concentrations, described earlier, suggests formation of Fe bridged ternary complexes. Thus, inner sphere Fe – DOM and As – DOM complexes and As – Fe – DOM coordination complex both were likely formed and detected.

BROADER IMPLICATIONS

The mobility of arsenic in reducing aquifers is known to be greatly influenced by the presence of DOM. The importance of the humic-like portion of the DOM pool has also recently gained attention with respect to arsenic mobility (Mladenov et al., 2015). Fluorescent and aromatic moieties in the DOM molecule have been described to contribute towards arsenic mobility by serving as electron shuttles (*Lovley et al., 1998; Nevin et al., 2000; Kappler et al., 2004, Mladenov et al., 2010, 2015*). Complexation of arsenic directly with DOM molecules (binary) or via Fe-bridging (ternary) has been considered as another significant mechanism controlling arsenic mobility. However, the role of non-aromatic DOM moieties in arsenic mobility has rarely been reported. Our results from ^{1}H NMR analyses of As – DOM binding suggest that the non-fluorescent and non-aromatic moieties of DOM molecules such as methyl, methylene, methine and carbonyl groups, which cover a substantial fraction of the DOM molecular structure, actually play an active role in As – DOM binary complex formation. These new findings assert the importance and role of DOM in arsenic mobility.

Chapter 7 - A new influence on iron dissolution in Bangladesh sediments: electron shuttling by groundwater fulvic acids

ABSTRACT

The electron shuttling behavior of fulvic acid and its role in accelerating iron (Fe) reduction were experimentally demonstrated more than two decades ago, and the environmental relevance of this mechanism is only now being understood. Here we show that fulvic acids isolated from high and low arsenic groundwater aquifers in the Bengal Basin can be reduced by Geobacter metallireducens, and are subsequently capable of reducing Fe(III) to Fe(II). Moreover, all four Bangladesh groundwater fulvic acids had higher Fe(III) to Fe(II) conversion rates compared to Suwannee River Fulvic Acid, a commercially-available FA isolated from a terrestrially-dominated surface water source. Until now, microbially-mediated reductive dissolution of Fe (oxy)hydroxides, driven by the availability of labile organic matter, was widely accepted as the main control on arsenic mobilization in reducing aquifers. Our evidence for the electron shuttling ability of Bangladesh FAs implicates electron shuttling as another important control on elevated As concentrations in groundwater of the Bengal Basin.

INTRODUCTION

Humic-like moieties in dissolved organic matter (DOM) have been reported to interact and enhance the reductive dissolution process of iron and arsenic in the presence of iron-reducing bacteria (IRB) under diverse environmental conditions (*Scott et al., 1998; Redman et al., 2002; Kappler et al., 2004; Oremland et al., 2004; Bauer et al., 2006; Mladenov et al., 2007, 2008, 2010, 2013, 2015; Wolf et al., 2009; Reza et al., 2010; Palmer et al., 2010; Legg et al., 2012; Vaxevanidou et al., 2012; Zheng et al., 2012; Lee, 2013; Pi et al., 2015*). An acceleration of reductive dissolution of Fe by humic substances was shown by Lovley et al., (1996). In

experiments with anthraquinone-2,6,-disulfonate (AQDS, a humic analog), Lovley et al., (1996) showed that AQDS was reduced to anthrahydroquinone-2,6-disulfonate (AHDS) by *G. metallireducens* and *S. alga*, and AHDS could abiotically transfer electrons to Fe (III) with the regeneration of AQDS. Further it was demonstrated that other groups of bacteria (including iron, sulfate and nitrate reducing bacteria) were capable of reducing the humic substances (HS) and abiotically reducing metals (*Lovley et al., 1996, 1998*). Scott et al. (1998) proposed that organic radicals in HS, which are primarily quinone groups, were reduced by accepting electrons from G. metallireducens and that this capacity of HS to accept electrons was higher in sedimentary HS than that in aquatic HS. It was further investigated that the reduced HS (AHDS) could serve as electron donors for a wide group of bacteria (*Lovley et al., 1999*).

Klapper et al. (2002) reported that the electron accepting capacity of HS extracted from soil, freshwater and sea water varied with the source and that the excitation emission matrix spectra (EEMS) of HS were altered significantly after microbial reduction. In another study, humic acids from a freshwater lake were shown to have higher electron-accepting (i.e. oxidized HS) capacity near surface and higher electron-donating (i.e. reduced HS) capacity at depth, which was correlated with the presence of IRB at deeper layers (*Kappler et al., 2004*). Jiang (2008) investigated that the concentration of HS do not limit their ability to shuttle electrons and accelerate metal reduction, even at lower concentrations (<5 mgL^{-1} C) common in marine and subsurface environments. Similar study in the groundwater environment (Mladenov et al., 2008) showed that the DOM with reduced fluorescence components (semiquinone-like and hydroquinone-like) was linked with potential electron-shuttling role in the dissolution of metal oxides in the groundwater beneath the seasonal swamp of the Okavango Delta in northwestern Botswana. HS extracted from deep aquifer

in Germany stimulated the microbial iron reduction at concentrations of HS as low as 1 mgL^{-1} (*Wolf et al., 2009*).

The large human population residing in the Ganga-Meghana-Brahmaputra River basin, mainly in parts of eastern India and Bangladesh, is at health risk due to drinking groundwater with high dissolved arsenic (As) concentration (> 10 µgL^{-1}, WHO guidelines) (*Bhattacharya et al., 1997; Nickson et al., 1998; Smith et al., 2000; McArthur et al., 2001; Dowling et al., 2002; Roychowdhury et al., 2002; Ravenscroft et al., 2005; Acharyya and Shah, 2006; Datta et al., 2009, 2011; Sankar et al., 2014*). The As in groundwater is natural and mobilized from oxidized iron minerals via microbially-mediated reductive dissolution (*McArthur et al., 2001; Dowling et al., 2002; Hasan et al., 2007*). This process is primarily driven by labile organic carbon that was deposited in the sediments in the past (*McArthur et al., 2004; Sengupta et al., 2008; Datta et al., 2011*) or drawn to depth from ponds and other surface water sources (*Harvey et al., 2006; Neumann et al., 2010*). Studies have shown that HS were present in abundance in the reducing aquifer of Bangladesh (*Reza et al., 2010*) and play a dual role (*Mladenov et al., 2010*) as a labile substrate as well as an electron shuttle and implicated in significantly accelerating the reductive dissolution resulting in elevated arsenic levels. Further, Mladenov (2015) isolated fulvic acid (FA) groundwater in Araihazar, Bangladesh spanning an age gradient (<5 to >30 years old) and investigated source and reactive characteristics in relation with dissolved As concentration.

In general, these studies (*Mladenov et al., 2008, 2010, 2015; Reza et al., 2010*) have hypothesized that the HS in high As groundwater serve as electron shuttles to accelerate Fe reduction or As reduction and thereby promote mobilization of As from sediments. However, direct evidence that the HS isolated from these groundwaters are capable of shuttling the electron is still lacking. To our knowledge, the mechanism of electron shuttling by HS in the geologic

setting of Bengal basin has not been tested. In the present study, we evaluate the electron shuttling abilities of five large volume FA samples isolated in Mladenov (2015) under environmentally relevant conditions with *Geobacter metallireducens*. We also investigate the influence of Suwanee River Fulvic Acid (SRFA, a commercially available terrestrial HS) on growth rate of *G. metallireducens*.

Propagation of Geobacter metallireducens

Geobacter metallireducens Lovley et al. (ATCC 53774) pure culture was used and initial cultures were propagated by incubating the cells at 30^0C in freshly prepared ferric citrate medium (ATCC 1768) for 7 days. The pH of the medium was maintained between $6.8 - 7.0$ after bubbling 80% N_2 and 20% CO_2. Suwanee River Fulvic Acid (SRFA) was used to study the growth rate of *G. metallireducens* and was obtained from International Humic Substances Society (IHSS # 2S101H). Ferric citrate (Fisher # 3388) and Goethite (*Schwertmann and Cornell, 2007*) were used as liquid and solid phase electron acceptor respectively. Dissolved Fe^{2+} was quantified by Ferrozine method (*Stookey, 1970*) on a UV-Spectrophotometer. Bangladesh Fulvic Acid (BFA) samples were isolated from the groundwater ranging from $7 - 15$ m depths and <5 to >30 years old age. (*Mladenov et al., 2015*). The study site was located in the Ganges Brahmaputra Delta (GBD) in central Bangladesh and underlay Holocene aquifers ($5 - 30$ m, elevated As) and deep Holocene aquifers ($40 - 90$ m, low As) separated by one or multiple layers of fine-grained sediment (*Zheng et al., 2005*). BFA samples were re-dissolved in 18.2 MΩ-cm Milli-Q ultra-pure water to obtain final concentration of 2 mg.mL^{-1}. Nutrients (as per ATCC 1768, except ferric citrate) were added and dissolved to BFA solutions in appropriate amounts. An industrial grade N_2 gas was bubbled through the BFA solutions for 1 hour in 18 x 150 mm glass anaerobic tubes and tubes

were sealed under N_2 head with 20 mm blue butyl rubber stopper and aluminum seal. 100 μL of each BFA sample was analyzed on Horiba Aqualog fluorometer to acquire fluorescence data.

Figure 25: *G. metallireducens* cells transfer from the ATCC 1768 medium to Bangladesh Fulvic Acid medium by successive filtration process.

Electron shuttling experimental setup

Humic substances used in the electron shuttling experiments have been previously described (Mladenov et al., 2015). In brief, chemical characterization of bulk water samples that were used to isolate BFA revealed that two of the samples, K12.1 at 7.5 m and K10.2 at 11 m, were found to be younger than 5 years old with $^3H/^3He$ age (*Mladenov et al., 2015*). Another water sample K8.3 collected at 14.8 m depth was found to have $^3H/^3He$ age greater than 30 years in the same study. Table 8 shows the chemical parameters for bulk water and BFA isolates adapted from Mladenov (2015). Briefly, the sample K8.3 shows high arsenic concentration related with high Ar:Al ratio and low % AA-like fluorescence.

Table 8 Bulk water and BFA isolate properties (From *Mladenov et al., 2015*)

Sample	Depth	Bulk Water Properties								BFA Isolate Properties			
		Age	As_T	As^{3+}	Fe_T	DOC	SUVA	AA	FI	SUVA	Ar:Al	FI	AA
KSW	0	N.A.	23.3	40	0.01	4.80	2.66	5.7	1.65	4.36	0.4	1.69	11
K12.1	7.5	<5	2	90	0.5	0.59	1.60	24	1.47	3.86	0.54	1.48	4.9
K10.2	11	<5	69	100	3.5	0.92	1.72	8	1.46	5.16	0.22	1.45	4.1
K8.3	14.8	>30	363	94	11	0.93	2.24	4	1.49	4.71	0.64	1.40	3.7

Depth is in meters below ground; Age is determined as $^3H/^3He$; As_T and As^{3+} is in μgL^{-1}; FT and DOC is in mgL^{-1}; SUVA is in $L.mg^{-1}.m^{-1}$; AA is % amino acid like fluorescence of overall fluorescence; FI, Ar:Al are dimensionless.

Characteristics of microbially reduced HS by tracking the changes in its fluorescence signature have been studied (Klapper et al., 2002) with surface and marine DOM. In this study, we quantified the changes key fluorescence indices for HS (K12.1) isolated from 7.5 m depth and characterized by 2 μgL^{-1} As_T and 0.5 mgL^{-1} of Fe_T and younger age (<5 years). The fluorescence data was acquired from the sterile filtered sample just after adding clean bacterial cells to BFA solution and after 7 days of incubation followed by sterile filtration.

As per ATCC 53774 propagation protocol, frozen vial was thawed under anaerobic conditions and an aliquot of pure culture was transferred into previously prepared 10 ml of ferric citrate medium into sealed anaerobic test tube by a sterilized needle. After 7-day incubation, 0.5 mL aliquot from the first test tube was transferred to second, three such transfers were made. Fe^{2+} concentration was measured at each stage to monitor the growth using Ferrozine method. In order to obtain healthy bacterial cells possibly free from any dissolved iron trace, a successive filtration process was used as described in Figure 25. From the actively growing culture, 5 ml was filtered through 0.2-micron nylon sterilized syringe filter, pre-rinsed with 20 ml of anaerobic (N_2 purged) 18.2 MΩ-cm Milli-Q ultra-pure water. The filtrate contained the medium constituents, microbially produced Fe^{2+} and remainder ferric citrate while bacterial cells were retained on the filter. This

filter was then backwashed using 2 mL of ultra-pure water to collect bacterial cells. To this, 3 mL of ultra-pure water was added and total 5 mL volume was again filtered through a new filter. This process was successively repeated four times to avoid any traces of culture medium and Fe^{2+}. At the end of 5th backwash, 400 µL of solution containing bacterial cells per 1 mL of the BFA medium was added for inoculation. After 7-day incubation under anaerobic conditions and room temperature, BFA sample was filtered through 0.2 µm sterile filter to separate bacterial cells (Figure 26). The filtrate aliquot of 1 mL was added to 1 mL of 55.93 mM freshly prepared ferric citrate solution in a 1.5 mL micro centrifuge tube. After allowing specific reaction times (0, 2, 4, 5, 6, 7 and 8 hours), an aliquot of the sample was tested for Fe^{2+} concentration using Ferrozine method.
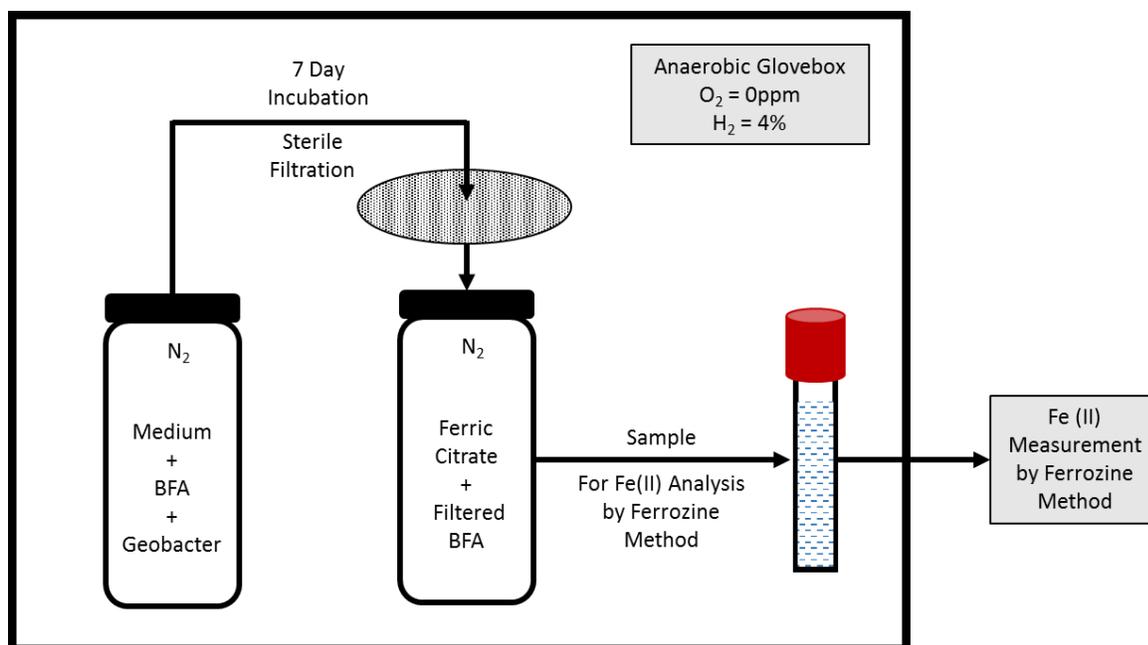
Figure 26: Procedure to microbially reduce Bangladesh Fulvic Acid, sterile filter and measure Fe^{2+} using Ferrozine method.

Influence of HS on growth of bacteria
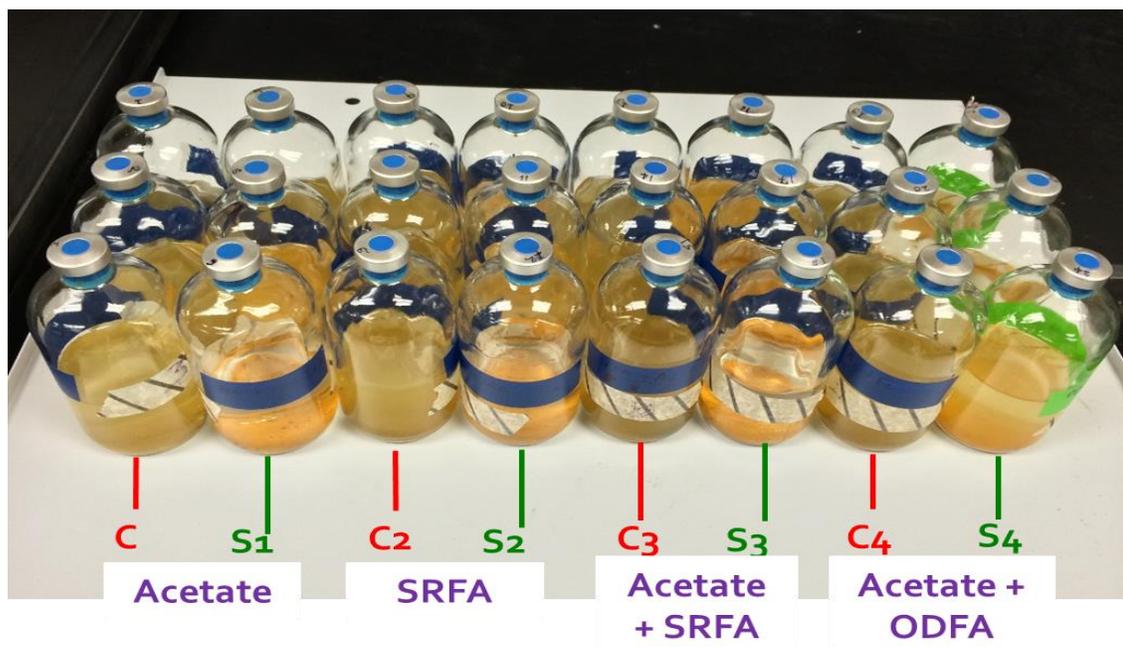
Figure 27 Samples used for the experiment. "C" in red indicates control samples; "S" in green indicates live cultures; SRFA stands for Suwanee River Fulvic Acid; and ODFA stands for Okavango Delta Fulvic Acid.

Table 9 Composition of growth medium

Type	Compound	Concentration
Primary Electron Donor	CH3COONa	2 mM
Primary Electron Acceptor	FeOOH	6 mM
	NaHCO3	5 mM
Medium Composition	K2HPO4	1 uM
	NH4Cl	50 uM
Humic Substances	Suwanee River Fulvic Acid	2 mgL^{-1}
	Okavango Delta Fulvic Acid	2 mgL^{-1}

Sodium acetate (2 mM) as primary electron donor and Goethite (10 mM) as primary electron acceptor were added to a 250 mL glass serum bottle containing 100 mL of ATCC 1768 medium (Figure 27, Table 9). The medium was bubbled with 80% N_2 and 20% CO_2 to achieve final pH of 6.8 − 7. The bottles were sealed under N_2 head and sterilized in autoclave at liquid cycle. One sample was prepared with HS by adding 6 mgL^{-1} of SRFA while the other sample only

had acetate. A 0.2 mL aliquot of *G. metallireducens* culture was injected into each sample. Blanks

were prepared in similar way without adding the bacteria. Sample bottles were incubated at room

temperature under anaerobic conditions for 18 days. Fe^{2+} concentrations were measured using

Ferrozine method to monitor the bacterial growth in all the samples. An iterative algorithm

(Geochemist's Workbench 10.0 Professional) was used to model theoretical growth of the bacteria

using Monod kinetic equation (*Roden et al., 2006*) modified to include thermodynamic potential

factor F_T (*Bethke et al., 2008*) and surface properties of Goethite to simulate environmentally

relevant conditions. Fe^{2+} concentrations measured during the experiment were fitted to the

modeled values to obtain kinetic rate constant.

$$r = k * [X] * \frac{mD}{mD + kD} * \frac{(\frac{[X]}{mA})}{(\frac{[X]}{mA}) + kA} * FT$$

$$FT = 1 - \exp(\frac{dG_R + n * dP}{x * R * TK})$$

Figure 24 Combination of experimental and biogeochemical model data.

$$r = k * [X] * \frac{mD}{mD + kD} * \frac{\left(\frac{[X]}{mA}\right)}{\left(\frac{[X]}{mA}\right) + kA} * FT \qquad\qquad FT = 1 - \exp\left(\frac{dGR + n * dP}{x * R * T}\right)$$

Rate of iron reaction (r) can be expressed by the above equation, where k is reaction rate constant, X is biomass concentration, mA and mD are molality of electron acceptor and donor respectively, kA and kD are half saturation constants for electron acceptor and donor respectively. Thermodynamic potential factor (F_T) is calculated by second equation where dG_R is the free energy change of the metabolic reaction in kJ/mol, m is the number of ATPs produced, dG_P is the free energy change of ATP synthesis in kJ/mol, X is the average number of times the rate determining step occurs, R is the gas constant and T is absolute temperature (*Jin et al., 2013*).

RESULTS

Microbial reduction of BFA

Prior to inoculation, fluorescence data were acquired for all the samples (Table 10). Fluorescence index (FI) for BFA samples (K12.1, K10.2 and K8.3) was found to be 1.43, 1.36 and 1.38 respectively while 1.50 for KSW. Fluorescence data was acquired for BFA (K12.1) and SRFA after incubating with clean iron reducing bacteria cells for five days with growth nutrients and anaerobic conditions. The results revealed the decrease in spectral slope ratio (S_R) by 26.04 % and 5.42 % respectively in K12.1 and SRFA sample. Fluorescence index (FI) was increased by 5.5 % in K12.1 sample and by 11.7 % in SRFA sample. Humification index (HIX) was decreased by 26.41 % in K12.1 and by 25.18% in SRFA sample.

Table 10 Optical properties of BFA samples measured just before the experiment and changes in properties of two samples K12.1 and SRFA. All the indices are dimensionless.

	Before Reduction				After Reduction			
	S_R	FI	FrI	HIX	SR	FI	FrI	HIX
KSW	0.75	1.50	0.54	16.68	-	-	-	-
K12.1	0.73	1.43	0.54	15.45	0.54	1.51	0.54	11.36
K10.2	0.72	1.36	0.51	11.64	-	-	-	-
K8.3	0.96	1.38	0.52	15.48	-	-	-	-
SRFA	0.74	1.24	0.42	22.33	0.70	1.39	0.42	16.70

Electron shuttling by Bangladesh Fulvic Acids

Using 4 different types of Bangladesh fulvic acids (BFAs), we found the Fe(III) was reduced to Fe(II) in each electron shuttling experiment. For sample K12.1, 7 data points were recorded over time showing that after 8 hours 95% of Fe(III) was converted to Fe(II) and after 4 hours 64% of Fe(III) was converted to Fe(II). Between 328.07 µM and 530.43 µM of Fe^{2+} was produced over the 8-hour period. In electron shuttling experiments with KSW, KS10, and KS8 fulvic acids, we allowed Fe(III) to react for 4 hours. KS8 had the highest conversion of Fe(III), with 87% (489 µM) converted to Fe(II) (Table 11). Although AQDS and SRFA were microbially reduced and reacted with the Fe^{3+} solution, they produced 51.05 µM and 103.73 µM, respectively, immediately upon reaction, and only 271.67 µM and 134.05 µM after 24 h of reaction time (Table 11).

Table 11 Fe^{2+} produced during abiotic reduction of Fe^{3+} by Bangladesh fulvic acids and average % conversion of Fe^{3+}.

Sample	Time (hours)	Fe^{2+} (µM)	Average Conversion %
KSW	4	352.73 ± 2.84 (350.52 – 355.93)	0.63
K12.1	0	328.07 ± 2.66 (326.1 – 331.1)	0.59
	2	332.72 ± 1.63 (331.68 – 334.60)	0.60
	4	358.31± 2.80 (356.45 – 361.53)	0.64
	5	489.42 ± 7.06 (472.63 – 486.38)	0.86
	6	510.54 ± 4.54 (507.52 – 515.76)	0.91
	7	516.70 ± 2.83 (514.85 – 519.96)	0.92
	8	530.43 ± 3.059 (528.45 – 533.95)	0.95
K10.2	4	363.79 ± 15.76 (351.22 – 381.46)	0.65
K8.3	4	489.03 ± 4.1 (486.24 – 493.73)	0.87
SRFA	0	103.73 ± 0.27 (103.42 – 103.92)	0.19
SRFA	24	134.05 ± 1.71 (132.62 – 135.95)	0.24
AQDS	0	51.05 ± 1.48 (49.62 – 52.57)	0.091
AQDS	24	271.67 ± 2.17 (269.24 – 273.39)	0.49

Influence of HS on growth of bacteria

A population of Geobacter metallireducens was incubated using sodium acetate (2 mM) as the electron donor and Goethite (10 mM) as the solid phase electron acceptor (Fe^{3+}), with and without SRFA (6 mgL^{-1}). Growth of *G. metallireducens* was monitored by measuring Fe^{2+} using Ferrozine method (Figure 26). When acetate (primary electron donor) was not added to the system, Fe^{2+} increased from 0.36 µM to 35.8 µM only. With acetate but without SRFA, the Fe^{2+} concentration increased from 0.37 µM to 260.6 µM. In the presence of SRFA, the Fe^{2+} concentration increased from 0.43 µM to 366.04 µM. The rate of Fe^{3+} reduction was also observed

to be faster in presence of SRFA than in its absence. Our biogeochemical model calibrated with experimental data predicted that the maximum Fe^{2+} would have been produced ~2.5 days early in presence of SRFA
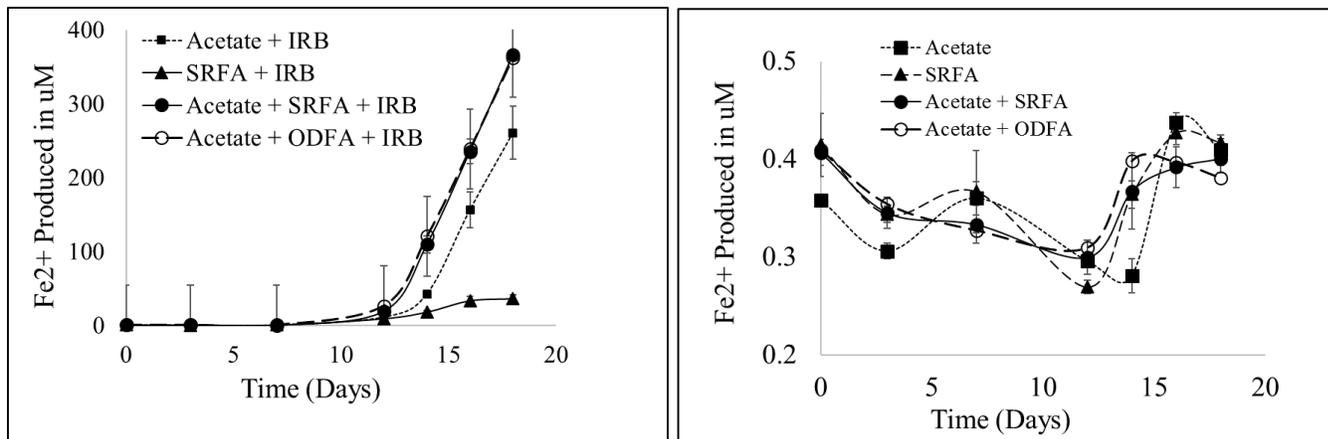
Figure 29: Graph to left shows the Fe^{2+} generated during growth of *G. metallireducens* in different mediums (only with acetate, only with SRFA/ODFA and with both acetate and SRFA/ODFA). The graph to the right shows the blanks i.e. Fe^{2+} measured in mediums without *G. metallireducens*.

than that in the absence of SRFA. The reaction rate constant for microbial Fe^{3+} reduction was estimated as $10^{-3.82}$ mol.mg^{-1}. s^{-1} in absence of SRFA and $10^{-3.69}$ mol.mg^{-1}s^{-1} (~1.33 times greater) in its presence, Response of microbial growth to various environmental parameters was also evaluated using sensitivity analysis. It was observed (Figure 30) that the increase in pH decreases the rate of growth and Fe^{3+} reduction. It was also observed that concentration of electron acceptor (Fe^{3+}) was not a major limitation for microbial growth. The presence of 0.8 mM Goethite was found to be enough to achieve maximum efficiency of Fe^{3+} reduction. At higher Goethite concentrations (up to 50 mM), the efficiency of reaction remained constant at maximum value.
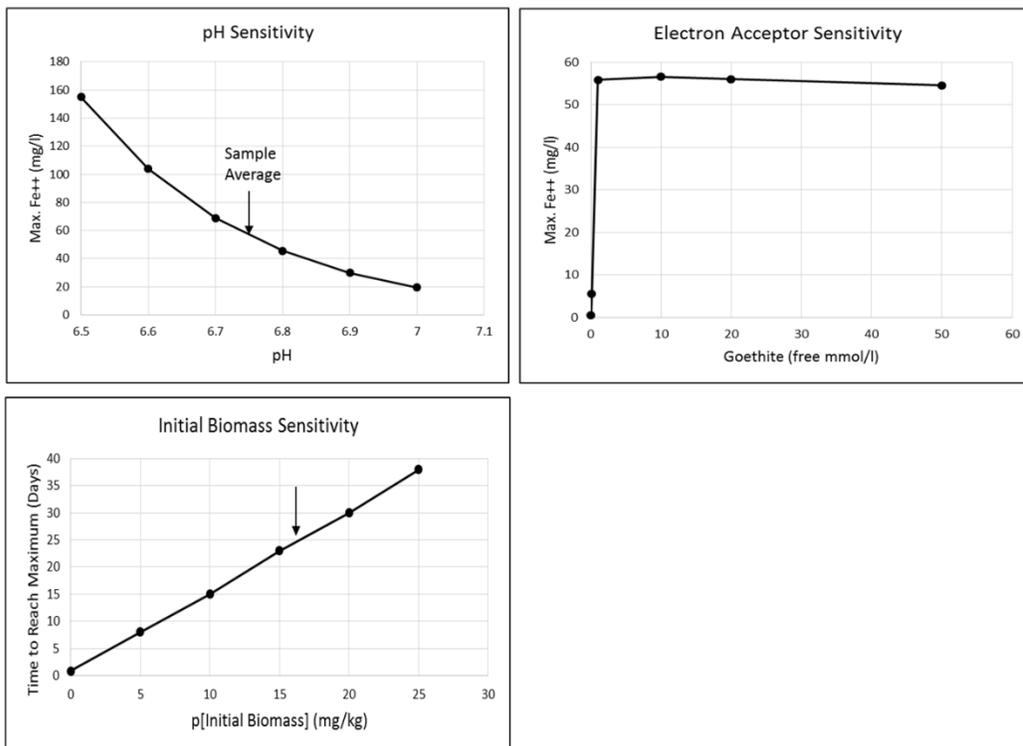
Figure 25 Sensitivity of pH (top left), electron acceptor concentration (top right) and initial biomass concentration (bottom left) on microbial iron reduction.

DISCUSSION

In laboratory studies, the role of HS as intermediate electron acceptors in microbial respiration of iron, sulfate and nitrate reducing bacteria, has been well established (*Lovley et al., 1996, 1998 and 1999; Scott et al., 1998*). Here, we show for the first time that humic substances isolated from groundwater and surface water in Bangladesh are capable of shuttling electrons to from Geobacter to Fe(III). After the microbially reduced BFAs were filtered through a 0.2-micron sterile filter and the filtrate was reacted with Fe^{3+}, the generation of Fe^{2+} (Figure 25 and 26) can be attributed solely to abiotic iron reduction by the reduced BFA. Interestingly, the older KW8 fulvic acid, which had the most terrestrially-derived characteristics (low FI), produced a greater number of moles of Fe^{2+} abiotically than the other fulvic acids, which had higher protein-like

fluorescence. This greater electron shuttling capacity of the more terrestrially-derived fulvic acid is consistent with the notion that in groundwater with higher fulvic acid concentrations and greater terrestrially-derived DOM, As concentrations will be higher because of the ability of humic substances to participate in electron shuttling reactions (Mladenov et al., 2010; 2015). Our results further show that as FI of the BFAs decreased (signaling more lignaceous and terrestrially derived organic matter), the moles of Fe^{2+} produced after 4 h of reaction increased ($R^2 = 0.80$). Indeed, the BFAs with the fresher and more microbially-derived organic matter, highest protein-like fluorescence, and lowest groundwater As and Fe concentrations had lower Fe^{3+} conversion rates (at 63% or 19.70 mg L^{-1}) in 4 hours of reaction than the older, more lignaceous KW8 fulvic acid (Table 11).

The results showing that the electron shuttling ability of SRFA was much lower than that of the native fulvic acids indicated that there is great variability among fulvic acids in terms of their chemical reactivity. The more rapid conversion of Fe(III) by the BFAs suggests that the humic moieties in groundwater in the Bengal Basin are more well-suited to electron transfer than those isolated from a surface water system (the Suwannee River), even if the DOM of that system is also characterized by lignaceous and terrestrially-derived compounds.

Fluorescence signature

An increase of 5.51% in FI was observed in the sample that was primarily characterized as terrestrially-dominated with FI of 1.432, which increased to 1.51 after 7 days of incubation with bacterial cells. However, it is important to note here that, FI was measured in the samples after the acetate was added. This result is consistent with prior studies that report increases in FI to be associated with microbial activities (*McKnight et al., 2001; Cory and McKnight, 2005*). Similarly, S_R calculated by taking the ratio of two spectral slopes, $S_{275-295}$ which is indicative of molecular

weight and $S_{350\text{-}400}$ which is indicative of contributions from terrestrially derived DOM (*Helms et al., 2008*) was 0.729 prior to incubation with bacterial cells. After the 7 days incubation, S_R decreased to 0.539 (26.04%), suggesting decrease in molecular weight possibly due to microbial processing i.e. microbial production or preservation of long wavelength absorbing substances (H*elms et al., 2008; Moran et al., 2000; Vahatalo and Wetzel, 2004*). Additionally, HIX of 15.45 for the sample which is typical for fulvic acids (Zsolnay et al., 1998) was decreased to 11.37 (26.42%) after 5 days of incubation. This decrease is consistent with other studies that report the decrease in HIX denotes change in strong humic character of DOM to a DOM with humic character still important but with weak recent autochthonous or a component of bacterial origin (*Huguet et al., 2009*). Similar trend was observed when SRFA was incubated i.e. 11.7 % increase in FI, 5.42 % decrease in SR and 25.18% decrease in HIX.

Increased rate of Fe^{3+} reduction

The control samples 1) Goethite and acetate, 2) Goethite and SRFA/ODFA, 3) Goethite, acetate and SRFA/ODFA without the bacterial cells, showed no Fe^{3+} reduction. In first case, it indicated that labile carbon was not able to reduce Goethite by itself, which is consistent with many other studies (*McArthur et al., 2004; Sengupta et al., 2008; Datta et al., 2011*). Secondly, SRFA seemed to be incapable of reducing Goethite in absence of bacteria. In other words, abiotic electron transfer seemed to be possible only when the HS were reduced by bacteria prior to come in contact with Fe^{3+} in solution or in mineral form. The third experiment suggested that in the presence of labile carbon and HS that are not microbially reduced, but in absence of bacteria, the biotic Fe^{3+} reduction was not possible which was in agreement with many other studies (*Bethke et al., 2008, 2011*). At the same time the inability of abiotic Fe^{3+} reduction by HS that were not microbially reduced, was underlined.

G. metallireducens, is also known to be capable of extracellular electron transfer to solid phase minerals in order to conduct metabolic activities (*Lovley et al., 1996, 1998; Nevin and Lovley, 2000; Bethke et al., 2008, 2011; Lee et al., 2013; Pi et al., 2015; Mladenov et al., 2015*). Our experiments with *G. metallireducens* grown in the presence of the solid phase electron acceptor, Goethite, and in the presence and absence of SRFA further showed that addition of fulvic acid did increase microbial reduction of Fe^{3+} to Fe^{2+}. The rate of microbial growth was also observed to be faster in presence of SRFA (Figure 29). Similar results were observed when ODFA was used instead of SRFA.

Nevertheless, microbial growth in experiments with acetate but without SRFA, followed a typical lag-growth phase curve and bacterial cells using the labile carbon electron donor directly reduced Fe^{3+}. In experiments with only SRFA, but with no other source of carbon, much lower Fe^{3+} reduction was observed (Figure 26). This result indicates that bacteria do not use SRFA as a primary electron donor. This is consistent with the findings of Harvey et al. (2002) and others showing that labile carbon is needed to set off the cascade of Fe-reductive dissolution. Interestingly, when bacterial cells were grown with acetate as well as HS, the Fe^{3+} reduction, once again followed the lag-growth phase curve, but also with increased rate. The presence of SRFA seemed to enhance the ability of bacterial cells to reduce Fe^{3+}, possibly via mechanism of abiotic electron transfer explained earlier section.

Environmental Implications

The role of sedimentary organic matter and HS in mobilizing Fe and As in reducing aquifers throughout the Bengal Basin has been discussed in many studies. However, the exact mechanism that HS interact with the microorganisms and the sources of iron required attention. Electron shuttling abilities of HS have been reported in laboratory studies and also linked with the

subsurface geochemistry. The process of abiotic electron transfers in this mechanism, however, have been addressed rarely in the literature, particularly for this specific geological setting.

In this study, we experimentally evaluated the ability of fulvic acid isolated from the groundwater in reducing Holocene aquifers of Bangladesh with varying dissolved As ($2 - 363$ µg/L) and Fe ($0.5 - 11$ mg/L) concentrations. As discussed in this study, the fulvic acid isolated from high As sites had higher abilities to reduce Fe^{3+} abiotically. This finding provides experimental evidence supporting a widely postulated electron shuttling mechanism responsible for As mobilization in the Bengal Basin. Further, using Goethite, a solid phase mineral, similar to sedimentary iron minerals found in Bengal Basin aquifers, we showed the increase in rate of Fe^{3+} reduction in presence of HS. Our results from the electron shuttling experiment showed that the fulvic acids extracted from Bangladesh aquifer were able to transform more Fe^{3+} to Fe^{2+} than SRFA. Together, it can be expected that BFA may have better capability of transferring the electrons to solid phase electron acceptor such as Goethite than SRFA. This finding supports the idea that the mechanism of electron shuttling holds true in environmentally relevant scenarios where major electron acceptor is iron minerals.

Chapter 8 - Groundwater Modeling

Introduction

Nearly 2 billion people worldwide rely on groundwater as the main source of drinking water (*Van Geen, 2013*). Shallow groundwater (<30 m) in south and south-east Asia is affected by microbial pathogens due to poor sanitation and excessive use of fertilizer and pesticides. However, deep groundwater resources experience less contaminants and require little or no treatment. A growing public health concern is focused on chronic exposure to natural and geogenic contaminants that are mobilized from sediment to groundwater under certain redox conditions. Within Bengal Basin in south Asia arsenic (As) contamination is reported as the greatest natural mass poisoning in human history (*Bhattacharya et al., 1997; Nickson et al., 1998; Smith et al., 2000; McArthur et al., 2001; Dowling et al., 2002; Paul, 2004; Ravenscroft et al., 2005, Routh et al., 2005; Acharya and Shah, 2007; Datta et al., 2011; Sankar et al., 2014*). Arsenic affected areas across the world include Vietnam, Cambodia, China, Taiwan, Mongolia, Chile, Mexico, Argentina, Germany and USA (*Smedley and Kinniburgh, 2002; Mukherjee et al., 2006*).

The regions affected by arsenic contamination are predominantly low-lying, topographically flat floodplains of rivers (*Winkel et al., 2008*). For example, the Bengal basin in south Asia is a flood plain of three major rivers Ganges – Meghana – Brahmaputra which provides groundwater to over 100 million people in south and south-east Asia. Likewise, the Mahomet Bedrock Valley aquifer in central Illinois, USA provides groundwater for over 1 million residents of central Illinois (*Kelly et al., 2005*). These sites have different geography, geology and hydrology, however, some of the key processes that mobilize arsenic into groundwater are similar, such as the reductive dissolution of iron oxides via oxidation of labile carbon by microorganisms (*Nickson et al., 1998; Van Geen et al., 2002; Zheng et al., 2005; Berg et al., 2008; Mladenov et*

al., 2010). The transport of dissolved organic matter through sedimentary organic matter with groundwater now is an important factor driving arsenic mobilization.

In this chapter, groundwater flow models of two arsenic contaminated sites, the alluvial aquifer in West Bengal, India and Mahomet Bedrock Valley (MBV) aquifer in USA are studied. A groundwater modeling approach is used to simulate the key processes in arsenic mobilization in two aquifer systems geographically distinct from each other but comparable in hydrologic and geologic settings. Movement of organic matter and its reactivity which mobilizes arsenic is modeled using reactive transport modeling.

Hydrogeology (West Bengal Aquifer)

The Bengal basin was formed as a result of India-Asia collision as the flexural subsidence of the Indian lithosphere created Ganges Plain foreland basin in front of the Himalayan mountain ranges during late Quaternary period (*Singh, 2004; Sinha et al., 2005*). This basin was named as the GBM delta since it is formed due to sediment deposition by the meandering of three major rivers Ganges, Meghana and Brahmaputra (*Morgan and McIntyre, 1959; McArthur et al., 2011; Mukherjee et al., 2008; Hoque et al., 2011*). The basin spans from the northern Himalayan mountain ranges to the southern Precambrian, Peninsular Indian craton. The regional study area consists of eastern Bengal basin, bounded by River Ganges, River Hooghly and Bay of Bengal, as shown in Figure 31.
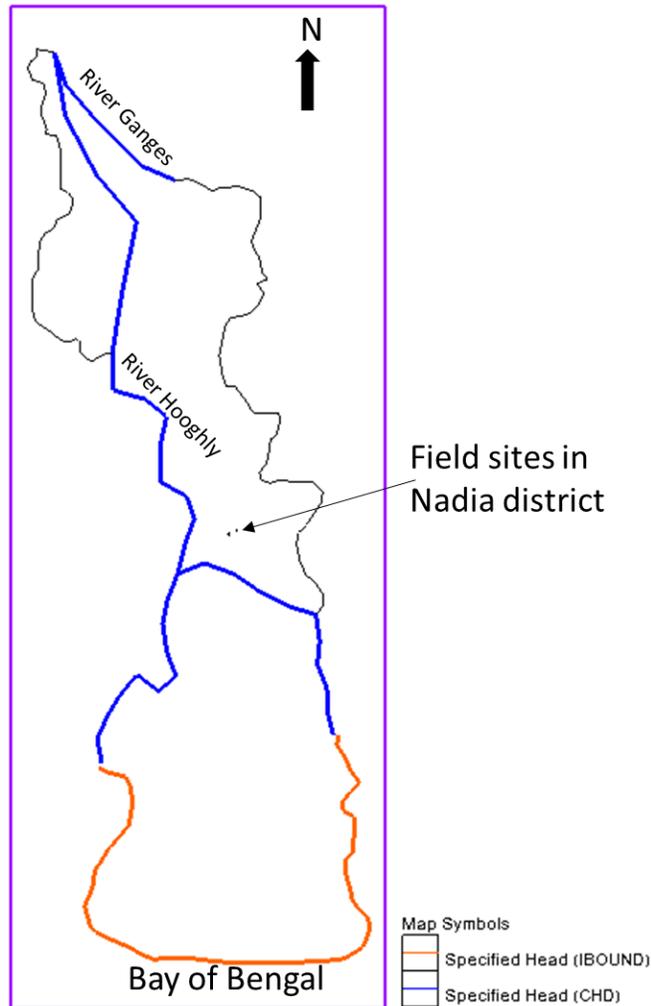
Figure 26 Regional model domain and boundary conditions.

The basin has been chrono-stratigraphically classified to hold two major types of sedimentary units older Pleistocene and younger Holocene unit (*Morgan and McIntyre, 1959; Mukherjee et al., 2008; Datta et al., 2011; McArthur et al., 2008 and 2011*). McArthur (2008) reported that the current paleo-inter-fluvial areas (highlands) in the basin were exposed and a thin layer of paleosol was deposited during the last glacial maximum (~20 ka before present) when sea level was substantially lower. The low-stand of sea level caused deep erosion in paleo-channels (current low-lying areas) in the basin by paleo-rivers followed by weathering due to heavy rainfall

during the warmer climate regime. Afterwards, a widespread paleosol of impermeable clay developed that has been found widely today across the basin (*McArthur et al., 2008; Hozque et al., 2011*). Rajmahal hills to West and north-west boundaries of the basin are basalt lava traps of lower Jurassic age and are the upper part of Gondwana system. The Shillong plateau (Garo or Khasi or Jaintia hills) is composed of Archean quartzite, slates and schists with massive granitic intrusions with interbedded basaltic traps, overlain by Eocene sandstones and limestones beds which mark the northeastern boundary of the Bengal Basin. Tripura hills and Chittagong marks the northeastern and southeastern boundary of the basin, while the western boundary is marked by Chottonagpur plateau composed of granites, amphibolite, carbonates and quartzities of Precambrian age (*Morgan and McIntyre, 1959*). River Ganges from northwest and River Brahmaputra from northeast brings sediments from Himalayas, River Meghana brings sediments from Shillong Plateau (*Morgan and McIntyre, 1959*). The Regional stratigraphy and commonly found sediment types are shown in Figure 32.

The hydrological controls in the Bengal basin have been discussed in Mukherjee et al., (2007). The Bengal basin groundwater system is influenced by rainfall due to the southeast monsoon wind, with October/November to May/June considered to be the dry seasons while June/July to September/October are wet seasons. CGWB (1994) reported the annual rainfall ranges from 1200 mm to 2000 mm and in the delta region, precipitation exceeds annual potential evapotranspiration (*Allison, 1998*). Frequent floods occur in the lowlands of the basin due to heavy rainfall during the monsoon period and the snow melt from Himalayas.

Given the flat topography, the northern part of the Bengal basin has a hydraulic gradient of 1 m/km while the southern part near the delta region has lower hydraulic gradient of 0.01 m/km (*Mukherjee et al., 2007*). Alluvial aquifers in this area have been found to be highly productive in

terms of available pumping rates with water table mostly within 15 m below ground level. Although seasonal variations occur based on irrigation pumping, the average yearly water table remains consistent, suggesting that there is sufficient recharge replenishing the groundwater systems (*BGS/DPHE, 2001*).

The estimated transmissivity (T) values vary from 3300 to 7000 m2/day in northern district of Murshidabad, 5000 to 8800 m2/day in North 24-Paraganas and 500 to 3000 m2/day in South 24-Paraganas, the hydraulic conductivity (K) have been reported to vary from 10 to 100 m/day (*BGS/DPHE, 2001, Figure 33*) and the porosity of alluvial aquifers have been reported to be 0.2 (*Harvey, 2002*). Natural groundwater flux to the Bay of Bengal from Bengal basin was estimated to be 2E11 m3/year which was 19% of the total surface water flux (*Basu et al., 2001*) and 15% of the Ganges-Brahmaputra river flux (*Dowling et al., 2003*). The river Bhagirathi – Hooghly is considered to be a losing stream along most of its length and recharges the shallow aquifers (*Ghosh and Mukherjee, 2002*).
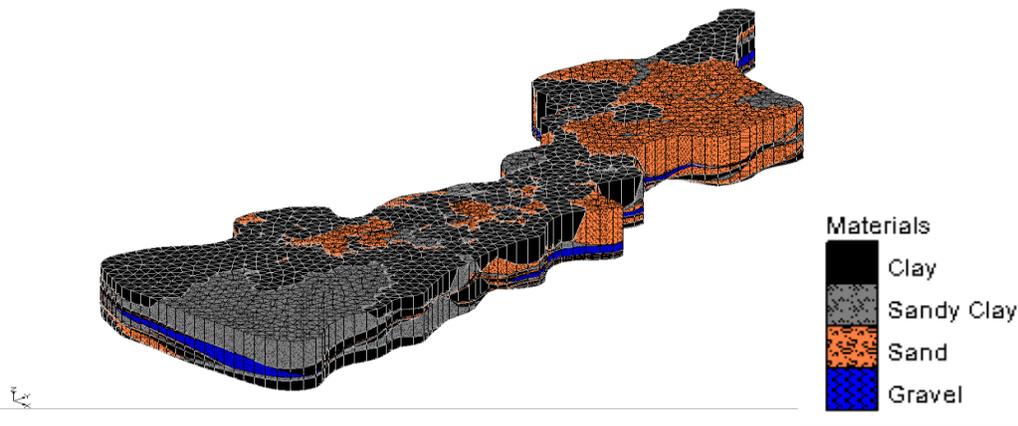
Figure 27 Regional stratigraphic model based on borehole data from Mukherjee et al., 2007
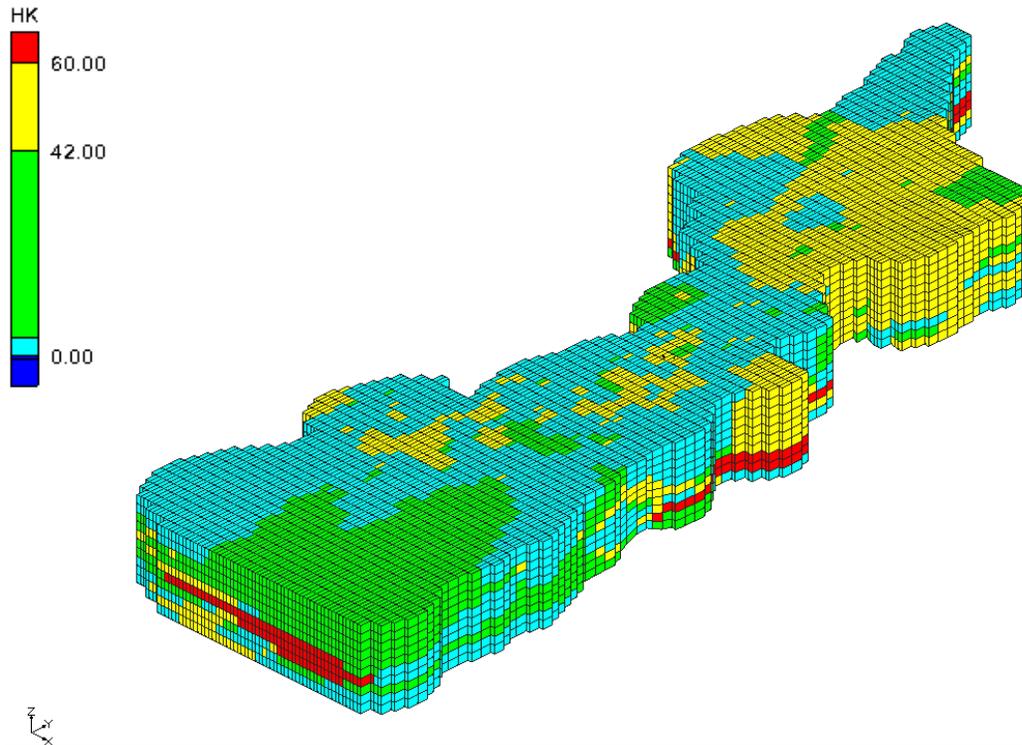
Figure 28 Hydraulic conductivities in regional model

Flow Model (West Bengal Aquifer)

The regional model area is bounded in the north, west and east by the river Ganges, Hooghly and Ichamati Rivers respectively and to the south by the Bay of Bengal. The study area is 335 km in length and 110 km in width and a 3-D rectangular grid of cell size 1.5 Km (West – East), 4 Km (North-South) and 30 m in depth was used to map hydrologic boundaries and stratigraphy. The rivers were defined as specified head boundaries, with the heads at nodes defined using SRTM-90m DEM. The Bay of Bengal has a constant specified head of 0 m. The initial heads in all the cells were set to be equal to the surface elevations, defined by the DEM. A uniform recharge of 1.8 mm/year was applied to the top layer of model area as estimated by Mukherjee et al. (2007) from seasonal rainfall, evapotranspiration and irrigation return flow. Groundwater abstraction of 0.06 mm/year was defined using evenly distributed wells across the study area

pumping at 20 m depth based upon estimated pumping discharges. All hydrological and geological units were georeferenced by projecting to UTM Zone 45 coordinate system with WGS84 as the datum and the regional model was run as a steady state model. Heads were computed (Figure 34) by Newton-Raphson formulation for USGS MODFLOW-2005 with upstream weighting (UPW) flow package for improved solution in unconfined groundwater flow conditions (*Niswonger et al., 2011*).
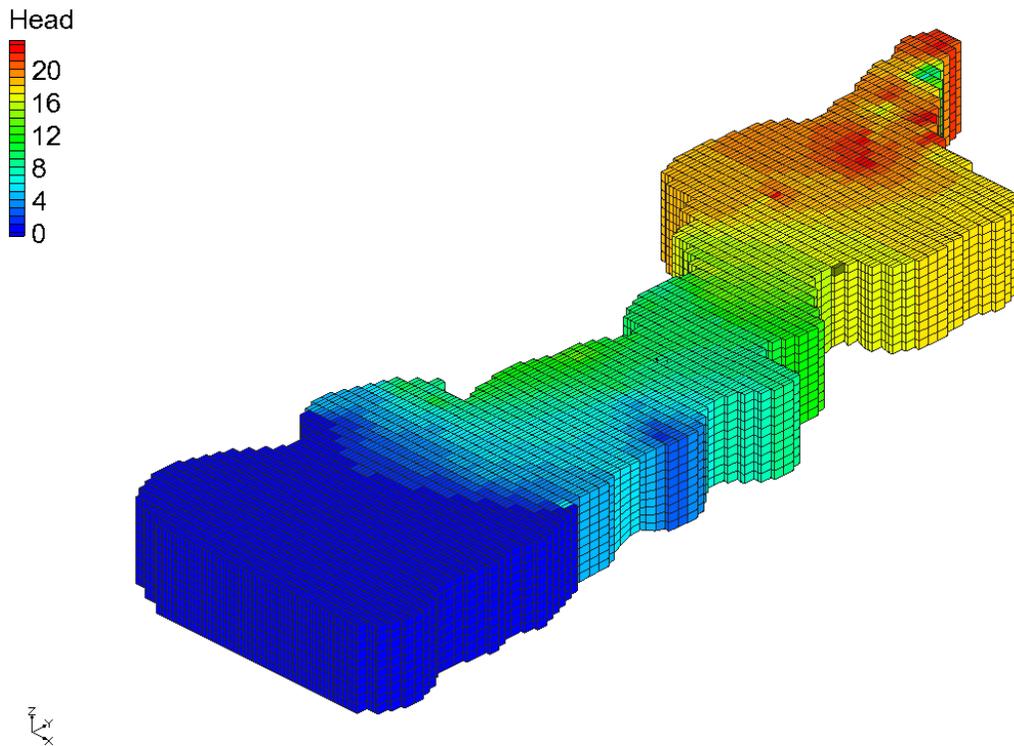
Figure 29 Hydraulic heads (in m above mean sea level) computed in the regional model

A local scale model was constructed using the regional model in two steps. First, a grid frame of 10 Km (West-East) and 16 Km (North-South) was mapped on regional model with the study sites in Nadia district in the center of the grid frame. The model boundaries were set as specified head boundaries and the heads at four corner nodes were defined by the heads computed from the regional model. A telescopic grid approach was used to obtain higher resolution in an

intermediate model and the new grid was designed with cell size of 103 m x 169 m. The starting

heads and the surface elevations were defined by interpolating (IDW) the layer data from regional

model. The local stratigraphy was defined by interpolating (Figure 35) from 3-D regional

stratigraphy model and heads were computed using a steady state MODFLOW model (Figure 35).

The local model was further refined for a smaller grid frame of 4.9 Km (West-East) and 2.2 Km

(North-South) with a grid cell size of 50 m x 22 m x 30 m. Once again, head specified boundary

conditions were defined from the heads computed in intermediate scale model. The heads

computed (Figure 36) in this local model were used for transport analyses.
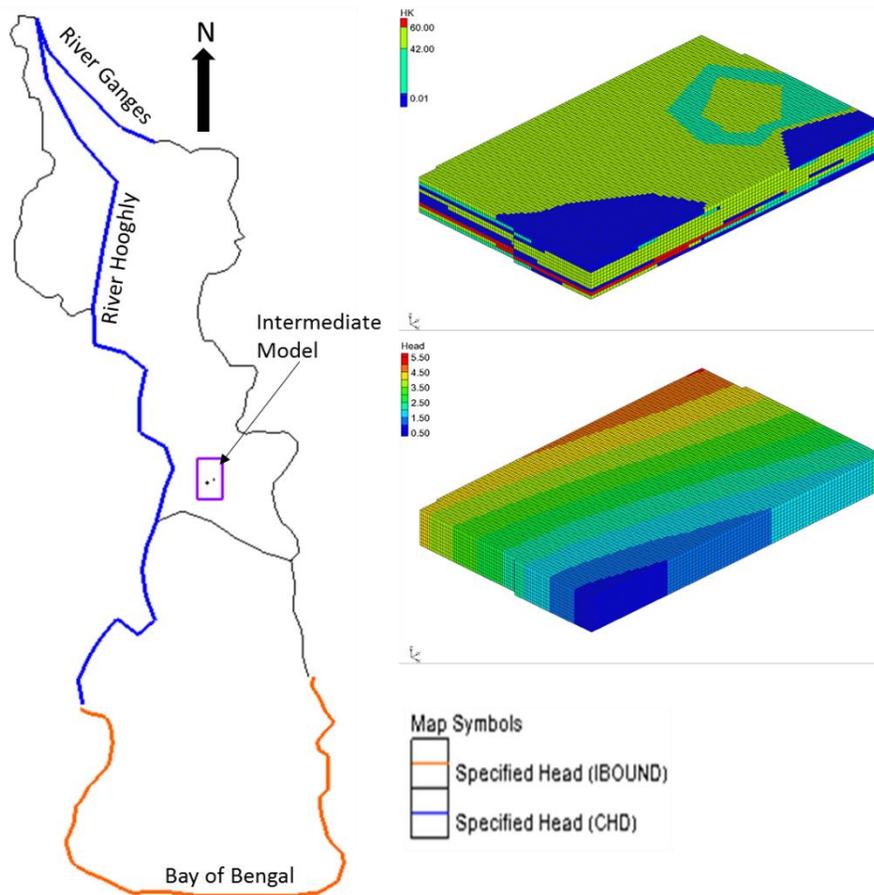
Figure 30 Location of the grid used for local model 1 (left), hydraulic conductivity of intermediate model (top right), hydraulic heads (in m above mean sea level) computed for intermediate model (bottom right)
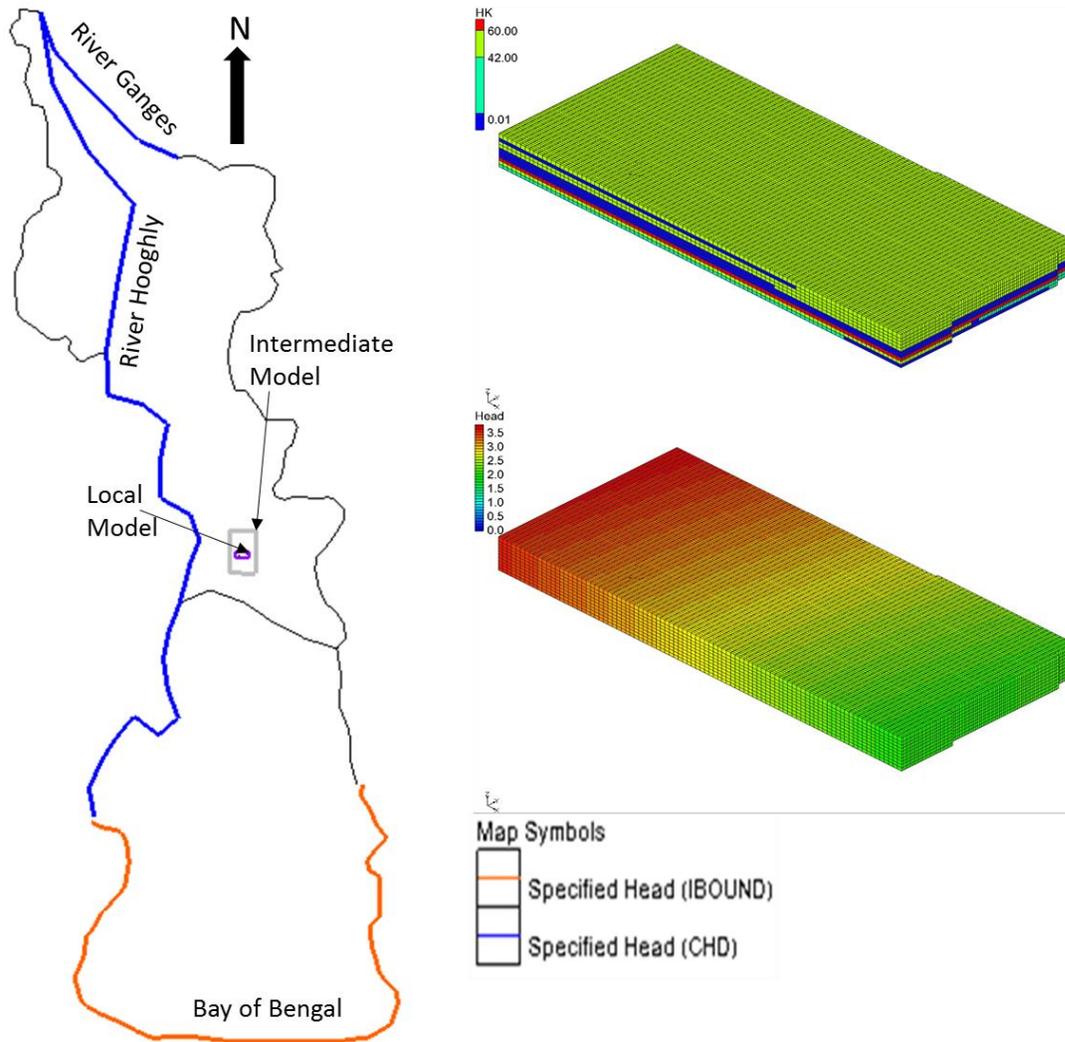
Figure 31 Location of the grid used for local model (left), hydraulic conductivity of local model (top right), hydraulic heads (in m above mean sea level) computed for local model (bottom right)

Transport Model (West Bengal Aquifer)

Acetotrophic iron reduction was modeled in the local model domain using a modified Monod rate law (*Roden, 2006; Jin et al., 2013*) with Fe (III) as electron acceptor. The fate and transport of an electron donor in a multidimensional saturated porous media was modeled using,

$$\frac{d[D]}{dt} = -\frac{\mu m}{RD} * \left([X] + \frac{\rho[X']}{\phi}\right) * \left(\frac{[D]}{KD + [D]}\right) * \left(\frac{[A]}{KA + [A]}\right)$$

Where, [D] and [A] is the concentrations of electron donor and acceptor respectively in mgL^{-1}, μ_m is the rate of substrate utilization in day^{-1}, R_D is retardation factor for electron donor, [X] and [X'] are concentrations of aqueous phase and solid phase bacteria in mgL^{-1} and $mgkg^{-1}$ respectively, K_D and K_A are half-saturation coefficients for electron donor and acceptor respectively in mgL^{-1}. It was assumed that the degradation of electron donor occurs only in the aqueous phase.

The fate and transport of an electron acceptor Fe^{3+} in the aquifer was modeled using,

$$\frac{d[A]}{dt} = -\frac{YA/D * \mu m}{RA} * \left([X] + \frac{\rho[X']}{\phi}\right) * \left(\frac{[D]}{KD + [D]}\right) * \left(\frac{[A]}{KA + [A]}\right)$$

Where, $Y_{A/D}$ is the stoichiometric yield coefficient for electron acceptor and donor, R_A is the retardation factor for electron acceptor. Then the fate and transport of bacteria was modeled using,

$$\frac{d[X]}{dt} = \frac{Kdet * \rho * [X']}{\phi} - Katt[X] - Ke[X] - YX/D * \mu m * \left([X] + \frac{\rho[X']}{\phi}\right) * \left(\frac{[D]}{KD + [D]}\right) * \left(\frac{[A]}{KA + [A]}\right)$$

where, K_{det} and K_{att} are bacterial attachment and detachment coefficients in day^{-1}, $Y_{X/D}$ is the stoichiometric yield coefficient for the biomass and electron donor. The growth of solid-phase bacteria was modeled using,

$$\frac{d[X']}{dt} = \frac{Katt * \phi * [X]}{\rho} - Kdet[X'] + \frac{YX}{D} * \mu m * [X'] * \left(\frac{[D]}{KD + [D]}\right) * \left(\frac{[A]}{KA + [A]}\right) - Ke * [X']$$

Where K_e is the endogenous cell death or decay coefficient in day^{-1}. The stoichiometric equation for Acetotrophic iron reduction was described by the equation below.

$$CH_3COO^- + 8FeOOH_{(S)} + 15H^+ \rightarrow 2HCO_3^- + 8Fe^{2+} + 12H_2O \quad Log\ K = 82.854$$

The rate law for iron reducing bacteria was described (*Roden, 2006; Jin et al., 2013*) by equation below, with F_T as the thermodynamic potential factor.

$$r = k * [X] * \frac{mD}{mD + kD} * \frac{\frac{[X]}{mA}}{\left(\frac{[X]}{mA}\right) + kA} * FT$$

Transport was modeled using MT3DMS-RT3D (Figure 38). Three mobile species represent electron donor, electron acceptor and aqueous phase bacteria and one immobile phase represents bacteria attached to sediments were used and the stress period was set to 30 years with increments 1 year. Advection was modeled using standard finite difference method. Dispersion was modeled using longitudinal dispersivity values of 6, 10, 40 and 60 m for Clay, Sandy Clay, Sand and Gravels respectively with ratio of transverse to longitudinal dispersivity as 0.3 and the ratio of vertical to longitudinal dispersivity as 0.1 and porosity is 0.3. Sorption was accounted using a linear isotherm with reaction parameters $\mu_{max} = 3.16$ day^{-1}, $K_D = 0.05$ mgL^{-1}, $K_A = 14$ mgL^{-1}, $Y_{X/D} = 0.1525$, $Y_{A/D} = 4.75$, $K_{decay} = 0.0009$ day^{-1}, $K_{att} = 70$ day^{-1} and $K_{det} = 1$ day^{-1}. The initial concentrations of electron donor, electron acceptor, aqueous phase bacteria and solid phase bacteria were assigned as 0.02 mgL^{-1}, 20 mgL^{-1}, 2.0e-9 mgL^{-1} and 2.0e-9 mgL^{-1} respectively.

The particles were tracked backwards in time from the locations of sampling tube-wells within the study area to 10, 20 and 30 years (Figure 37) using a post-processor MODPATH. The constant concentrations of electron donor (100 mgL^{-1} in high arsenic site and 5 mgL-1 in low arsenic site) were assigned to the end points of the particles tracked to 30 years. This was done to ascertain whether DOM source could exist with this concentration at these locations and reproduce

what was measured in the field. This shows that the source of carbon must be closer than the 30-year travel zone.

The concentrations of electron donor (organic carbon) and dissolved Fe^{2+} which was the product of biogeochemical reaction were predicted by using a RT3D forward model (Figure 38). The concentrations of Fe^{2+} predicted by the model were compared with the measured Fe^{2+} concentrations at the end of 30 years. It can be seen from Figure 39 that the concentrations of Fe^{2+} at the end of 10 years were spatially varying within the study sites, but at the end of 30 years, all the sampling sites showed maximum Fe^{2+} concentration due to diffusion.
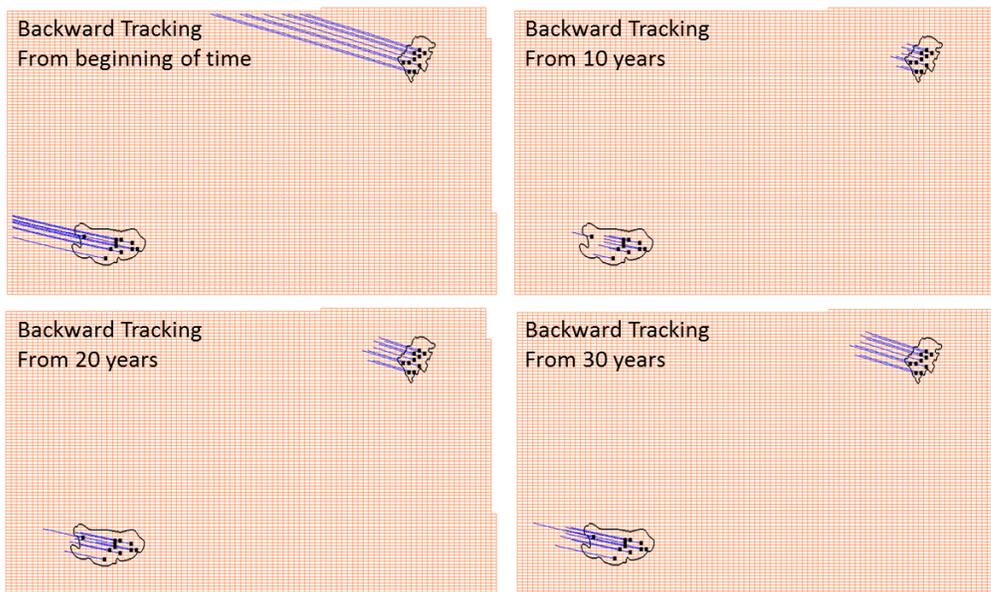
Figure 32 Particles path line tracked backward in time from the beginning of time (top left), from 10 years (top right), 20 years (bottom left) and 30 years (bottom right), Bengal basin aquifer.
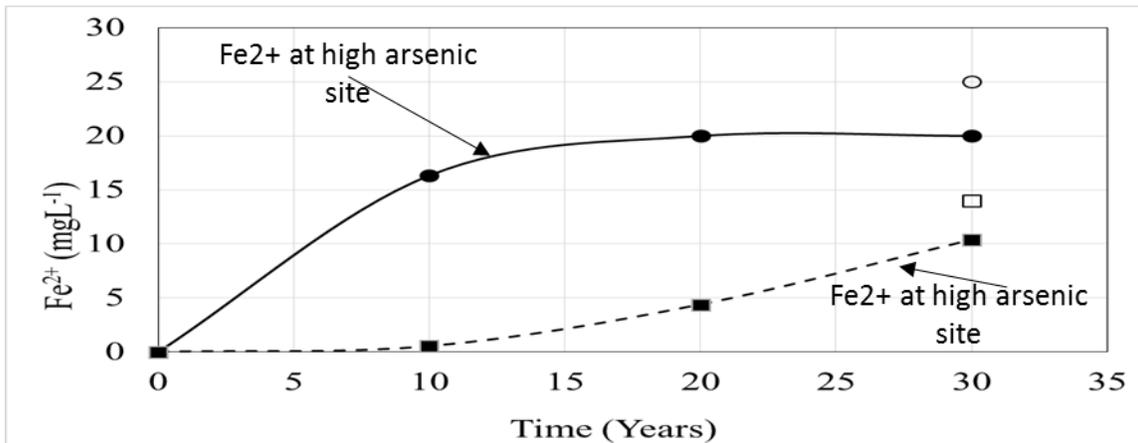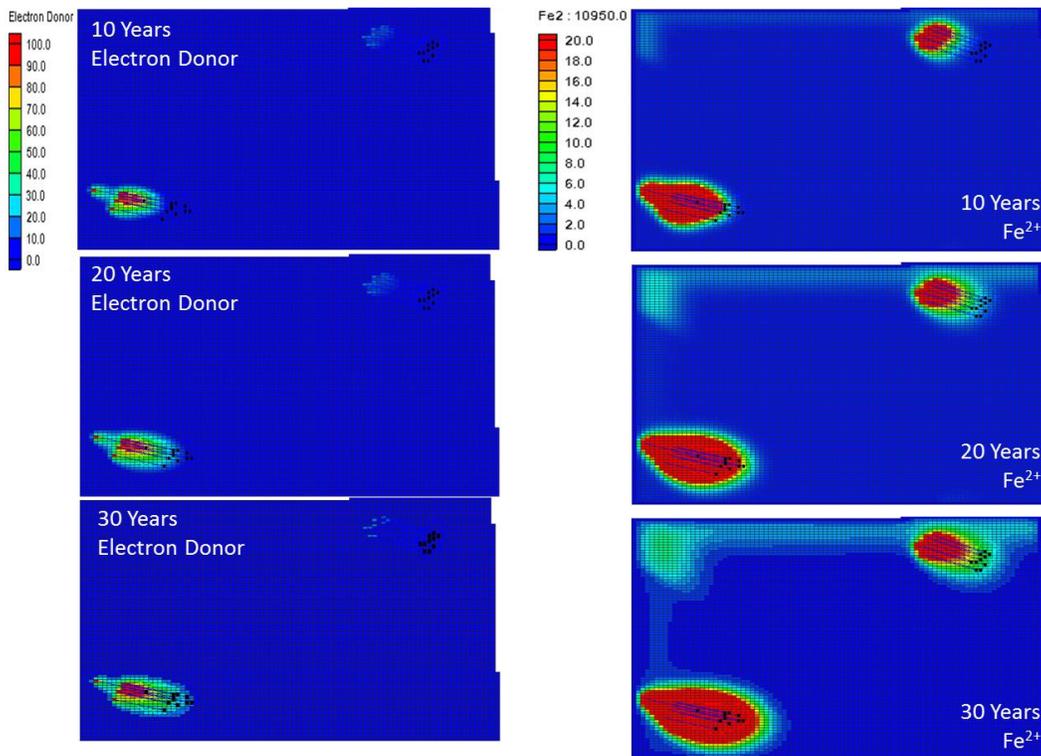
Figure 33 Transport of electron donor (left, top-bottom 10, 20 and 30 years), generation and transport of Fe^{2+} (right, top – bottom, 10, 20 and 30 years). Graph at the bottom shows the concentrations of Fe^{2+} at high arsenic site (filled circle) and at low arsenic site (filled box), open symbols indicate the observed values of Fe^{2+} in the field at respective study sites.

To evaluate the impacts of biogeochemical reaction if continued for another 30 years, the particles from the tube-well locations were tracked forward in time for 10, 20 and 30 years. The locations of the tube-wells were assigned a constant concentration of electron donor (100 mgL^{-1} in high arsenic site and 5 mgL-1 in low arsenic site) and Fe^{2+} concentrations were modeled forward in time for 10, 20 and 30 years (Figure 40). This illustrated that the persistent levels of Fe^{2+} that continue to exist in the study region, although in much dispersed pattern.
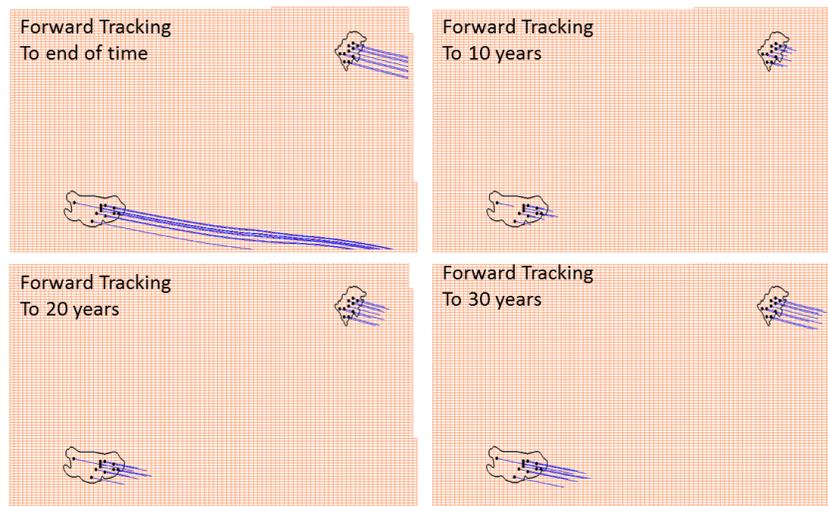
Figure 34 Particles path line tracked forward in time to the end of time (top left), to 10 years (top right), 20 years (bottom left) and 30 years (bottom right), Bengal basin aquifer.
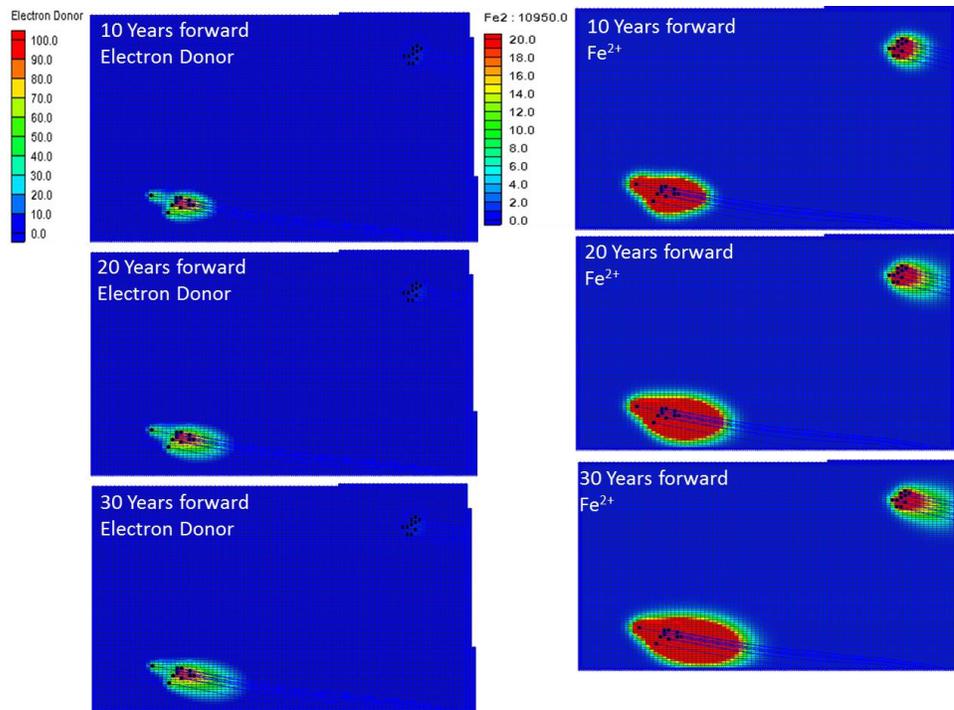
Figure 35 Transport of electron donor (left, top-bottom 10, 20 and 30 years in future), generation and transport of Fe^{2+} (right, top – bottom, 10, 20 and 30 years in future.

Hydrogeology (Mahomet Bedrock Valley Aquifer)

The Mahomet bedrock valley (Figure 39) follows an east-west trend and is located in east central Illinois and western Indiana. The sand member (Mahomet Sand Member) is composed of glacial outwash sand and gravel within the Mahomet valley lowland as by tills deposited during Pleistocene continental glaciation. This bedrock valley ranges from 13 -18 km in horizontal width and is incised in bedrock and buried beneath 100 m of Pleistocene glacial drift (Kempton et al., 1991). Clean sand and gravel (average 30 m thick and maximum 60 m) forms the main channel of Mahomet Bedrock Valley aquifer (Figure 41) with silty beds occur throughout. The Pennsylvanian, Mississippian, Devonian and Silurian rocks define the bedrock geology of this area (*Panno et al., 1994*), and are the western and eastern boundaries are formed by the Illinois and Indiana rivers. The groundwater flow in the aquifer is generally from east to west and the aquifer

122

discharges into the Mackinaw River (north-west), Sangamon River (south-west, south-east) and

Illinois River (west).
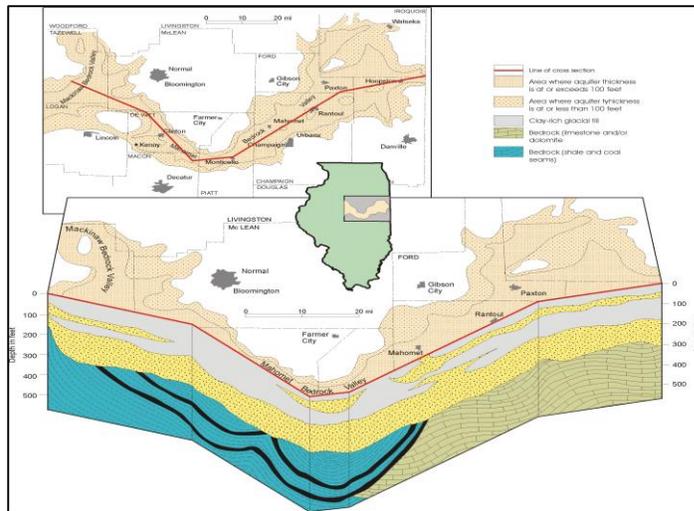
Figure 36 Location of Mahomet Bedrock Valley aquifer and section view (source: ISGS).
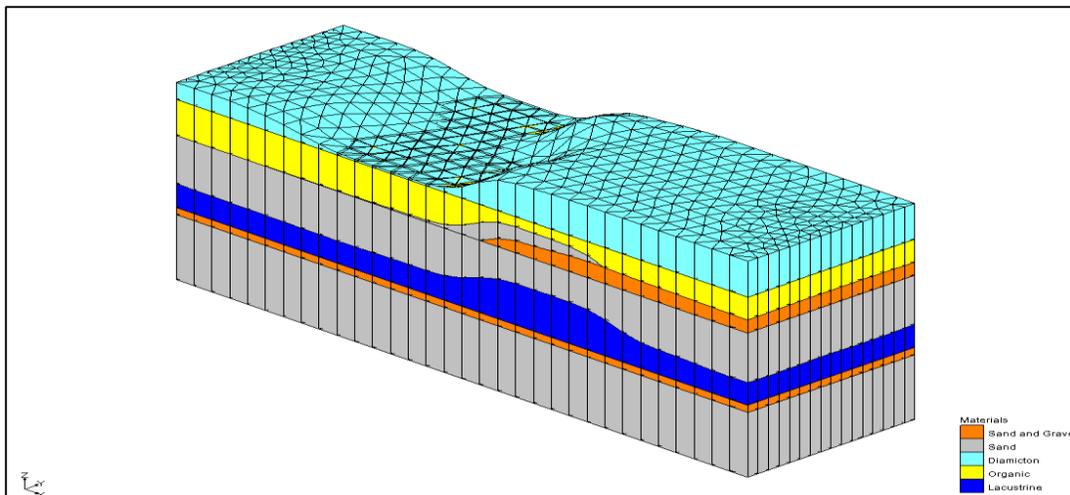
Figure 37 Stratigraphy of the proposed study area (Van Geen, 2013 IDRA proposal) near Bloomington, IL. The study area is in Tazewell and McLean counties and spans 30 km east-west and 10 km north-south.

Transmissivities for the sand member range from 7×10^{-4} to 8×10^{-2} m^2/s and were determined by pumping tests. The median hydraulic conductivity (Figure 42) was found to be 120 m/day and the vertical hydraulic conductivities range from 0.864 mm/day to 17.28 mm/day (*Kempton et al., 1991*). The hydraulic gradient is 19 cm/km (*Panno et al., 1994*), and vertical leakage of precipitation and snowmelt occurs through the overlying glacial deposits to recharge the aquifer. The estimated average annual recharge rate for the sand member in Mahomet aquifer is 250 m^3/day/km^2 (*Visocky and Schicht, 1969*). Analyses of dissolved organic matter quality was conducted for groundwater samples from proposed study area (*Van Geen et al., 2013*) and the details are provided in the Appendix.
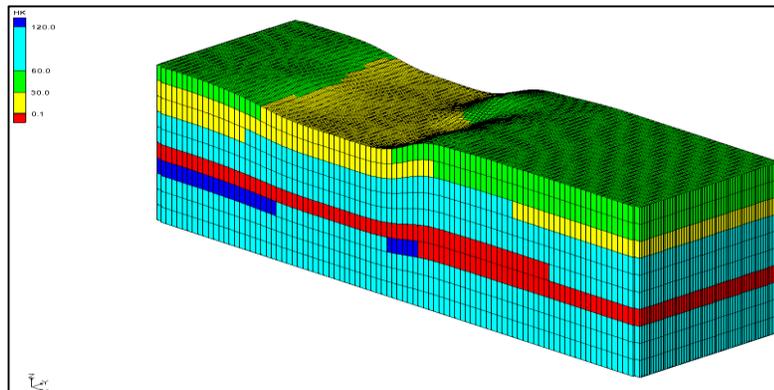
Figure 38 Hydraulic conductivities of the model domain defined by the study area in MBV aquifer.

Flow Model (Mahomet Aquifer)

The model domain in Figure 43 spans about 30 km east-west and 10 km north-south. A 3-D rectangular grid of cell size 318 m (east-west) and 135 m (north-south) and 10 m in depth was used to map hydrologic boundaries and stratigraphy. Heads boundaries were specified based on the heads computed in earlier study (*Van Geen et al., 2013*) and groundwater heads in the local model
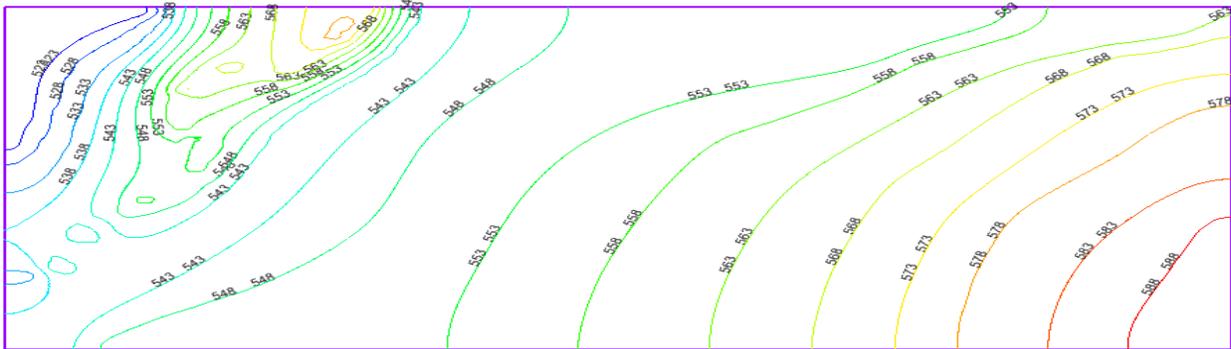
Figure 40 Groundwater heads (in ft above mean sea level) computed in MBV aquifer local model
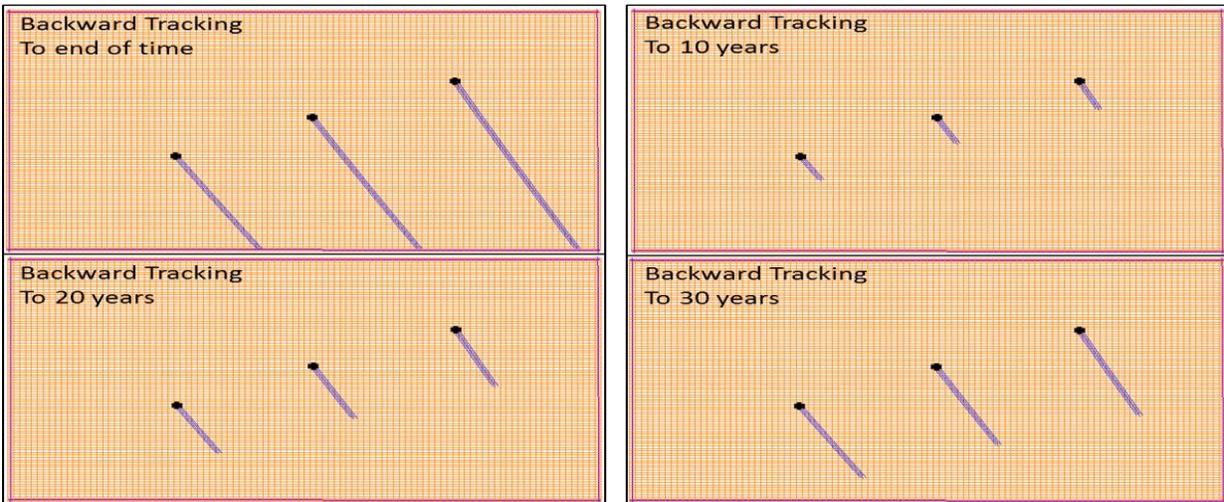
Figure 39 Particles path line tracked backward in time from the beginning of time (top left), from 10 years (top right), 20 years (bottom left) and 30 years (bottom right), MBV aquifer.

were computed (Figure 44) by running a steady-state MODFLOW model and were used for reactive transport analyses. This local model was constructed using the same telescoping mesh procedure described earlier for the Bengal Basin model.

The source of electron donor was located by tracking the particles from proposed drilling sites backwards in time for 10 years, 20 years and 30 years using MODPATH (Figure 45). Acetotrophic iron reduction reactive transport model described for Bengal basin aquifer study was also applied to MBV aquifer proposed study area (Figure 46).
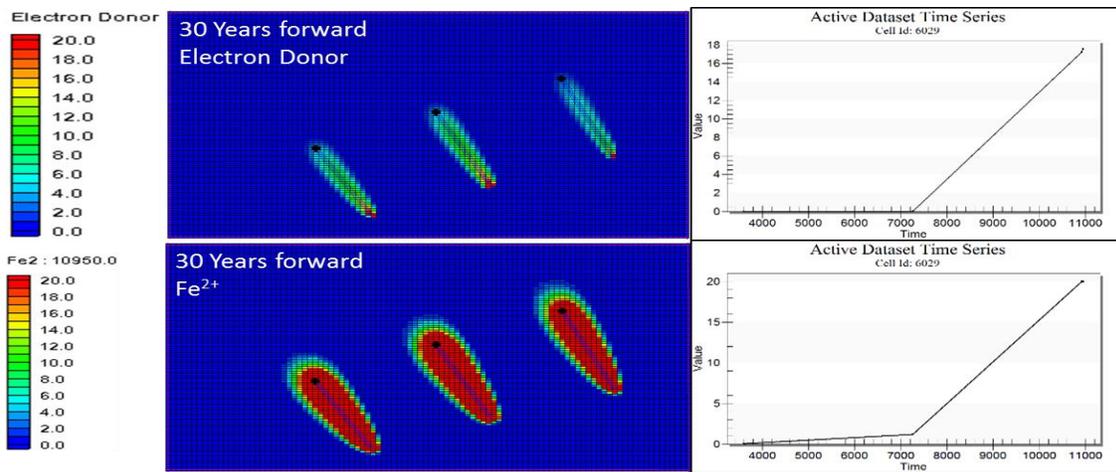
Figure 41 Transport of electron donor (top left) and increase in electron donor concentration at proposed drilling site 1 (top right), generation and transport of Fe^{2+} (bottom left) and increase in the concentration at proposed drilling site 1 (bottom right).

Conclusions

Groundwater models were constructed of two aquifers to study arsenic transport, with the results consistent with previous studies. Groundwater heads in the regional model of West Bengal aquifer ranged between 23.68 m on north and 0 m on south boundaries, while the heads in the local model 2 range between 3.7 m on north-western and 1.9 m on south-eastern boundaries. Major rivers Ganga and Hooghly recharge the aquifer and the groundwater in the study area (local model 2) is mainly recharged by the river Hooghly. The particles tracking post-processing at the local model 2 indicated that the groundwater traveled about 270 m in 10 years which translates to the groundwater velocity of 7.4 cm/day. The flow was mainly observed within the layers rather than across the layers. These results are in agreement with the flow model given by *Mukherjee et al., 2007*. In contrast, the groundwater heads in MBV aquifer local model ranged between 590 ft on south-eastern and 520 ft on north-west boundary. A particle was observed to travel 2.23 – 5.23 – 5.23 km in 30 years which translates to the groundwater velocity of 20.36 – 48.4 cm/day. This observation is in agreement with earlier studies (*Holm et al., 2004; Kelly et al., 2005; Van Geen et al., 2013*) which described the groundwater flowing into Mackinaw bedrock valley of the MBV aquifer.

Transport models were implemented using MT3DMS-RT3D, and the coefficients for arsenic reactive processes were used from the studies in chapters 5-7. These results were used to quantify the possible proximity of DOM sources to boreholes that reproduce their measured arsenic or iron concentrations. Reactive transport model in Bengal basin domain suggested that the source of electron donor may be within 500 m of the tube-wells sampled in the direction of the flow. In the contrast, due to higher groundwater velocity, in the MBV aquifer, the source of carbon may be within 5 km along the direction of the flow. These observations were made by simulating

the reactions over 30-year period, however, the concentrations of sedimentary organic carbon which serve as electron donor for iron reducing bacteria has been shown to be deposited during geologic time. In Bengal basin, presence of clay patches that are rich in organic matter are well-known. Flow of groundwater through these patches moves the organic carbon and it is then involved in mobilizing iron and arsenic. The reactive transport modeling provided an insight on how closely the source of electron donor needs to be so that diffusion does not overrule the transport process. Hence, this model helps understanding the patchy nature of organic carbon and its consequences on reductive dissolution of iron minerals and subsequent arsenic mobilization.

Chapter 9 - Pre and Post-Monsoon Quality of Dissolved Organic Matter in High Arsenic Sites (Nadia District) and Low Arsenic Sites (Hooghly District), West Bengal

Introduction

Arsenic (As) contaminated groundwater (>10 ugL-1, WHO guideline) in the alluvial aquifers of Ganges-Meghana-Brahmaputra basin in south Asia has been responsible for severe health threats to over 100 million people. Microbiological and geochemical processes are known to mobilize naturally occurring sediment bound As in the aquifer. Briefly, reductive dissolution of oxidized iron (Fe) minerals by iron reducing bacteria under reducing conditions has been attributed to release of dissolved Fe and As in the groundwater. The microorganisms utilize labile carbon primarily from older sedimentary depositions and also transported recently from surficial sources as an electron donor and abundant oxyhydroxides of iron serve as the primary electron acceptor. Sedimentary organic matter also contains significant amounts of humic substances that have undergone microbial processing. Microorganisms cannot utilize humic substances as a primary electron donor for the metabolic activities, however, humic substances accelerate the metabolism by serving as an electron shuttle between the bacteria and the electron acceptor (Lovley et al., 1996, 1998, 1999; Scott et al., 1998; Nevin and Lovley, 2000; Klapper et al., 2002; Kappler et al., 2004; Jiang et al., 2008; Wolf et al., 2009; Mladenov et al., 2010, 2015). Additionally, humic substances form aqueous complexes with dissolved Fe and As, which maintains their concentrations in the solution. In general, the presence, transport and reactivity of labile and humic organic matter are important factors in mobilizing As in the particular hydro-geologic setting in Bengal basin aquifer.

In West Bengal (India), one of the As-affected regions, shallow groundwater (<40 m deep) is the main source of drinking water. Typically, shallow aquifers of Holocene age (gray color sediments) have been found to be high in dissolved As concentrations while deeper and older aquifers of Pleistocene age (orange sediments) are low in dissolved As (Fendorf et al., 2010). The aquifers are recharged primarily by the monsoonal precipitation ranging between 1295-3945 mm during June-September. The water table fluctuates considerably from dry months (2.2 – 5.5 m) to wet months (0.1 – 6.4 m) below sea level (Majumder et al., 2016). Earlier studies showed that during monsoon, the organic carbon can be transported to the shallow aquifers when the surface waterbodies are hydraulically connected to the aquifer (*Kocar et al., 2008; Polizzotto et al., 2008; Lawson et al., 2013*). A recent study (Majumder et al., 2016) examined the influence of monsoonal recharge on hydrochemistry and showed a significant increase in As concentration during the post-monsoon season in Nadia district, West Bengal. This study also indicated the possibility of inflow of organic carbon to the aquifer during the monsoonal recharge. Thus the significantly high monsoonal recharge in this region may have important implications in transporting organic carbon in the aquifer as well as altering the chemical characteristics of dissolved organic matter (DOM) and hence in the arsenic mobility. However, little is known about the alterations in the chemical characteristics of DOM that may take place during monsoonal recharge processes in shallow aquifer.

In the current study, the emphasis is on characterizing the chemical quality of DOM in the groundwater during pre and post monsoon season. Shallow (50 to 150 ft) groundwater samples from two sites in Nadia district and deep (200 to 460 ft) groundwater samples from two sites in Hooghly district were collected during pre and post monsoon. Samples were analyzed for several chemical parameters and detailed spectroscopic analyses to characterize DOM.

Materials and Methods

Study Site
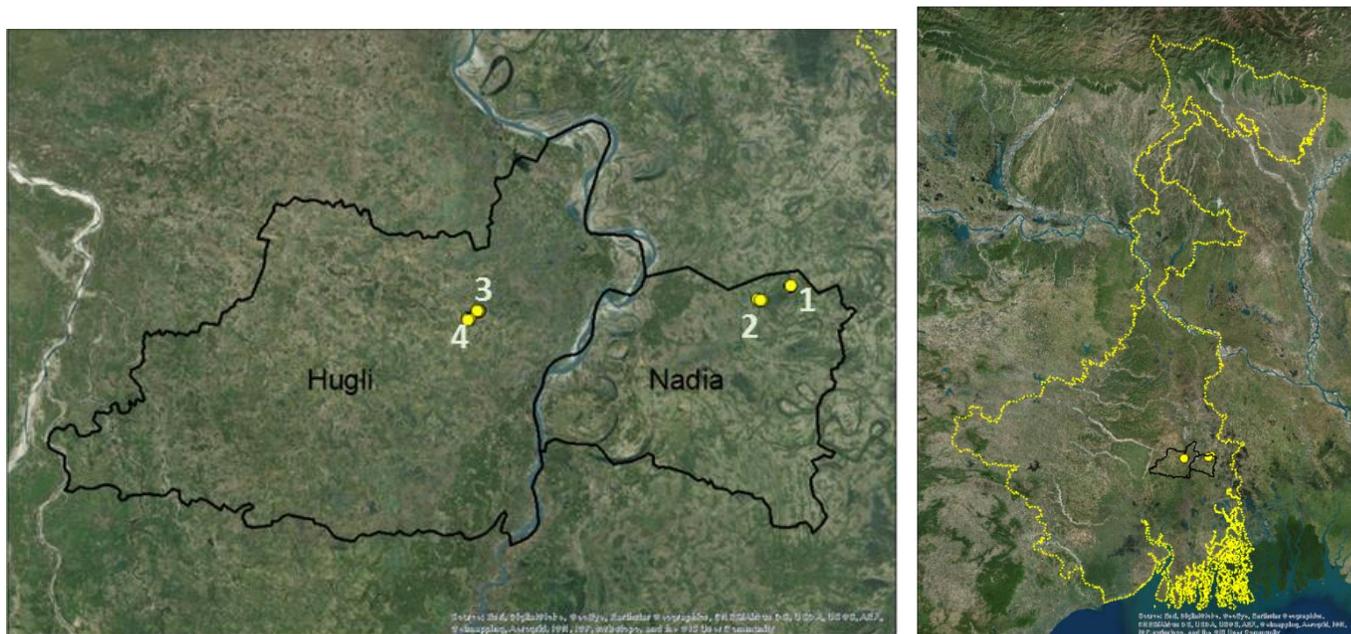
Figure 42 Map of study area (left) showing district boundaries and locations of sampling sites, location of sampling sites in the West Bengal state (right). (1) Chakudanga, (2) Shahispur, (3) Bele and (4) Radhanagar.

Groundwater samples were collected from existing drinking water tube wells at Chakudanga (23°4'57.42"N, 88°38'9.96"E) and Shahispur (23° 4'18.47"N, 88°36'34.96"E) located in Nadia district and at Bele (23° 3'40.55"N, 88°21'7.81"E) and Radhanagar (23° 3'18.22"N, 88°20'41.10"E) located in Hooghly district as shown in Figure 47. River Hooghly flowing north-south marks the boundary between Nadia and Hooghly district. Chakudanga, Shahispur sites are located ~12 km east of the river while Bele and Radhanagar sites are located ~12 km west of the river. Chakudanga and Shahispur sites overly on shallow alluvial aquifer of Holocene age with generally high dissolved Fe and As concentrations, while deeper older Pleistocene age aquifer occurs beneath other two sites (Mukherjee et al., 2007; Harald et al., 2013) with significantly lower dissolved Fe and As concentrations (Biwas et al., 2011; Bhowmick et al., 2013; Majumder et al.,

2016). All four study sites are within 25 km distance and receive the monsoonal recharge at similar rates. The detailed locations of sampled tube wells is shown in Figure 48.
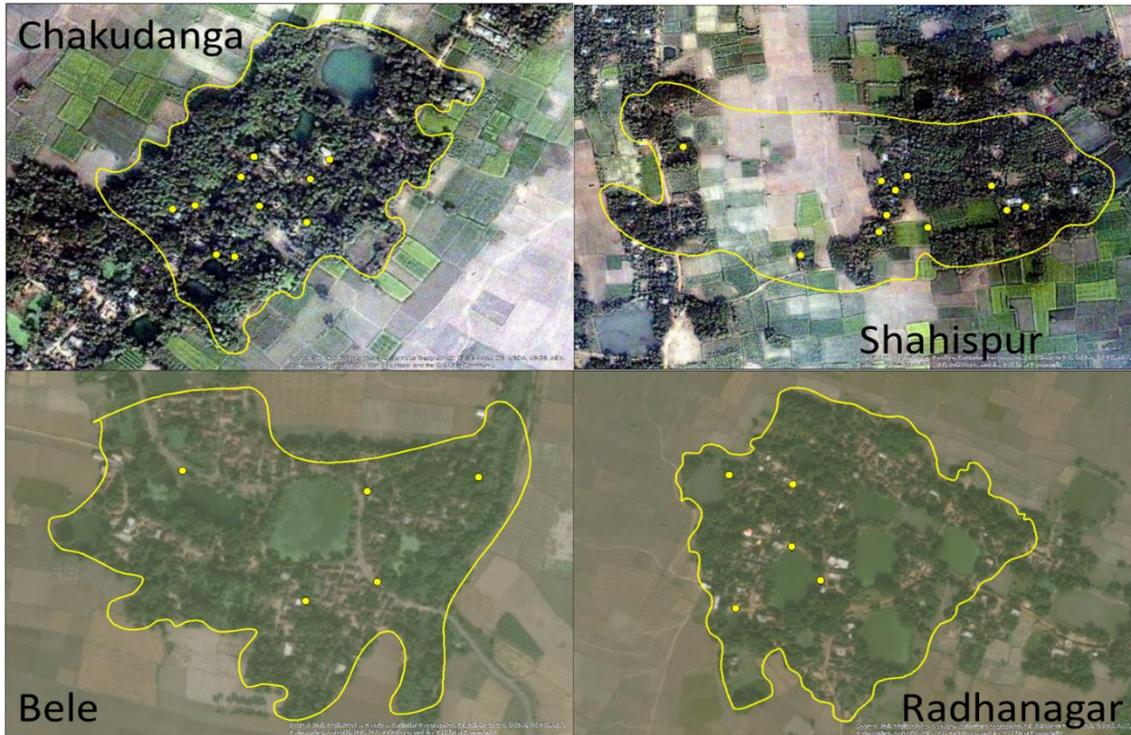
Figure 43 Locations of tube-wells sampled at four study sites (yellow circles)

Sample Collection and Storage

Groundwater samples were collected from each location during 4th-11th June 2015 (pre-monsoon) and 20th July – 13th August 2015 (post monsoon). The monsoon rains began around 15th June 2015 in the study area. Surface water samples (n = 10) were also collected only in July 2015 (post monsoon) as most surface water sources were dried during summer. Groundwater samples were also collected from four piezometers installed at Chakudanga and Shahispur. Geographic coordinates of all the tube-wells were recorded using a handheld GPS device.

Tube-wells were pumped for at least 45 minutes to remove accumulated water before collecting the samples. Three types of samples, 1) filtered acidified with 70% hydrochloric acid,

2) filtered acidified with 70% nitric acid and 3) filtered unacidified were collected in 60 mL and 125 mL HDPE bottles pre-rinsed with sample water. Filtration was done in the field by using a handheld vacuum pump device and 200 µL of stock acid was added immediately with pre-rinsed (300 mL of sample) GFF filters. All the bottles were appropriately labeled and stored at 4^0C in dark until analyzed. Groundwater from the piezometers was pumped using an electric pump for at least 1 hour before collecting the samples. Surface water samples were collected directly from the water body, at the center wherever possible.

Chemical Analyses

Dissolved oxygen was measured using a probe in the flowing water during the pumping while the pH was measured in stagnant water sample collected in a clean and rinsed container. Filtered sample (0.7 µm GFF) was used to measure alkalinity using a field titration kit (Chemetrics K9810 and K9815). Arsenic was measured using a color strips analysis kit (HACH 2800000 and HACH 2822800) and iron using (Chemetrics K6210 and K6210D) immediately after sample collection. Samples were transported to San Diego State University and Kansas State University for further analyses.

Filtered unacidified samples (1.5 mL) were tested for eight inorganic (chloride, bromide, fluoride, nitrate, nitrite, phosphate, sulfate and arsenate) and five organics (acetate, citrate, formate, lactate and oxalate) anions using Dionex Ion Chromatography System. Non-purgeable organic carbon (NPOC) and total nitrogen (TN) was measured using a Shimadzu Total Organic Carbon Analyzer (detailed protocol in Appendix) on samples acidified with hydrochloric acid. Total arsenic was measured using ICP-MS on samples acidified with nitric acid.

Spectroscopic Analyses of DOM

Absorbance and fluorescence data were acquired for filtered unacidified samples using Jobin Yvon Aqualog Fluorometer. Approximately 4 mL of sample was placed in a clean quartz cuvette of 0.01 m path length. Incident wavelengths ranged from 240 nm to 450 nm with increment of 3nm, and emission spectra were obtained from 212 nm to 619 nm with 3.28 nm increment. The integration time used was 1s. Ultra-pure water (18.3 MΩ cm Milli-Q) was used as a blank and for Raman normalization. Excitation-emission matrices (EEMs) were corrected for the inner-filter effect, Raman and Rayleigh (1st and 2nd order) scattering. Applications of absorbance and fluorescence spectroscopy are explained in detail in Chapter 4, and the protocol for applying corrections to the data is provided in the Appendix.

A parallel factor analyses (PARAFAC) model was built using total of 78 EEMs obtained from pre and post monsoon samples from 39 tube-wells. The DOM Fluor toolbox (Stedmon and Bro, 2008) was used for building and validating the model. All the EEMs were normalized by dividing the EEM by the maximum intensity of that EEM. The detailed procedure of developing and validating the model is explained in Chapter 4. In brief, a three-component model was validated by split half analysis and random initialization technique. For all the samples, the difference between actual and modeled EEM intensities did not exceed 10% of the intensity in the original EEM (Cawley et al., 2012), which was used as the criteria for acceptable model fit (Stedmon and Bro, 2008). From the PARAFAC components, humic to protein like ratio (Humic:Protein) was developed as described earlier in Chapters 4 & 5. As only three components were identified in this model (unlike 4 components in Murshidabad PARAFAC model in Chapter 5), the ratio of terrestrial to microbial DOM (terr: microb) was not developed.

Bulk Proteins

Filtered unacidified water sample (10 mL) was placed into 50 mL polypropylene Falcon conical centrifuge tube was instantaneously frozen using slurry of 99.5 % ethyl alcohol (Sigma 459844) and dry ice for about 15-20 minutes. The frozen samples were dried using a freeze drying unit at -150^0C for 24 hours. After the sample was completely sublimed, 1 mL of 18.3 MOhm-cm ultrapure water was added to the centrifuge tube and the solution was centrifuged using a 1.5 mL micro-centrifuge tube at 10000xG for 5 minutes. Supernatant of the centrifuged solution was used for the bulk protein analysis by a modified Lowry method (Hartree, 1972) using modified Lowry protein assay kit (Thermo Scientific 23240). The detailed information on the chemical reactions and procedure is explained in Chapter 4. In brief, the bulk proteins of the pre-concentrated water sample were reacted with reagents to form a blue colored aqueous complex and absorbance was measured at 750 nm. The standard curve was prepared using a common protein bovine serum albumin.

Results

Spatial variation in chemical and DOM characteristics

The average total As concentrations (Table 12) were greater for shallow groundwater samples (118.8 μgL^{-1} at Chakudanga and 201.46 μgL^{-1} at Shahispur) than deeper groundwater samples (0.71 μgL^{-1} at Bele and 4.34 μgL^{-1} at Radhanagar). However, two tube-wells at Radhanagar with depth of 360 ft and 340 ft had exceptionally higher total As concentrations as 132.02 μgL^{-1} and 715.22 μgL^{-1}. Dissolved Fe^{2+} concentrations measured using field test kits were found to be in the range of $25 - 30$ mg. mL^{-1} and $60 - 135$ mg. mL^{-1} for Chakudanga and Shahispur samples respectively while lower concentrations were found at Bele and Radhanagar sites as 0.1 $- 0.6$ mg. mL^{-1} and $0.2 - 45$ mg.mL^{-1}. Exceptionally higher Fe^{2+} concentrations in two tube-well

samples at Radhanagar (300 mg. mL^{-1} each) were consistent with higher total As concentrations at these two tube-wells. Similarly, higher DOC and TN concentrations were found in shallow aquifer samples (1.28 mg. mL^{-1} of DOC and 1.89 mg. mL^{-1} of DON at Chakudanga; 1.24 mg. mL^{-1} of DOC and 2.12 mg. mL^{-1} of DON at Shahispur) as compared to that in deeper aquifer samples (0.64 mg.mL^{-1} of DOC and 0.4 mg.mL^{-1} of DON at Bele; 0.78 mg.mL^{-1} of DOC and 0.68 mg.mL^{-1} of DON at Radhanagar). Similarly, the DOM characteristics showed distinction between shallow and deeper aquifer samples (Table 13), for example HIX and Humic:Protein values were higher in Chakudanga and Shahispur as compared to those in Bele and Radhanagar samples. Again exceptionally higher HIX and Humic:Protein values were observed for the two tube-wells at Radhanagar corresponding to higher total As and Fe^{2+} concentrations. For deeper aquifer samples, values of β:α were higher than for shallower samples. This spatial variation observed for all chemical parameters and DOM characteristics remained same in samples collected during pre- as well as post-monsoon seasons.

Pre- and post-monsoon variation in chemical and DOM characteristics

Pre- and post-monsoon average total As (Table 12) at Chakudanga was 118.8 µgL^{-1} and 122.3 µgL^{-1} respectively. Similarly, Shahispur had average total As concentrations in the same range (i.e. 201.46 µgL^{-1} (pre-monsoon) and 187.7 µgL^{-1}). By contrast, Bele had much lower (P<0.05) total As concentrations 0.71 µgL^{-1} and 0.94 µgL^{-1} for pre and post-monsoon conditions, respectively. Radhanagar also had lower (P<0.05) total As concentrations at 4.34 µgL^{-1} (pre-monsoon) and 4.23 µgL^{-1} (post-monsoon) than Chakudanga and Shahispur sites As concentrations, except the two wells that had exceptionally higher concentrations of 132.02 µgL^{-1} and 715.22 µgL^{-1} (pre-monsoon) and 107.12 µgL^{-1} and 686.16 µgL^{-1} (post-monsoon). Lower DOC and DON concentrations (P<0.05) were observed in Bele and Radhanagar both pre and post-monsoon. Slight

increase in the chlorides concentration at Chakudanga and decrease at Shahispur sites was observed between pre- and post-monsoon conditions (P<0.05), however no such decrease was observed for Bele and Radhanagar samples.

DOM chemical characteristics are listed in Table 13 for pre and post-monsoon conditions. Groundwater samples at all the sites had low absorbance at 254 nm. No significant difference was observed within the samples or pre- and post-monsoon conditions. Spectral slope ratio (S_R) was also consistent for all the samples except for one sample from Bele that had SR of 68 and was considered as an outlier. Specific ultra violet absorbance (SUVA) values were found to be 3.85 and 4.28 L.mg-1.m-1 for Chakudanga and Shahispur (pre-monsoon) which decreased to 2.1 and 2.29 L.mg-1.m-1 post-monsoon. Fluorescence index (FI) for Chakudanga and Shahispur was found to be 1.63 and 1.53 (pre-monsoon) respectively while average FI at Bele and Radhanagar was 1.5 and 1.49 (pre-monsoon) respectively. In post-monsoon condition, FI at Chakudanga and Shahispur did not change significantly, but at Bele and Radhanagar significant increase (P<0.05) in FI was observed (FI = 1.99 and 1.85 respectively). Pre-monsoon freshness index (β:α) was observed to be 0.75 and 0.73 for Chakudanga and Shahispur respectively, while it was significantly higher (P<0.05) at Bele and Radhanagar (0.99 and 0.94 respectively). This pattern of β:α continued in the post-monsoon conditions. Much higher humification index (HIX) values were observed for Chakudanga and Shahispur (6.33 and 6) in pre-monsoon conditions as compared to Bele and Radhanagar (1.32 and 1.21), again this pattern was observed to be repeating in post-monsoon conditions. Humic:Protein ratio values obtained from the PARAFAC components (Figure 49) were significantly higher (P<0.05) for samples from Chakudanga and Shahispur (5.64 and 5.28) as compared to that in Bele and Radhanagar (1.29 and 1.01). This pattern of Humic: Protein ratio repeated in post-monsoon conditions as well. Bulk protein content at all four sites was observed

137

to be similar in pre and post monsoon conditions, except at Bele, slightly lower bulk protein content

$(0.74 \text{ mg. mL}^{-1})$ was observed during post-monsoon condition.

Table 12 Pre and Post-monsoon hydrochemistry

Pre-monsoon Hydrochemistry						
Site	Depth (ft)	Total As (μgL^{-1})	[2]DOC (mgL^{-1})	[3]DON (mgL^{-1})	Chlorides (mgL^{-1})	[4]Fe $^{2+}$ (mgL^{-1})
Chakudanga	68.50 ± 15.28 (50-105)	118.86 ± 38.57 (52.74 – 187.84)	1.28 ± 0.29 (0.9 – 1.77)	1.89 ± 0.42 (1.17 – 2.38)	9.99 ± 12.03 (1.94 – 42.45)	29.5 ± 1.581 (25 - 30)
Shahispur	84.20 ± 31.95 (50 - 150)	201.46 ± 76.55 (49.53 – 315.01)	1.24 ± 0.22 (0.98 – 1.76)	2.12 ± 0.54 (1.06 – 2.86)	13.66 ± 10.46 (4.12 – 35.83)	94.5 ± 26.5 (60 - 135)
Bele	264 ± 58.99 (200 - 320)	0.71 ± 0.4 (0.44 – 1.41)	0.64 ± 0.12 (0.50 – 0.81)	0.40 ± 0.04 (0.34 – 0.44)	16.47 ± 5.10 (9.43 – 22.03)	0.26 ± 0.195 (0.1 – 0.6)
Radhanagar	333 ± 30.55 (300 - 360)	4.34 ± 5.43* (1.07 – 10.62)	0.78 ± 0.17 (0.61 – 0.97)	0.68 ± 0.3 (0.38 - 1)	14.67 ± 0.37 (14.28 – 15.03)	15.2 ± 25.81 (0.2 - 45)
Post-monsoon Hydrochemistry						
Chakudanga	68.50 ± 15.28 (50-105)	122.3 ± 39.23 (49.84 – 185.1)	1.39 ± 0.29 (0.86 – 1.72)	1.86 ± 0.39 (1.2 – 2.26)	10.37 ± 11.34 (1.71 – 40.11)	29 ±2.4 (25 - 30)
Shahispur	84.20 ± 31.95 (50 - 150)	187.7 ± 72.76 (42.61 – 299.7)	0.94 ± 0.29 (0.57 – 1.64)	2.1 ± 0.54 (0.97 – 2.94)	11.89 ± 7.65 (3.56 – 27.41)	26 ± 2.1 (25 – 30)
Bele	264 ± 58.99 (200 - 320)	0.94 ± 0.40 (0.55 – 1.48)	0.36 ± 0.02 (0.33 – 0.4)	0.45 ± 0.07 (0.33 – 0.55)	16.16 ± 5.05 (9.27 – 21.9)	1.5 ± 0 (1.5 – 1.5)
Radhanagar	333 ± 30.55 (300 - 360)	4.23 ± 4.66 (1.49 – 9.62)	0.41 ± 0.07 (0.35 – 0.50)	0.84 ± .027 (0.53 – 1.06)	14.58 ± 0.41 (14.19 – 15.01)	1.5 ± 0 (1.5 – 1.5)

[1]All numbers are expressed as average value ± standard deviation, minimum – maximum range in parenthesis.

[2]Dissolved (non-purgeable) organic carbon

[3]Dissolved organic nitrogen

[3]Fe^{2+} measured in the field using test kits.

*Two wells at Radhanagar had exceptionally high (132.02 and 715.22 μgL^{-1}) pre-monsoon and (107.12 μgL^{-1} and 686.16 μgL^{-1}) post-monsoon total As concentrations.

Chakudanga, Shahispur (Holocene aquifer); Bele, Radhanagar (Pleistocene aquifer)

Table 13 Pre and post-monsoon characteristics of DOM

Site	[2]Abs254 (A.U.)	[3]S_R	SUVA (L.mg^{-1}.m^{-1})	[4]FI	[4] β:α	[4]HIX	[5]Humic:protein	Bulk Protein (mg.mL^{-1})
Pre-monsoon DOM characteristics								
Chakudanga	0.048 ± 0.007 (0.03 – 0.06)	1.4 ± 0.25 (1 – 1.9)	3.85 ± 0.6 (3.05 – 4.98)	1.63 ± 0.03 (1.58 – 1.69)	0.75 ± 0.02 (0.71 – 0.78)	6.33±2.42 (3.07 – 9.75)	5.64 ± 2.93 (1.99 – 10.01)	1.12 ± 0.58 (0.40 – 2.23)
Shahispur	0.05 ± 0.01 (0.03 – 0.06)	1.47 ± 0.27 (1.13 – 1.94)	4.28 ± 0.88 (2.75 – 6.15)	1.53 ± 0.07 (1.42 – 1.64)	0.73 ± 0.03 (0.68 – 0.79)	6 ± 2.56 (2.78 – 9.6)	5.28 ± 3.36 (1.74 – 11.03)	1.30 ± 0.18 (0.94 – 1.48)
Bele	0.02 ± 0.003 (0.01 – 0.02)	3.01 ± 3.2 (0.90 – 8.58)	2.93 ± 0.88 (1.96 ± 4.20)	1.5 ± 0.28 (1.23 – 1.97)	0.99 ± 0.09 (0.88 – 1)	1.32 ± 0.69 (0.84 – 2.46)	1.29 ± 0.86 (0.71 2.77)	1.17 ± 0.40 (0.77 – 1.76)
Radhanagar	0.04 ± 0.01 (0.02 – 0.05)	1.84 ± 0.73 (1.24 – 2.67)	4.97 ± 0.96 (4.01 – 5.95)	1.49 ± 0 .13 (1.39 – 1.64)	0.94 ± 0.08 (0.87 – 1)	1.21 ± 0.49 (0.73 – 1.72)	1.01 ± 0.56 (0.51 – 1.63)	1.25 ± 0.37 (0.82 – 1.47)
Post-monsoon DOM characteristics								
Chakudanga	0.03 ± 0.009 (0.02 – 0.05)	1.32 ± 0.23 (0.9 – 1.61)	2.1 ± 0.44 (1.32 – 2.99)	1.64 ± 0.06 (1.5 – 1.73)	0.76 ± 0.03 (0.72 – 0.83)	6.67 ± 2.21 (3.21 – 9.11)	6.47 ± 2.85 (2.37 – 9.75)	1.16 ± 0.39 (0.59 – 1.49)
Shahispur	0.04 ± 0.01 (0.03 – 0.06)	1.52 ± 0.56 (0.96 – 2.77)	2.29 ± 0.49 (1.66 – 3.36)	1.6 ± 0.06 (1.51 – 1.68)	0.71 ± 0.03 (0.66 – 0.77)	6.72 ± 1.61 (3.33 – 8.7)	5.91 ± 2.11 (2.11 – 8.91)	1.36 ± 0.22 (1.03 – 1.8)
Bele	0.016 ± 0.007 (0.006 – 0.025)	14.63 ± 30.04 (0.08 – 68.37)	3.68 ± 1.63 (1.44 – 5.37)	1.99 ± 0.06 (1.93 – 1.99)	0.98 ± 0.08 (0.94 - 1)	0.82 ± 0.14 (0.69 – 1.06)	0.66 ± 0.1 (0.56 – 0.80)	0.74 ± 0.09 (0.66 – 0.86)
Radhanagar	0.02 ± 0.01 (0.01 – 0.04)	1.51 ± 0.43 (1.01 – 1.77)	3.24 ± 1.47 (1.57 – 4.34)	1.85 ± 0.11 (1.74 – 1.96)	0.97 ± 0.05 (0.91 - 1)	1.53 ± 0.63 (1.09 – 2.26)	1.25 ± 0.71 (0.82 – 2.08)	1.3 ± 0.14 (1.15 – 1.43)

[1]All numbers are expressed as average value ± standard deviation, minimum – maximum range in parenthesis.
[2]Absorbance at 254 nm.
[3]Spectral Slope Ratio (S_{275_295} / S_{350_400})
[4]Fluorescence Index (FI), Freshness Index (β:α), Humification Index (HIX)
[5]Ratio of humic like to protein like component obtained by PARAFAC model = (C1+C2) / (C3), Figure 49
Chakudanga, Shahispur (Holocene aquifer); Bele, Radhanagar (Pleistocene aquifer)
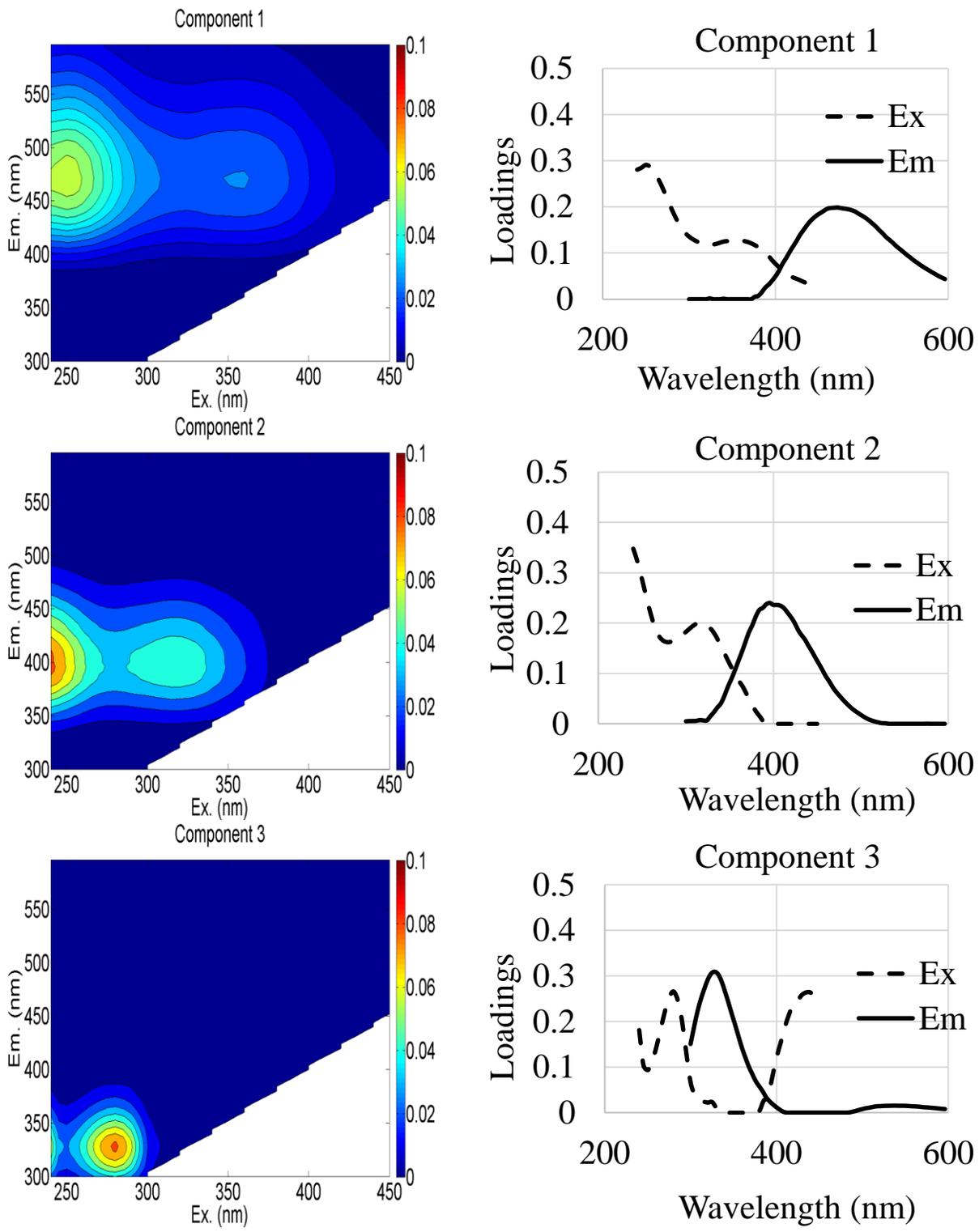
Figure 44 EEM spectra (left) and emission-excitation curve (right) showing loadings of three PARAFAC components identified in the model

Difference in pre- and post-monsoon chemical and DOM quality with respect to the depth

The pre- and post-monsoon chloride concentrations varied (decreased and/or increased) at only shallower depth (within 100 ft) while the concentrations at greater depths remained unchanged (Figure 50). Similarly, total As concentrations varied (decreased and/or increased) after the monsoon within 200 ft depth and for the samples at greater depths, the concentrations remained unchanged. However, two tube-wells with exceptionally high total As at Radhanagar showed a positive increase after the monsoon (i.e. total As concentrations at these tube-wells decreased after the monsoon). The DOC concentrations at shallow depth (within 150 ft) varied (decreased and/or increased) however, the concentrations at greater depth particularly decreased after the monsoon. Contrastingly, DON concentrations were mostly unchanged or increased after the monsoon in shallow as well as deep groundwater samples. The field measured Fe^{2+} concentrations showed a decline after the monsoon at shallow depth while remained unchanged at greater depths.

Humic:Protein ratio varied (decreased and/or increased) at shallow depths and remained unchanged at deeper samples, except one deep (460 ft) groundwater sample from Shahispur (typically high As, shallow Holocene aquifer domain) showed a positive difference i.e. the Humic:Protein ratio decreased in this sample (Figure 51). The differences in HIX values followed the same trend as Humic:Protein ratio. Interestingly, FI values at shallow depths did not change after the monsoon, but FI in samples at greater depths indicated a negative difference, i.e. the FI values at deep (below 200 ft) groundwater samples increased after the monsoon. A positive difference (decrease in value after the monsoon) at shallow depths and negative difference (increase in value after the monsoon) was observed for SUVA. Bulk protein content at the shallow

142

depths were found to have decreased after the monsoon while at greater depths it remained unchanged.
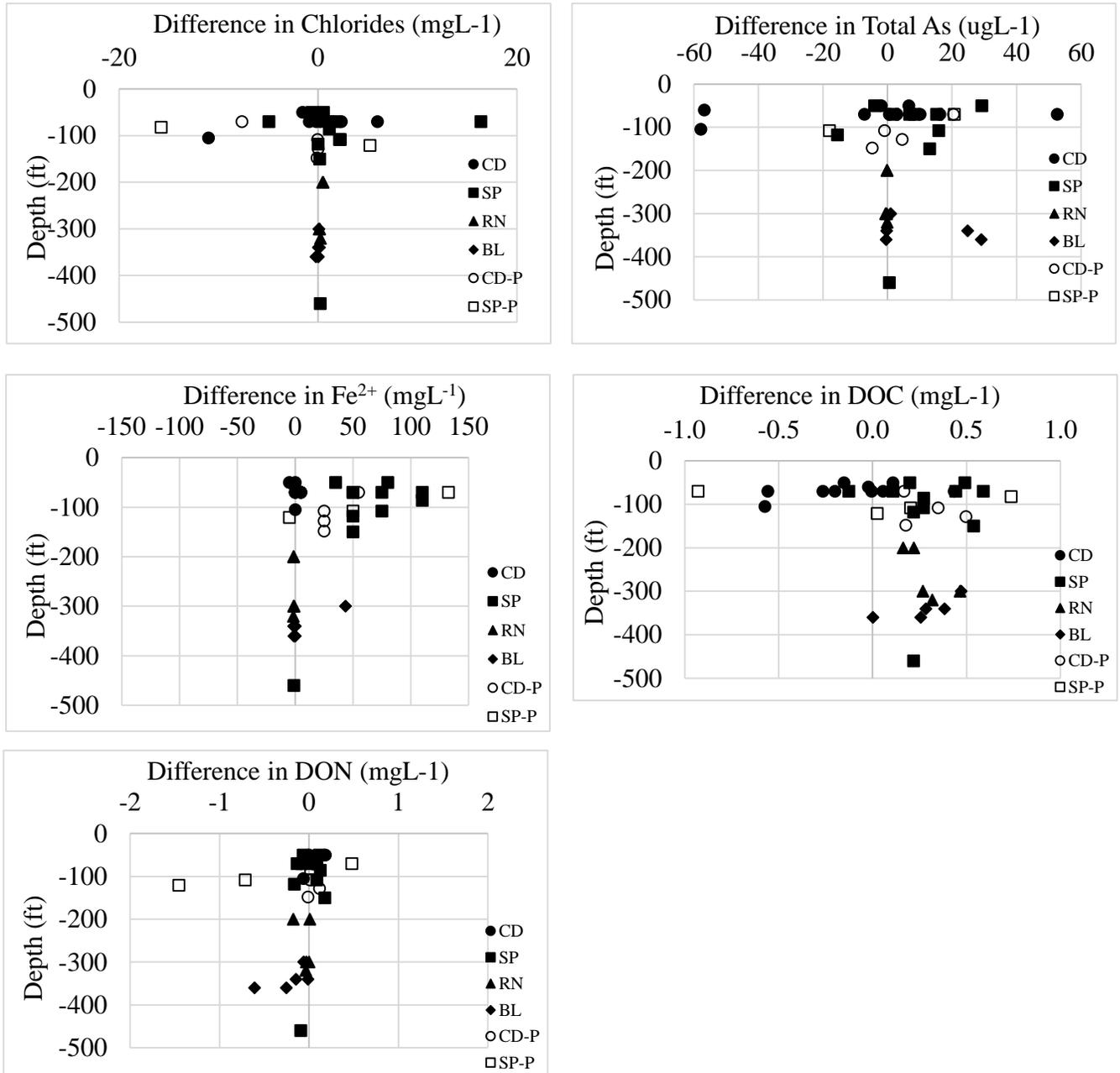
Figure 45 Scatterplots showing the difference between Pre and Post-monsoon values for hydrochemical parameters. X-axis indicate the difference [(Pre-monsoon) – (Post-monsoon)] in respective units and Y-axis indicate the depth in ft. Legend indicate, Chakudanga (CD), Shahispur (SP), Radhanagar (RN), Bele (BL), Chakudanga Piezometers (CD-P) and Shahispur-Piezometers (SP-P)
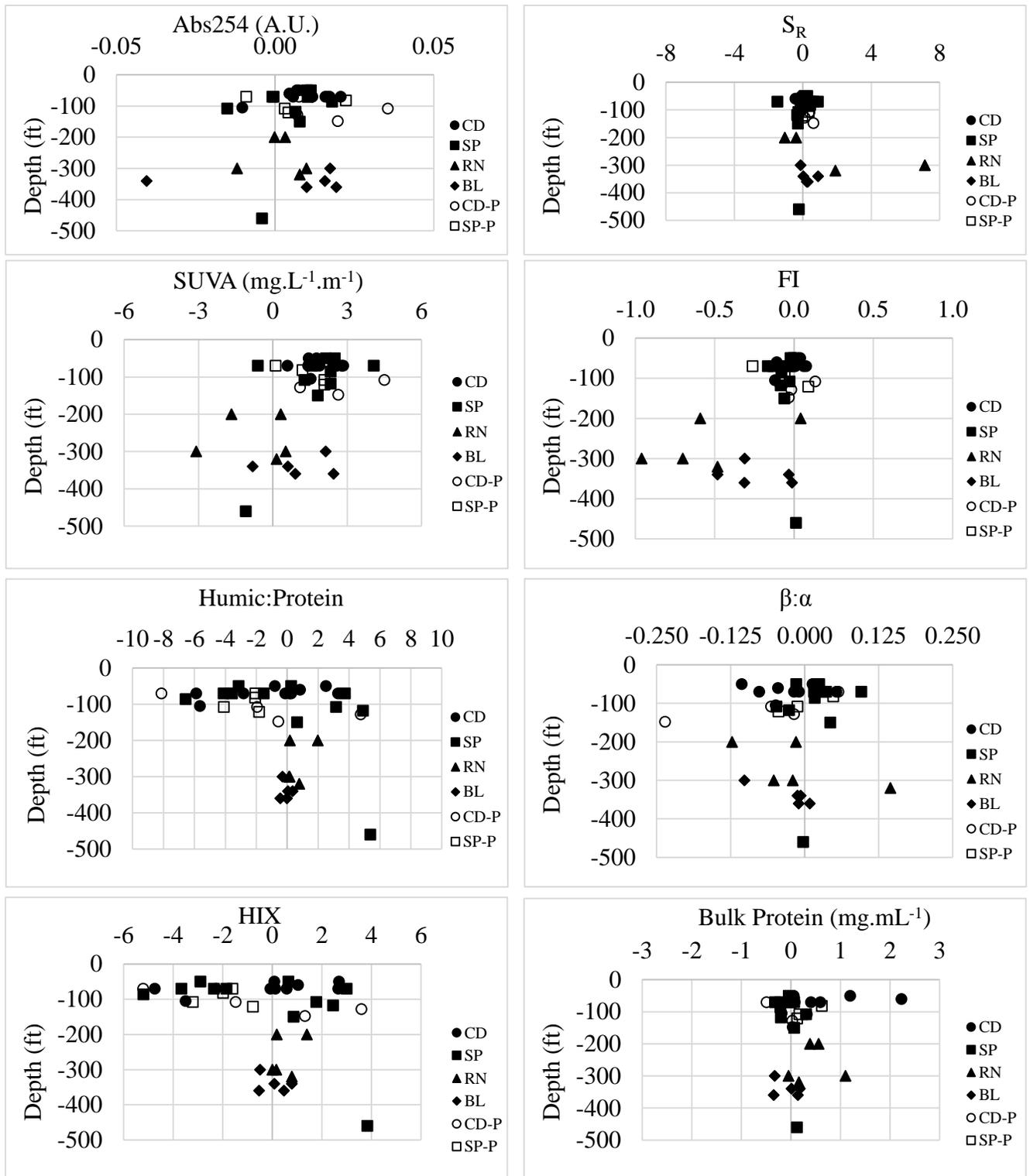
Figure 46 Scatterplots showing the difference between Pre and Post-monsoon values for various DOM characteristics. X-axis indicate the difference [(Pre-monsoon) – (Post-monsoon)] in respective units and Y-axis indicate the depth in ft. Legend indicate, Chakudanga (CD), Shahispur (SP), Radhanagar (RN), Bele (BL), Chakudanga Piezometers (CD-P) and Shahispur-Piezometers (SP-P)

Among the DOM characteristics, FI values in deeper samples were found to increase during post-monsoon condition while for the shallower aquifer samples, FI values did not change significantly (Figure 51). S_R values in shallower as well as deeper samples did not change significantly except one sample from Radhanagar at 300 ft depth, where the S_R value decreased. SUVA values at shallower depths were found to have decreased for most of the samples while in deeper samples, four samples showed the increase in SUVA values. The HIX varied at shallower depths and remained unchanged in deeper samples except for one deep tube-well from Shahispur where the HIX decreased. Humic to protein ratio shows the very similar trend to HIX values. Bulk protein values in deeper samples remained unchanged, while there was variation in bulk protein content of shallower samples.

Conclusions

Variation in chlorides concentration in the samples collected from shallow aquifers and no change in the concentrations in the samples collected from deeper aquifers indicate that the shallow aquifer may be experiencing vertical recharge during monsoon. Chloride being a conservative anion which does not react, can be considered as a tracer in this setting. In comparison, other chemical species such as arsenic are influenced by other environmental factors such as redox potential. Increased FI values at greater depths in post-monsoon season may be indicative of increased microbial humic substances. Humic to protein ratio and HIX values varied at shallower depths suggesting mixing with freshwater and input from recent organic matter. These values remained unchanged at greater depths which suggests that extent of mixing was limited. These observations are in agreement with earlier study Majumder et al., 2016 that suggested the occurrence of vertical recharge in shallow aquifers associated with release of additional arsenic in the groundwater.

Chapter 10 - Conclusions

Hypothesis # 1: Higher arsenic concentrations in Holocene aquifers and lower concentrations in Pleistocene aquifers are linked with the contrasting quality of DOM in the aquifers.

Dissolved organic matter in groundwater in Holocene and Pleistocene aquifers in West Bengal, India was characterized. A PARAFAC model based on fluorescence data identified four unique fluorescent components of DOM in the groundwater. Organic matter in groundwater in Holocene aquifer was found to be microbially-processed and humic-like, while that in Pleistocene aquifer was more protein-like in character. Dominance of humic-like DOM in groundwaters in Holocene aquifers may be attributed to arsenic mobilization. Absence of humic-like DOM in groundwater in Pleistocene aquifer reflects the lack of microbial processing of DOM and may be linked with the lower arsenic concentrations.

Hypothesis 2 Humic substances act as intermediate electron shuttles and the rate of microbial iron/arsenic reduction is accelerated by the presence of humic substances.

Fulvic acids extracted from high arsenic groundwater in Bangladesh were used to test their ability to shuttle the electron between microorganism and the electron acceptor. The results indicated that the Geobacter metallireducens, iron reducing bacteria were capable of reducing the Bangladesh fulvic acids. The reduced fulvic acids further reduced the ferric citrate to Fe^{2+}. This finding provides an experimental evidence to a widely postulated electron shuttling mechanism responsible for As mobilization in the Bengal basin aquifers. Experiment with solid phase electron acceptor (Goethite) showed the significant increase in the rate of microbial iron reduction upon addition of humic substances which supports the idea that the mechanism of electron shuttling

holds true in environmentally relevant scenarios where major electron acceptor is oxidized iron minerals.

Hypothesis 3 Arsenic and iron forms aqueous complexes with dissolved organic matter.

Complexation of arsenic directly with DOM molecules (binary) or via Fe-bridging (ternary) has been considered as another significant mechanism controlling arsenic mobility. However, the role of non-aromatic DOM moieties in arsenic mobility has rarely been reported. Fluorescence titrations with dissolved iron and dissolved organic matter showed the quenching of fluorescence indicating formation of binary aqueous complex between iron and DOM. Our results from ^{1}H NMR analyses of As – DOM binding suggest that the non-fluorescent and non-aromatic moieties of DOM molecules such as methyl, methylene, methine and carbonyl groups, which cover a substantial fraction of the DOM molecular structure, actually play an active role in As – DOM binary complex formation. These new findings assert the importance and role of DOM in arsenic mobility.

Hypothesis 4 Groundwater flow and biogeochemical transport results in spatially discontinuous arsenic concentrations.

Groundwater models were developed for Bengal basin aquifer, India and Mahomet bedrock valley aquifer, USA to understand the variability of dissolved arsenic. Biogeochemical reactions involved in arsenic mobilization were modeled using a multicomponent reactive transport model using MT3DMS-RT3D code. Backward tracking of particles from the field sampling sites provided the proximity where the source of electron donor (organic carbon) would need to be in order to produce observed concentrations of dissolved iron and arsenic. A forward reactive transport model was developed to predict the spread of arsenic contamination in the future.

Hypothesis 5 Monsoonal recharge influences the quality of dissolved organic matter in shallow alluvial aquifer and subsequently the arsenic mobility.

Groundwater samples were collected and analyzed from shallow and deep aquifers in West Bengal, India during dry and wet seasons. Dissolved organic matter in the groundwater was examined in detail using absorbance and fluorescence spectroscopy along with hydro-chemical parameters. Results suggested that the monsoonal recharge influence the chemical quality of groundwater only at shallow depths, while the quality of DOM was observed to vary at greater depths as well. Variation in humification index and humic to protein ratio in shallow aquifers indicated the mixing and possibly increase in the rate of arsenic mobility.

Chapter 11 - Bibliography

1. Acharyya, S.K., Lahiri, S., Raymahashay, B.C., Bhowmik, A., 2000. Arsenic toxicity of groundwater in parts of the Bengal basin in India and Bangladesh: The role of Quaternary stratigraphy and Holocene sea-level fluctuation. Environ. Geol. 39, 1127–1137. doi:10.1007/s002540000107

2. Acharyya, S.K., Shah, B. a., 2007. Arsenic-contaminated groundwater from parts of Damodar fan-delta and west of Bhagirathi River, West Bengal, India: Influence of fluvial geomorphology and Quaternary morphostratigraphy. Environ. Geol. 52, 489–501. doi:10.1007/s00254-006-0482-z

3. Ahmed, K.M.M., Bhattacharya, P., Hasan, M.A.A., Akhter, S.H.H., Alam, S.M.M.M.M., Bhuyian, M.A.H.A.H., Imam, M.B.B., Khan, A.A., Sracek, O., 2004. Arsenic enrichment in groundwater of the alluvial aquifers in Bangladesh : an overview. Appl. Geochemistry 19, 181–200. doi:10.1016/j.apgeochem.2003.09.006

4. Aiken, G.R., Mcknight, I.D.M., Thorn, I.K.A., Thurman, E.M., 1992. Isolation of hydrophilic organic acids from water using nonionic macroporous resins. Org. Geochem. 18, 567–573.

5. Al Lawati, W.M., Rizoulis, A., Eiche, E., Boothman, C., Polya, D. a., Lloyd, J.R., Berg, M., Vasquez-Aguilar, P., van Dongen, B.E., 2012. Characterisation of organic matter and microbial communities in contrasting arsenic-rich Holocene and arsenic-poor Pleistocene aquifers, Red River Delta, Vietnam. Appl. Geochemistry 27, 315–325. doi:10.1016/j.apgeochem.2011.09.030

6. Alan H. Welch, D.B. Westjohn, Dennis R. Helsel, R.B.W., 2000. Arsenic in groundwater of the united states: Occurrence and Geochemistry. Ground Water.

7. America, N., Mukherjee, S.C., 2004. Groundwater arsenic contamination and its health effects in the Ganga-Meghna- Brahmaputra plain {. J. Environ. Monit.

8. American, A., Standard, N., 2012. Standard Test Methods for Acidity or Alkalinity of Water 1 1–8. doi:10.1520/D1067-11.2

9. Anger, P., Bharadwaj, P., Novotny, L., 2006. Enhancement and Quenching of Single-Molecule Fluorescence. Phys. Rev. Lett. 96, 113002. doi:10.1103/PhysRevLett.96.113002

10. Anisotropy, F., 2006. Fluorescence Anisotropy 576–576. doi:10.1007/3-540-29623-9_7040

11. Annual Conference 2007 , Royal Geographical Society , London Session key : BSG-session 3 Arsenic contaminated aquifers : a study of the Ganga levee zones in Bihar , India Department of Environment and Water Management , A . N . College , Patna Department , 2007.

12. Antunes, M.C.G., Pereira, C.C.C., Esteves da Silva, J.C.G., 2007. MCR of the quenching of the EEM of fluorescence of dissolved organic matter by metal ions. Anal. Chim. Acta 595, 9–18. doi:10.1016/j.aca.2006.12.017

13. Armienta, M. a, Segovia, N., 2008. Arsenic and fluoride in the groundwater of Mexico. Environ. Geochem. Health 30, 345–53. doi:10.1007/s10653-008-9167-8

14. Baker, a, 2001. Fluorescence excitation-emission matrix characterization of some sewage-impacted rivers. Environ. Sci. Technol. 35, 948–53.

15. Baker, A., 2001. Fluorescence Excitation - Emission Matrix Characterization of Some Sewage-Impacted Rivers. Environ. Sci. Technol. 35, 948–953.

16. Baker, A., Elliott, S., Lead, J.R., 2007. Effects of filtration and pH perturbation on freshwater organic matter fluorescence. Chemosphere 67, 2035–43. doi:10.1016/j.chemosphere.2006.11.024

17. Bauer, M., Blodau, C., 2006. Mobilization of arsenic by dissolved organic matter from iron oxides, soils and sediments. Sci. Total Environ. 354, 179–90. doi:10.1016/j.scitotenv.2005.01.027

18. Bauer, P., Gumbricht, T., 2003. Hydrological modelling and resource management in the Okavango Delta 130–137.

19. Bauer-Gottwein, P., Langer, T., Prommer, H., Wolski, P., Kinzelbach, W., 2007. Okavango Delta Islands: Interaction between density-driven flow and geochemical reactions under evapo-concentration. J. Hydrol. 335, 389–405. doi:10.1016/j.jhydrol.2006.12.010

20. Bazlen, W.R., Gedney, W.C., Rossi, J. V, Babcock, L., Shaffer, S., Vargas, A., Johnson, T., 2001. Framework for a Ground-Water Quality Monitoring and Assessment Program for 599.

21. Beaulieu, B., Ramirez, R.E., 2013. Arsenic remediation field study using a sulfate reduction and zero-valent iron PRB. Groundw. Monit. Remediat. 33, 85–94. doi:10.1111/gwmr.12007

22. Berg, M., Trang, P.T.K., Stengel, C., Buschmann, J., Viet, P.H., Van Dan, N., Giger, W., Stüben, D., 2008. Hydrological and sedimentary controls leading to arsenic contamination of groundwater in the Hanoi area, Vietnam: The impact of iron-arsenic ratios, peat, river bank deposits, and excessive groundwater abstraction. Chem. Geol. 249, 91–112. doi:10.1016/j.chemgeo.2007.12.007

23. Bethke, C.M., Ding, D., Jin, Q., Sanford, R. a., 2008. Origin of microbiological zoning in groundwater flows. Geology 36, 739. doi:10.1130/G24859A.1

24. Bethke, C.M., Sanford, R.A., Kirk, M.F., Jin, Q., Flynn, T.M., 2011. The thermodynamic ladder in geomicrobiology. Am. J. Sci. 311, 183–210. doi:10.2475/03.2011.01

25. Bhattacharya, P., Chatterjee, D., Jacks, G., 1997. Occurrence of Arsenic-contaminatedGroundwater in Alluvial Aquifers from Delta Plains, Eastern India: Options for Safe Drinking Water Supply. Int. J. Water Resour. Dev. 13, 79–92. doi:10.1080/07900629749944

26. Bhattacharya, P., Claesson, M., Bundschuh, J., Sracek, O., Fagerberg, J., Jacks, G., Martin, R.A., Storniolo, A.D.R., Thir, J.M., 2006. Distribution and mobility of arsenic in the Río Dulce alluvial aquifers in Santiago del Estero Province, Argentina. Sci. Total Environ. 358, 97–120. doi:10.1016/j.scitotenv.2005.04.048

27. Bhowmick, S., Nath, B., Halder, D., Biswas, A., Majumder, S., Mondal, P., Chakraborty, S., Nriagu, J., Bhattacharya, P., Iglesias, M., Roman-Ross, G., Guha Mazumder, D., Bundschuh, J., Chatterjee, D., 2013. Arsenic mobilization in the aquifers of three physiographic settings of West Bengal, India: understanding geogenic and anthropogenic influences. J. Hazard. Mater. 262, 915–23. doi:10.1016/j.jhazmat.2012.07.014

28. Bieroza, M.Z., Bridgeman, J., Baker, a., 2010. Fluorescence spectroscopy as a tool for determination of organic matter removal efficiency at water treatment works. Drink. Water Eng. Sci. 3, 63–70. doi:10.5194/dwes-3-63-2010

29. Biswas, A., Majumder, S., Neidhardt, H., Halder, D., Bhowmick, S., Mukherjee-Goswami, A., Kundu, A., Saha, D., Berner, Z., Chatterjee, D., 2011. Groundwater chemistry and redox processes: Depth dependent arsenic release mechanism. Appl. Geochemistry 26, 516–525. doi:10.1016/j.apgeochem.2011.01.010

30. Blum, M.D., Roberts, H.H., 2012. The Mississippi Delta Region: Past, Present, and Future. Annu. Rev. Earth Planet. Sci. 40, 655–683. doi:10.1146/annurev-earth-042711-105248

31. Braissant, O., Decho, a. W., Dupraz, C., Glunk, C., Przekop, K.M., Visscher, P.T., 2007. Exopolymeric substances of sulfate-reducing bacteria: Interactions with calcium at alkaline pH and implication for formation of carbonate minerals. Geobiology 5, 401–411. doi:10.1111/j.1472-4669.2007.00117.x

32. Burton, E.D., Johnston, S.G., Bush, R.T., 2011. Microbial sulfidogenesis in ferrihydrite-rich environments: Effects on iron mineralogy and arsenic mobility. Geochim. Cosmochim. Acta 75, 3072–3087. doi:10.1016/j.gca.2011.03.001

33. Burton, E.D., Johnston, S.G., Planer-Friedrich, B., 2013. Coupling of arsenic mobility to sulfur transformations during microbial sulfate reduction in the presence and absence of humic acid. Chem. Geol. 343, 12–24. doi:10.1016/j.chemgeo.2013.02.005

34. Buschmann, J., Berg, M., 2009. Impact of sulfate reduction on the scale of arsenic contamination in groundwater of the Mekong, Bengal and Red River deltas. Appl. Geochemistry 24, 1278–1286. doi:10.1016/j.apgeochem.2009.04.002

35. Buschmann, J., Kappeler, A., Lindauer, U., Kistler, D., Berg, M., Sigg, L., 2006. Arsenite and Arsenate Binding to Dissolved Humic Acids: Influence of pH, Type of Humic Acid, and Aluminum. Environ. Sci. Technol. 40, 6015–6020. doi:10.1021/es061057+

36. C.G.E.M. van Beek, D. van der K., 1982. Sulfate-reducing bacteria in groundwater from clogging and nonclogging shallow wells in the Netherlands River Region. Ground Water.

37. Cabanlss, S.E., 1992. Synchronous Fluorescence Spectra of Metal-Fulvic Acid Complexest. Environ. Sci. Technol. 26, 1133–1139.

38. Campbell, J.R., Craw, D., Frew, R., Horton, T., Chamberlain, C.P., 2004. Geochemical signature of orogenic hydrothermal activity in an active tectonic intersection zone, Alpine Fault, New Zealand. Miner. Depos. 39, 437–451. doi:10.1007/s00126-004-0421-4

39. Cardoza, L. a. LA, Korir, A. a. K., Otto, W.H.W., Wurrey, C.J., Larive, C.K., 2004. Applications of NMR spectroscopy in environmental science. Prog. Nucl. Magn. Reson. Spectrosc. 45, 209–238. doi:10.1016/j.pnmrs.2004.06.002

40. Catrouillet, C., Davranche, M., Dia, A., Bouhnik-Le Coz, M., Marsac, R., Pourret, O., Gruau, G., 2014. Geochemical modeling of Fe(II) binding to humic and fulvic acids. Chem. Geol. 372, 109–118. doi:10.1016/j.chemgeo.2014.02.019

41. Cawley, K.M., Wolski, P., Mladenov, N., Jaffé, R., 2012. Dissolved organic matter biogeochemistry along a transect of the okavango delta, botswana. Wetlands 32, 475–486. doi:10.1007/s13157-012-0281-0

42. Chakraborti, D., Das, B., Rahman, M.M., Chowdhury, U.K., Biswas, B., Goswami, a B., Nayak, B., Pal, A., Sengupta, M.K., Ahamed, S., Hossain, A., Basu, G., Roychowdhury, T., Das, D., 2009. Status of groundwater arsenic contamination in the state of West Bengal, India: a 20-year study report. Mol. Nutr. Food Res. 53, 542–51. doi:10.1002/mnfr.200700517

43. Chakraborti, D., Mukherjee, S.C., Pati, S., Sengupta, M.K., Rahman, M.M., Chowdhury, U.K., Lodh, D., Chanda, C.R., Chakraborti, A.K., Basu, G.K., 2003. Arsenic Groundwater Contamination in Middle Ganga Plain, Bihar, India: A Future Danger? Environ. Health Perspect. 111, 1194–1201. doi:10.1289/ehp.5966

44. Chakraborti, D., Rahman, M.M., Das, B., Nayak, B., Pal, A., Sengupta, M.K., Hossain, M.A., Ahamed, S., Sahu, M., Saha, K.C., Mukherjee, S.C., Pati, S., Dutta, R.N., Quamruzzaman, Q., 2013. Groundwater arsenic contamination in Ganga–Meghna–Brahmaputra plain, its health effects and an approach for mitigation. Environ. Earth Sci. 70, 1993–2008. doi:10.1007/s12665-013-2699-y

45. Chauhan, V.S., Nickson, R.T., Chauhan, D., Iyengar, L., Sankararamakrishnan, N., 2009. Ground water geochemistry of Ballia district, Uttar Pradesh, India and mechanism of arsenic release. Chemosphere 75, 83–91. doi:10.1016/j.chemosphere.2008.11.065

46. Chauhan, V.S., Yunus, M., Sankararamakrishnan, N., 2012. Geochemistry and mobilization of arsenic in Shuklaganj area of Kanpur-Unnao district, Uttar Pradesh, India. Environ. Monit. Assess. 184, 4889–901. doi:10.1007/s10661-011-2310-5

47. Chen, B., Nam, S.N., Westerhoff, P.K., Krasner, S.W., Amy, G., 2009. Fate of effluent organic matter and DBP precursors in an effluent-dominated river: A case study of wastewater impact on downstream water quality. Water Res. 43, 1755–1765. doi:10.1016/j.watres.2009.01.020

48. Cheng, W.P., Chi, F.H., 2002. A study of coagulation mechanisms of polyferric sulfate reacting with humic acid using a fluorescence-quenching method. Water Res. 36, 4583–91.

49. Chien, Y., Bleam, W., 1998. Two-dimensional NOESY nuclear magnetic resonance study of pH-dependent changes in humic acid conformation in aqueous solution. Environ. Sci. Technol. 32, 3653–3658.

50. Chin, Y.P., Aiken, G., O'Loughlin, E., 1994. Molecular weight, polydispersity, and spectroscopic properties of aquatic humic substances. Environ. Sci. Technol. 28, 1853–8. doi:10.1021/es00060a015

51. Coble, P.G., 1996. Characterization of marine and terrestrial DOM in seawater using excitation-emission matrix spectroscopy. Mar. Chem. 51, 325–346. doi:10.1016/0304-4203(95)00062-3

52. Coble, P.G., Del Castillo, C.E., Avril, B., 1998. Distribution and optical properties of CDOM in the Arabian Sea during the 1995 Southwest Monsoon. Deep. Res. Part II Top. Stud. Oceanogr. 45, 2195–2223. doi:10.1016/S0967-0645(98)00068-X

53. Coble, P.G., Green, S.A., Blough, N. V, Gagosian, R.B., 1990. Characterization of dissolved organic matter in the Black Sea by fluorescence spectroscopy. Nature 348, 432–435.

54. Cole, J.J., Prairie, Y.T., Caraco, N.F., McDowell, W.H., Tranvik, L.J., Striegl, R.G., Duarte, C.M., Kortelainen, P., Downing, J. a., Middelburg, J.J., Melack, J., 2007. Plumbing the Global Carbon Cycle: Integrating Inland Waters into the Terrestrial Carbon Budget. Ecosystems 10, 172–185. doi:10.1007/s10021-006-9013-8

55. Commission, P., Bhavan, Y., 2007. REPORT OF THE TASK FORCE ON FORMULATING ACTION PLAN FOR REMOVAL OF ARSENIC CONTAMINATION IN WEST BENGAL 001.

56. Cook, R.L., 2004. Coupling NMR to NOM. Anal. Bioanal. Chem. 378, 1484–503. doi:10.1007/s00216-003-2422-z

57. Cook, R.L., McIntyre, D.D., Langford, C.H., Vogel, H.J., 2003. A comprehensive liquid-state heteronuclear and multidimensional NMR study of Laurentian fulvic acid. Environ. Sci. Technol. 37, 3935–44. doi:10.1021/es026196f

58. Corp, B.H., 1988. High-Speed Amino Acid Analysis (AAA) on 1 . 8 µm Reversed-Phase (RP) Columns Application Authors 1–14.

59. Correction for Determining the Humification Index of Dissolved Organic Matter ", 2002. 36, 200692.

60. Cory, R.M., Boyer, E.W., Mcknight, D.M., 2011. Forest Hydrology and Biogeochemistry. Ecological Studies 216, 117–135. doi:10.1007/978-94-007-1363-5

61. Cory, R.M., McKnight, D.M., 2005. Fluorescence spectroscopy reveals ubiquitous presence of oxidized and reduced quinones in dissolved organic matter. Environ. Sci. Technol. 39, 8142–9.

62. Cory, R.M., Miller, M.P., Mcknight, D.M., Guerard, J.J., Miller, P.L., 2010. OCEANOGRAPHY : METHODS Effect of instrument-specific response on the analysis of fulvic acid fluorescence spectra 67–78.

63. Couture, R.M., Van Cappellen, P., 2011. Reassessing the role of sulfur geochemistry on arsenic speciation in reducing environments. J. Hazard. Mater. 189, 647–652. doi:10.1016/j.jhazmat.2011.02.029

64. Couture, R.-M., Wallschläger, D., Rose, J., Van Cappellen, P., 2013. Arsenic binding to organic and inorganic sulfur species during microbial sulfate reduction: a sediment flow-through reactor experiment. Environ. Chem. 10, 285. doi:10.1071/EN13010

65. Craw, D., Koons, P.O., Horton, T., Chamberlain, C.P., 2002. Tectonically driven fluid flow and gold mineralisation in active collisional orogenic belts: comparison between New Zealand and western Himalaya. Tectonophysics 348, 135–153. doi:10.1016/S0040-1951(01)00253-0

66. Cullen, W.R., Reimer, K.J., 1989. Arsenic speciation in the environment. Chem. Rev. 89, 713–764. doi:10.1021/cr00094a002

67. Datta, S., Mailloux, B., Jung, H.-B., Hoque, M. a, Stute, M., Ahmed, K.M., Zheng, Y., 2009. Redox trapping of arsenic during groundwater discharge in sediments from the Meghna riverbank in Bangladesh. Proc. Natl. Acad. Sci. U. S. A. 106, 16930–5. doi:10.1073/pnas.0908168106

68. Datta, S., Neal, A.W., Mohajerin, T.J., Ocheltree, T., Rosenheim, B.E., White, C.D., Johannesson, K.H., 2011. Perennial ponds are not an important source of water or dissolved organic matter to groundwaters with high arsenic concentrations in West Bengal, India. Geophys. Res. Lett. 38, 1–5. doi:10.1029/2011GL049301

69. Dhar, R.K., Zheng, Y., Saltikov, C.W., Radloff, K. a., Mailloux, B.J., Ahmed, K.M., Van Geen, A., 2011. Microbes enhance mobility of arsenic in pleistocene aquifer sand from Bangladesh. Environ. Sci. Technol. 45, 2648–2654. doi:10.1021/es1022015

70. Dowling, C.B., 2002. Geochemical study of arsenic release mechanisms in the Bengal Basin groundwater. Water Resour. Res. 38, 1–18. doi:10.1029/2001WR000968

71. Duursma, Egbert K., and M.M., Duursma, E.K., Marchand., M., 1974. Aspects of organic marine pollution. Oceanogr. Mar. Biol. An Annu. Rev. 12, 315–431.

72. Earl, W.L., T., J.C., 1998. Applications of NMR spectroscopy to the study of the chemistry of environmental interfaces., Structure and surface reactions of soil particles1.

73. Eiche, E., Neumann, T., Berg, M., Weinman, B., van Geen, A., Norra, S., Berner, Z., Trang, P.T.K., Viet, P.H., Stüben, D., 2008. Geochemical processes underlying a sharp contrast in groundwater arsenic concentrations in a village on the Red River delta, Vietnam. Appl. Geochemistry 23, 3143–3154. doi:10.1016/j.apgeochem.2008.06.023

74. Excitation, M., 1990. Multiphoton Excitation and Microscopy 18.1. 607–621.

75. Fan, T.W.-M., Higashi, R.M., Lane, A.N., 2000. Chemical Characterization of a Chelator-Treated Soil Humate by Solution-State Multinuclear Two-Dimensional NMR with FTIR and Pyrolysis-GCMS. Environ. Sci. Technol. 34, 1636–1646. doi:10.1021/es991127v

76. Fang, X., Mao, J., Cory, R.M., McKnight, D.M., Schmidt-Rohr, K., 2011. 15N and 13C{14N} NMR investigation of the major nitrogen-containing segment in an aquatic fulvic acid: evidence for a hydantoin derivative. Magn. Reson. Chem. 49, 775–80. doi:10.1002/mrc.2816

77. Features, B., 2012. CQA Arsenic Removal Media 4–5.

78. Fellman, J.B., D'Amore, D. V., Hood, E., Boone, R.D., 2008. Fluorescence characteristics and biodegradability of dissolved organic matter in forest and wetland soils from coastal temperate watersheds in southeast Alaska. Biogeochemistry 88, 169–184. doi:10.1007/s10533-008-9203-x

79. Fellman, J.B., Hood, E., D'Amore, D. V., Edwards, R.T., White, D., 2009a. Seasonal changes in the chemical quality and biodegradability of dissolved organic matter exported from soils to

streams in coastal temperate rainforest watersheds. Biogeochemistry 95, 277–293. doi:10.1007/s10533-009-9336-6

80. Fellman, J.B., Hood, E., Edwards, R.T., Jones, J.B., 2009b. Uptake of Allochthonous Dissolved Organic Matter from Soil and Salmon in Coastal Temperate Rainforest Streams. Ecosystems 12, 747–759. doi:10.1007/s10021-009-9254-4

81. Fellman, J.B., Hood, E., Spencer, R.G.M., 2010. Fluorescence spectroscopy opens new windows into dissolved organic matter dynamics in freshwater ecosystems: A review. Limnol. Oceanogr. 55, 2452–2462. doi:10.4319/lo.2010.55.6.2452

82. Fellman, J.B., Miller, M.P., Cory, R.M., D'Amore, D. V, White, D., 2009. Characterizing dissolved organic matter using PARAFAC modeling of fluorescence spectroscopy: a comparison of two models. Environ. Sci. Technol. 43, 6228–34.

83. Fendorf, S., Michael, H. a, van Geen, A., 2010. Spatial and temporal variations of groundwater arsenic in South and Southeast Asia. Science 328, 1123–1127. doi:10.1126/science.1172974

84. Fluorophores, N., 1998. Novel Fluorophores.

85. Flynn, T.M., Sanford, R. a, Ryu, H., Bethke, C.M., Levine, A.D., Ashbolt, N.J., Santo Domingo, J.W., 2013. Functional microbial diversity explains groundwater chemistry in a pristine aquifer. BMC Microbiol. 13, 146. doi:10.1186/1471-2180-13-146

86. Fujii, M., Imaoka, A., Yoshimura, C., Waite, T.D., 2014. Effects of molecular composition of natural organic matter on ferric iron complexation at circumneutral pH. Environ. Sci. Technol. 48, 4414–24. doi:10.1021/es405496b

87. Fujiwara, M., 2006. Fluorescence Lifetime Imaging Microscopy: Two 414, 633–642. doi:10.1016/S0076-6879(06)14033-1

88. Gao, S., Fujii, R., Chalmers, A.T., Tanji, K.K., 2004. Evaluation of Adsorbed Arsenic and Potential Contribution to Shallow ...

89. Gao, S., Goldberg, S., Herbel, M.J., Chalmers, a. T., Fujii, R., Tanji, K.K., 2006. Sorption processes affecting arsenic solubility in oxidized surface sediments from Tulare Lake Bed, California. Chem. Geol. 228, 33–43. doi:10.1016/j.chemgeo.2005.11.017

90. Gendron, R.P., 2010. & Evolution Classification Caminalcules 62, 570–576.

91. Geucke, T., Deowan, S. a., Hoinkis, J., Pätzold, C., 2009. Performance of a small-scale RO desalinator for arsenic removal. Desalination 239, 198–206. doi:10.1016/j.desal.2008.03.018

92. Goldberg, S., 2002. Competitive Adsorption of Arsenate and Arsenite on Oxides and Clay Minerals. Soil Sci. Soc. Am. J. 66, 413. doi:10.2136/sssaj2002.4130

93. Goldman, J., Rounds, S., 2012. Applications of Fluorescence Spectroscopy for Monitoring Water Quality in an Urban Watershed Approach :

94. Goldserg, S., 1985. (1986) Chemical Modeling of Arsenate Adsorption on Aluminum and Iron Oxide Minerals. Soil Sci. Soc. Am. J. 50, 1154–1157.

95. Gotkowitz, M., Ellickson, K., Clary, A., Bowman, G., Standridge, J., Sonzogni, W., 2008. Effect of Well Disinfection on Arsenic in Ground Water. Ground Water Monit. Remediat. 28, 60–67. doi:10.1111/j.1745-6592.2008.00192.x

96. Haiber, S., Burba, P., Herzog, H., Lambert, J., 1999. Elucidation of aquatic humic partial structures by multistage ultrafiltration and two-dimensional nuclear magnetic resonance spectrometry. Fresenius. J. Anal. Chem. 364, 215–218. doi:10.1007/s002160051326

97. Harshman, R. a, 1970. Foundations of the PARAFAC procedure: Models and conditions for an "explanatory" multimodal factor analysis. UCLA Work. Pap. Phonetics 16, 1– 84.

98. Hartree, E.F., 1972. Determination of Protein: A Modification of the Lowry Method That Gives a Linear Photometric Response. Anal. Biochem. 48, 422–427.

99. Harvey, C.F., Ashfaque, K.N., Yu, W., Badruzzaman, a. B.M., Ali, M.A., Oates, P.M., Michael, H. a., Neumann, R.B., Beckie, R., Islam, S., Ahmed, M.F., 2006. Groundwater dynamics and arsenic contamination in Bangladesh. Chem. Geol. 228, 112–136. doi:10.1016/j.chemgeo.2005.11.025

100. Harvey, C.F., Swartz, C.H., Badruzzaman, a B.M., Keon-Blute, N., Yu, W., Ali, M.A., Jay, J., Beckie, R., Niedan, V., Brabander, D., Oates, P.M., Ashfaque, K.N., Islam, S., Hemond, H.F., Ahmed, M.F., 2002. Arsenic mobility and groundwater extraction in Bangladesh. Science 298, 1602–6. doi:10.1126/science.1076978

101. Hasan, M.A., Ahmed, K.M., Sracek, O., Bhattacharya, P., Brömssen, M., Broms, S., Fogelström, J., Mazumder, M.L., Jacks, G., 2007. Arsenic in shallow groundwater of Bangladesh: Investigations from three different physiographic settings. Hydrogeol. J. 15, 1507–1522. doi:10.1007/s10040-007-0203-z

102. He, Y.T., Fitzmaurice, A.G., Bilgin, A., Choi, S., O'Day, P., Horst, J., Harrington, J., James Reisinger, H., Burris, D.R., Hering, J.G., 2010. Geochemical processes controlling arsenic mobility in groundwater: A case study of arsenic mobilization and natural attenuation. Appl. Geochemistry 25, 69–80. doi:10.1016/j.apgeochem.2009.10.002

103. Helms, J.R., Stubbins, A., Ritchie, J.D., Minor, E.C., Kieber, D.J., Mopper, K., 2008. Absorption spectral slopes and slope ratios as indicators of molecular weight, source, and photobleaching of chromophoric dissolved organic matter. Limnol. Oceanogr. 53, 955–969. doi:10.4319/lo.2008.53.3.0955

104. Henderson, R.K., Baker, a, Murphy, K.R., Hambly, a, Stuetz, R.M., Khan, S.J., 2009. Fluorescence as a potential monitoring tool for recycled water systems: a review. Water Res. 43, 863–81. doi:10.1016/j.watres.2008.11.027

105. Hertkorn, N., Permin, A., Perminova, I., Kovalevskii, D., Yudov, M., Petrosyan, V., Kettrup, A., 2002. Comparative Analysis of Partial Structures of a Peat Humic and Fulvic Acid Using One- and Two-Dimensional Nuclear Magnetic Resonance Spectroscopy. J. Environ. Qual. 31, 375–387. doi:10.2134/jeq2002.3750

106. Hertkorn, N., Benner, R., Frommberger, M., Schmitt-Kopplin, P., Witt, M., Kaiser, K., Kettrup, A., Hedges, J.I., 2006. Characterization of a major refractory component of marine dissolved organic matter. Geochim. Cosmochim. Acta 70, 2990–3010. doi:10.1016/j.gca.2006.03.021

107. Hertkorn, N., Schmitt-Kopplin, P., 1998. Two dimensional NMR spectroscopy of humic substances. Proc 9th Int Conf Int Humic Subst. Soc. 21–25.

108. Hirsh, E., Tsao, A., 1997. United States Patent [19].

109. Holbrook, R.D., DeRose, P.C., Leigh, S.D., Rukhin, A.L., Heckert, N.A., 2006. Excitation-emission matrix fluorescence spectroscopy for natural organic matter characterization: a quantitative evaluation of calibration and spectral correction procedures. Appl. Spectrosc. 60, 791–9. doi:10.1366/000370206777886973

110. Holm, T.R., 2004. WMRC Reports.

111. Holm, T.R., 1995. Ground-Water Quality in the Mahomet Aquifer , McLean , Logan , and Tazewell Counties Ground-Water Quality in the Mahomet Aquifer , McLean , Logan , and Tazewell Counties.

112. Hood, E., Fellman, J., Spencer, R.G.M., Hernes, P.J., Edwards, R., D/'Amore, D., Scott, D., 2009. Glaciers as a source of ancient and labile organic matter to the marine environment. Nature 462, 1044–1047.

113. Hood, E., Williams, M.W., McKnight, D.M., 2005. Sources of dissolved organic matter (DOM) in a Rocky Mountain stream using chemical fractionation and stable isotopes. Biogeochemistry 74, 231–255. doi:10.1007/s10533-004-4322-5

114. Hoque, E., Wolf, M., Teichmann, G., Peller, E., Schimmack, W., Buckau, G., 2003. Influence of ionic strength and organic modifier concentrations on characterization of aquatic fulvic and humic acids by high-performance size-exclusion chromatography. J. Chromatogr. A 1017, 97–105. doi:10.1016/j.chroma.2003.08.038

115. Hossain, M.A., Mukharjee, A., Sengupta, M.K., Ahamed, S., Das, B., Nayak, B., Pal, A., Rahman, M.M., Chakraborti, D., 2006. Million Dollar Arsenic Removal Plants in West Bengal , India : Useful or Not ? 41, 216–225.

116. Hossain, M.A., Sengupta, M.K., Ahamed, S., Rahman, M.M., Mondal, D., Lodh, D., Das, B., Nayak, B., Roy, B.K., Mukherjee, A., Chakraborti, D., 2005. Ineffectiveness and poor reliability of arsenic removal plants in West Bengal, India. Environ. Sci. Technol. 39, 4300–6.

117. Hua, B., Yang, J., Veum, K., Jones, J., Deng, B., 2009. Determination of disinfection byproduct precursors in lake water by fluorescence EEM- PARAFAC technique 1–15.

118. Hudson, N., Baker, A., Ward, D., Reynolds, D.M., Brunsdon, C., Carliell-Marquet, C., Browning, S., 2008. Can fluorescence spectrometry be used as a surrogate for the Biochemical Oxygen Demand (BOD) test in water quality assessment? An example from South West England. Sci. Total Environ. 391, 149–58. doi:10.1016/j.scitotenv.2007.10.054

119. Hudson, N., Reynolds, D., 2007. FLUORESCENCE ANALYSIS OF DISSOLVED ORGANIC MATTER IN NATURAL , WASTE AND POLLUTED WATERS — A REVIEW 649, 631–649. doi:10.1002/rra

120. Huguet, A., Vacher, L., Relexans, S., Saubusse, S., Froidefond, J.M., Parlanti, E., 2009. Properties of fluorescent dissolved organic matter in the Gironde Estuary. Org. Geochem. 40, 706–719. doi:10.1016/j.orggeochem.2009.03.002

121. Huntsman-Mapila, P., Mapila, T., Letshwenyo, M., Wolski, P., Hemond, C., 2006. Characterization of arsenic occurrence in the water and sediments of the Okavango Delta, NW Botswana. Appl. Geochemistry 21, 1376–1391. doi:10.1016/j.apgeochem.2006.05.003

122. Huq, S.M.I., Nesa, L., Chowdhury, M.T.A., Joardar, J.C., 2011. Disposal of Arsenic Filter Sludge in Soil and its Consequences 5, 165–176.

123. Hussam, a., Habibuddowla, M., Alauddin, M., Hossain, Z. a., Munir, a. K.M., Khan, a. H., 2003. Chemical Fate of Arsenic and Other Metals in Groundwater of Bangladesh: Experimental Measurement and Chemical Equilibrium Model. J. Environ. Sci. Heal. Part A 38, 71–86. doi:10.1081/ESE-120016882

124. Hussam, A., Munir, A.K.M., 2010. SONO Water Filter : A Sustainable Solution for Arsenic Crisis and Clean Drinking Water SONO Water Filter : A Sustainable Solution for Arsenic Crisis and Clean Drinking Water 1–2.

125. Hussam, A., Munir, A.K.M., 2007. A simple and effective arsenic filter based on composite iron matrix: development and deployment studies for groundwater of Bangladesh. J. Environ. Sci. Health. A. Tox. Hazard. Subst. Environ. Eng. 42, 1869–78. doi:10.1080/10934520701567122

126. Ishii, S.K.L., Boyer, T.H., 2012. Behaviour of Reoccurring PARAFAC Components in Fluorescent Dissolved Organic Matter in Natural and Engineered Systems: A Critical Review.

127. Iv, J.P.T., Saunders, J.A., 2006. Groundwater geochemistry, geology and microbiology of arsenic contaminated holocene alluvial aquifers, Manikganj, Bangladesh.

128. Jaffé, R., McKnight, D., Maie, N., Cory, R., McDowell, W.H., Campbell, J.L., 2008. Spatial and temporal variations in DOM composition in ecosystems: The importance of long-term monitoring of optical properties. J. Geophys. Res. 113, G04032. doi:10.1029/2008JG000683

129. Jennifer A. Wilkie, J.G.H., 1995. Adsorption of arsenic onto hydrous ferrix oxide: effects of adsorbate/adsorbent ratios and co-occuring solutes. Colloids Surfaces A 107.

130. Jiang, J., Bauer, I., Paul, A., Kappler, A., 2009. Arsenic redox changes by microbially and chemically formed semiquinone radicals and hydroquinones in a humic substance model quinone. Environ. Sci. Technol. 43, 3639–45.

131. Jiang, J., Kappler, A., 2008. Kinetics of microbial and chemical reduction of humic substances: implications for electron shuttling. Environ. Sci. Technol. 42, 3563–9.

132. Jin, H., Wen, H., Yang, H., Liu, Z., Ren, Z., Che, G., Zhao, Z., 2003. Arsenic poisoning of Bangladesh groundwater. Sci. Technol. 395, 16–18.

133. Jin, Q., Roden, E.E., Giska, J.R., 2013. Geomicrobial Kinetics: Extrapolating Laboratory Studies to Natural Environments. Geomicrobiol. J. 30, 173–185. doi:10.1080/01490451.2011.653084

134. Kalbitz, K., Geyer, W., Geyer, S., 1999. Spectroscopic properties of dissolved humic substances—a reflection of land use history in a fen area. Biogeochemistry 47, 219–238. doi:10.1007/BF00994924

135. Kalbitz, K., Geyer, W., Geyer, S., 1999. Spectroscopic properties of dissolved humic substances ? a reflection of land use history in a fen area. Biogeochemistry 47, 219–238. doi:10.1007/BF00994924

136. Kalle, K., 1949. Fluoreszenz und Gelbstoff im Bottnischen und Finnischen Meerbusen. Dtsch. Hydrogr. Zeitschrift 2, 117–124. doi:10.1007/BF02225972

137. Kappler, A., Benz, M., Schink, B., Brune, A., 2004. Electron shuttling via humic acids in microbial iron(III) reduction in a freshwater sediment. FEMS Microbiol. Ecol. 47, 85–92. doi:10.1016/S0168-6496(03)00245-9

138. Kar, S., Maity, J.P., Jean, J.-S., Liu, C.-C., Nath, B., Yang, H.-J., Bundschuh, J., 2010. Arsenic-enriched aquifers: Occurrences and mobilization of arsenic in groundwater of Ganges Delta Plain, Barasat, West Bengal, India. Appl. Geochemistry 25, 1805–1814. doi:10.1016/j.apgeochem.2010.09.007

139. Keimowitz, a R., Mailloux, B.J., Cole, P., Stute, M., Simpson, H.J., Chillrud, S.N., 2007. Laboratory investigations of enhanced sulfate reduction as a groundwater arsenic remediation strategy. Environ. Sci. Technol. 41, 6718–24.

140. Khan, A.H., Rasul, S.B., Munir, A.K.M., Habibuddowla, M., Alauddin, M., Newaz, S.S., Hussam, A., Diagnostic, S., Island, S., 2008. Journal of Environmental Science and Health , Part A : Toxic / Hazardous Substances and Environmental Engineering Appraisal of a simple arsenic removal method for ground water of 37–41.

141. Khandaker, N.R., Brady, P. V, Krumhansl, J.L., 2009. ARSENIC REMOVAL FROM DRINKING WATER : A HANDBOOK FOR COMMUNITIES 0–51.

142. Kirk, M.F., 2000. Geothite synthesis 5–7.

143. Kirk, M.F., Holm, T.R., Park, J., Jin, Q., Sanford, R. a., Fouke, B.W., Bethke, C.M., 2004. Bacterial sulfate reduction limits natural arsenic contamination in groundwater. Geology 32, 953. doi:10.1130/G20842.1

144. Kirk, M.F., Roden, E.E., Crossey, L.J., Brealey, A.J., Spilde, M.N., 2010. Experimental analysis of arsenic precipitation during microbial sulfate and iron reduction in model aquifer sediment reactors. Geochim. Cosmochim. Acta 74, 2538–2555. doi:10.1016/j.gca.2010.02.002

145. Klapper, L., McKnight, D.M., Fulton, J.R., Blunt-Harris, E.L., Nevin, K.P., Lovley, D.R., Hatcher, P.G., 2002. Fulvic acid oxidation state detection using fluorescence spectroscopy. Environ. Sci. Technol. 36, 3170–5.

146. Knappett, P.S.K., Escamilla, V., Layton, A., McKay, L.D., Emch, M., Williams, D.E., Huq, R., Alam, J., Farhana, L., Mailloux, B.J., Ferguson, A., Sayler, G.S., Ahmed, K.M., van Geen, A., 2011. Impact of population and latrines on fecal contamination of ponds in rural Bangladesh. Sci. Total Environ. 409, 3174–3182. doi:10.1016/j.scitotenv.2011.04.043

147. Korak, J.A., Dotson, A.D., Summers, R.S., Rosario-ortiz, F.L., 2013. Critical analysis of commonly used fluorescence metrics to characterize dissolved organic matter 9.

148. Krstulovic, a M., Brown, P.R., Rosie, D.M., Champlin, P.B., 1977. High-performance liquid-chromatographic analysis for tryptophan in serum. Clin. Chem. 23, 1984–8.

149. Kulkarni, H., Ozbek, P.O., 2012. OCCURRENCE OF CYCLO-SILOXANES IN WASTEWATER TREATMENT PLANTS – QUANTIFICATION AND MONITORING.

150. Kulp, T.R., Hoeft, S.E., Miller, L.G., Saltikov, C., Murphy, J.N., Han, S., Lanoil, B., Oremland, R.S., 2006. Dissimilatory arsenate and sulfate reduction in sediments of two hypersaline, arsenic-rich soda lakes: Mono and Searles Lakes, California. Appl. Environ. Microbiol. 72, 6514–26. doi:10.1128/AEM.01066-06

151. Laboratory Experiment 2 : Alkalinity and Acidity, 2012. 2–5.

152. Lakowicz, J.R., 2006. Solvent and Environmental Effects 205–235. doi:10.1007/978-0-387-46312-4_6

153. Lam, B., Baer, A., Alaee, M., Lefebvre, B., Moser, A., Williams, A., 2007a. Major Structural Components in F 41.

154. Lam, B., Baer, A., Alaee, M., Lefebvre, B., Moser, A., Williams, A., Simpson, A.J., 2007b. Major Structural Components in Freshwater Dissolved Organic Matter. Environ. Sci. Technol. 41, 8240–8247. doi:10.1021/es0713072

155. Langner, P., Mikutta, C., Kretzschmar, R., 2011. Arsenic sequestration by organic sulphur in peat. Nat. Geosci. 5, 66–73. doi:10.1038/ngeo1329

156. Larsen, L.G., Aiken, G.R., Harvey, J.W., Noe, G.B., Crimaldi, J.P., 2010. Using fluorescence spectroscopy to trace seasonal DOM dynamics, disturbance effects, and hydrologic transport in the Florida Everglades. J. Geophys. Res. 115, G03001. doi:10.1029/2009JG001140

157. Lawaetz, a J., Stedmon, C. a, 2009. Fluorescence intensity calibration using the Raman scatter peak of water. Appl. Spectrosc. 63, 936–40. doi:10.1366/000370209788964548

158. Lee, S.W., 2013. Enhancement of arsenic mobility by Fe(III)-reducing bacteria from iron oxide minerals. J. Mater. Cycles Waste Manag. 15, 362–369. doi:10.1007/s10163-013-0132-y

159. Lee, Y., Nam, S., 2002. Reflection on Kinetic Models to the Chlorine Disinfection for Drinking Water Production 40, 119–124.

160. Legg, T.M., Zheng, Y., Simone, B., Radloff, K. a, Mladenov, N., González, A., Knights, D., Siu, H.C., Rahman, M.M., Ahmed, K.M., McKnight, D.M., Nemergut, D.R., 2012. Carbon, metals, and grain size correlate with bacterial community structure in sediments of a high arsenic aquifer. Front. Microbiol. 3, 82. doi:10.3389/fmicb.2012.00082

161. Lin, H.H.T., Wang, M.C.M., Li, G.G.C., 2004. Complexation of arsenate with humic substance in water extract of compost. Chemosphere 56, 1105–1112. doi:10.1016/j.chemosphere.2004.05.018

162. Liu, G., Cai, Y., 2011. Complexation of Arsenite with Dissolved Organic Matter: Conditional Distribution Coefficients and Apparent Stability Constants. Chemosphere 81, 890–896. doi:10.1016/j.chemosphere.2010.08.002.Complexation

163. Liu, G., Fernandez, A., Cai, Y., 2011a. Supporting Information: Complexation of Arsenite with Humic Acid in the Presence of Ferric Iron. Environ. Sci. Technol. 45, 1–11.

164. Liu, G., Fernandez, A., Cai, Y., 2011b. Complexation of arsenite with humic acid in the presence of ferric iron. Environ. Sci. Technol. 45, 3210–6. doi:10.1021/es102931p

165. Lloyd, T., 1996. Multi-Wavelength Molecular Fluorescence Spectrometry for Quantitative Characterization of Organic Matter 30, 1565–1574.

166. Loiselle, S. a., Bracchini, L., Dattilo, A.M., Ricci, M., Tognazzi, A., Cézar, A., Rossi, C., 2009. The optical characterization of chromophoric dissolved organic matter using wavelength distribution of absorption spectral slopes. Limnol. Oceanogr. 54, 590–597. doi:10.4319/lo.2009.54.2.0590

167. Loucks, D.P., Speight, V., 2008. Technologies for clean WaTer.

168. Lovley, 1996. 1996_Nature_Humic substances as electron acceptors_Lovley.pdf.

169. Lovley, D.R., Coates, J.D., Blunt-Harris, E.L., Phillips, E.J.P., Woodward, J.C., 1996. Humic substances as electron acceptors for microbial respiration. Nature 382, 445–448.

170. Lovley, D.R., Fraga, J.L., Blunt-Harris, E.L., Hayes, L. a., Phillips, E.J.P., Coates, J.D., 1998. Humic Substances as a Mediator for Microbially Catalyzed Metal Reduction. Acta Hydrochim. Hydrobiol. 26, 152–157. doi:10.1002/(SICI)1521-401X(199805)26:3<152::AID-AHEH152>3.0.CO;2-D

171. Lovley, D.R., Fraga, J.L., Coates, J.D., Blunt-Harris, E.L., 1999. Humics as an electron donor for anaerobic respiration. Environ. Microbiol. 1, 89–98.

172. Lovley, D.R., Phillips, E.J.P., 1988. Novel Mode of Microbial Energy Metabolism : Organic Carbon Oxidation Coupled to Dissimilatory Reduction of Iron or Manganese Novel Mode of Microbial Energy Metabolism : Organic Carbon Oxidation Coupled to Dissimilatory Reduction of Iron or Manganese 54.

173. Lovley, D.R., Phillips, E.J.P., 1986. Organic Matter Mineralization with Reduction of Ferric Iron in Anaerobic Sediments Organic Matter Mineralization with Reduction of Ferric Iron in Anaerobic Sediments 51.

174. Lowers, H. a., Breit, G.N., Foster, A.L., Whitney, J., Yount, J., Uddin, M.N., Muneem, A.A., 2007. Arsenic incorporation into authigenic pyrite, Bengal Basin sediment, Bangladesh. Geochim. Cosmochim. Acta 71, 2699–2717. doi:10.1016/j.gca.2007.03.022

175. Luster, J., Lloyd, T., Sposito, G., Fry, I. V., 1996. Multi-Wavelength Molecular Fluorescence Spectrometry for Quantitative Characterization of Copper(II) and Aluminum(III) Complexation by Dissolved Organic Matter. Environ. Sci. Technol. 30, 1565–1574. doi:10.1021/es950542u

176. Mailloux, B.J., Trembath-Reichert, E., Cheung, J., Watson, M., Stute, M., Freyer, G. a, Ferguson, A.S., Ahmed, K.M., Alam, M.J., Buchholz, B.A., Thomas, J., Layton, A.C., Zheng, Y., Bostick, B.C., van Geen, A., 2013. Advection of surface-derived organic carbon fuels microbial reduction in Bangladesh groundwater. Proc. Natl. Acad. Sci. U. S. A. 110, 5331–5. doi:10.1073/pnas.1213141110

177. Management, B., 2002. Best Management Practices for 8–11.

178. Manciulea, A., Baker, A., Lead, J.R., 2009. A fluorescence quenching study of the interaction of Suwannee River fulvic acid with iron oxide nanoparticles. Chemosphere 76, 1023–7. doi:10.1016/j.chemosphere.2009.04.067

179. Mandal, B.K., 1996. arsenic in groundwater.pdf. Curr. Sci.

180. Mann, H.B., Whitney, D.R., 1947. On a Test of Whether one of Two Random Variables is Stochastically Larger than the Other. Ann. Math. Stat. 18, 50–60. doi:10.1214/aoms/1177730491

181. Manning, B.A., Goldberg, S., 1996. M O D E L I N G A R S E N A T E COMPETITIVE A D S O R P T I O N O N KAOLINITE , M O N T M O R I L L O N I T E A N D ILLITE 44.

182. Masamba, W., 2006. Influence of dissolved organic matter and microbial processes on the mobilization of trace elements in Okavango Delta groundwater 1–5.

183. McArthur, J.M., Banerjee, D.M., Hudson-Edwards, K. a., Mishra, R., Purohit, R., Ravenscroft, P., Cronin, a., Howarth, R.J., Chatterjee, a., Talukder, T., Lowry, D., Houghton, S., Chadha, D.K., 2004. Natural organic matter in sedimentary basins and its relation to arsenic in anoxic ground water: The example of West Bengal and its worldwide implications. Appl. Geochemistry 19, 1255–1293. doi:10.1016/j.apgeochem.2004.02.001

184. McArthur, J.M., Ravenscroft, P., Banerjee, D.M., Milsom, J., Hudson-Edwards, K.A., Sengupta, S., Bristow, C., Sarkar, A., Tonkin, S., Purohit, R., 2008. How paleosols influence groundwater flow and arsenic pollution: A model from the Bengal Basin and its worldwide implication. Water Resour. Res. 44, 1–30. doi:10.1029/2007WR006552

185. McArthur, J.M., Ravenscroft, P., Safiulla, S., Thirlwall, M.F., 2001. Arsenic in groundwater: Testing pollution mechanisms for sedimentary aquifers in Bangladesh. Water Resour. Res. 37, 109–117. doi:10.1029/2000WR900270

186. McArthur P. AU3 - Safiullah, S. AU4 - Thirlwall, M.F., J.M.A.-R., 2001. Arsenic in groundwater: testing pollution mechanisms for sedimentary aquifer in Bangladesh RN - Water. Resour. Res., vol. 37, pp. 109-117. Water Resour. Res. 37, 109–117.

187. McCarthy, T.S., 2006. Groundwater in the wetlands of the Okavango Delta, Botswana, and its contribution to the structure and function of the ecosystem. J. Hydrol. 320, 264–282. doi:10.1016/j.jhydrol.2005.07.045

188. Mcknight, D.M., Boyer, E.W., Westerhoff, P.K., Doran, P.T., Kulbe, T., Andersen, D.T., 2013. Organic Material and Aromaticity characterization of dissolved organic matter for indication Spectrofluorometric of precursor organic material and aromaticity.

189. Mcknight, D.M., Boyer, E.W., Westerhoff, P.K., Doran, P.T., Kulbe, T., Andersen, D.T., 2008. Spectrofluorometric Characterization of Dissolved Organic Matter for Indication of Precursor Organic Material and Aromaticity Published by : American Society of Limnology and Oceanography Stable URL : http://www.jstor.org/stable/2670577 46, 38–48.

190. McKnight, D.M., Boyer, E.W., Westerhoff, P.K., Doran, P.T., Kulbe, T., Andersen, D.T., 2001. Spectrofluorometric characterization of dissolved organic matter for indication of precursor organic material and aromaticity. Limnol. Oceanogr. 46, 38–48. doi:10.4319/lo.2001.46.1.0038

191. Measurements, F.L., 1983. Frequency-Domain Lifetime Measurements.

192. Menard, C., Burt, D., Collins, M.R., 2007. Arsenic Removal Using Aged Rapid Sand Filter Media by.

193. Miao, Z., Carreón-Diazconti, C., Carroll, K.C., Brusseau, M.L., 2014. The impact of biostimulation on the fate of sulfate and associated sulfur dynamics in groundwater. J. Contam. Hydrol. 164, 240–50. doi:10.1016/j.jconhyd.2014.06.010

194. Michael, H. a, Voss, C.I., 2008. Evaluation of the sustainability of deep groundwater as an arsenic-safe resource in the Bengal Basin. Proc. Natl. Acad. Sci. U. S. A. 105, 8531–8536. doi:10.1073/pnas.0710477105

195. Michael, H.A., Voss, C.I., 2009a. Controls on groundwater flow in the Bengal Basin of India and Bangladesh: Regional modeling analysis. Hydrogeol. J. 17, 1561–1577. doi:10.1007/s10040-008-0429-4

196. Michael, H.A., Voss, C.I., 2009b. Estimation of regional-scale groundwater flow properties in the Bengal Basin of India and Bangladesh. Hydrogeol. J. 17, 1329–1346. doi:10.1007/s10040-009-0443-1

197. Mikutta, C., Kretzschmar, R., 2011. Spectroscopic evidence for ternary complex formation between arsenate and ferric iron complexes of humic substances. Environ. Sci. Technol.

198. Miller, M.P., McKnight, D.M., Cory, R.M., Williams, M.W., Runkel, R.L., 2006. Hyporheic exchange and fulvic acid redox reactions in an Alpine stream/wetland ecosystem, Colorado Front Range. Environ. Sci. Technol. 40, 5943–5949. doi:10.1021/es060635j

199. Miller, M.P., Simone, B.E., McKnight, D.M., Cory, R.M., Williams, M.W., Boyer, E.W., 2010. New light on a dark subject: comment. Aquat. Sci. 72, 269–275. doi:10.1007/s00027-010-0130-2

200. Mladenov, N., Huntsman-Mapila, P., Wolski, P., Masamba, W.R.L., McKnight, D.M., 2008. Dissolved organic matter accumulation, reactivity, and redox state in ground water of a recharge wetland. Wetlands 28, 747–759. doi:10.1672/07-140.1

201. Mladenov, N., López-Ramos, J., McKnight, D.M., Reche, I., 2009. Alpine lake optical properties as sentinels of dust deposition and global change. Limnol. Oceanogr. 54, 2386–2400. doi:10.4319/lo.2009.54.6_part_2.2386

202. Mladenov, N., Mcknight, D.M., Macko, S. a., Norris, M., Cory, R.M., Ramberg, L., 2007. Chemical characterization of DOM in channels of a seasonal wetland. Aquat. Sci. 69, 456–471. doi:10.1007/s00027-007-0905-2

203. Mladenov, N., McKnight, D.M., Wolski, P., Ramberg, L., 2005. Effects of annual flooding on dissolved organic carbon dynamics within a pristine wetland, the Okavango Delta, Botswana. Wetlands 25, 622–638. doi:10.1672/0277-5212(2005)025[0622:EOAFOD]2.0.CO;2

204. Mladenov, N., Wolski, P., Hettiarachchi, G.M., Murray-Hudson, M., Enriquez, H., Damaraju, S., Galkaduwa, M.B., McKnight, D.M., Masamba, W., 2013. Abiotic and biotic factors influencing the mobility of arsenic in groundwater of a through-flow island in the Okavango Delta, Botswana. J. Hydrol. 518, 326–341. doi:10.1016/j.jhydrol.2013.09.026

205. Mladenov, N., Zheng, Y., Miller, M.P., Nemergut, D.R., Legg, T., Simone, B., Hageman, C., Rahman, M.M., Ahmed, K.M., McKnight, D.M., 2010. Dissolved organic matter sources and consequences for iron and arsenic mobilization in Bangladesh aquifers. Environ. Sci. Technol. 44, 123–8. doi:10.1021/es901472g

206. Mladenov, N., Zheng, Y., Simone, B., Bilinski, T.M., McKnight, D.M., Nemergut, D., Radloff, K. a., Rahman, M.M., Ahmed, K.M., 2015. Dissolved Organic Matter Quality in a Shallow Aquifer of Bangladesh: Implications for Arsenic Mobility. Environ. Sci. Technol. 150827163840003. doi:10.1021/acs.est.5b01962

207. Mohajerin, T.J., Neal, A.W., Telfeyan, K., Sasihharan, S.M., Ford, S., Yang, N., Chevis, D. a., Grimm, D. a., Datta, S., White, C.D., Johannesson, K.H., 2014. Geochemistry of tungsten and arsenic in aquifer systems: A comparative study of groundwaters from west bengal, india, and nevada, usa. Water. Air. Soil Pollut. 225. doi:10.1007/s11270-013-1792-x

208. Moore, J.C., DeVries, J.W., Lipp, M., Griffiths, J.C., Abernethy, D.R., 2010. Total Protein Methods and Their Potential Utility to Reduce the Risk of Food Protein Adulteration. Compr. Rev. Food Sci. Food Saf. 9, 330–357. doi:10.1111/j.1541-4337.2010.00114.x

209. Moran, M.A., Sheldon, W.M., Zepp, R.G., 2000. Carbon loss and optical property changes during long-term photochemical and biological degradation of estuarine dissolved organic matter. Limnol. Oceanogr. 45, 1254–1264. doi:10.4319/lo.2000.45.6.1254

210. Morgan, J.P., G., M.W., 1959. Quaternery geology of the Bengal Basin, East Pakistan and India. Bull. Geol. Soc. Am. 70, 319–342.

211. Morgan, J.P., Mcintire, W.G., 1959. Geological Society of America Bulletin QUATERNARY GEOLOGY OF THE BENGAL BASIN , EAST. doi:10.1130/0016-7606(1959)70

212. Morris, K.F., Cutak, B.J., Dixon, A.M., Larive, C.K., 1999. Analysis of diffusion coefficient distributions in humic and fulvic acids by means of diffusion ordered NMR spectroscopy. Anal. Chem. 71, 5315–21. doi:10.1021/ac9907585

213. Moruzzi, R.B., de Oliveira, S.C., 2013. Mathematical modeling and analysis of the flocculation process in chambers in series. Bioprocess Biosyst. Eng. 36, 357–63. doi:10.1007/s00449-012-0791-4

214. Mukherjee, A., Fryar, A.E., Howell, P.D., 2007a. Regional hydrostratigraphy and groundwater flow modeling in the arsenic-affected areas of the western Bengal basin, West Bengal, India. Hydrogeol. J. 15, 1397–1418. doi:10.1007/s10040-007-0208-7

215. Mukherjee, A., Fryar, A.E., Rowe, H.D., 2007b. Regional-scale stable isotopic signatures of recharge and deep groundwater in the arsenic affected areas of West Bengal, India. J. Hydrol. 334, 151–161. doi:10.1016/j.jhydrol.2006.10.004

216. Mukherjee, A., Fryar, A.E., Scanlon, B.R., Bhattacharya, P., Bhattacharya, A., 2011. Elevated arsenic in deeper groundwater of the western Bengal basin, India: Extent and controls from regional to local scale. Appl. Geochemistry 26, 600–613. doi:10.1016/j.apgeochem.2011.01.017

217. Murphy, E.M., Zachara, J.M., Smith, S.C., 1990. Influence of mineral-bound humic substances on the sorption of hydrophobic organic compounds. Environ. Sci. Technol. 24, 1507–1516. doi:10.1021/es00080a009

218. Murphy, K.R., Butler, K.D., Spencer, R.G.M., Stedmon, C. a, Boehme, J.R., Aiken, G.R., 2010. Measurement of dissolved organic matter fluorescence in aquatic environments: an interlaboratory comparison. Environ. Sci. Technol. 44, 9405–12. doi:10.1021/es102362t

219. Murphy, K.R., Stedmon, C. a., Graeber, D., Bro, R., 2013. Fluorescence spectroscopy and multi-way techniques. PARAFAC. Anal. Methods 5, 6557. doi:10.1039/c3ay41160e

220. Nebbioso, A., Piccolo, A., 2013. Molecular characterization of dissolved organic matter (DOM): a critical review. Anal. Bioanal. Chem. 405, 109–24. doi:10.1007/s00216-012-6363-2

221. Neumann, R.B., Ashfaque, K.N., Badruzzaman, a. B.M., Ashraf Ali, M., Shoemaker, J.K., Harvey, C.F., 2010. Anthropogenic influences on groundwater arsenic concentrations in Bangladesh. Nat. Geosci. 3, 46–52. doi:10.1038/ngeo685

222. Nevin, K.P., Lovley, D.R., 2000. Lack of production of electron-shuttling compounds or solubilization of Fe(III) during reduction of insoluble Fe(III) oxide by Geobacter metallireducens. Appl. Environ. Microbiol. 66, 2248–2251. doi:10.1128/AEM.66.5.2248-2251.2000

223. Nevin, K.P., Lovley, D.R., 2000. Lack of Production of Electron-Shuttling Compounds or Solubilization of Fe (III) during Reduction of Insoluble Fe (III) Oxide by Geobacter metallireducens Lack of Production of Electron-Shuttling Compounds or Solubilization of Fe (III) during Reduct. doi:10.1128/AEM.66.5.2248-2251.2000.Updated

224. Newman, D.K., Kennedy, E.K., Coates, J.D., Ahmann, D., Ellis, D.J., Lovley, D.R., Morel, F.M., 1997. Dissimilatory arsenate and sulfate reduction in Desulfotomaculum auripigmentum sp. nov. Arch. Microbiol. 168, 380–8.

225. Nickson, R.T., McArthur, J.M., Ravenscroft, P., Burgess, W.G., Ahmed, K.M., 2000. Mechanism of arsenic release to groundwater, Bangladesh and West Bengal. Appl. Geochemistry 15, 403–413. doi:10.1016/S0883-2927(99)00086-4

226. Ohno, T., 2002a. Fluorescence inner-filtering correction for determining the humification index of dissolved organic matter. Environ. Sci. Technol. 36, 742–6.

227. Ohno, T., 2002b. Response to Comment on "Fluorescence Inner-Filtering Correction for Determining the Humification Index of Dissolved Organic Matter" †. Environ. Sci. Technol. 36, 4196–4196. doi:10.1021/es020113d

228. Ohno, T., Amirbahman, A., Bro, R., 2008. Parallel factor analysis of excitation-emission matrix fluorescence spectra of water soluble soil organic matter as basis for the determination of conditional metal binding parameters. Environ. Sci. Technol. 42, 186–92.

229. Onstott, T.C.C., Chan, E., Polizzotto, M.L.L., Lanzon, J., DeFlaun, M.F.F., 2011. Precipitation of arsenic under sulfate reducing conditions and subsequent leaching under aerobic conditions. Appl. Geochemistry 26, 269–285. doi:10.1016/j.apgeochem.2010.11.027

230. Oremland, R.S., 2003. The ecology of arsenic 300, 939–944.

231. Oremland, R.S., Hoeft, S.E., Santini, J.M., Bano, N., Hollibaugh, R.A., Hollibaugh, J.T., 2002. Anaerobic Oxidation of Arsenite in Mono Lake Water and by a Facultative , Anaerobic Oxidation of Arsenite in Mono Lake Water and by a Facultative , Arsenite-Oxidizing Chemoautotroph , Strain MLHE-1. doi:10.1128/AEM.68.10.4795

232. Oremland, R.S., Stolz, J.F., Hollibaugh, J.T., 2004. The microbial arsenic cycle in Mono Lake, California. FEMS Microbiol. Ecol. 48, 15–27. doi:10.1016/j.femsec.2003.12.016

233. Osburn, C.L., Handsel, L.T., Mikan, M.P., Paerl, H.W., Montgomery, M.T., 2012. Fluorescence tracking of dissolved and particulate organic matter quality in a river-dominated estuary. Environ. Sci. Technol. 46, 8628–36. doi:10.1021/es3007723

234. Palmer, N.E., von Wandruszka, R., 2010. Humic acids as reducing agents: The involvement of quinoid moieties in arsenate reduction. Environ. Sci. Pollut. Res. 17, 1362–1370. doi:10.1007/s11356-010-0322-2

235. Parlanti, E., Wörz, K., Geoffroy, L., Lamotte, M., Wo, K., Geo, L., Lamotte, M., 2000. Dissolved organic matter ¯uorescence spectroscopy as a tool to estimate biological activity in a coastal zone submitted to anthropogenic inputs. Org. Geochem. 31, 1765–1781. doi:10.1016/S0146-6380(00)00124-8

236. Pellegrini, C., 2010. Investigating the Suitability of UV/Vis Spectrophotometric Methods for Analyzing Arsenic in Urban Soils for use in Undergraduate Laboratory Courses.

237. Perrette, Y., Delannoy, J., Desmet, M., Lignier, V., Destombes, J., 2005. Speleothem organic matter content imaging. The use of a Fluorescence Index to characterise the maximum emission wavelength. Chem. Geol. 214, 193–208. doi:10.1016/j.chemgeo.2004.09.002

238. Peuravuori, J., Pihlaja, K., 1997. Molecular size distribution and spectroscopic properties of aquatic humic substances. Anal. Chim. Acta 337, 133–149. doi:10.1016/S0003-2670(96)00412-6

239. Pi, K., Wang, Y., Xie, X., Huang, S., Yu, Q., Yu, M., 2015. Geochemical effects of dissolved organic matter biodegradation on arsenic transport in groundwater systems. J. Geochemical Explor. 149, 8–21. doi:10.1016/j.gexplo.2014.11.005

240. Plasmon-, S., 2000. Engineering : 861–871.

241. Polizzotto, M.L., Kocar, B.D., Benner, S.G., Sampson, M., Fendorf, S., 2008. Near-surface wetland sediments as a source of arsenic release to ground water in Asia. Nature 454, 505–508. doi:10.1038/nature07093

242. Postma, D., Larsen, F., Minh Hue, N.T., Duc, M.T., Viet, P.H., Nhan, P.Q., Jessen, S., 2007. Arsenic in groundwater of the Red River floodplain, Vietnam: Controlling geochemical processes and reactive transport modeling. Geochim. Cosmochim. Acta 71, 5054–5071. doi:10.1016/j.gca.2007.08.020

243. Process, A.R., 2010. Prepared in cooperation with the City of Wichita , Kansas , Water Quality in the Equus Beds Aquifer and the Little Arkansas River Before Implementation of Large-Scale

Artificial Recharge , South-Central Kansas , 1995 – 2005 Equus Beds Aquifer — Artificial 1995–2005.

244. Proctor, C.J., Baker, a., Barnes, W.L., Gilmour, M. a., 2000. A thousand year speleothem proxy record of North Atlantic climate from Scotland. Clim. Dyn. 16, 815–820. doi:10.1007/s003820000077

245. Pullin, M.J., Cabaniss, S.E., 2003. The effects of pH, ionic strength, and iron–fulvic acid interactions on the kinetics of non-photochemical iron transformations. II. The kinetics of thermal reduction. Geochim. Cosmochim. Acta 67, 4079–4089. doi:10.1016/S0016-7037(03)00367-3

246. Quality, D., 1996. Iron in Drinking-water Background document for development of 2.

247. Rahaman, S., Sinha, a C., Pati, R., Mukhopadhyay, D., 2013. Arsenic contamination: a potential hazard to the affected areas of West Bengal, India. Environ. Geochem. Health 35, 119–32. doi:10.1007/s10653-012-9460-4

248. Ramberg, L., Wolski, P., Krah, M., Oppenheimer, H., 2006. Water balance and infiltration in a seasonal floodplain in the Okavango Delta, Botswana, 26, 677–690.

249. Ramberg, L., Wolski, P., Wolski, Æ.P., 2007. Growing islands and sinking solutes: processes maintaining the endorheic Okavango Delta as a freshwater system. Plant Ecol. 196, 215–231. doi:10.1007/s11258-007-9346-1

250. Ravenscroft, P., Burgess, W.G., Ahmed, K.M., Burren, M., Perrin, J., 2005. Arsenic in groundwater of the Bengal Basin, Bangladesh: Distribution, field relations, and hydrogeological setting. Hydrogeol. J. 13, 727–751. doi:10.1007/s10040-003-0314-0

251. Redman, A.D., Macalady, D.L., Ahmann, D., 2002. Natural organic matter affects arsenic speciation and sorption onto hematite. Environ. Sci. Technol. 36, 2889–96.

252. Reynolds, D.M., 2003. Rapid and direct determination of tryptophan in water using synchronous fluorescence spectroscopy. Water Res. 37, 3055–60. doi:10.1016/S0043-1354(03)00153-2

253. Reza, a. H.M.S., Jean, J.S., Lee, M.K., Liu, C.C., Bundschuh, J., Yang, H.J., Lee, J.F., Lee, Y.C., 2010. Implications of organic matter on arsenic mobilization into groundwater: Evidence from northwestern (Chapai-Nawabganj), central (Manikganj) and southeastern (Chandpur) Bangladesh. Water Res. 44, 5556–5574. doi:10.1016/j.watres.2010.09.004

254. Rhine, E.D., Phelps, C.D., Young, L.Y., 2006. Anaerobic arsenite oxidation by novel denitrifying isolates. Environ. Microbiol. 8, 899–908. doi:10.1111/j.1462-2920.2005.00977.x

255. Ritter, K., Aiken, G.R., Ranville, J.F., Bauer, M., Macalady, D.L., 2006. Evidence for the aquatic binding of arsenate by natural organic matter-suspended Fe(III). Environ. Sci. Technol. 40, 5380–7.

256. Roberts, H., 1997. Dynamic changes of the Holocene Mississippi River delta plain: the delta cycle. J. Coast. Res. 13, 605–627.

257. Roccaro, P., Vagliasindi, F.G. a., Korshin, G. V., 2009. Changes in NOM Fluorescence Caused by Chlorination and their Associations with Disinfection by-Products Formation. Environ. Sci. Technol. 43, 724–729. doi:10.1021/es801939f

258. Roden, E.E., 2006. Geochemical and microbiological controls on dissimilatory iron reduction. Comptes Rendus Geosci. 338, 456–467. doi:10.1016/j.crte.2006.04.009

259. Roden, E.E., Kappler, A., Bauer, I., Jiang, J., Paul, A., Stoesser, R., Konishi, H., Xu, H., 2010. Extracellular electron transfer through microbial reduction of solid-phase humic substances. Nat. Geosci. 3, 417–421. doi:10.1038/ngeo870

260. Rodriguez-Freire, L., Sierra-Alvarez, R., Root, R., Chorover, J., Field, J.A., 2014. Biomineralization of arsenate to arsenic sulfides is greatly enhanced at mildly acidic conditions. Water Res. 66, 242–253. doi:10.1016/j.watres.2014.08.016

261. Rose, A.L., Waite, T.D., 2003. Kinetics of iron complexation by dissolved natural organic matter in coastal waters. Mar. Chem. 84, 85–103. doi:10.1016/S0304-4203(03)00113-0

262. Rostad, C.E., Leenheer, J. a., 2004. Factors that affect molecular weight distribution of Suwannee river fulvic acid as determined by electrospray ionization/mass spectrometry. Anal. Chim. Acta 523, 269–278. doi:10.1016/j.aca.2004.06.065

263. Roy, J., 2007. Estimating the Economic Benefits of Arsenic Removal in India : A Case Study from West Bengal.

264. Roychowdhury, T., Uchino, T., Tokunaga, H., Ando, M., 2002. Arsenic and other heavy metals in soils from an arsenic-affected area of West Bengal, India. Chemosphere 49, 605–618. doi:10.1016/S0045-6535(02)00309-0

265. Ryan, D.K., Weber, J.H., 1982. Fluorescence quenching titration for determination of complexing capacities and stability constants of fulvic acid. Anal. Chem. 54, 986–990. doi:10.1021/ac00243a033

266. S.V.Panno, K.C.Hackley, K.Cartwright, C.L.L., S.V. Panno, K.C. Hackley, K.C. and C.L.L., 1994. Hydrochemistry of the Mahomet bedrock valley aquifer, east-central Illinois: Indicators of recharge and ground-water flow. Ground Water 32.

267. Saha, D., 2009. Arsenic groundwater contamination in parts of middle Ganga plain , Bihar 97, 753–755.

268. Saha, D., Sarangam, S.S., Dwivedi, S.N., Bhartariya, K.G., 2009. Evaluation of hydrogeochemical processes in arsenic-contaminated alluvial aquifers in parts of Mid-Ganga Basin, Bihar, Eastern India. Environ. Earth Sci. 61, 799–811. doi:10.1007/s12665-009-0392-y

269. Sankar, M.S., Vega, M. a., Defoe, P.P., Kibria, M.G., Ford, S., Telfeyan, K., Neal, a., Mohajerin, T.J., Hettiarachchi, G.M., Barua, S., Hobson, C., Johannesson, K., Datta, S., 2014. Elevated arsenic and manganese in groundwaters of Murshidabad, West Bengal, India. Sci. Total Environ. 488-489, 570–579. doi:10.1016/j.scitotenv.2014.02.077

270. Santín, C., Yamashita, Y., Otero, X.L., Álvarez, M.Á., Jaffé, R., 2009. Characterizing humic substances from estuarine soils and sediments by excitation-emission matrix spectroscopy and parallel factor analysis. Biogeochemistry 96, 131–147. doi:10.1007/s10533-009-9349-1

271. Sarkar, S., Blaney, L.M., Gupta, A., Ghosh, D., SenGupta, A.K., 2008. Arsenic Removal from Groundwater and Its Safe Containment in a Rural Environment: Validation of a Sustainable Approach. Environ. Sci. Technol. 42, 4268–4273. doi:10.1021/es702556t

272. Sarkar, S., Gupta, A., Biswas, R.K., Deb, A.K., Greenleaf, J.E., Sengupta, A.K., 2005. Well-head arsenic removal units in remote villages of Indian subcontinent: field results and performance evaluation. Water Res. 39, 2196–206. doi:10.1016/j.watres.2005.04.002

273. Sasidharan, S., 2013. GEOCHEMICAL SIGNIFICANCE OF ARSENIC AND MANGANESE TOXICITY IN.

274. Saunders, J.A., Lee, M.-K.K., Shamsudduha, M., Dhakal, P., Uddin, A., Chowdury, M.T., Ahmed, K.M., 2008. Geochemistry and mineralogy of arsenic in (natural) anaerobic groundwaters. Appl. Geochemistry 23, 3205–3214. doi:10.1016/j.apgeochem.2008.07.002

275. Schnoor, J.L., 1987. Processes, coefficients and models for simulating toxic organics and heavy metals in surface water, EPA.

276. Sciences, O., Kingdom, U., 2009. Metal Complexation by Humic Substances in Seawater 43, 7192–7197.

277. Sciences, P., 2001. Interpretation of heteronuclear and multidimensional NMR spectroscopy of humic substances 495–510.
278. Scott, D.T., McKnight, D.M., Blunt-Harris, E.L., Kolesar, S.E., Lovley, D.R., 1998. Quinone Moieties Act as Electron Acceptors in the Reduction of Humic Substances by Humics-Reducing Microorganisms. Environ. Sci. Technol. 32, 2984–2989. doi:10.1021/es980272q
279. Selim Reza, a. H.M., Jean, J.-S., Lee, M.-K., Kulp, T.R., Hsu, H.-F., Liu, C.-C., Lee, Y.-C., 2012. The binding nature of humic substances with arsenic in alluvial aquifers of Chianan Plain, southwestern Taiwan. J. Geochemical Explor. 114, 98–108. doi:10.1016/j.gexplo.2012.01.002
280. Sengupta, S., Mcarthur, J.M., Sarkar, a., Leng, M.J., Ravenscroft, P., Howarth, R.J., Banerjee, D.M., 2008. Do ponds cause arsenic-pollution of groundwater in the Bengal Basin? An answer from West Bengal. Environ. Sci. Technol. 42, 5156–5164. doi:10.1021/es702988m
281. Shah, B. a., 2007. Role of Quaternary stratigraphy on arsenic-contaminated groundwater from parts of Middle Ganga Plain, UP–Bihar, India. Environ. Geol. 53, 1553–1561. doi:10.1007/s00254-007-0766-y
282. Shah, B.A., 2013. Status of groundwater arsenic pollution in Holocene aquifers from parts of the Ghaghara Basin, India: Its relation to geomorphology and hydrogeological setting. Phys. Chem. Earth, Parts A/B/C 58-60, 68–76. doi:10.1016/j.pce.2013.04.015
283. Sharma, A.K., Tjell, J.C., Mosbæk, H., 2006. Health effects from arsenic in groundwater of the Bengal delta : Effects of iron and water storage practices. Environ. Geoscinces 1, 17–29. doi:10.1306/eg.07310404035
284. Sharma, P., 2010. As-mineral-humic substance interactions – Influence of natural organic matter on sorption and mobility of As.
285. Sharma, P., Ofner, J., Kappler, A., 2010. Formation of binary and ternary colloids and dissolved complexes of organic matter, Fe and As. Environ. Sci. Technol. 44, 4479–85. doi:10.1021/es100066s
286. Simpson, A., Burdon, J., 2001. Interpretation of heteronuclear and multidimensional NMR spectroscopy of humic substances. Eur. J. Soil Sci. 52, 495–509.
287. Simpson, A.A.J., McNally, D.J.D., Simpson, M.M.J., 2011. NMR spectroscopy in environmental research: from molecular interactions to global processes. Prog. Nucl. Magn. Reson. Spectrosc. 58, 97–175. doi:10.1016/j.pnmrs.2010.09.001
288. Simpson, A.A.J., Simpson, M.M.J., Soong, R., 2012. Nuclear magnetic resonance spectroscopy and its key role in environmental research. Environ. Sci. Technol. 46, 11488–96. doi:10.1021/es302154w
289. Singh, A.K., 2006. Chemistry of arsenic in groundwater of Ganges-Brahmaputra river basin. Curr. Sci.
290. Smedley, P.., Kinniburgh, D.., 2002. A review of the source, behaviour and distribution of arsenic in natural waters. Appl. Geochemistry 17, 517–568. doi:10.1016/S0883-2927(02)00018-5
291. Smith, A., Lingas, E., Rahman, M., 2000. Contamination of drinking-water by arsenic in Bangladesh: a public health emergency: RN - Bull. W.H.O., v. 78, p. 1093-1103. Bull. World Health Organ. 78, 1093–1103.
292. Snoeyink, V.L., Jenkins, D., 1980. Water Chemistry.
293. Spencer, R.G.M., Bolton, L., Baker, A., 2007. Freeze/thaw and pH effects on freshwater dissolved organic matter fluorescence and absorbance properties from a number of UK locations. Water Res. 41, 2941–50. doi:10.1016/j.watres.2007.04.012

294. Stedmon, C. a, Markager, S., Bro, R., 2003. Tracing dissolved organic matter in aquatic environments using a new approach to fluorescence spectroscopy. Mar. Chem. 82, 239–254. doi:10.1016/S0304-4203(03)00072-0

295. Stedmon, C. a., Seredyńska-Sobecka, B., Boe-Hansen, R., Le Tallec, N., Waul, C.K., Arvin, E., 2011. A potential approach for monitoring drinking water quality from groundwater systems using organic matter fluorescence as an early warning for contamination events. Water Res. 45, 6030–6038. doi:10.1016/j.watres.2011.08.066

296. Stedmon, C.A., Bro, R., 2008. Characterizing dissolved organic matter fluorescence with parallel factor analysis: a tutorial. Limnol. Oceanogr. Methods 6, 572–579. doi:10.4319/lom.2008.6.572

297. Stedmon, C.A., Markager, S., 2009. Resolving the variability in dissolved organic matter fluorescence in a temperate estuary and its catchment using PARAFAC analysis 50, 686–697.

298. Steed, R., 2010. Analysis of Amino Acids by HPLC.

299. Stollenwerk, K.G., Breit, G.N., Welch, A.H., Yount, J.C., Whitney, J.W., Foster, A.L., Uddin, M.N., Majumder, R.K., Ahmed, N., 2007. Arsenic attenuation by oxidized aquifer sediments in Bangladesh. Sci. Total Environ. 379, 133–50. doi:10.1016/j.scitotenv.2006.11.029

300. Survey, U.S.G., 1989. Characterization of the international humic substances society standards and reference fulvic and humic acids by solution state Carbon – 13 (13C) and Hydrogen-1 (1H) nuclear magnetic resonance spectrometry.

301. Sutton, N.B., van der Kraan, G.M., van Loosdrecht, M.C.M., Muyzer, G., Bruining, J., Schotting, R.J., 2009. Characterization of geochemical constituents and bacterial populations associated with As mobilization in deep and shallow tube wells in Bangladesh. Water Res. 43, 1720–1730. doi:10.1016/j.watres.2009.01.006

302. Tahura, S., Shahidullah, S.M., Rahman, T., Milton, A.H., 1998. Evaluation of An Arsenic Removal Household Device : Bucket Treatment Unit (BTU) 158–170.

303. Technology, D.N.A., 2000. DNA Technology 21.

304. Teymouri, B., 2007. Fluorescence Spectroscopy and Parallel Factor Analysis of Waters from Municipal Waste Sources.

305. Thanabalasingam, P., Pickering, W.F., 1986. Arsenic sorption by humic acids. Environ. Pollut. Ser. B, Chem. Phys. 12, 233–246. doi:10.1016/0143-148X(86)90012-1

306. Thesis, D., 2000. Derivatives for HPLC Analysis.

307. Thorn, K., Folan, D., MacCarthy, P., 1989. Characterization of the international humic substances society standard and reference fulvic and humic acids by solution state carbon-13 and Hydrogen-1 nuclear magnetic resonance spectroscopy [WWW Document]. USGS. URL http://pubs.usgs.gov/wri/1989/4196/report.pdf (accessed 1.14.16).

308. Thurman, E.M., Malcolm, R.L., 1981. Preparative isolation of aquatic humic substances. Environ. Sci. Technol. 15, 463–6. doi:10.1021/es00086a012

309. Time-Resolved Protein Fluorescence, 2000.

310. Tulonen, T., 2004. Role of allochthonous and autochthonous dissolved organic matter (DOM) as a carbon source for bacterioplankton in boreal humic lakes. Dr. Thesis.

311. Ujitake, N.F., 2012. Notes A Method for Quantitative Analysis of Aquatic Humic Substances in Clear Water Based on Carbon Concentration 28, 28–31.

312. Vähätalo, A. V., Wetzel, R.G., 2004. Photochemical and microbial decomposition of chromophoric dissolved organic matter during long (months-years) exposures. Mar. Chem. 89, 313–326. doi:10.1016/j.marchem.2004.03.010

313. Valencia, S., Marín, J.M., Restrepo, G., Frimmel, F.H., 2013. Application of excitation-emission fluorescence matrices and UV/Vis absorption to monitoring the photocatalytic degradation of commercial humic acid. Sci. Total Environ. 442, 207–14. doi:10.1016/j.scitotenv.2012.10.058

314. van Dongen, B.E., Rowland, H. a L., Gault, A.G., Polya, D. a., Bryant, C., Pancost, R.D., 2008. Hopane, sterane and n-alkane distributions in shallow sediments hosting high arsenic groundwaters in Cambodia. Appl. Geochemistry 23, 3047–3058. doi:10.1016/j.apgeochem.2008.06.012

315. van Geen, A., 2011. International Drilling to Recover Aquifer Sands (IDRAs) and Arsenic Contaminated Groundwater in Asia. Sci. Drill. 49–52. doi:10.2204/iodp.sd.12.06.2011

316. Vaxevanidou, K., Giannikou, S., Papassiopi, N., 2012. Microbial arsenic reduction in polluted and unpolluted soils from Attica, Greece. J. Hazard. Mater. 241-242, 307–15. doi:10.1016/j.jhazmat.2012.09.048

317. Vivian, J.T., Callis, P.R., 2001. Mechanisms of tryptophan fluorescence shifts in proteins. Biophys. J. 80, 2093–109. doi:10.1016/S0006-3495(01)76183-8

318. von Brömssen, M., Jakariya, M., Bhattacharya, P., Ahmed, K.M., Hasan, M.A., Sracek, O., Jonsson, L., Lundell, L., Jacks, G., 2007. Targeting low-arsenic aquifers in Matlab Upazila, Southeastern Bangladesh. Sci. Total Environ. 379, 121–32. doi:10.1016/j.scitotenv.2006.06.028

319. Walker, M., Kristensen, T.B., Huuse, M., Piotrowski, J. a, Clausen, O.R., 2009. A morphometric analysis of tunnel valleys in the eastern North Sea based on 3D seismic data. J. Quat. Sci. 22, 801–815. doi:10.1002/jqs

320. Wang, K., Dickinson, L.C., Ghabbour, E.A.E., Davies, G., Xing, B., 2003. Proton spin-lattice relaxation times of humic acids as determined by solution NMR. Soil Sci. 168, 128–136. doi:10.1097/01.ss.0000055308.24681.3f

321. Wang, S., Mulligan, C.N.C., 2006. Effect of natural organic matter on arsenic release from soils and sediments into groundwater. Environ. Geochem. Health 28, 197–214. doi:10.1007/s10653-005-9032-y

322. Warwick.P., Inam, E., Evans, N., 2005. Institutional Repository Arsenic ' s interactions with humic acid. Environ. Chem.

323. Weishaar, J.L., Aiken, G.R., Bergamaschi, B. a., Fram, M.S., Fujii, R., Mopper, K., 2003. Evaluation of Specific Ultraviolet Absorbance as an Indicator of the Chemical Composition and Reactivity of Dissolved Organic Carbon. Environ. Sci. Technol. 37, 4702–4708. doi:10.1021/es030360x

324. Williams, C.J., Frost, P.C., Xenopoulos, M. a., 2013. Beyond best management practices: Pelagic biogeochemical dynamics in urban stormwater ponds. Ecol. Appl. 23, 1384–1395. doi:10.1890/12-0825.1

325. Wilson, H.F., Xenopoulos, M. a., 2008. Effects of agricultural land use on the composition of fluvial dissolved organic matter. Nat. Geosci. 2, 37–41. doi:10.1038/ngeo391

326. Wilson, S.D., Roadcap, G.S., Herzog, B.L., Larson, D.R., 1998. Hydrogeology and Ground-Water Availability in Southwest McLean and Southeast Tazewell Counties Part 2 : Aquifer Modeling Hydrogeology and Ground-Water Availability in Southwest McLean and Southeast Tazewell Counties Part 2 : Aquifer Modeling and Final Rep.

327. Wolf, M., Kappler, A., Jiang, J., Meckenstock, R.U., 2009. Effects of humic substances and quinones at low concentrations on ferrihydrite reduction by Geobacter metallireducens. Environ. Sci. Technol. 43, 5679–85.

328. Wolski, P., Savenije, H.H.G., 2006. Dynamics of floodplain-island groundwater flow in the Okavango Delta, Botswana. J. Hydrol. 320, 283–301. doi:10.1016/j.jhydrol.2005.07.027

329. Wolski, P., Savenije, H.H.G., Murray-Hudson, M., Gumbricht, T., 2006. Modelling of the flooding in the Okavango Delta, Botswana, using a hybrid reservoir-GIS model. J. Hydrol. 331, 58–72. doi:10.1016/j.jhydrol.2006.04.040

330. Wolthers, M., Charlet, L., van Der Weijden, C.H., van der Linde, P.R., Rickard, D., 2005. Arsenic mobility in the ambient sulfidic environment: Sorption of arsenic(V) and arsenic(III) onto disordered mackinawite. Geochim. Cosmochim. Acta 69, 3483–3492. doi:10.1016/j.gca.2005.03.003

331. Wu, F., Tanoue, E., 2001. Sensitive determination of dissolved tryptophan in freshwater by alkaline hydrolysis and HPLC. Anal. Sci. 17, 1063–6.

332. Wu, F.C., Evans, R.D., Dillon, P.J., Cai, Y.R., 2007. Rapid quantification of humic and fulvic acids by HPLC in natural waters. Appl. Geochemistry 22, 1598–1605. doi:10.1016/j.apgeochem.2007.03.043

333. Yadav, A., Garg, V.K., 2009. Feasibility of nutrient recovery from industrial sludge by vermicomposting technology. J. Hazard. Mater. 168, 262–8. doi:10.1016/j.jhazmat.2009.02.035

334. Yamashita, Y., Jaffé, R., Jaffé, R., 2008. Characterizing the interactions between trace metals and dissolved organic matter using excitation-emission matrix and parallel factor analysis. Environ. Sci. Technol. 42, 7374–7379. doi:10.1021/es801357h

335. Yan, M., Korshin, G. V, 2014. Comparative Examination of Effects of Binding of Different Metals on Chromophores of Dissolved Organic Matter. Environ. Sci. Technol. 48, 3177–3185.

336. Yan, M.Q., Li, M.Y., Wang, D.S., Xiao, F., 2013. Optical property of iron binding to Suwannee River fulvic acid. Chemosphere 91, 1042–1048. doi:10.1016/j.chemosphere.2013.01.069

337. Yang, X., Steward, D.R., de Lange, W.J., Lauwo, S.Y., Chubb, R.M., Bernard, E. a., 2010. Data model for system conceptualization in groundwater studies. Int. J. Geogr. Inf. Sci. 24, 677–694. doi:10.1080/13658810902967389

338. Zhang, H., Qu, J., Liu, H., Zhao, X., 2009. Characterization of isolated fractions of dissolved organic matter from sewage treatment plant and the related disinfection by-products formation potential. J. Hazard. Mater. 164, 1433–8. doi:10.1016/j.jhazmat.2008.09.057

339. Zheng, R., Sun, G., Zhu, Y., 2012. Effects of microbial processes on the fate of arsenic in paddy soil. Chinese Sci. Bull. 58, 186–193. doi:10.1007/s11434-012-5489-0

340. Zheng, Y., Stute, M., van Geen, a., Gavrieli, I., Dhar, R., Simpson, H.J., Schlosser, P., Ahmed, K.M., 2004. Redox control of arsenic mobilization in Bangladesh groundwater. Appl. Geochemistry 19, 201–214. doi:10.1016/j.apgeochem.2003.09.007

341. Zheng, Y., van Geen, a., Stute, M., Dhar, R., Mo, Z., Cheng, Z., Horneman, a., Gavrieli, I., Simpson, H.J., Versteeg, R., Steckler, M., Grazioli-Venier, a., Goodbred, S., Shahnewaz, M., Shamsudduha, M., Hoque, M. a., Ahmed, K.M., 2005. Geochemical and hydrogeological contrasts between shallow and deeper aquifers in two villages of Araihazar, Bangladesh: Implications for deeper aquifers as drinking water sources. Geochim. Cosmochim. Acta 69, 5203–5218. doi:10.1016/j.gca.2005.06.001

342. Zobrist, J., Dowdle, P.R., Davis, J. a., Oremland, R.S., 2000. Mobilization of Arsenite by Dissimilatory Reduction of Adsorbed Arsenate. Environ. Sci. Technol. 34, 4747–4753. doi:10.1021/es001068h

343. Zsolnay, Á., 2003. Dissolved organic matter: artefacts, definitions, and functions. Geoderma 113, 187–209. doi:10.1016/S0016-7061(02)00361-0

344. Zsolnay, A., Baigar, E., Jimenez, M., 1998. DIFFhRENTIATING WITH FLUORESCENCE SPECTROSCOPY THE SOURCES OF 38, 45–50.

Appendices

Appendix A - Total organic carbon / Total nitrogen analysis standard operating procedure.

TOC-L CPH/CPN (Shimadzu) Total Organic Carbon Analyzer
Before getting started
- Turn on compressed air 300kPa for gas going to the instrument and 1500 psi for pressure inside the cylinder (if <500s pi pressure, replace gas cylinder).

Machine Start Up
- Turn on the instrument. Allow it to warm up at least 1 hour.
- Check the **Maintenance Sheet** inside the TOC binder for daily checks!
- Make sure to check the list beneath each **TOC sample log sheet**.
- Open TOC-L Sample Editor software. Click Monitor on bottom left of screen. When all setting has stabilized, there will be an "OK" next to each setting and a green Ready will be indicated:
  - Furnace   = 680^0C   OK
  - Humidifier   = 1.0^0C   OK
  - Position, fluctuation, noise   all OK
  - SSM TC temp, SSM IC temp   all OK

To run samples with Auto sampler, using existing calibration curve
1. Press "New" button to open new Sample Worksheet
2. Left click on row 1 then right click and choose "insert-sample"
3. Choose "Edit parameters manually" and click next
4. Choose your analysis type, manual dilution =1, No. of determinations=1, click "Next"
   - Be aware that when doing NPOC and TN simultaneously, you will only be allowed to select one calibration curve for comparison, otherwise you will be able to use three for comparison
5. Click button with three dots and choose appropriate calibration curve then click "Next"
6. Injection parameters should be the same as the calibration curve that was created otherwise see the following:
   - NPOC: units = mg/l, injection volume= 200um, no. of injections = 3 / 4, SD max = 0.1, CV Max = 2%, No. of washes = 2, Auto dilution = 1, Sparge gas flow = 80ml, sparge time = 1:30 min (3 min if necessary), acid addition = 1.5%, check the box next to Multiple Injections
   - TN: units = mg/l, injection volume= 200um, no. of injections = 3 / 4, SD max = 0.1, CV Max = 2%, No. of washes = 2, Auto dilution = 1, acid addition = 1.5%, check the box next to Multiple Injections
7. Use default setting for peak time parameters (4:50 min max) then click next
8. Click "none" for pharmaceutical water testing then click finish.
9. To add more than one sample using the same analysis just copy and paste the one you just made. Names of each sample can be added by clicking under "sample name" and typing the name.
10. Click on the "view vial settings" icon in the upper right. Assign vial numbers to samples with a blank coming from "off line" or vial "0" then click "OK"

11. Click the "Connect" icon at the top middle of the screen. An initialization window should pop up.
12. Once initialization is complete and the machine is ready, a green "Ready" icon will appear in the upper right. Press "Start" and choose to shut the instrument down.

To make a new calibration curve
1. Click on the second tab (for calibration curve) of the window in the top left of the screen
2. Click "New"
3. Click "Next"
4. Checkmark the box next to "Use dilution from standard solution" and click "Next"
5. Choose the type of analysis, checkmark the boxes next to "Zero shift" and "Multiple injections." Type in a file name using the following format: Analysis type (NPOC…) _Concentration range… (Ex. NPOC_0.1-1mg/L). Then click "Next."
6. Choose units, No. of injections (usually 2/3 or 3/4), SD Max = 0.1, CV Max = 2%, acid addition for TC, NPOC should be at least 1.5%, select sparge time (minimum 1:30min), then click "Next"
7. Click "add", enter in standard solution concentration and calibration point concentration (eg. 10 mg/l and 5 mg/l), auto dilution = 1, click "OK", add as many as necessary and make sure injection volume in upper right corner is enough for type of analysis (eg. low concentrations will need higher volume) then click "Next" and "Finish"
8. Press "New" button in upper left corner to open new Sample Worksheet
9. Left click on row 1 then right click and choose "insert-calibration curve." Choose the calibration curve you just created.
10. Follow steps 10-12 above to run calibration curve.

Filling the auto-sampler
- Fill vial 0 with FRESH!!! milliQ.
- Load the tray with standards – samples –standards. I suggest:
  - Vial #1   =   milliQ
  - Vial #2   =   low C water
  - Vial #3   =   0.10 standard
  - Vial #4   =   0.25 standard
  - Vial #5   =   0.50 standard
  - Vial #6   =   1.0 standard
  - Vial #7   =   2.0 standard
  - Vial #8   =   5.0 standard
  - Next one vial of milliQ
  - Next all your samples
  - Next one vial of milliQ
  - Next all your standards again.
- To avoid CO2 entering samples and causing higher DOC concentrations to be measured, fill vials to near the top every time. For 40 mL vials, use 35 mL of sample.
- For low DOC measurements with the high sensitivity catalyst, do not run samples higher than 5 mg/L. TOC analyzer in E-420 is more sensitive at low concentrations so this may be a better option.
- If you expect some higher DOC samples, place a vial of milliQ water after them. This avoids contamination of the next sample.

Machine Shut Down
- DO NOT turn off the instrument using the on/off button!!! The instrument needs to cool down (from 680^0C) with fans inside. Otherwise the instrument will be destroyed.
- If your analysis is done and you have not previously told the machine to shut down, click "Shutdown" button in upper right of screen and select "shut down instrument"
- If you need to stop the auto sampler in the middle of a run, follow the instructions on P 221 of the manual to end the analyses and perform instrument shut down. DO NOT press the on/off button.

Notes:
- ✓ Always run standards at start and end of sample measurement.
- ✓ A set of standards remains fairly stable for at least 1.5 weeks. After that make new standards. A 1000 mg/L KHP stock solution remains stable for at least one month, so you do not have to weigh out the dry KHP every time you make standards.
- ✓ Always write down or record the results as soon as possible. The heat sensitive paper can be easily damaged and deteriorates when exposed to sunlight or water or heat.
- ✓ Even an excellent calibration curve will definitely change over time due to aging of the catalyzer and other components. Use the results of your two standard runs to make a NEW calibration curve for that day (expected standard concentrations vs. measured standard concentrations). Use the equation of this regression line to correct your DOC results.
- ✓ TOC vials should be cleaned (3x with DI water) and combusted before use (500^0C for 2 hrs.; cover with aluminum foil during combustion).

Appendix B - Analysis of Fe^{2+} by Ferrozine method

Ferrozine (the disodium salt of 3-(2-pyridyl)-5,6-bis (4-phenylsulfonic acid)-1,2,4-triazine) reacts with ferrous iron to form a stable magenta complex that is soluble in water. The visible absorption spectrum of the ferrous-Ferrozine complex has a single sharp peak with maximum absorbance at 562 nm. Beer-Lambert law is obeyed to about 4 mg/L Fe. The complex will form in solution between pH 4 and 9. References – Stookey (1970) and Gibbs (1976)

Reagents

Ferrozine solution – add per liter 1 g of Ferrozine and 11 g of HEPES (or 12 g of HEPES disodium salt). Adjust the pH to 7.0 and store at 4°C. Note – the original Ferrozine method used an ammonium acetate buffer instead of HEPES.

Ferrous iron standards – add 0.70213 g of ferrous ammonium sulfate hexahydrate $(Fe(NH_4)_2(SO_4)_2 \cdot 6H_2O$; FW 392.14) to 100 mL of DI. This equates to about 1000 mg/L ferrous iron. Make dilutions from this solution to obtain standards ranging in concentration from as low as 0.1 mg/L and as high as 10 mg/L, depending on the Fe content you expect to find in your samples. All standards, including the 1000 mg/L starting solution, need to be made fresh the day of the analysis. You can adjust the procedure to accommodate a different range of iron concentrations.

Procedure

- Add 5 mL of Ferrozine reagent to a 10 mL test tube.
- Add 2 mL of sample. Mix and observe color. The solution will become pale violet or purple in color if ferrous iron is present. A deep blue/purple indicates that too much ferrous iron is present. If this is the case, dilute the sample (alternatively, you can just use less sample and keep track of volumes).
- Measure absorbance at 562 nm. Be sure to include a blank consisting of 5 mL of Ferrozine and 2 mL of DI water. Record the absorbance.
- Calculate sample concentration from a standard line.

Phenanthroline Method

Ferrous iron is chelated by three molecules of 1,10-phenanthroline forming an orange-red complex. The colored solution obeys Beer's law with maximum absorbance at 510 nm. Reference – Eaton et al (1995).

Reagents

Store reagents in glass stoppered bottles. HCl and ammonium acetate solutions are stable indefinitely if tightly stoppered. The Phenanthroline solution is stable for several months.

HCl – concentrated

Ammonium acetate buffer solution – dissolve 25 g $NH_4C_2H_3O_2$ in 15 mL water. Add 70 mL concentrated (glacial) acetic acid.

Phenanthroline solution (10X Standard Methods concentration) – dissolve 5 g 1,10-phenanthroline monohydrate $(C_{12}H_8N_2 \circ H_2O)$ in 500 mL water by stirring and heating to 80°. Do not boil. Discard the solution if it darkens. Heating is unnecessary if 3 mL of HCl is added. 2 mL of this solution is sufficient for no more than 0.05 mg Fe (i.e, 2 mL for up to 10 mg/L iron in samples using 5 mL sample sizes).

Iron standards – slowly add 20 mL of concentrated H_2SO_4 to 50 mL of water and dissolve 1.404 g of ferrous ammonium sulfate $(Fe(NH_4)_2(SO_4)_2, 6H_2O)$. Add 0.1 N potassium permanganate $(KMnO_4)$ dropwise until a faint pink color persists. Dilute to 1000 mL with water. 1 mL contains

200 µg Fe (200 mg/L). Prepare standards daily for use from this stock. Make three 10-fold dilutions.

Procedure – Sample Prep

- Acidify 5 mL of sample (or standard) with 0.1 mL of concentrated HCl (2%) at time of collection. This will slow down oxidation of ferrous iron to ferric iron and prevent adsorption to the walls of the container.
- Add 2 to 4 mL of Phenanthroline solution (2 mL can handle up to 10 mg/L Fe(II) in 5 mL samples).
- Add 1 mL $NH_4C_2H_3O_2$ solution with vigorous stirring.
- Measure color intensity at 510 nm within 5 to 10 minutes. Do not expose to sunlight. Color development is rapid in the presence of excess Phenanthroline.

Additional Notes

Phenanthroline solution as suggested by Standard Methods:

Dissolve 100 mg 1,10-phenanthroline monohydrate ($C_{12}H_8N_2 \cdot H_2O$) in 100 mL water by stirring and heating to 80°. Do not boil. Discard the solution if it darkens. Heating is unnecessary if 2 drops of HCL are added. One mL of this solution is sufficient for no more than 100 µg Fe.

Alternative iron standards:

Degas DI water in 125 mL serum bottles: 1 containing 100 mL and 1 with 98 mL, and 2 with 90 mL. After the bottles have degassed for at least 30 minutes, add 0.226974 g $FeCl_2$ to the 100 mL bottle. This should correspond to about 1000 mg/L ferrous iron. Stopper all of the bottles loosely and let them degas for another 30 minutes. Stopper them tightly and crimp an aluminum seal on the bottle. Make a 50-fold dilution, and two 10-fold dilutions.

References

- Eaton, A.D., Clesceri, L.S., and Greenberg, A.E., 1995, Standard Methods for the Examination of Water and Wastewater: Washington, DC, American Public Health Association, American Water Works Association, and Water Environmental Federation.
- Gibbs, C.R., 1976, Characterization and application of ferrozine iron reagent as a ferrous iron indicator: Analytical Chemistry, v. 48, p. 1197-1201.
- Stookey, L.L., 1970, Ferrozine - a new spectrophotometric reagent for iron: Analytical Chemistry, v. 42, p. 779-781.

Appendix C - Protocol for EEMs acquisition with Aqualog

Sample Preparation

- Samples should be filtered using a pre-rinsed filter
- Allow samples to warm to room temperature
- To acidify or not acidify?
    - If you have dilute samples (meaning they have low DOC concentration or low absorbance), then it is best to NOT acidify because acidification can change the conformation of the DOM molecules, resulting in lower fluorescence intensity.
    - If you have samples that contain metals, such as iron or copper, consider lowering the pH to 2-3. This will dissociate the DOM-metal complexes and minimize the metal quenching effects.

Startup

- Turn on the instrument 1st and then turn on the computer 2nd.
- Allow the lamp to warm up approximately 45 minutes before running a sample
- Rinse a clean quartz cuvette with ultra-pure water ~20 times.
- Clean the sides of the 3-Q-10 sealed water sample with kim-wipes.
- Clean the two Quinine sulfate cells (blank and sample) with kim-wipes.
- Initial software steps
    - Make a folder on the desktop of in the C: drive under your name in which to save your sample results for the day – we recommend saving your samples into a sub-folder named with the date YYMMDD (e.g. "120504" for May 4, 2012)
    - Open the Aqualog logbook.xls on the desktop and enter your name and date.
    - Open the Aqualog software.

Cuvette check (for contamination)

- Click on the "H2O" button "Aqualog main experiment menu".
- Click on "Spectra".
- Click on "Emission 2D".
- You may be asked to name a new project. Use this format: PYYMMDD.
- Load the experiment file "cuvette_check.xml" (located in C:\PublicDocuments\Jobin Yvon\Data\).
- Check that the settings are
    - Integration time = 0.25 sec
    - Increment = 2.33 nm
    - Gain = high
    - Excitation = 240 nm
    - "Sample only" box is checked.
- "Run" the sample and look for any peaks between emission 300 and 400 nm that are not noise. If there is an obvious peak, clean the cuvette again and re-run this check.
- To see the peak values, double click on the figure. Then click the "Data Reader" icon (square with cross hairs inside) to select the peak.
- Record the highest peak between emission 300 and 400 nm in the Aqualog logbook.xls.

Water Raman scan

- Click on the "H2O" button "Aqualog main experiment menu".

- Click on "Spectra".
- Click on "Emission 2D".
- Load the experiment file "water raman.xml" (located in the "Startup" folder).
- Check that the settings are
    - Integration time = 0.25 sec
    - Increment = 4.65 nm
    - Gain = high
    - Excitation = 350 nm
    - "Sample only" box is checked.
- "Run" the sample and record the raman peak at ~397 nm (Raman peak X and Y) in the Aqualog logbook.xls.
- Calculate the area under the raman peak.
    - Double-click on the graph.
    - Click the up and down arrow ("Data Selector" arrow) which allows you to narrow the range of the emission wavelength so that only the raman peak is in view.
    - Click "Analysis" → "Baseline"
    - Goal: "integrate peaks" should be selected, Next
    - "Baseline mode, Constant" should be "custom" and set Y = 0. Next, Next.
    - Click on "find", Next
    - Select "Fix width for all peaks" as the integration window width and set "Left half width" to "25". Right half width should automatically set to "25". Finish.
    - Go to the "Integration Result1" tab to find the area. The area is in the 2nd column entitled "Integral result of Sc/Rc, Area". Paste this value into the Aqualog logbook.xls.
    - Also record this area in your lab notebook every day.

***If you change your integration time when you run your sample, then re-run the Water Raman scan with the new integration time. ***

Quinine sulfate scan
- Click on the box with "Q.U" in it.
- Do not change any settings.
- Check that the settings are
    - Integration time = 0.1 sec
    - Increment = 0.41 nm
    - Gain = med
    - Excitation = 347.5 nm
    - "Sample and blank" box is checked.
  - Record the emission at 450 nm (observed) in the Aqualog logbook.xls and in your lab notebook.

3D EEM acquisition
- Click on the "H2O" button "Aqualog main experiment menu".
- Click on "3D".
- Click on EEM 3D CCD + absorbance.
- Load the experiment file "3DeemNEW.xml" from the Startup folder.
- Check that the settings are:
    - Integration time = 0.25 sec

- o Increment = 3 nm and 3.28 nm
- o Gain = high
- o "Sample and blank" circle is selected.
- First run ultra-pure water as a sample to check for any contamination on the cuvette or in the ultrapure water system
  1. Enter a name for the sample (eg. "MQ") in the Data Identifier box.
  2. Enter a name for the blank (with this format: BYYMMDD) in the "Collect blank" box.
  3. Click run.
  4. You will be asked to insert the blank and then the sample.
  5. Your blank-subtracted EEM spectra will show up as an uncorrected waterfall plot.
  6. Make sure you are at the waterfall plot screen. Click the following in this order:
     a. the "Inner filter correct" button (which is a small square at the upper left corner of the button)
     b. the "Rayleigh masking" button – select both first and second order and set the wavelength to 12.
     c. The "Normalize 3D" button –
        i. enter the Raman area you recorded earlier into the "Divide by a specified value" box.
        ii. Or normalize to the quinine sulfate emission value you recorded earlier.
  7. Edit the contour plot to make it easier to view.
  8. Double-click the "Processed contour: IFE_RM_NRM" plot.
  9. Set range from 0 (zero, no negative values) to the maximum intensity.
  10. Change the first layer to the color white.
  11. Select contours at all major levels.
- Perform steps 1-11 on the next samples EXCEPT now you can use the "blank from file" (no need to run the blank each time).
- You can select "Collect" → "Previous experimental setup" for the next EEM acquisition (don't have to click the H2O button, etc. every time).
- Write each sample's name in your lab notebook (full description) along with the short filename you used to name the 3dEEM.

***If you change your integration time when you run your sample, then run a new blank (enter a name with this format: BYYMMDDb) using the new integration time. ***

Shut down
- Save the project.
- Download and correct the data according to the Corrections Protocol.
- Shut down the software.
- Shut down the computer.
- *****Shut down the instrument*****
- Clean all cuvettes.
- Clean or put away all beakers, pens, notebooks, etc.

Cuvette cleaning

You can put a dirty cuvette into water with hydrogen peroxide (a 10:1 solution) for a few hours to clean it. Best if you can put it in direct sunlight as well.

Appendix D - Protocol for correcting EEMs and calculating indices using MATLAB with Aqualog

STEP 1: Exporting raw data from the instrument
1. You are already in Aqualog program. If not, double click on Aqualog icon on desktop.
2. Click on "File" and select "HJY Export"
3. In HJY_Export dialog box, click on the button just to the right of "Export Graph(s)" field.
4. In Graph Browser dialog box, select on the desired project folder icon (not individual files) and click on button with two right arrows. Click "OK".
5. Again HJY_Export dialog box will pop up with selected graphs in "Export Graph(s)" field. Make sure the "File Format" is "ASCII". Click "OK".
6. "File Location for batch exporting" window will open. Create a new folder with name "Raw_Data" and provide this folder address to export the data.
7. A warning "File Exists!" will appear for each sample. Always click "YES" to replace the existing file.
8. Save and close the Aqualog program.

STEP 2: Reviewing raw data flies
1. Open the folder where raw data is exported.
2. Make sure the folder contains:
   a. Seven (7) raw files for each sample
   b. Only one (1) Raman File
   c. Cuvette Check Files (may be 1 or more)
   d. A QS Unit file
3. Close the folder.

STEP 3: Correcting and calculating indices
1. Open "MATLAB R2014a" program by double clicking on the shortcut created on desktop home screen.
2. Browse for folder with name "AqualogCode" folder using "Browse for Folder" button to the left of address bar.
3. Right click on "AqualogCode" folder and then select "Add to Path >> Selected Folders and Subfolders".
4. Repeat step 2 & 3 for "Raw_Data" folder.
5. In the Command Window, type command "ProcessData" followed by the address of "Raw_Data" folder copied from the address bar in the format given below, and hit Enter:
   >> ProcessData ('C:\Users\harshad\Desktop\ Raw_Data\')

6. You will be asked to answer following interactive questions:
   a. Is dilution Factor same for all samples? Enter
      i. Enter 1 for YES
         0 for NO
   b. For all samples, is Integration Time exactly SAME as Integration time used for Raman?

        i. Enter 1 for YES
            0 for NO
   c. Do all samples have exactly SAME integration time?
        i. Enter 1 for YES
            0 for NO
   d. Method for absorbance data extrapolation?
   e. Enter 0 for Linear
        1 for Nonlinear (recommended)
7. The command window will show the message "Process Completed" when it is done. Then type command "close all" and hit Enter.

STEP 4: Review the results
1. Review the results in respective folders as given below:
   a. Absorbance Graphs in "*.png" format
      >>Raw_Data >> Abs Spectra Graphs >> Graphs
   b. Intensity of absorbance @ 254 nm
      >> Raw_Data >> Abs Spectra Graphs >> Results >> Results.txt
      NOTE: Open the "*.txt" from MS Excel
   c. Calculated Raman Area
      >> Raw_Data >> raman >> "*.csv"
   d. 3D EEM contour plots in "*.png" format
      >> Raw_Data >> Results >> EEM Graphs
   e. Graph of maximum emission @ 370 nm in "*.png" format
      >> Raw_Data >> Results >> MaxEm
   f. Table of calculated indices
      >> Raw_Data >> Results >> Results.txt
      NOTE: Open the "*.txt" from MS Excel
   g. Files ready for PARAFAC analysis
      >> Raw_Data >> Results >> Data4Parafac
2. To close the MATLAB, type the command "quit" and hit Enter.

STEP 5: PARAFAC
1. Create a new folder say "Parafacfiles" to store files ready for parafac obtained from 3
      ">> Raw_Data >> Results >> Data4Parafac"
Note: This is important when you have raw files in different folders. You will run corrections code to individual folder. For PARAFAC, we want all files ready for PARAFAC in single folder.
2. In the Command Window, type command "dataprep4pf" followed by the address of "Parafacfiles" folder copied from the address bar in the format given below, and hit Enter:
      >> dataprep4pf ('C:\Users\harshad\Desktop\Raw Data\Parafacfiles\')
3. You will see some objective questions on the screen as below:
   a. Do you want to normalize the EEMs?
      i. Enter 1 for YES (recommended)
      ii. Enter 0 for NO

4. A new folder named "PF" will be created in "Current Folder" window in main MATLAB window. Right click on this folder and add this folder to path with folders and subfolders option. Open this folder by double clicking on it. After you open this folder, you will see three files as:
   a. em.csv
   b. ex.csv
   c. fl.csv
5. In the Command Window, type command "loadpfdata" followed by the address of "PF" folder copied from the address bar in the format given below, and hit Enter:
   >> loadpfdata ('C:\Users\harshad\Desktop\Raw Data\Parafacfiles\PF\')
6. Now, you will see another file created "pf.mat". This is the dataset we'll be using for PARAFAC analysis.
7. Follow the steps given in Stedmon and Bro, 2008 tutorial for PARAFAC analysis.

Appendix E - Raw Data for Murshidabad groundwater DOM characteristics

Table A 1 Raw data for Murshidabad groundwater DOM characteristics. All numbers are in Raman Units.

Sample Name	PARAFAC				Fluorescence								Absorbance			
	C1	C2	C3	C4	FI	FrI	HIX	Peak A	Peak B	Peak T	Peak C	Peak M	abs254	S275_295	S350_400	SR
High Arsenic TW																
TW 101 BM F (01).csv	1.82	1.43	0.39	0.20	1.74	0.75	9.40	1.89	0.22	0.28	1.00	1.16	0.07	-0.02	-0.01	1.15
TW 102 BM F (01).csv	1.24	1.00	0.25	0.26	1.78	0.78	7.57	1.35	0.16	0.21	0.68	0.82	0.05	-0.02	-0.01	1.66
TW 103 BM F (01).csv	1.04	0.81	0.27	0.00	1.71	0.75	7.97	1.03	0.12	0.16	0.58	0.66	0.04	-0.02	-0.01	1.12
TW 104 BM F (01).csv	2.37	1.72	0.29	0.83	1.74	0.73	10.45	2.65	0.22	0.32	1.23	1.52	0.07	-0.02	-0.02	0.91
TW 105 BM F (01).csv	0.56	0.48	0.19	0.00	1.71	0.79	5.67	0.60	0.11	0.12	0.32	0.38	0.03	-0.01	-0.01	1.46
TW 106 BM F (01).csv	1.83	1.40	0.29	0.71	1.82	0.76	9.14	2.10	0.23	0.32	1.00	1.19	0.06	-0.02	-0.02	0.96
TW 107 BM F (01).csv	1.05	0.84	0.24	0.18	1.81	0.77	7.00	1.10	0.14	0.19	0.58	0.70	0.04	-0.02	-0.02	1.17
TW 139 BM F (01).csv	0.68	0.57	0.26	0.12	1.78	0.80	3.65	0.74	0.27	0.18	0.36	0.49	0.04	-0.02	-0.01	1.75
TW100F (01).csv	1.00	0.78	0.25	0.17	1.83	0.77	5.69	1.05	0.15	0.18	0.54	0.65	0.04	-0.02	-0.02	1.11
TW139BM (01).csv	0.47	0.39	0.16	0.11	1.77	0.81	4.21	0.52	0.19	0.13	0.26	0.33	0.06	-0.01	0.00	2.34
TW139BM2 (01).csv	0.23	0.19	0.05	0.07	1.74	0.79	4.38	0.27	0.06	0.06	0.13	0.16	0.06	-0.01	-0.01	2.06
TW139BM3 (01).csv	2.26	1.76	0.53	1.00	1.77	0.78	4.16	2.53	0.53	0.63	1.24	1.60	0.05	-0.01	-0.01	2.18
TW 119 HK F (01).csv	1.04	0.76	0.23	0.01	1.71	0.73	9.49	1.02	0.12	0.16	0.53	0.62	0.06	-0.01	0.00	2.09
TW 121 HK F (01).csv	0.97	0.68	0.27	0.00	1.70	0.70	6.42	0.92	0.22	0.17	0.52	0.61	0.05	-0.01	-0.01	1.04
TW 122 HK F (01).csv	0.55	0.37	0.26	0.01	1.68	0.83	3.99	0.55	0.14	0.20	0.26	0.33	0.05	-0.01	-0.01	2.15
TW 124 HK F (01).csv	1.00	0.69	0.28	0.07	1.66	0.72	6.40	0.99	0.15	0.19	0.50	0.59	0.05	-0.01	-0.01	1.43
TW 127HK F (01).csv	0.72	0.51	0.37	0.05	1.71	0.88	3.48	0.75	0.29	0.32	0.36	0.45	0.04	-0.02	-0.02	1.12
TW 128 HK F (01).csv	0.37	0.25	0.10	0.03	1.66	0.73	7.41	0.38	0.06	0.07	0.19	0.23	0.02	-0.01	-0.01	1.18
TW 129 HB (01).csv	0.87	0.61	0.19	0.03	1.68	0.73	9.11	0.88	0.09	0.12	0.43	0.51	0.05	-0.01	-0.01	1.66
TW 137 HK F (01).csv	1.22	0.90	0.27	0.01	1.66	0.73	8.44	1.22	0.12	0.16	0.62	0.74	0.05	-0.01	-0.01	1.45
TW 137HK2 (01).csv	0.98	0.71	0.23	0.04	1.66	0.78	8.40	0.98	0.11	0.15	0.50	0.60	0.04	-0.02	-0.02	0.82
TW118HKF (01).csv	17.13	8.14	1.84	9.90	1.59	0.96	8.81	18.81	1.36	2.62	6.03	8.58	0.08	-0.01	-0.02	0.83
TW120HK F (01).csv	1.31	0.85	0.29	0.43	1.70	0.73	5.98	1.40	0.20	0.28	0.65	0.78	0.05	-0.02	-0.02	1.09
TW123HKF (01).csv	1.28	0.79	0.20	0.32	1.76	0.72	9.09	1.32	0.13	0.18	0.61	0.72	0.04	-0.02	-0.03	0.76
TW125HKF (01).csv	1.57	1.10	0.32	0.39	1.77	0.75	8.11	1.61	0.18	0.28	0.85	0.95	0.07	-0.02	-0.02	1.13
TW126HKF (01).csv	9.64	5.44	2.59	2.45	1.68	0.71	4.81	9.68	1.54	2.17	4.51	5.22	0.03	-0.02	-0.03	0.69
TW138HK F (01).csv	1.14	0.93	0.30	0.27	1.78	0.78	6.56	1.23	0.19	0.26	0.65	0.76	0.06	-0.02	-0.02	0.99
High Arsenic IW																
IW 101 F (01).csv	1.16	0.88	0.28	0.35	1.82	0.79	6.21	1.27	0.20	0.26	0.63	0.73	0.04	-0.02	-0.01	1.29
IW 102 BM F (01).csv	0.52	0.42	0.30	0.05	1.81	0.85	3.94	0.59	0.17	0.26	0.30	0.36	0.03	-0.02	-0.01	1.96
IW 103 HK F (01).csv	1.39	0.94	0.23	0.45	1.74	0.75	7.38	1.52	0.17	0.22	0.67	0.84	0.04	-0.02	-0.02	0.99
IW 104 HB F (01).csv	1.26	0.83	0.26	0.37	1.64	0.77	6.57	1.35	0.15	0.26	0.60	0.76	0.04	-0.02	-0.03	0.79
IW105HB F (01).csv	1.14	0.64	0.21	0.31	1.75	0.68	7.42	1.21	0.13	0.20	0.53	0.61	0.03	-0.02	-0.02	1.14

High Arsenic PW

PW 103 BM F (01).csv	3.71	2.73	1.88	1.13	1.64	0.81	4.58	4.00	1.31	1.63	1.90	2.51	0.30	-0.02	-0.01	1.35
PW 103 BM F 2 (01).csv	2.94	2.14	1.45	0.81	1.65	0.81	4.53	3.14	1.01	1.24	1.50	1.98	0.28	-0.02	-0.01	1.21
PW102 F (01).csv	6.22	4.37	2.18	1.63	1.70	0.77	6.09	6.40	1.40	2.00	3.27	4.01	0.38	-0.01	-0.02	0.84
PW104 (01).csv	2.15	1.58	0.68	0.96	1.58	0.83	6.01	2.41	0.55	0.68	1.04	1.50	0.25	-0.02	-0.01	1.27
PW104 F (01).csv	3.18	2.31	1.06	1.33	1.55	0.83	5.69	3.54	0.76	1.00	1.54	2.19	0.24	-0.02	-0.02	1.18
PW104B (01).csv	2.12	1.54	0.67	0.90	1.59	0.83	6.08	2.40	0.51	0.65	1.02	1.45	0.25	-0.02	-0.01	1.32
PW108F (01).csv	1.00	0.79	0.57	0.38	1.62	0.90	3.38	1.13	0.37	0.47	0.51	0.72	0.08	-0.02	-0.01	1.73
PW109F (01).csv	3.43	2.20	1.00	1.20	1.55	0.77	6.31	3.66	0.70	1.00	1.59	2.13	0.22	-0.02	-0.01	1.30
PW 110 (01).csv	11.48	5.30	3.21	9.51	1.59	1.12	5.55	13.57	2.67	3.63	4.12	6.06	0.17	-0.02	-0.01	1.30
PW110 F (01).csv	1.84	1.31	0.61	0.69	1.60	0.82	5.29	2.02	0.42	0.54	0.89	1.23	0.15	-0.02	-0.02	1.02
PW110B (01).csv	1.23	0.87	0.38	0.53	1.58	0.84	5.82	1.37	0.27	0.37	0.59	0.83	0.16	-0.02	-0.01	1.28

Low Arsenic TW

TW114NBKF (01).csv	1.59	1.56	0.91	0.44	1.81	0.81	2.19	1.90	0.54	0.57	0.96	1.27	0.02	-0.01	-0.01	2.54
TW 111 NB F (01).csv	0.65	0.39	0.17	0.03	1.54	0.66	7.25	0.63	0.11	0.12	0.32	0.35	0.05	-0.01	-0.01	1.66
TW 131 KHN F (01).csv	0.44	0.40	0.24	0.36	1.63	0.97	4.06	0.65	0.12	0.20	0.24	0.36	0.03	-0.01	-0.01	1.22
TW 132 KHN F (01).csv	0.72	0.82	0.61	0.87	1.81	1.09	3.02	1.24	0.44	0.53	0.48	0.74	0.05	-0.01	-0.01	1.84
TW130KHNF (01).csv	0.24	0.25	0.20	0.29	1.60	1.08	2.54	0.39	0.12	0.14	0.14	0.25	0.02	-0.02	-0.01	2.32
TW133KHN F (01).csv	6.96	5.90	4.83	10.12	1.68	1.00	3.04	11.28	3.03	4.74	3.95	5.75	0.04	-0.01	-0.01	1.84
TW134KHNF (01).csv	10.08	8.15	6.67	20.02	1.79	1.10	3.29	18.41	4.61	7.25	6.00	8.52	0.05	-0.02	-0.01	1.59
TW135KHN F (01).csv	0.99	0.98	0.70	1.75	1.76	1.07	3.47	1.89	0.46	0.71	0.63	0.93	0.03	-0.02	-0.02	1.10
TW136KHNF (01).csv	6.53	6.14	4.32	11.19	1.75	1.06	3.20	11.39	2.78	4.03	3.99	6.07	0.04	-0.01	-0.01	1.70

Low Arsenic IW

IW 106 KHN F (01).csv	0.76	0.82	0.53	1.20	1.74	1.07	3.30	1.39	0.33	0.51	0.49	0.75	0.04	-0.02	-0.01	1.67
IW 108 KHN F (01).csv	0.17	0.19	0.18	0.09	1.88	1.09	1.67	0.25	0.12	0.13	0.10	0.19	0.02	-0.02	-0.01	2.30
IW107KHN F (01).csv	0.55	0.55	0.41	0.73	1.62	1.03	3.07	0.98	0.28	0.34	0.34	0.51	0.03	-0.02	-0.01	1.59

Low Arsenic PW

PW 106 NB F 2 (01).csv	0.89	0.66	0.42	0.00	1.66	0.81	4.06	0.91	0.25	0.33	0.47	0.55	0.11	-0.02	-0.01	1.36
PW 106 NB F (01).csv	1.12	0.85	0.52	0.00	1.67	0.79	4.13	1.14	0.29	0.38	0.60	0.70	0.11	-0.01	-0.01	1.42
PW107F (01).csv	6.07	4.07	1.55	2.14	1.60	0.72	7.15	6.49	1.08	1.62	2.98	3.83	0.35	-0.02	-0.01	1.32
PW111F (01).csv	4.72	3.16	1.14	1.88	1.60	0.75	7.51	5.12	0.73	1.14	2.23	3.00	0.26	-0.02	-0.01	1.18
PW112F (01).csv	5.85	4.05	1.10	2.30	1.62	0.74	9.06	6.41	0.63	1.15	2.73	3.77	0.28	-0.02	-0.01	1.08

Appendix F - Raw data for complexation experiment

Table A 2 Fe-DOM Complexation. All numbers are in Raman Units.

Sample Name	abs254	S1	S2	SR	FI	FrI	HIX	A	B	T	C	M
SRFA12.5x0 (01)	0.313021	-0.011074	-0.014523	0.762458	1.272846	0.39614	26.10065	1.934195	0.040263	0.117277	0.979045	1.098955
SRFA12.5x0.1 (01)	0.293744	-0.010958	-0.014393	0.761359	1.263212	0.391162	24.063224	1.765517	0.050466	0.136185	0.899969	1.019426
SRFA12.5x1 (01)	0.289066	-0.010724	-0.013648	0.785711	1.256575	0.408712	21.258486	1.548537	0.055019	0.099854	0.793009	0.892511
SRFA12.5x10 (01)	0.404356	-0.009319	-0.013337	0.698746	1.353825	0.488008	11.434706	1.029929	0.014449	0.09973	0.531624	0.590821
SRFA12.5x20 (01)	0.516211	-0.007868	-0.01302	0.604283	1.453788	0.585558	7.276913	0.571402	0.014041	0.08383	0.303776	0.328067
SRFA12.5x5 (01)	0.355204	-0.010195	-0.01371	0.743615	1.285238	0.442376	14.471603	1.432879	0.006974	0.146794	0.70924	0.809268
SRFA6.25x0 (01)	0.186882	-0.010151	-0.012735	0.797102	1.247793	0.403704	24.572681	0.984353	0.032599	0.058348	0.490052	0.552964
SRFA6.25x0.1 (01)	0.181384	-0.010089	-0.012684	0.795386	1.27187	0.399273	21.899522	0.939332	0.028457	0.055854	0.463063	0.518239
SRFA6.25x1 (01)	0.183006	-0.009815	-0.012415	0.790551	1.299421	0.396835	20.585842	0.802509	0.039011	0.055787	0.394501	0.455274
SRFA6.25x10 (01)	0.309601	-0.007944	-0.012683	0.626334	1.358229	0.542689	7.250312	0.38444	0.01171	0.060891	0.190304	0.198496
SRFA6.25x20 (01)	0.417494	-0.00644	-0.012318	0.522836	1.431583	0.624039	4.258683	0.250547	0.017566	0.048776	0.127436	0.133329
SRFA6.25x5 (01)	0.247364	-0.008932	-0.012548	0.711767	1.397676	0.458962	20.207077	0.653167	0.00432	0.067938	0.321828	0.374179
SRFA12.5 (01)	0.258337	-0.013053	-0.019125	0.682498	1.270678	0.388967	5.023407	2.164612	1.26281	0.355449	1.062662	1.267864
SRFA6.25 (01)	0.133882	-0.012351	-0.016188	0.763004	1.289206	0.39484	4.985919	1.1145	0.674627	0.185039	0.533704	0.630971
SRFA6.25Fe0.1 (01)	0.122201	-0.012941	-0.0197	0.656869	1.292714	0.416786	4.616818	1.060783	0.733694	0.199033	0.509471	0.603823
SRFA6.25Fe1 (01)	0.122556	-0.012219	-0.0144	0.848555	1.364459	0.400054	3.910253	0.892649	0.777649	0.207526	0.43555	0.516889
SRFA6.25Fe10 (01)	0.232149	-0.008845	-0.014283	0.619273	1.434537	0.511122	3.961495	0.70147	0.503715	0.198883	0.347776	0.36844
SRFA6.25Fe20 (01)	0.520491	-0.006741	-0.012516	0.538642	1.546458	0.651262	1.335107	0.602892	1.28454	0.31748	0.289387	0.348085
SRFA6.25Fe5 (01)	0.183201	-0.010272	-0.015479	0.663608	1.305986	0.390198	5.456069	0.889953	0.5584	0.136214	0.441294	0.525124
SRFAFe0.1 (01)	0.239049	-0.013029	-0.01881	0.692666	1.272277	0.416135	5.640339	2.03166	1.087073	0.331291	0.973021	1.184517
SRFAFe1 (01)	0.221217	-0.012696	-0.018695	0.679109	1.281676	0.386558	8.726356	1.728978	0.610493	0.204463	0.845692	0.974564
SRFAFe10 (01)	0.325284	-0.010185	-0.015518	0.656332	1.367187	0.441127	8.322419	1.440072	0.519889	0.16394	0.706084	0.762776
SRFAFe20 (01)	0.411614	-0.008516	-0.01434	0.593874	1.467943	0.528913	6.773085	1.118586	0.368535	0.165639	0.565306	0.598673
SRFAFe5 (01)	0.290408	-0.011284	-0.016529	0.682645	1.310882	0.40921	8.602898	1.719947	0.422531	0.210546	0.845162	0.97945
SRFA12.5 (01)	0.258047	-0.013111	-0.019326	0.678436	1.277103	0.406828	4.540606	2.851835	1.600352	0.473564	1.380925	1.640761
SRFA6.25 (01)	0.13034	-0.012853	-0.018582	0.6917	1.233506	0.405148	5.380362	1.436234	0.844764	0.248672	0.69142	0.83786
SRFA6.25Fe0.1 (01)	0.121752	-0.013207	-0.02007	0.658079	1.289306	0.385125	4.44701	1.342411	0.8923	0.237856	0.639166	0.752201
SRFA6.25Fe1 (01)	0.12212	-0.012238	-0.017032	0.718537	1.31336	0.399509	3.619618	1.18069	0.935072	0.269768	0.571512	0.685218
SRFA6.25Fe10 (01)	0.235177	-0.008617	-0.013651	0.631211	1.42157	0.52275	3.883504	0.907465	0.610037	0.181421	0.450139	0.473176
SRFA6.25Fe20 (01)	0.518694	-0.006745	-0.012546	0.537646	1.491724	0.56929	1.20924	0.708736	1.608035	0.45399	0.360934	0.414704
SRFA6.25Fe5 (01)	0.182746	-0.01032	-0.01568	0.65821	1.339825	0.397331	5.04365	1.137113	0.674915	0.184212	0.561602	0.686285
SRFAFe0.1 (01)	0.23858	-0.013064	-0.01889	0.691583	1.26024	0.411642	5.888765	2.615945	1.289765	0.453302	1.239637	1.50879
SRFAFe1 (01)	0.222175	-0.012663	-0.018399	0.68825	1.27429	0.387699	8.07825	2.249184	0.739947	0.256976	1.087231	1.266172
SRFAFe10 (01)	0.324668	-0.01021	-0.015675	0.651356	1.379501	0.457101	6.872782	1.780427	0.603913	0.263952	0.895275	0.966623
SRFAFe20 (01)	0.410638	-0.008509	-0.014387	0.591437	1.413064	0.500015	5.940092	1.421549	0.371164	0.207542	0.726949	0.768167
SRFAFe5 (01)	0.290818	-0.011246	-0.016369	0.687007	1.351642	0.404435	9.452961	2.162574	0.489958	0.292512	1.078915	1.235592

As – DOM Complexation

Table A 3 As-DOM Complexation. All numbers are in Raman Units.

Sample Name	SRFA (mg/L)	As (ug/L)	abs254	S1	S2	SR	FI	FrI	HIX	A	B	T	C	M
P12.5x0ppb (01)	12.5	0	0.264	-0.013	-0.017	0.743	1.262	0.395	21.163	2.368	0.055	0.148	1.190	1.350
P12.5x1000ppb (01)	12.5	1000	0.266	-0.012	-0.017	0.716	1.300	0.428	15.195	2.100	0.053	0.185	1.110	1.163
P12.5x100ppb (01)	12.5	100	0.264	-0.013	-0.017	0.738	1.236	0.403	20.664	2.290	0.052	0.159	1.164	1.293
P12.5x10ppb (01)	12.5	10	0.262	-0.013	-0.018	0.726	1.232	0.398	16.888	2.209	0.039	0.154	1.142	1.284
P12.5x500ppb (01)	12.5	500	0.259	-0.013	-0.018	0.717	1.281	0.416	16.280	2.160	0.057	0.182	1.104	1.188
P12.5x50ppb (01)	12.5	50	0.266	-0.013	-0.017	0.739	1.217	0.410	17.819	2.329	0.064	0.189	1.181	1.316
P6.25x0ppb (01)	6.25	0	0.143	-0.012	-0.014	0.856	1.243	0.402	19.357	1.203	0.015	0.063	0.586	0.645
P6.25x0ppb (02)	6.25	0	0.138	-0.012	-0.016	0.778	1.285	0.395	19.799	1.197	0.033	0.069	0.595	0.666
P6.25x1000ppb (01)	6.25	1000	0.146	-0.012	-0.015	0.778	1.309	0.431	13.805	1.178	0.006	0.091	0.605	0.633
P6.25x100ppb (01)	6.25	100	0.141	-0.012	-0.016	0.778	1.280	0.400	13.857	1.208	0.039	0.081	0.596	0.672
P6.25x100ppb (02)	6.25	100	0.140	-0.012	-0.016	0.783	1.242	0.405	15.303	1.182	0.015	0.063	0.589	0.662
P6.25x10ppb (01)	6.25	10	0.139	-0.013	-0.016	0.796	1.233	0.421	19.491	1.097	0.019	0.082	0.567	0.634
P6.25x10ppb (02)	6.25	10	0.138	-0.013	-0.016	0.786	1.241	0.424	17.848	1.106	0.023	0.062	0.573	0.637
P6.25x500ppb (01)	6.25	500	0.139	-0.012	-0.015	0.755	1.399	0.477	12.626	1.197	0.019	0.107	0.613	0.667
P6.25x500ppb (02)	6.25	500	0.140	-0.012	-0.015	0.763	1.291	0.467	12.244	1.214	0.038	0.117	0.610	0.655
P6.25x50ppb (01)	6.25	50	0.138	-0.013	-0.016	0.776	1.240	0.416	21.636	1.134	0.012	0.114	0.576	0.655

Table A 4 Fe – As – DOM Complexation. All numbers are in Raman Units.

Sample Name	SRFA (mg/L)	Fe (mg/L)	As (ug/L)	abs254	S1	S2	SR	FI	FrI	HIX	A	B	T	C	M
P6.25 10 0 (01)	6.25	10	0	0.234614	-0.008829	-0.013852	0.637366	1.397253	0.43167	4.132365	0.813304	0.410313	0.267626	0.411105	0.480563
P6.25 10 10 (01)	6.25	10	10	0.242123	-0.009004	-0.014067	0.640113	1.396359	0.431985	4.659197	0.81542	0.425097	0.256388	0.4329	0.476215
P6.25 10 100 (01)	6.25	10	100	0.232412	-0.008503	-0.014751	0.57644	1.410062	0.414955	5.294467	0.794056	0.398569	0.204588	0.40335	0.464342
P6.25 10 1000 (01)	6.25	10	1000	0.231625	-0.008167	-0.013978	0.584279	1.388557	0.457231	6.464676	0.773337	0.220649	0.175105	0.387647	0.456587
P6.25 10 50 (01)	6.25	10	50	0.238044	-0.008771	-0.013977	0.627524	1.354532	0.428557	5.33666	0.791366	0.313295	0.196712	0.396124	0.464523
P6.25 10 500 (01)	6.25	10	500	0.233638	-0.008441	-0.013951	0.60501	1.393688	0.426895	4.325106	0.80448	0.451039	0.192768	0.401067	0.487252
P6.25 20 0 (01)	6.25	20	0	0.224058	-0.00523	-0.009404	0.556192	1.648455	0.637941	10.356329	0.642044	0.171524	0.140712	0.354542	0.255296
P6.25 20 10 (01)	6.25	20	10	0.361299	-0.006889	-0.012557	0.54863	1.522602	0.479529	4.245955	0.667856	0.186167	0.222759	0.319147	0.394338
P6.25 20 100 (01)	6.25	20	100	0.371802	-0.006835	-0.012468	0.54821	1.454766	0.4714	3.900022	0.642221	0.32919	0.255059	0.316437	0.382995
P6.25 20 1000 (01)	6.25	20	1000	0.354691	-0.0063	-0.012278	0.513139	1.482699	0.474402	3.822519	0.738918	0.212494	0.226056	0.35551	0.403988
P6.25 20 50 (01)	6.25	20	50	0.372384	-0.006832	-0.012478	0.547501	1.427698	0.482648	3.998543	0.613744	0.277531	0.257431	0.314714	0.392478
P6.25 20 500 (01)	6.25	20	500	0.371884	-0.006529	-0.012172	0.536405	1.428559	0.501776	3.278329	0.704783	0.601409	0.275971	0.353808	0.416477

Appendix G - Analyses of DOM quality for groundwater samples from Mahomet aquifer.

The role of dissolved organic matter (DOM) in the biogeochemical interactions resulting into iron (Fe) and arsenic (As) mobilization in reducing aquifers of West Bengal (India) has been documented recently. Heavy monsoonal recharge in this region is also an important hydrological control that influences the groundwater flow, redox conditions and the groundwater quality. Few studies have reported the effect of monsoonal recharge on levels of As, Fe and HCO_3^-, however its effect on the characteristics of DOM has not been studied yet. In this study, pre (PRM) and post-monsoon (PSTM) spectroscopic properties of DOM in the groundwater samples from shallow (50 – 150 ft) holocene aquifer (Nadia) and deep (200 – 360 ft) pleistocene aquifer (Hooghly) were examined using absorbance and 3-dimensional fluorescence spectroscopy followed by a three components parallel factor (PARAFAC) model. Total As, anions, dissolved organic carbon and nitrogen (DOC/DON) and bulk proteins were measured in the laboratory. Total As in shallow PRM and PSTM samples ranged from 50 to 315 µg/L and 42 to 300 µg/L respectively, while that in deep PRM and PSTM samples from 0.44 to 10.62 µg/L and 0.55 to 9.62 µg/L. At shallow depths, chlorides concentrations were found to have mixing effect from monsoonal recharge while at greater depths this effect did not exist. All other chemical and DOM properties showed variations (either increased or decreased) at shallow as well as greater depths after monsoonal recharge. In the shallow samples, decrease in total As was linked with decrease in DOC, slight increase in fluorescence index (FI), slight decrease in freshness index (β:α), decrease in specific ultraviolet absorbance ($SUVA_{254}$) and decrease in bulk proteins. In deep samples, increase in total As was linked with decrease in DOC, increase in FI, slight increase in β:α, decrease in $SUVA_{254}$ and decrease in bulk proteins. The chlorides (Cl^-) concentrations varied at shallow depth but remained unchanged at greater depths after the monsoonal recharge. Although the drastic increase in As was not observed in this study, the results indicate that the quality of DOM changes significantly after the monsoon. Changes in DOM quality at shallow depth may be linked directly to mixing due to recharge while the changes at greater depths may be linked to monsoonal recharge but via complex flow and biogeochemical transport reactions rather than simple mixing.

Table A 5 DOM Parameters for Mahomet Aquifer Samples. Numbers are expressed as average value ± standard deviation, minimum – maximum range in parenthesis.

Parameter	As < 50 ppb	As > 50 ppb
SR	1.07 ± 0.11 (0.94 – 1.26)	1.05 ± 0.16 (0.95 – 1.70)
FI	1.78 ± 0.03 (1.73 – 1.82)	1.76 ± 0.02 (1.72 – 1.80)
FrI	0.75 ± 0.02 (0.72 – 0.78)	0.73 ± 0.02 (0.68 – 0.76)
HIX	10.84 ± 2.37 (6.97 – 13.91)	12.87 ± 1.40 (10.72 – 15.70)
Peak A	4.46 ± 1.78 (2.36 – 6.73)	4.70 ± 1.32 (2.01 – 6.87)
Peak B	0.53 ± 0.39 (0.19 – 1.30)	0.35 ± 0.15 (0.07 – 0.68)
Peak T	0.94 ± 0.61 (0.37 – 2.11)	0.68 ± 0.24 (0.22 – 1.17)
Peak C	2.34 ± 0.93 (1.24 – 3.56)	2.46 ± 0.71 (1.01 – 3.69)
Peak M	2.64 ± 1.07 (1.34 – 4.05)	2.72 ± 0.78 (1.13 – 4.05)
H/B	7.25 ± 0.82 (5.65 – 8.32)	8.01 ± 0.32 (7.53 – 8.60)
NPOC (mg/l)	4.7 ± 2.16 (2.7 – 7.9)	4.4 ± 1.79 (1.98 – 8.86)

Table A 6 Statistical analyses of DOM parameters for Mahomet Aquifer samples.

Parameter	As<50 – As>50
SR	0.42
FI	0.10
FrI	0.02
HIX	0.02
Peak A	0.42
Peak B	0.28
Peak T	0.40
Peak C	0.44
Peak M	0.46
H/B	0.00

Values in shaded cells: P<0.05 indicate statistically different parameter

Table A 7 Comparison of DOM parameters in Mahomet Bedock Valley and Bengal Basin Aquifers. Numbers are expressed as average value ± standard deviation, minimum − maximum range in parenthesis. All peak intensitys are in R.U.

Parameter	Mahomet Aquifer (IL)	Bengal Basin (Murshidabad, India)
SR	1.06 ± 0.14 (0.94 − 1.70)	1.33 ± 0.47 (0.69 − 2.34)
FI	1.77 ± 0.02 (1.72 − 1.82)	1.73 ± 0.06 (1.59 − 1.83)
FrI	0.74 ±0.02 (0.68 − 0.78)	0.77 ± 0.06 (0.68 − 0.96)
HIX	12.22 ± 1.97 (6.97 − 15.70)	6.79 ± 1.98 (3.48 − 10.45)
Peak A	4.63 ± 1.45 (2.01 − 6.87)	1.99 ± 3.46 (0.27 − 18.81)
Peak B	0.40 ± 0.26 (0.07 − 1.30)	0.25 ± 0.32 (0.06 − 1.54)
Peak T	0.76 ± 0.40 (0.22 − 2.11)	0.35 ± 0.55 (0.06 − 2.62)
Peak C	2.42 ± 0.77 (1.01 − 3.69)	0.87 ± 1.20 (0.13 − 6.03)
Peak M	2.69 ± 0.86 (1.13 − 4.05)	1.08 ± 1.62 (0.16 − 8.58)
H/B	7.76 ± 0.63 (5.65 − 8.60)	8.53 ± 3.42 (3.31 − 19.10)
NPOC (mg/l)	4.51 ± 1.88 (1.97 − 8.86)	2.94 ± 1.97 (1.25 − 6.76)

Table A 8 Statistical analyses of DOM parameters in MBV and Bengal Basin aquifers

P	Mahomet - Bengal
SR	0.010
FI	0.006
FrI	0.009
HIX	<0.001
Peak A	<0.001
Peak B	<0.001
Peak T	<0.001
Peak C	<0.001
Peak M	<0.001
H/B	0.201

*Values in shaded cells: P<0.05 indicate statistically different parameter*
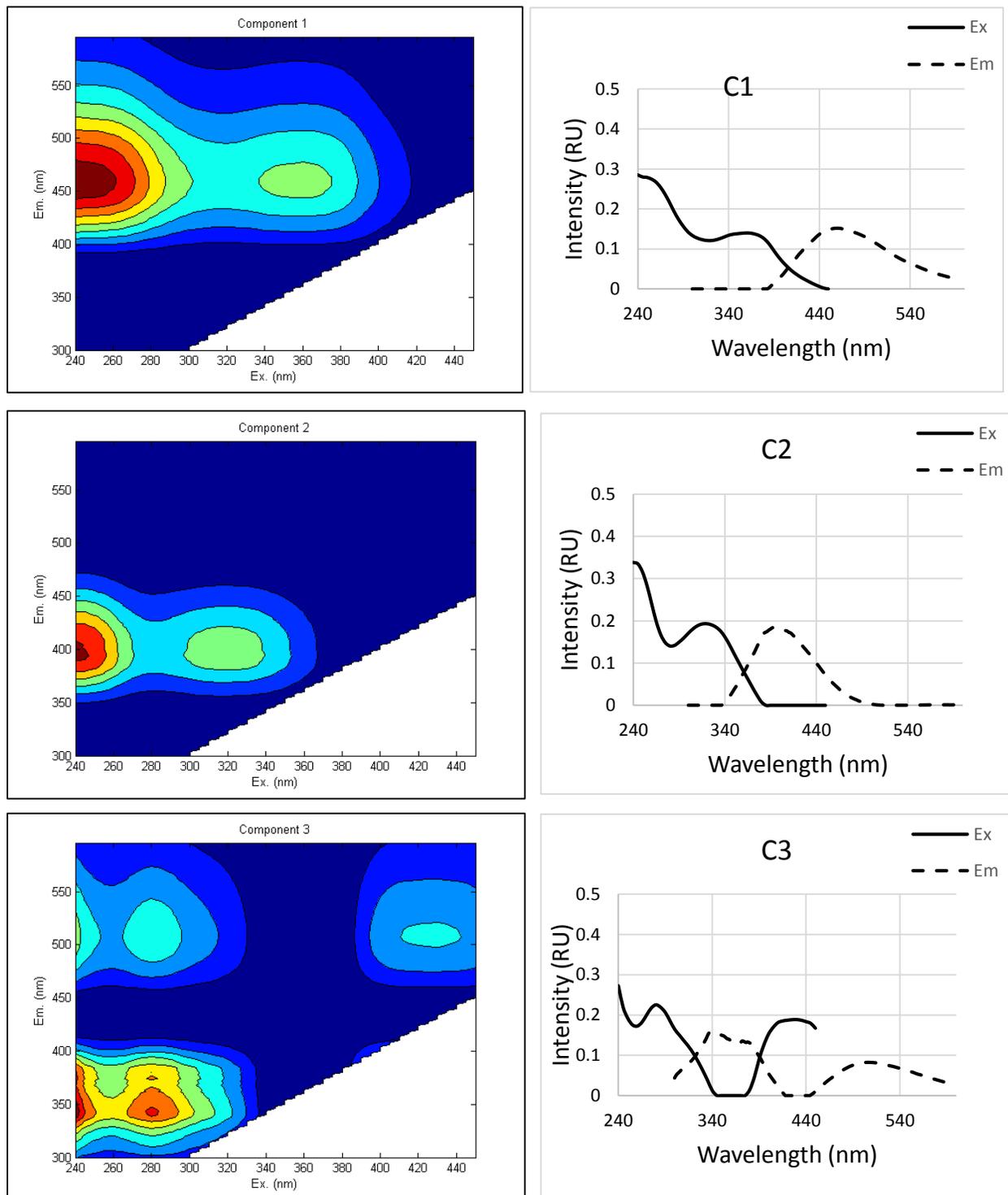
Figure A 1 Three component PARAFAC model for Mahomet Bedrock Valley Aquifer Groundwater samples.

Table A 9 DOM characteristics data: Mahomet Bedrock Valley Aquifer samples. C1, C2 and C3 are in Raman Units.

Name	Bulk Protein (mg/L)	NPOC (mg/L)	TN (mg/L)	abs254	S1	S2	SR	FI	FrI	HIX	C1	C2	C3
IL09	1.07	3.36	1.62	0.11	-0.02	-0.02	0.92	1.76	0.75	11.57	3.42	2.01	0.91
IL17	0.77	4.15	4.47	0.13	-0.02	-0.02	0.89	1.75	0.72	13.59	5.19	2.86	0.95
IL25	0.47	1.97	0.87	0.07	-0.01	-0.01	1.58	1.78	0.75	15.48	2.18	1.24	0.34
IL15	0.77	3.94	4.30	0.15	-0.02	-0.02	0.94	1.74	0.72	13.63	5.39	2.95	1.04
IL26	0.96	5.20	4.09	0.18	-0.02	-0.02	0.95	1.76	0.74	12.61	6.61	3.59	1.43
IL14	1.03	8.86	8.59	0.33	-0.01	-0.02	0.79	1.78	0.74	13.59	13.08	6.67	2.50
IL20	0.50	2.45	1.01	0.09	-0.02	-0.02	0.94	1.75	0.73	17.03	2.84	1.58	0.43
IL19	0.38	2.49	0.99	0.09	-0.02	-0.02	0.81	1.78	0.73	17.22	2.87	1.57	0.41
IL27	0.79	4.54	4.03	0.15	-0.02	-0.02	0.90	1.76	0.72	11.87	5.53	3.09	1.28
IL13	0.85	5.00	8.29	0.16	-0.02	-0.02	0.89	1.72	0.69	12.75	5.82	3.19	1.20
IL12	0.97	3.85	1.81	0.12	-0.02	-0.02	0.92	1.79	0.76	10.64	4.94	2.84	1.29
IL29	0.89	5.64	3.02	0.18	-0.02	-0.02	0.88	1.78	0.75	10.56	7.02	3.98	1.92
IL22	0.64	5.59	1.71	0.12	-0.02	-0.02	0.81	1.77	0.75	15.09	3.76	2.11	0.68
IL18	1.61	6.43	6.82	0.21	-0.02	-0.02	0.79	1.80	0.78	13.07	7.66	4.12	1.55
IL28	0.69	3.03	1.93	0.10	-0.02	-0.02	0.86	1.76	0.73	13.64	3.12	1.84	0.67
IL10	0.47	3.27	1.48	0.08	-0.01	-0.01	1.00	1.73	0.72	12.98	2.36	1.34	0.56
IL31	1.30	6.66	4.52	0.18	-0.02	-0.02	0.89	1.80	0.77	9.46	6.19	3.59	1.96
IL30	0.68	7.89	4.32	0.28	-0.01	-0.01	1.05	1.79	0.79	6.64	7.94	4.50	4.14
IL21	0.39	2.67	0.90	0.09	-0.02	-0.02	0.77	1.78	0.75	14.47	2.73	1.56	0.57
IL24	0.56	3.24	1.88	0.10	-0.02	-0.02	0.84	1.76	0.75	10.75	3.43	2.05	0.95

Table A 10 Raw chemical data provided by Holm R.

Name	Al27 ug/L	Si29 ug/L	P31 ug/L	S34 ug/L	Ca43 ug/L	Fe57 ug/L	Ba137 ug/L	Na23 ug/L	Mg25 mg/L	K39 ug/L	Mn55 mg/L	As75 ug/L	Sr88 ug/L
IL09	4.94	12949.67	43.30	45.00	44328.00	3998.69	59.28	27372.82	32.78	1536.55	0.01	176.50	468.59
IL17	6.34	13632.68	20.51	62.21	61174.18	1955.08	90.01	23151.43	38.87	2044.29	0.03	172.75	592.47
IL25	17.19	11843.37	33.24	52422.60	91434.56	3772.93	154.04	17724.30	85.05	1332.81	0.01	143.99	718.43
IL15	4.90	15952.43	323.33	71.17	57078.77	5599.05	151.91	18600.85	32.33	1979.19	0.03	120.51	559.31
IL26	12.80	12401.21	280.16	98.91	54975.39	4540.74	98.50	28619.47	37.37	2129.04	0.05	112.14	529.49
IL14	4.38	17819.20	237.12	150.82	70679.35	4400.30	241.59	34680.22	40.22	3101.68	0.03	110.61	471.23
IL20	27.90	12778.63	49.50	37.25	53104.79	1762.95	47.36	17941.31	32.75	1174.25	0.03	96.24	691.97
IL19	5.31	12417.77	47.54	30.23	51085.16	1695.12	46.52	17743.49	31.79	1159.95	0.02	95.25	670.29
IL27	6.29	14559.18	156.58	56.09	56399.82	2940.71	183.86	25334.49	35.20	2304.42	0.04	87.69	407.52
IL13	6.46	21797.76	204.88	82.89	########	8083.32	221.18	18757.12	46.90	2940.02	0.08	80.98	594.71
IL12	7.75	16818.92	58.54	65.75	54735.77	2292.71	113.97	27508.14	39.20	2216.02	0.01	77.19	341.71
IL29	7.31	12424.51	69.41	76.20	50549.91	1666.47	131.50	37314.85	37.19	2304.02	0.04	64.17	438.32
IL22	65.93	13913.18	70.63	42.00	50023.23	1623.32	127.18	27072.66	35.88	1747.13	0.04	54.38	369.16
IL18	7.45	15999.07	361.73	98.12	61129.81	2512.28	227.67	71882.22	31.80	1947.95	0.09	28.27	424.02
IL28	8.57	14691.88	134.56	40.99	53785.33	2657.62	144.73	22043.69	31.87	1696.03	0.04	24.08	331.88
IL10	7.85	13860.78	280.89	29.49	59901.49	4180.10	131.83	14554.93	32.84	1601.87	0.02	21.85	388.52
IL31	6.39	14957.69	254.27	10906.46	71276.11	4068.18	286.65	67947.46	40.43	2193.51	0.13	11.94	522.06
IL30	5.40	14665.70	255.29	10783.70	70463.37	3985.52	288.55	65809.34	37.77	2073.70	0.13	10.84	517.18
IL21	6.93	18289.68	246.87	31.38	61975.90	4083.78	159.76	23940.73	33.38	1807.44	0.02	9.55	263.62
IL24	32.44	14404.89	60.11	43.02	50814.57	2191.53	105.46	31962.40	33.43	2116.60	0.02	6.15	475.03

Table A 11 Anions (in ppm) data for Mahomet Bedrock Valley Aquifer samples

Name	Acetate	Arsenate	Bromide	Chloride	Citrate	Fluoride	Formate	Lactate	Nitrate	Nitrite	Oxalate	Phosphate	Sulfate
IL09	0.79	0.00	0.00	0.47	0.00	0.38	0.16	0.00	0.20	4.57	0.00	0.11	0.17
IL17	1.54	0.00	0.00	0.41	0.00	0.35	0.13	5.56	0.08	0.53	0.00	0.13	0.20
IL25	2.32	0.20	0.00	6.95	0.00	0.14	0.65	0.00	4.75	0.39	0.00	0.25	0.00
IL15	2.07	0.00	0.00	0.51	0.00	0.41	0.13	0.00	18.74	0.00	0.00	0.12	0.21
IL26	0.00	0.00	0.00	0.57	0.00	0.37	0.20	0.00	0.99	11.59	0.00	0.05	0.20
IL14	0.00	0.00	0.00	0.49	0.00	0.48	0.09	0.00	0.10	0.56	0.00	0.16	0.18
IL20	2.14	0.00	0.00	0.31	0.00	0.52	0.11	0.00	0.07	0.00	0.00	0.09	0.12
IL19	2.79	0.00	0.00	0.31	0.00	0.53	0.78	0.00	0.00	0.00	0.00	0.09	0.12
IL27	3.07	0.00	0.00	0.50	0.00	0.41	1.84	0.00	0.19	0.52	0.00	0.10	0.18
IL13	1.86	0.08	0.00	0.34	0.00	0.19	0.47	5.00	0.21	0.58	0.00	0.07	0.18
IL12	1.50	0.00	0.00	0.53	0.00	0.32	0.09	0.00	0.08	0.53	0.00	0.15	0.20
IL29	2.64	0.05	0.00	0.52	0.66	0.39	0.54	0.00	0.08	0.53	0.00	0.12	0.15
IL22	2.29	0.00	0.00	1.01	0.00	0.32	0.16	0.00	0.62	0.00	0.00	0.15	0.28
IL18	1.71	0.00	0.00	32.19	0.00	0.35	0.36	0.00	0.10	0.33	0.00	0.10	0.14
IL28	2.57	0.00	0.00	0.68	0.00	0.32	0.58	0.00	0.89	5.83	0.00	0.15	0.17
IL10	1.29	0.01	0.00	0.85	0.00	0.29	0.29	0.00	0.00	0.00	0.00	0.15	0.19
IL31	2.46	0.35	0.00	32.90	0.00	0.41	0.47	0.00	0.14	0.33	0.00	0.32	0.00
IL30	2.89	0.00	0.00	33.51	0.00	0.41	0.49	0.00	0.13	0.34	0.00	0.23	0.00
IL21	0.00	0.00	0.00	2.51	0.00	0.29	0.11	0.00	0.10	3.07	0.00	0.02	0.13
IL24	2.75	0.00	0.00	5.59	0.00	0.36	0.63	0.00	0.16	0.27	0.00	0.20	0.12

Appendix H - Maps showing distribution of geochemical parameters at Nadia / Hooghly district study sites
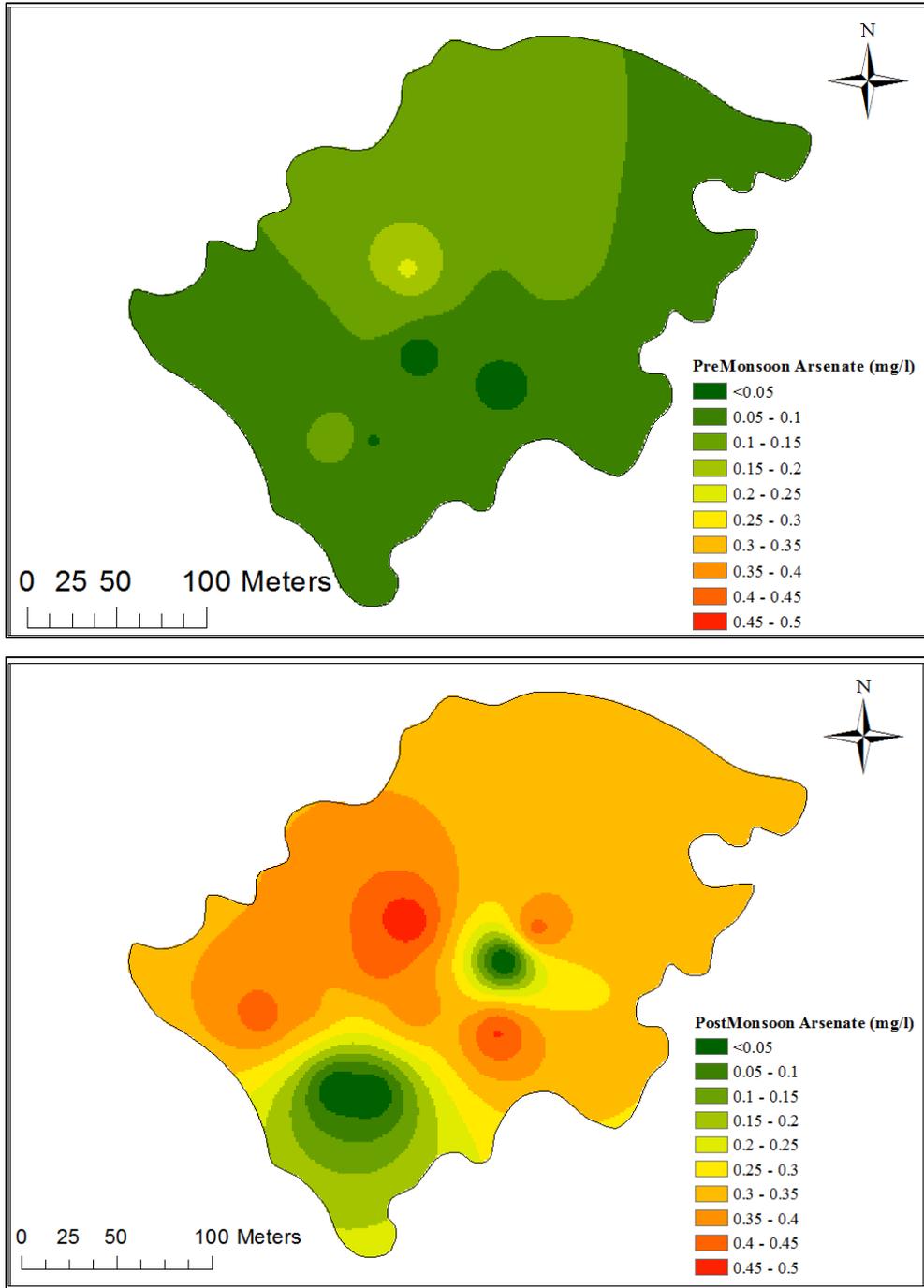
Figure A 2 Pre- and Post-Monsoon Arsenate Concentrations at Chakudanga
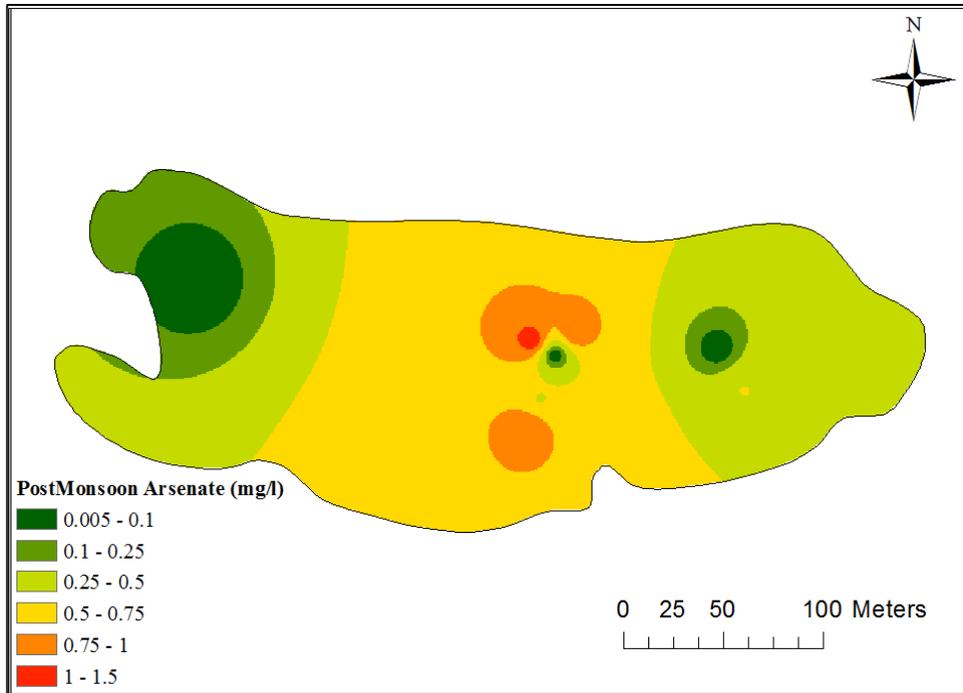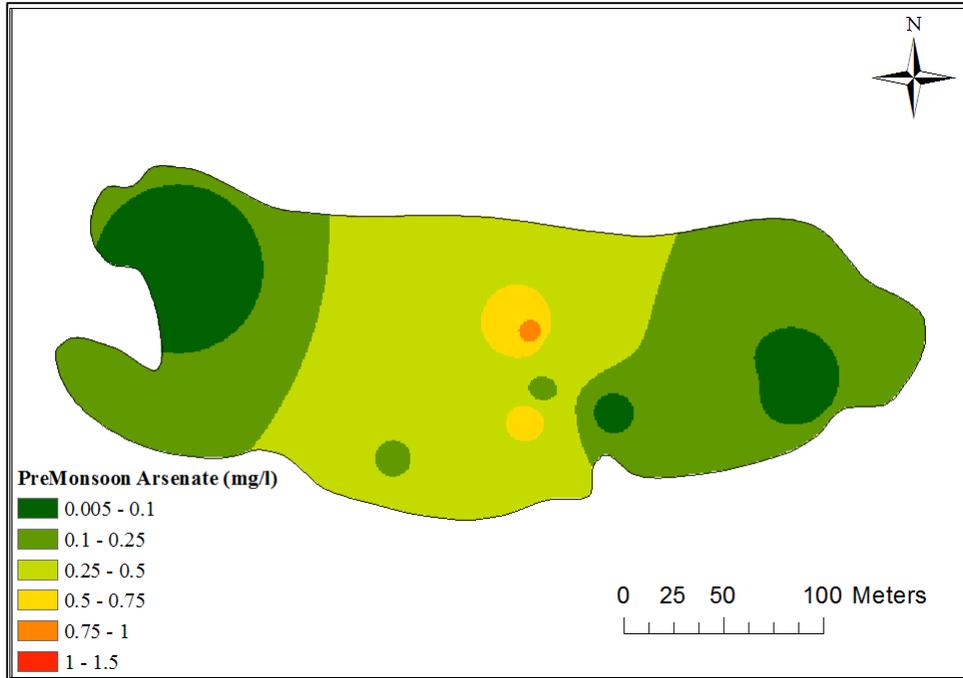
Figure A 3 Pre- and Post-Monsoon Arsenate Concentrations at Shahispur
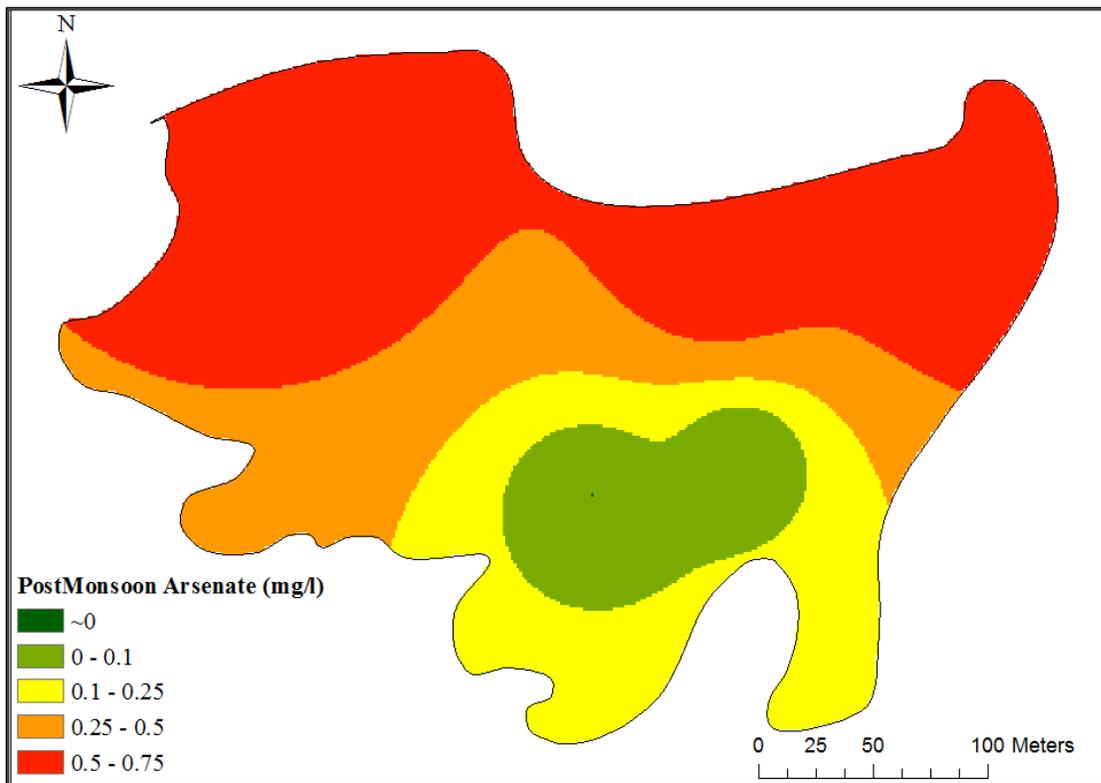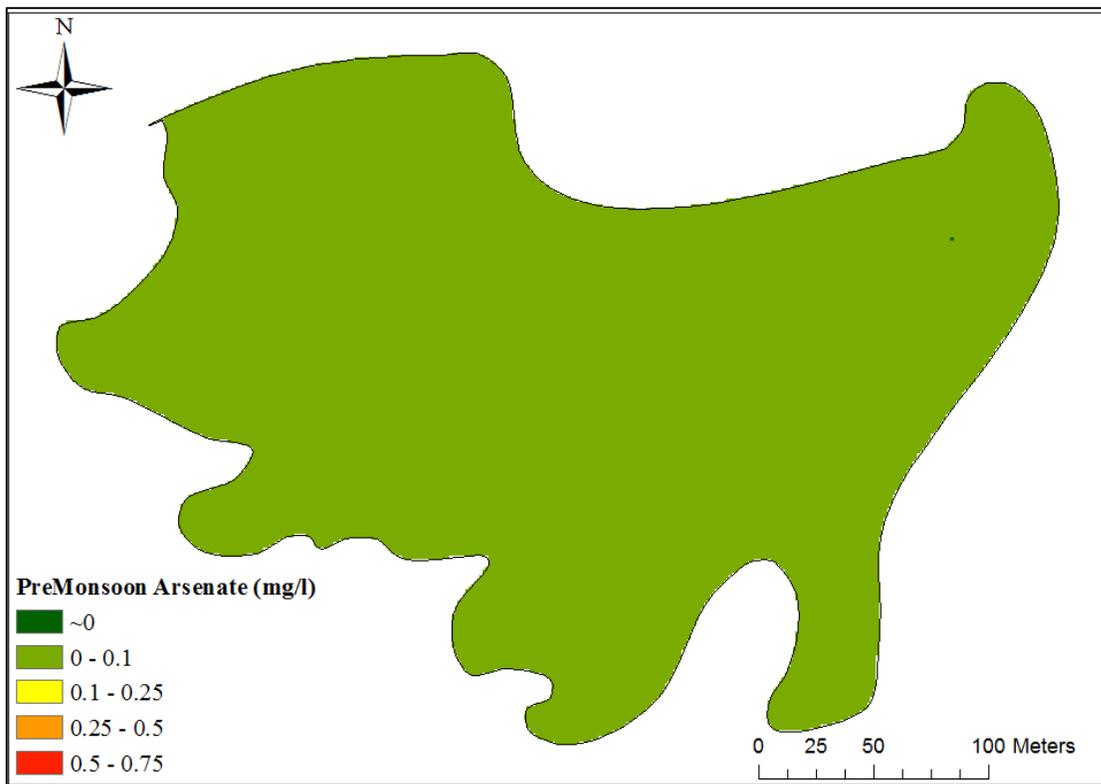
**Figure A 4 Pre- and Post-Monsoon Arsenate Concentration at Bele**
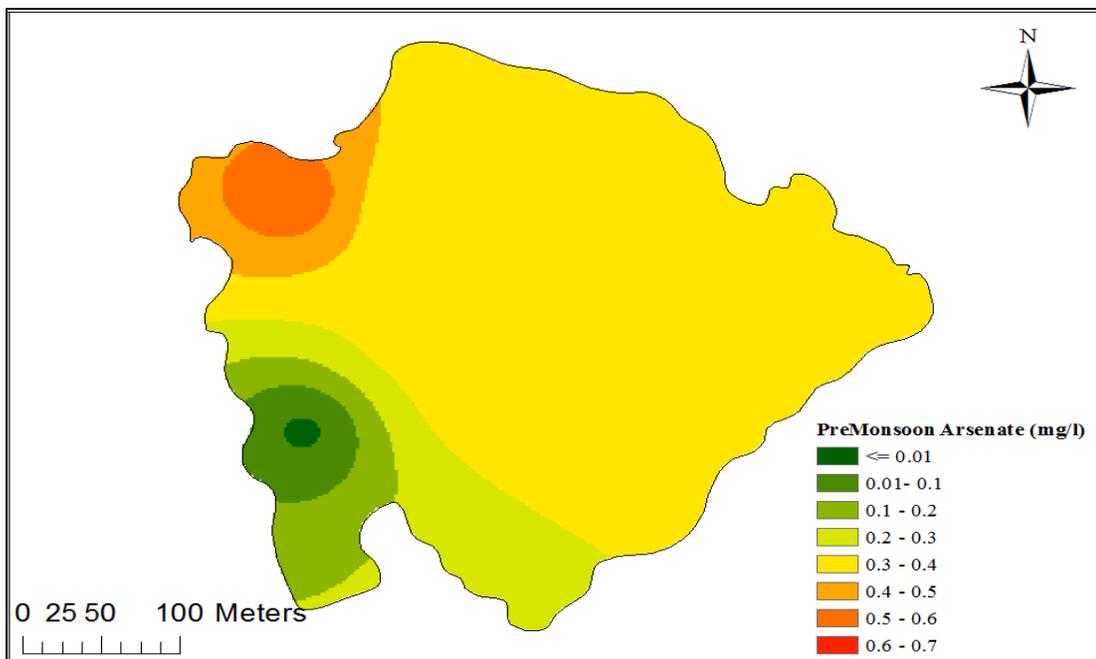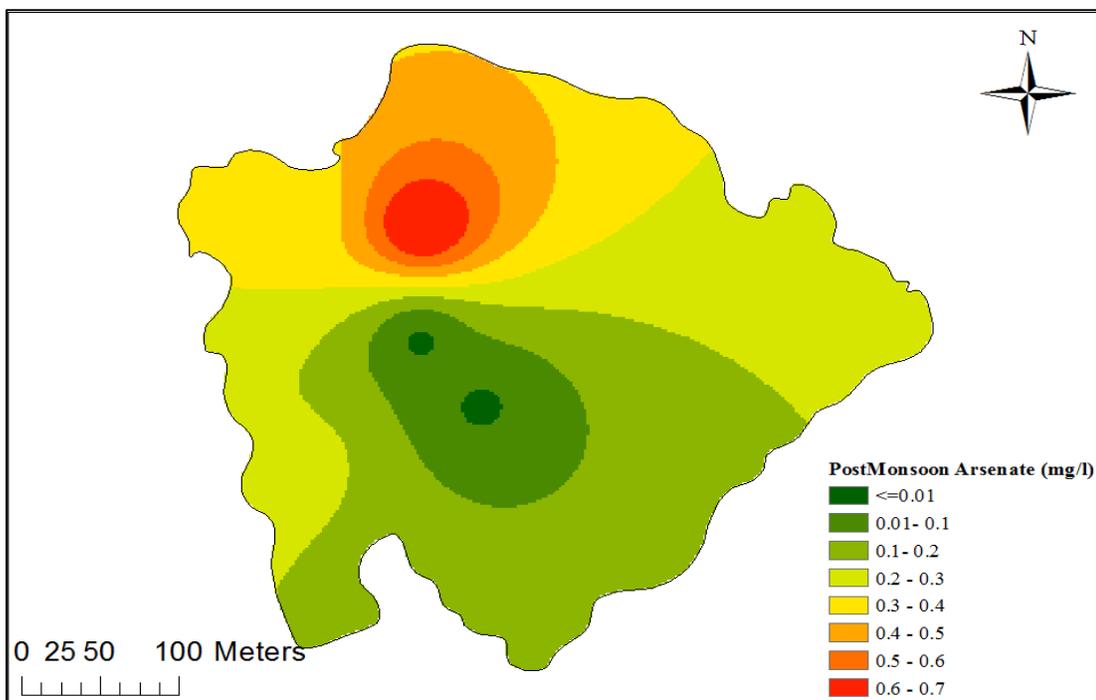
Figure A 5 Pre- and Post-Monsoon Arsenate Concentrations at Radhanagar
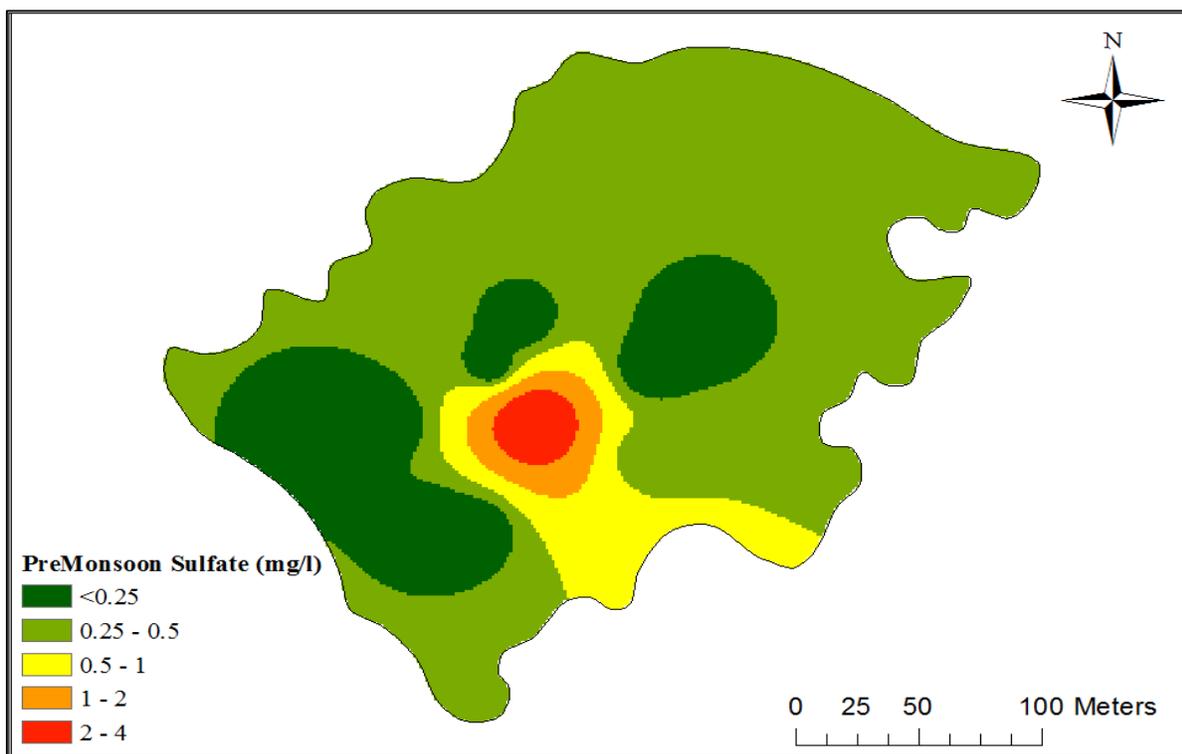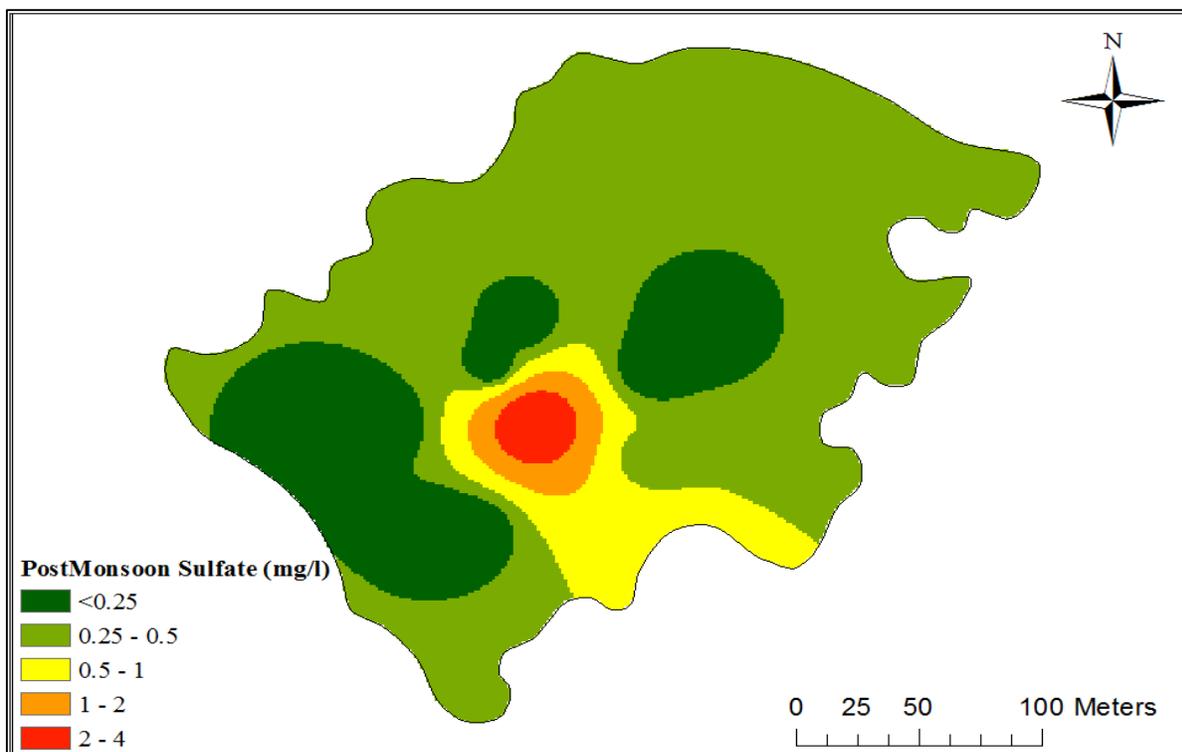
Figure A 6 Pre- and Post-Monsoon Sulfate Concentrations at Chakudanga
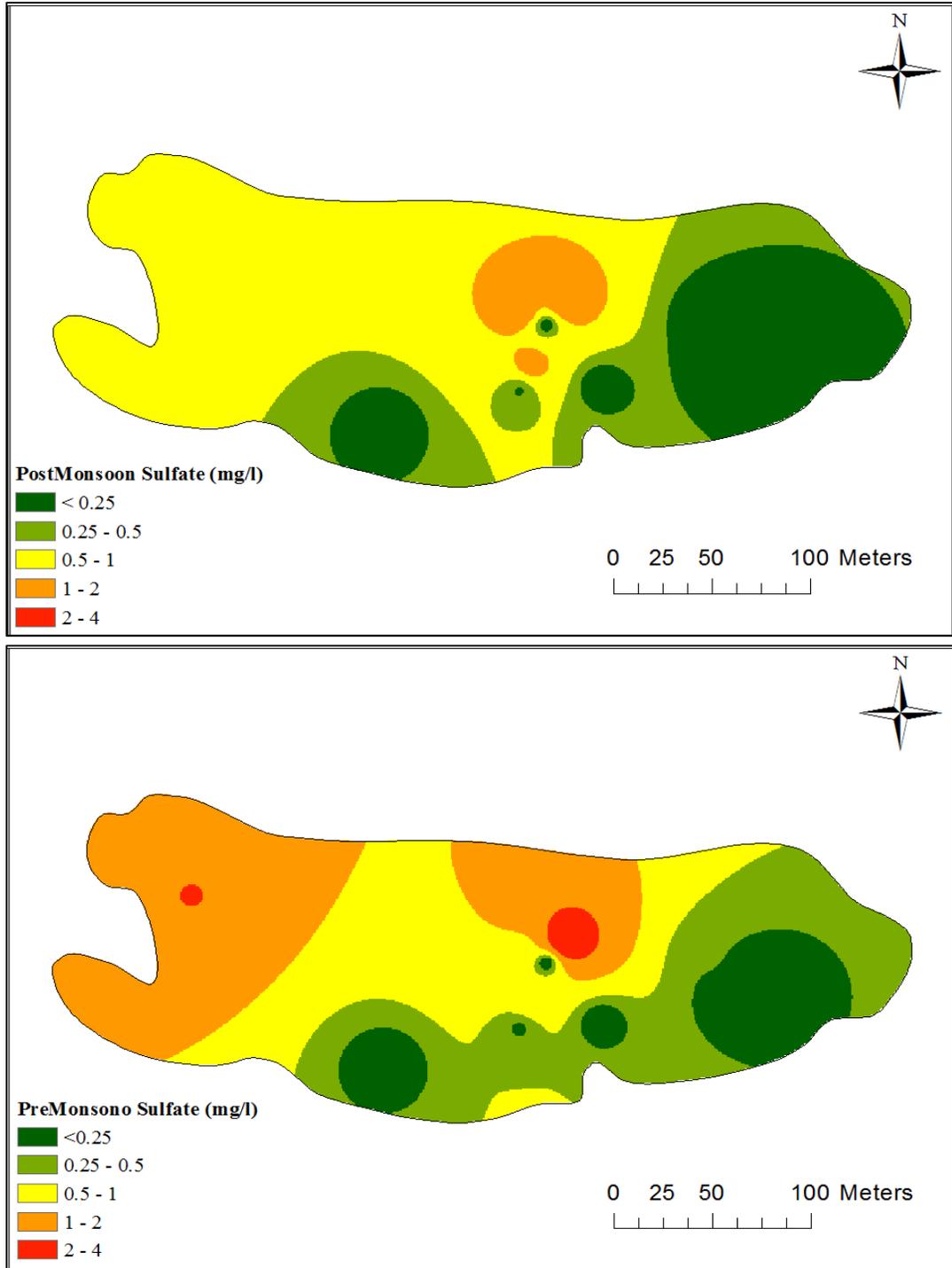
Figure A 7 Pre- and Post-Monsoon Sulfate Concentrations at Shahispur
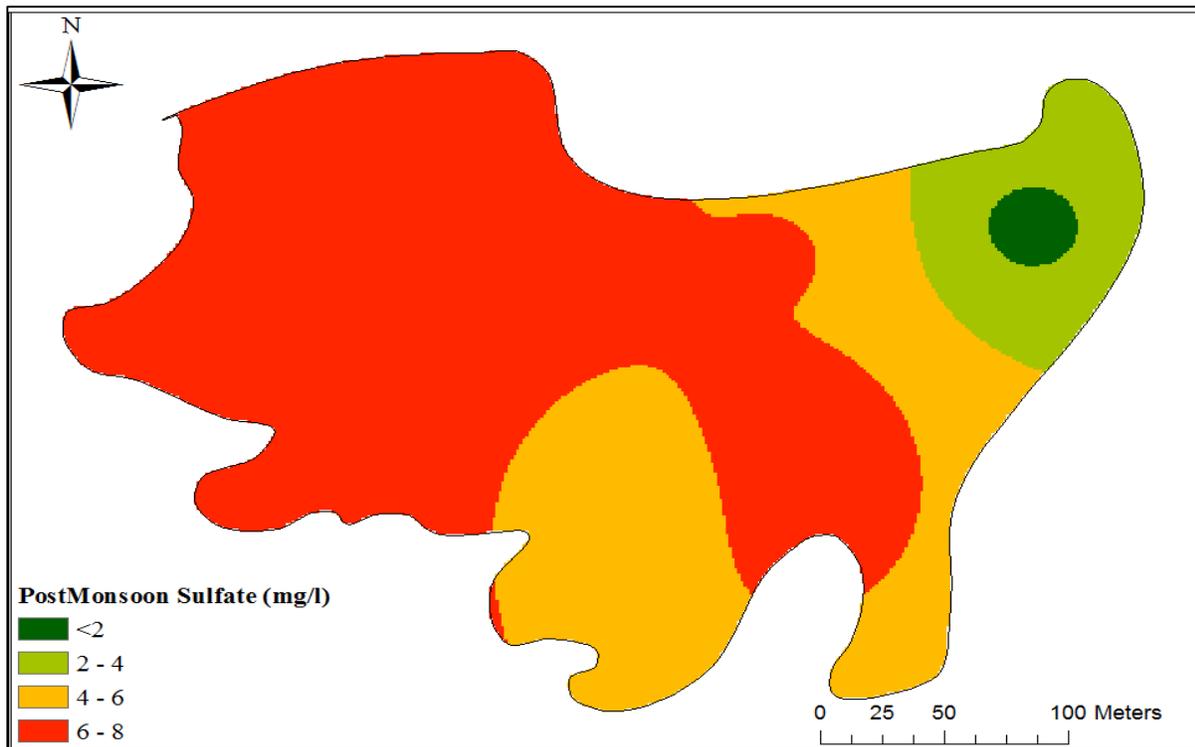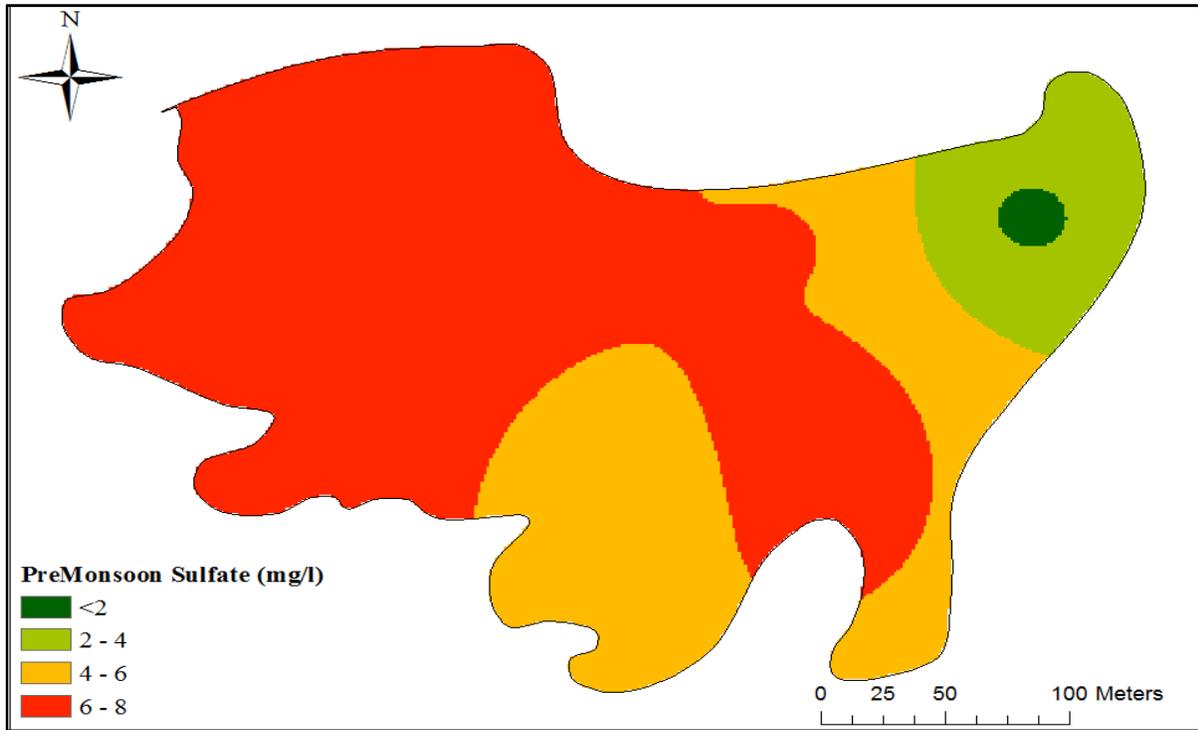
Figure A 8 Pre- and Post-Monsoon Sulfate Concentrations at Bele
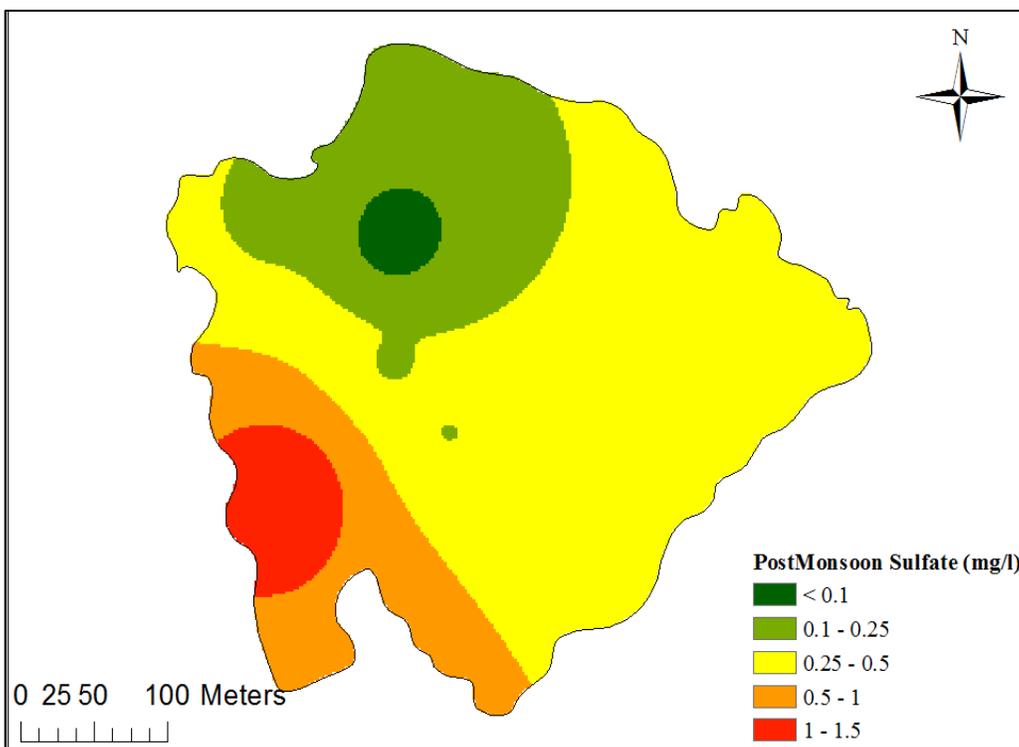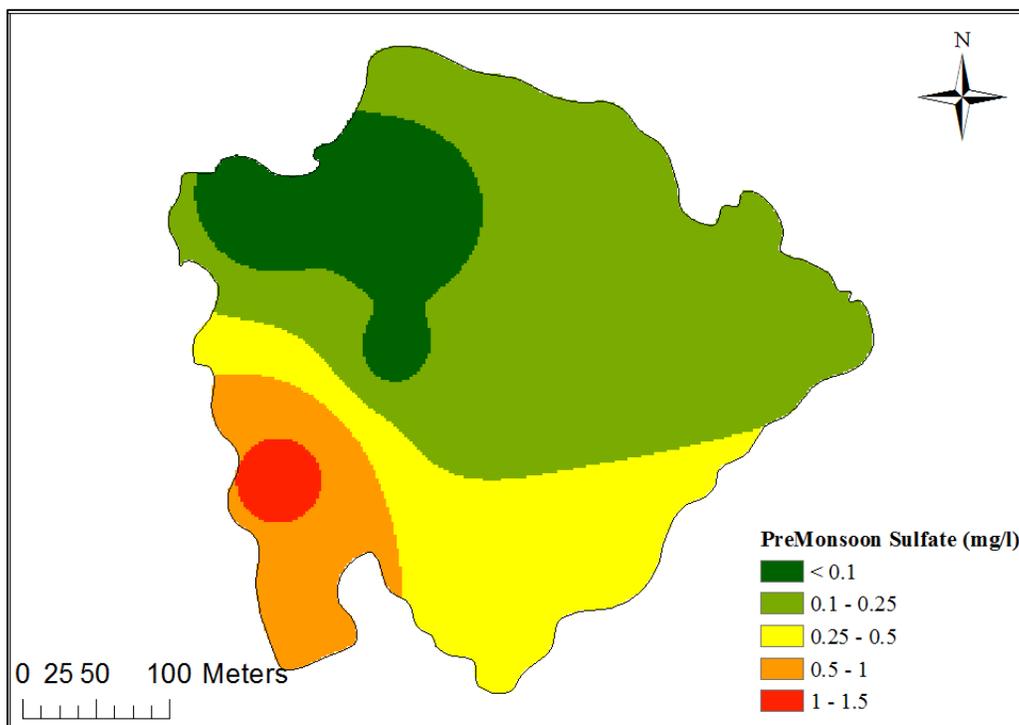
Figure A 9 Pre- and Post-Monsoon Sulfate Concentrations at Radhanagar
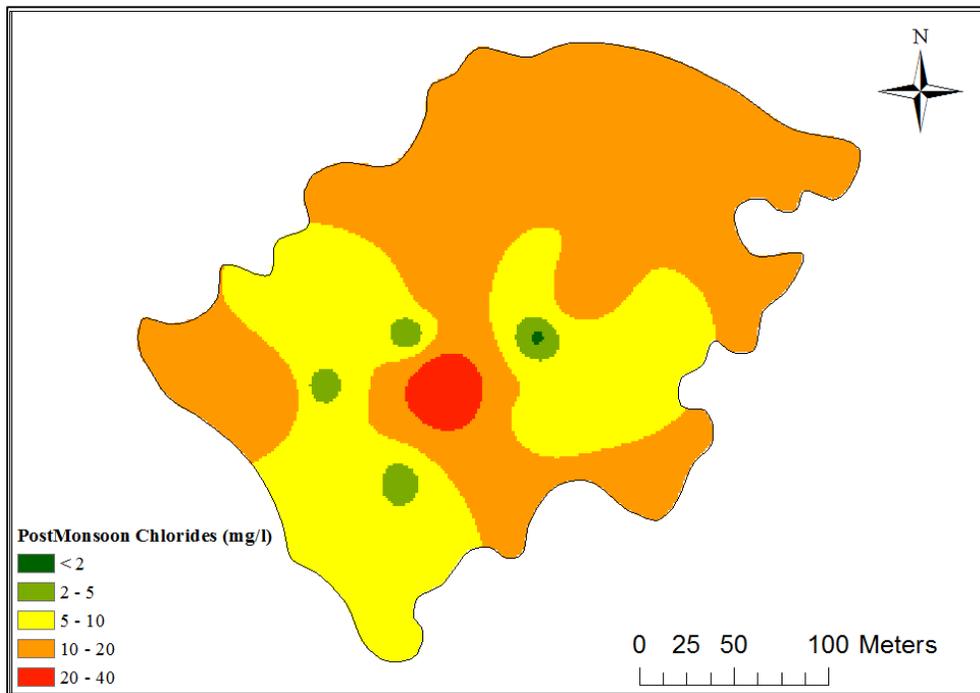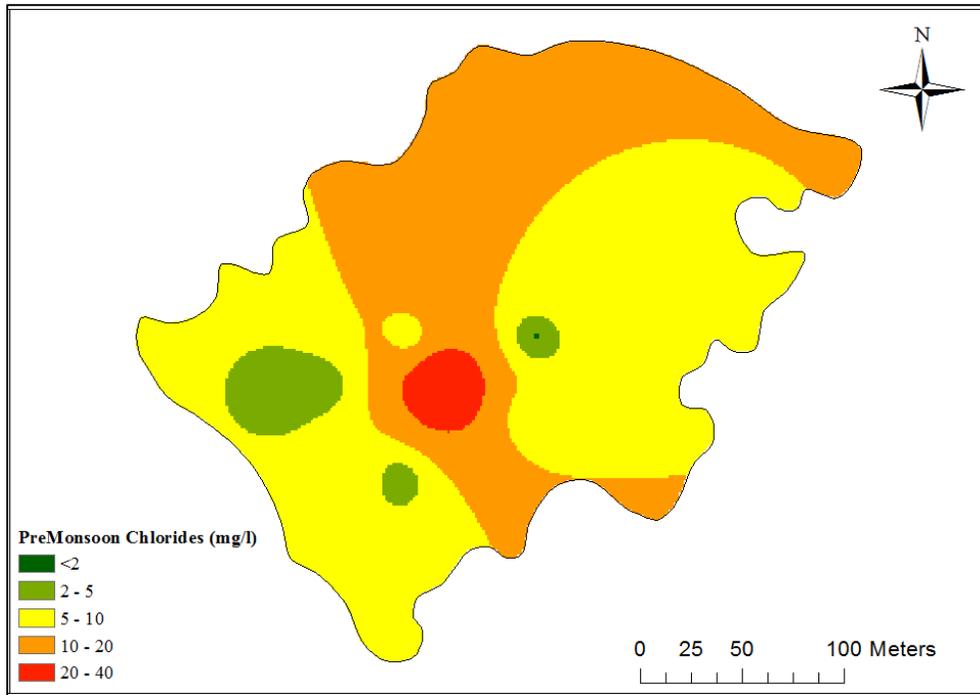
Figure A 10 Pre- and Post-Monsoon Chloride Concentrations at Chakudanga
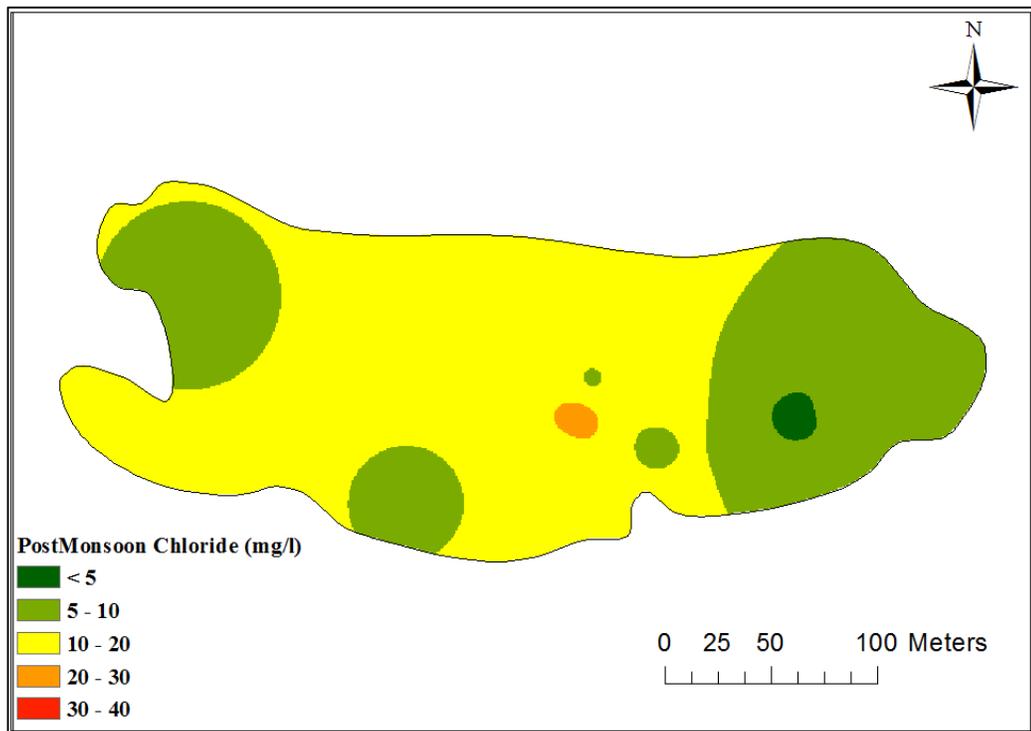
Figure A 11 Pre- and Post-Monsoon Chloride Concentrations at Shahispur
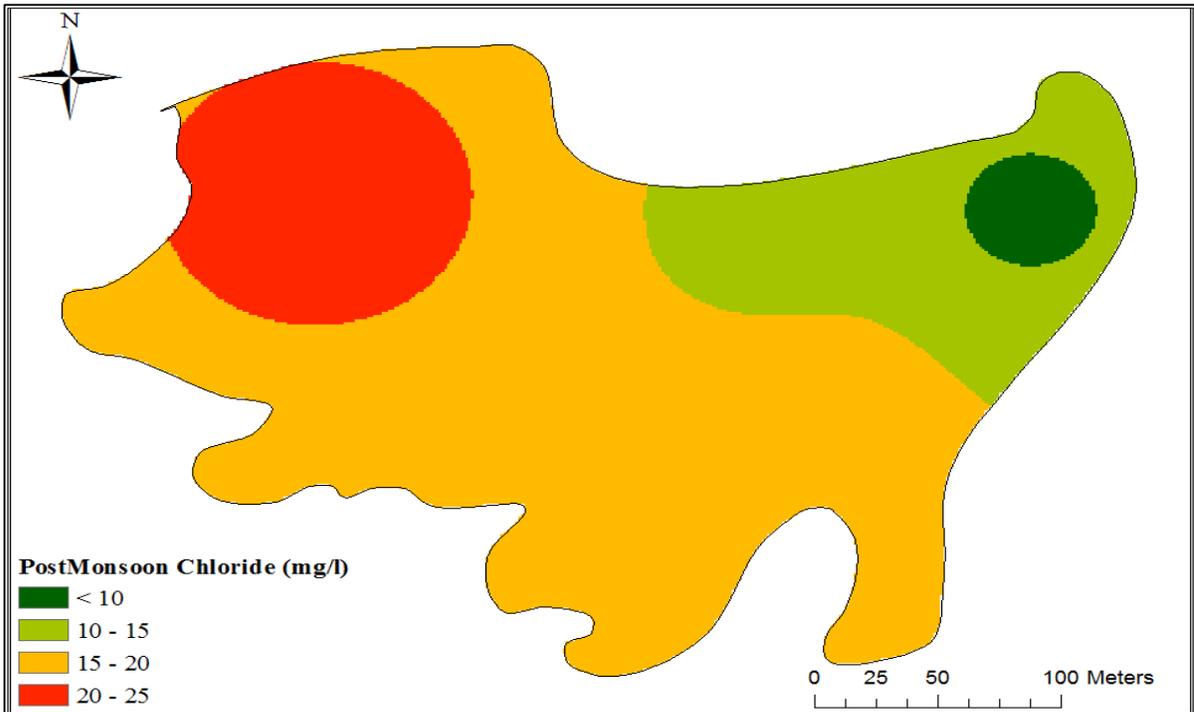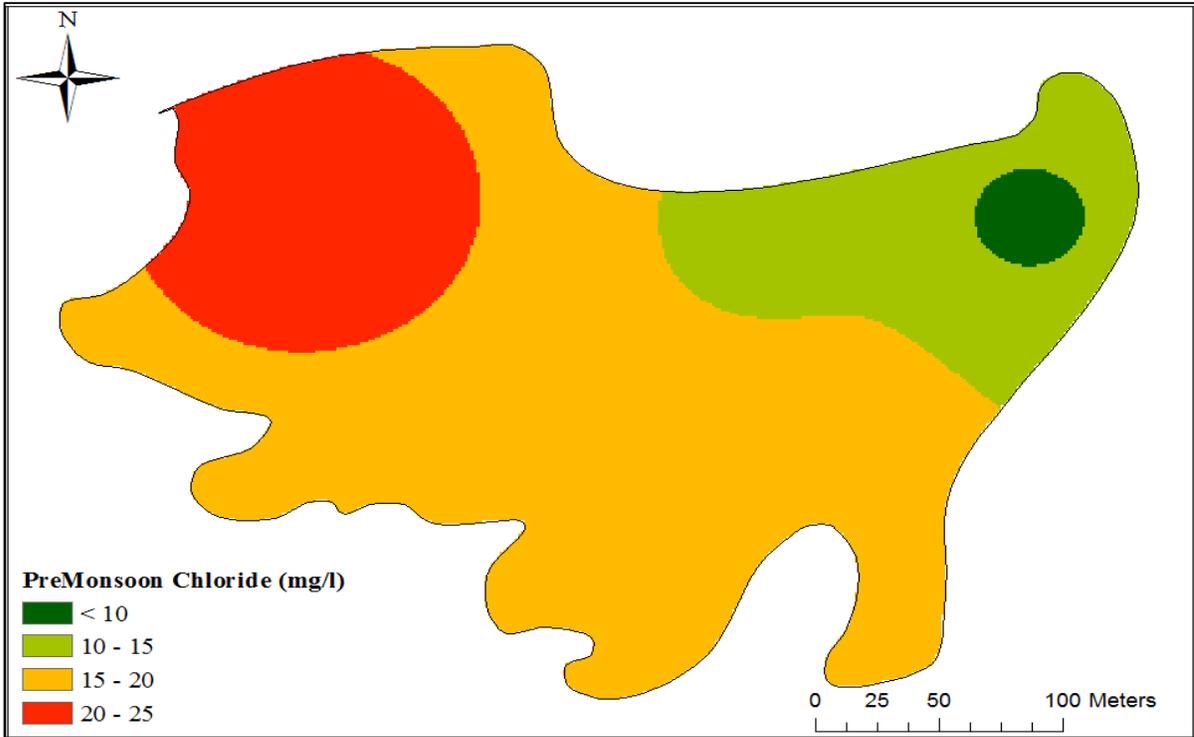
Figure A 12 Pre- and Post-Monsoon Chloride Concentrations at Bele
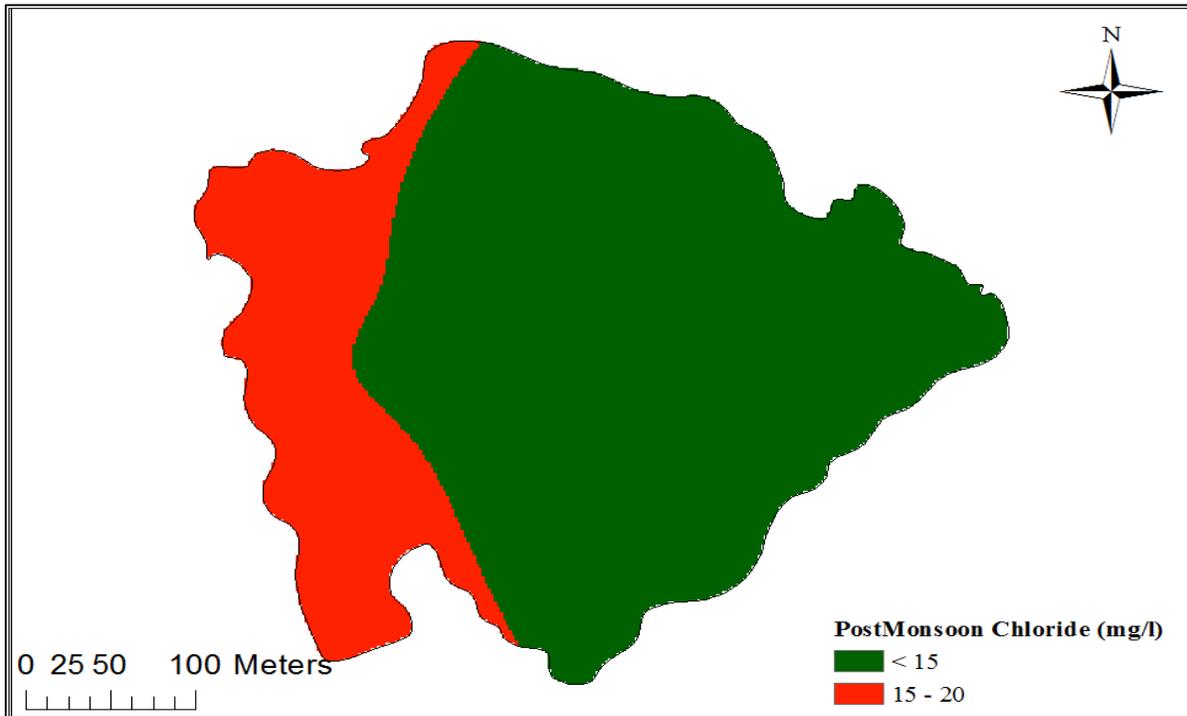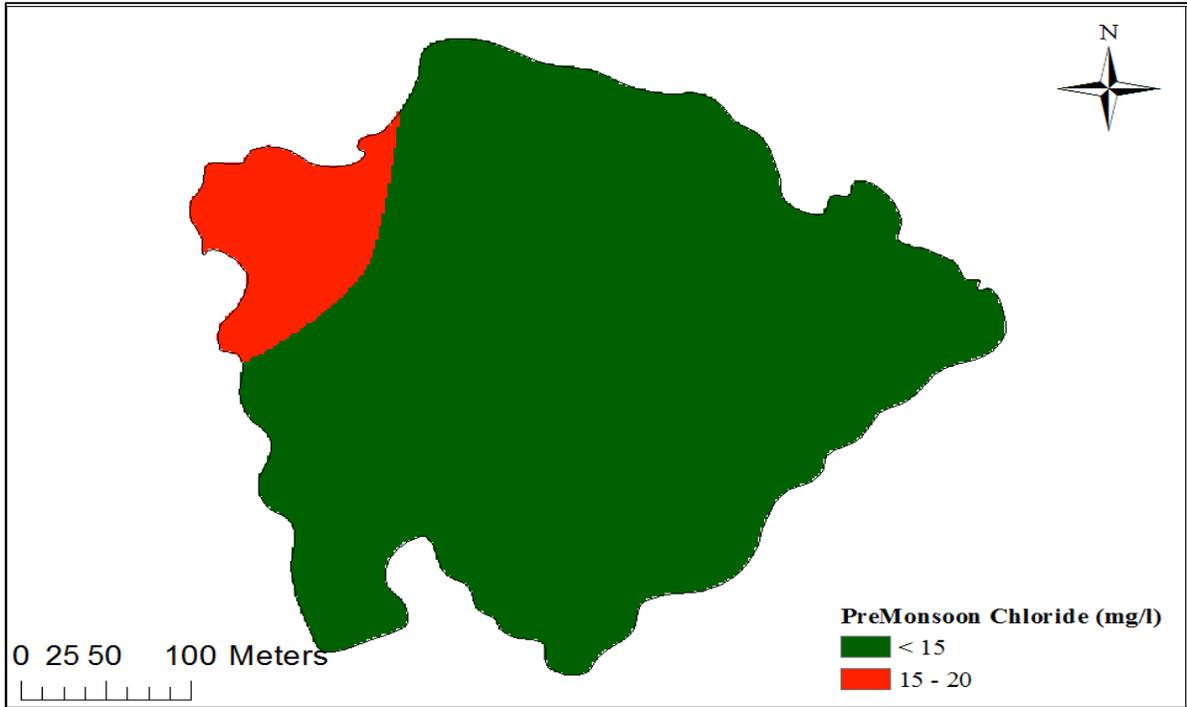
Figure A 13 Pre- and Post-Monsoon Chloride Concentrations at Radhanagar
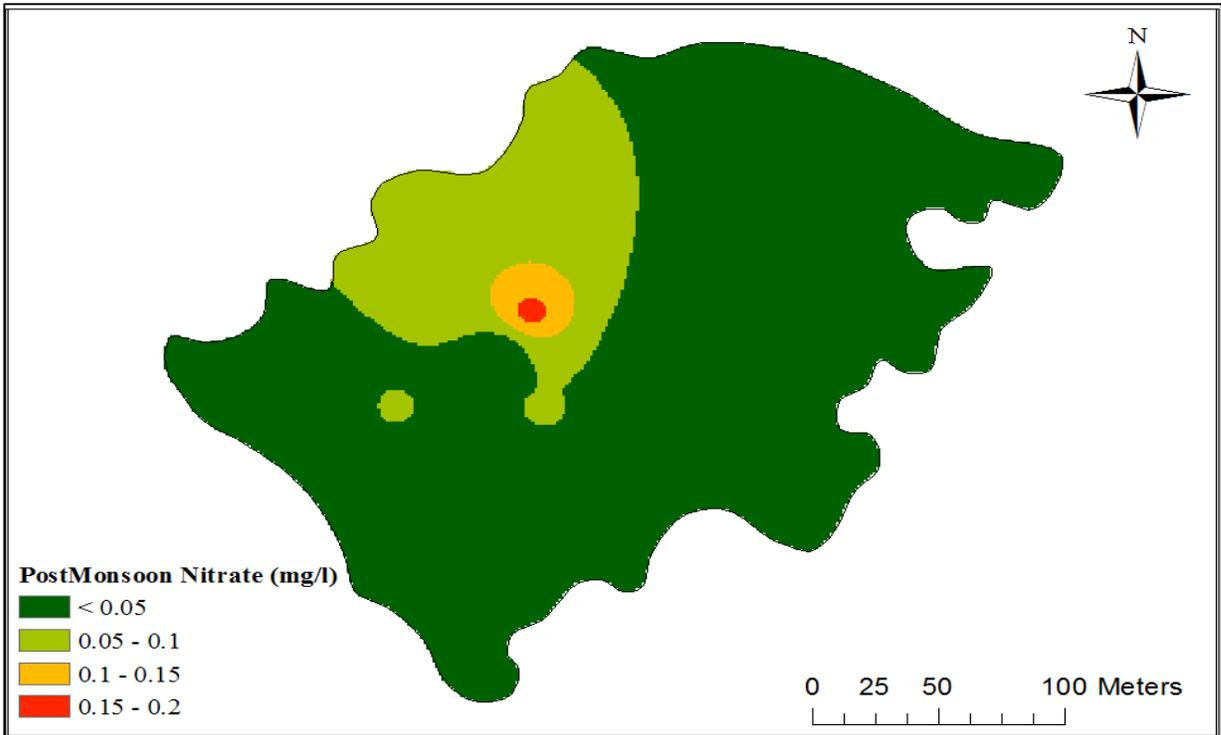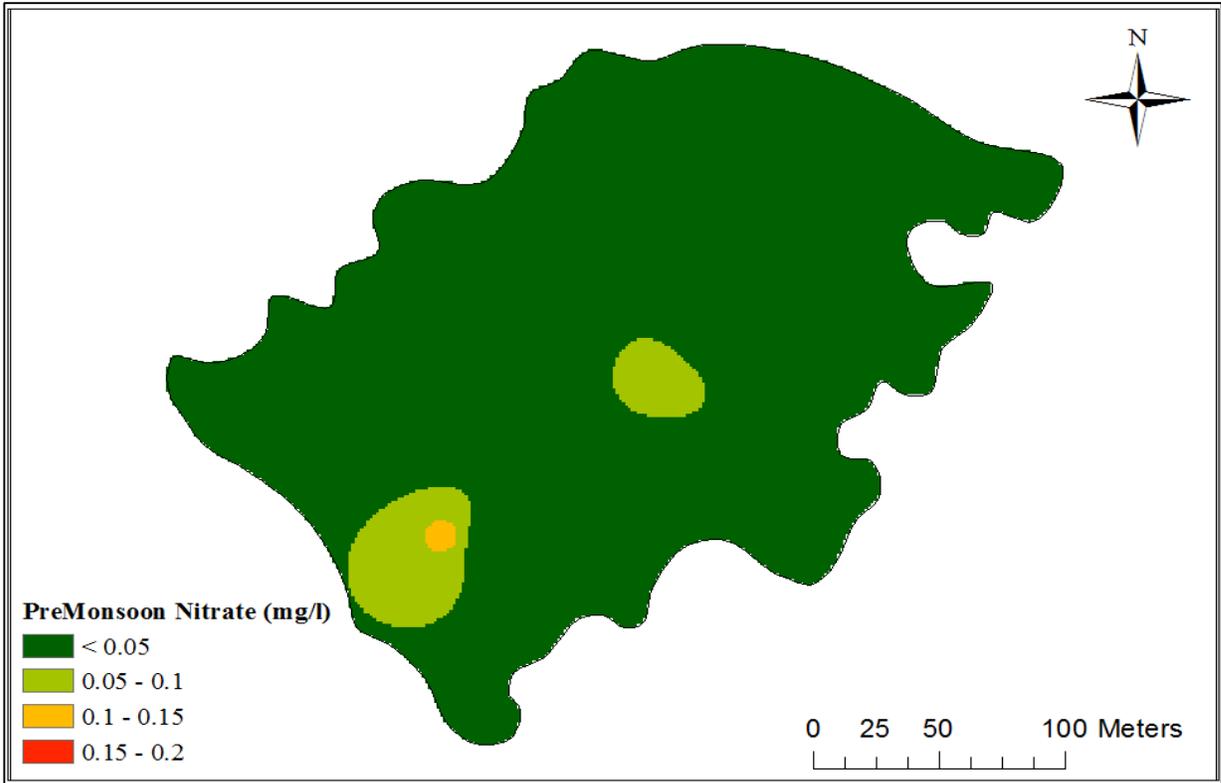
Figure A 14 Pre- and Post-Monsoon Nitrate Concentrations at Chakudanga
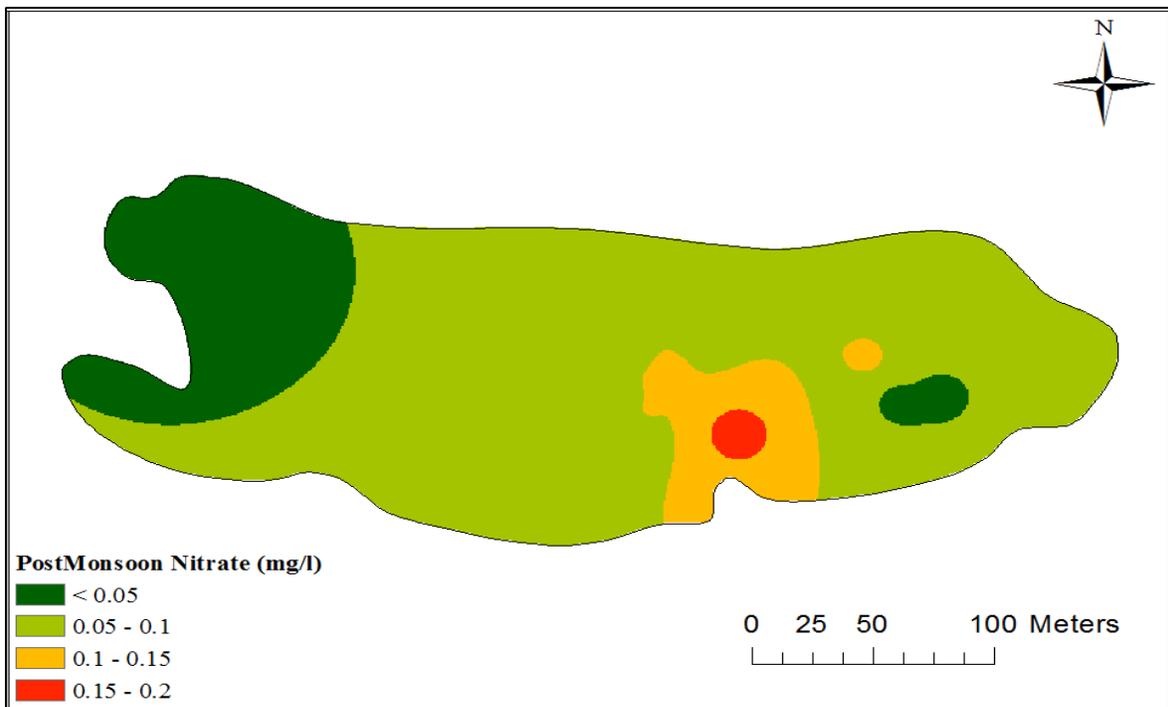
Figure A 15 Pre- and Post-Monsoon Nitrate Concentrations at Shahispur
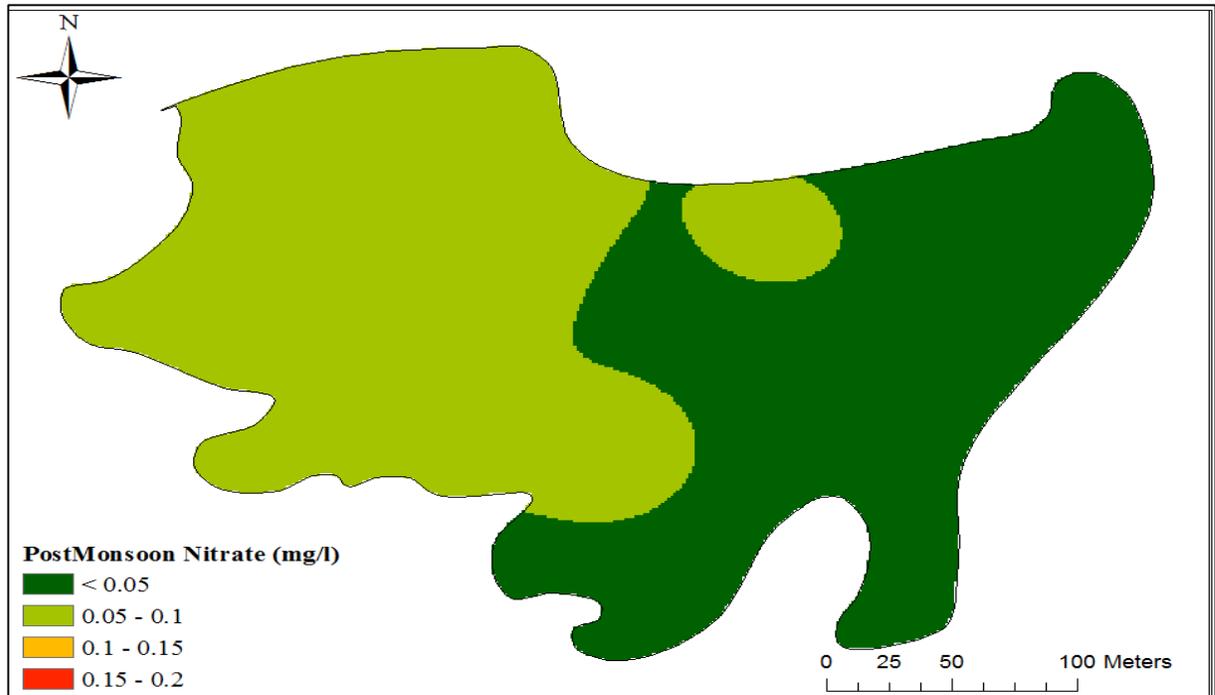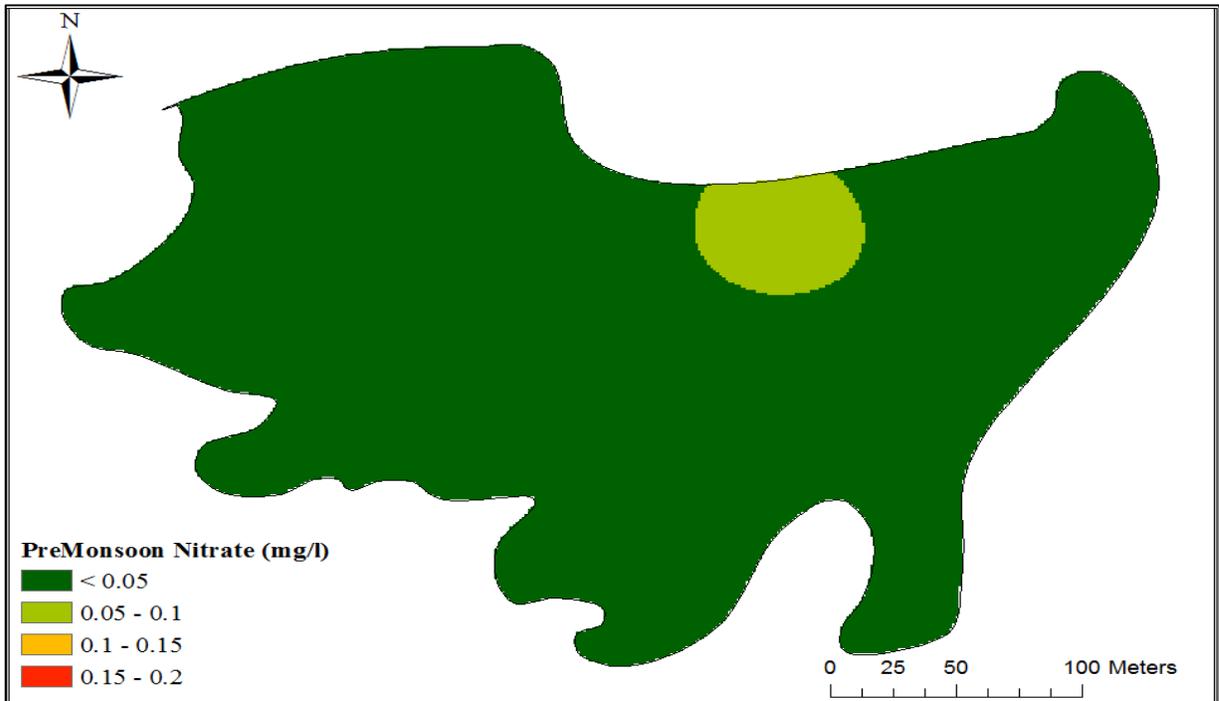
Figure A 16 Pre- and Post-Monsoon Nitrate Concentrations at Bele
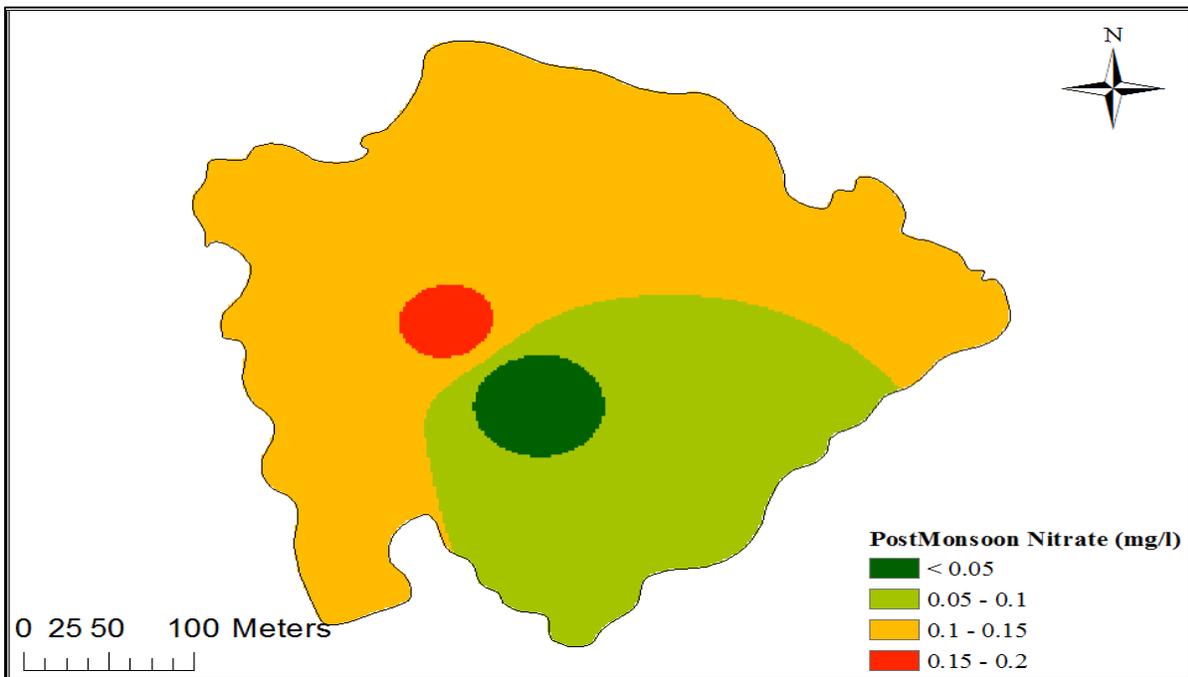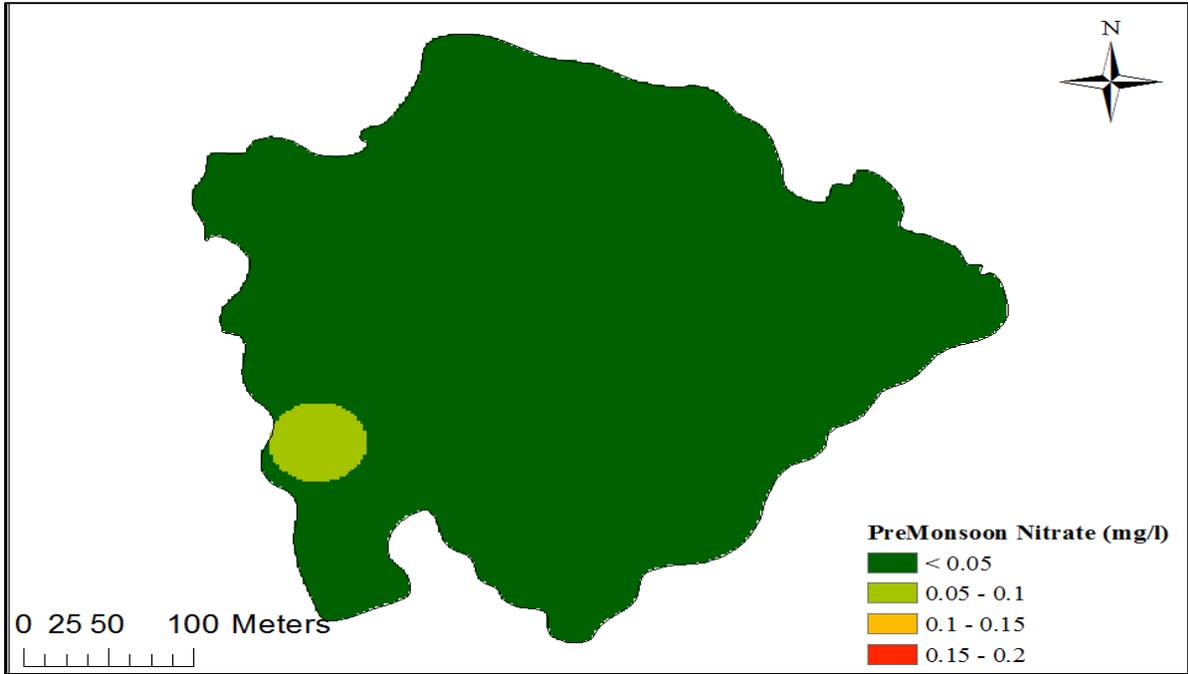
Figure A 17 Pre- and Post-Monsoon Nitrate Concentrations at Radhanagar
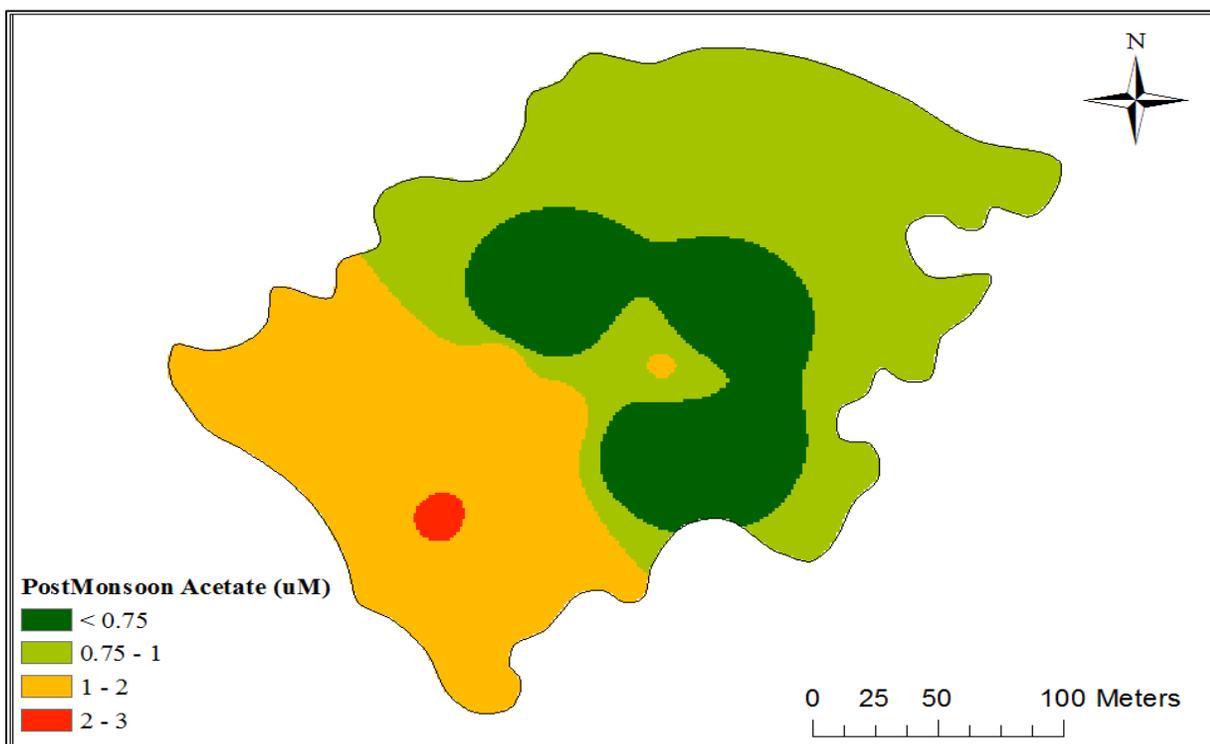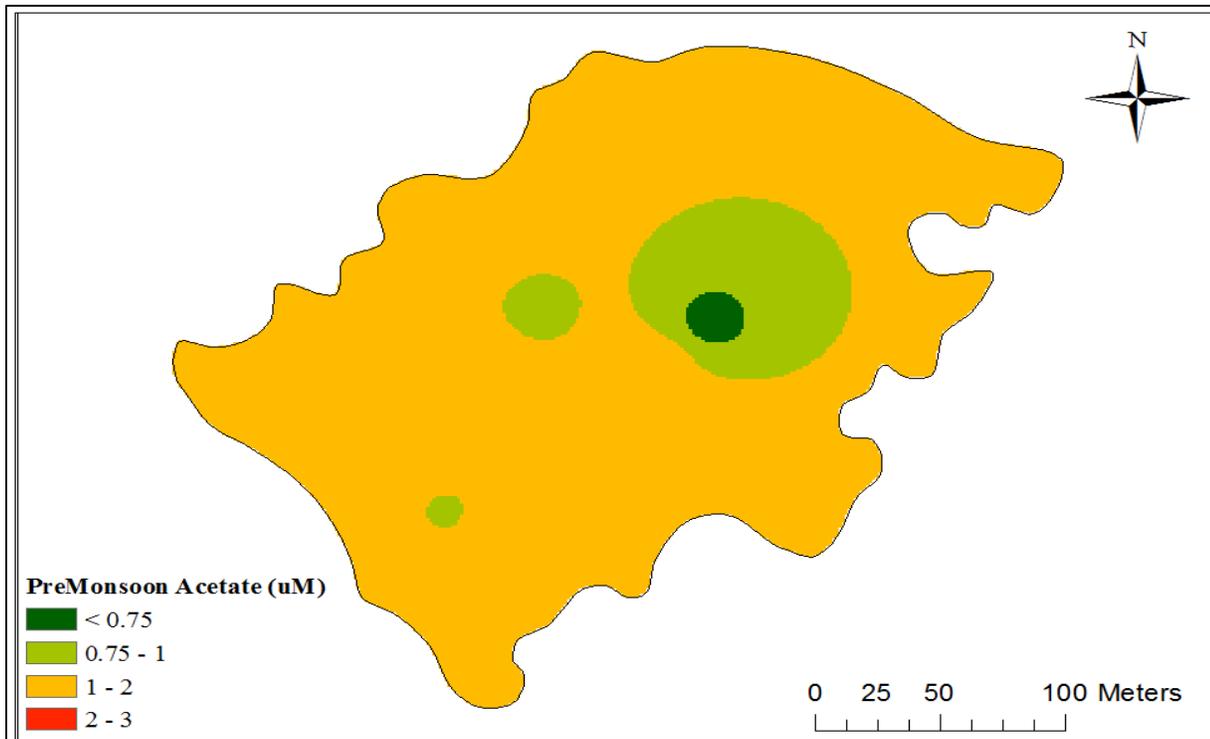
Figure A 18 Pre- and Post-Monsoon Acetate Concentrations at Chakudanga
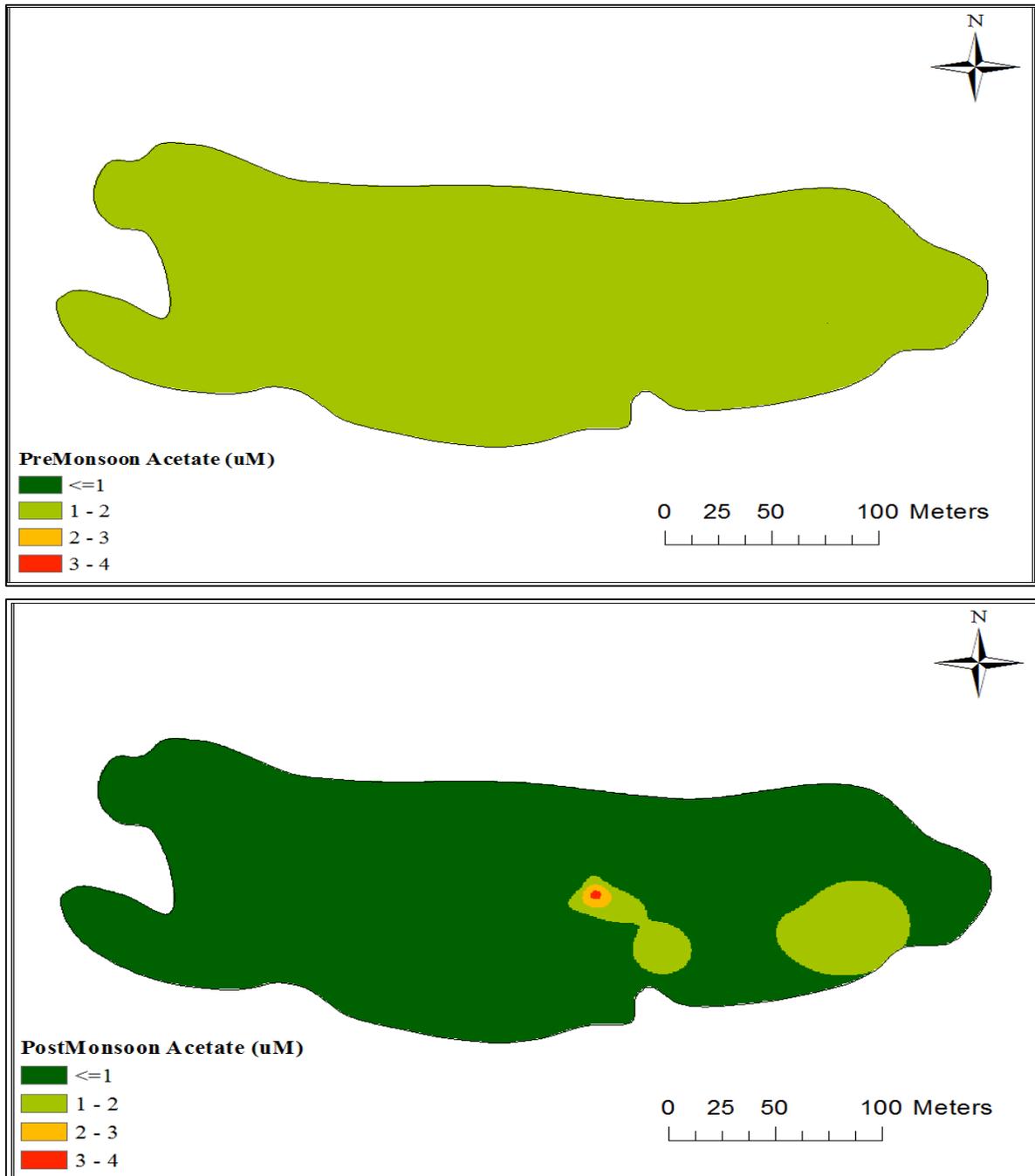
Figure A 19 Pre- and Post-Monsoon Acetate Concentrations at Shahispur
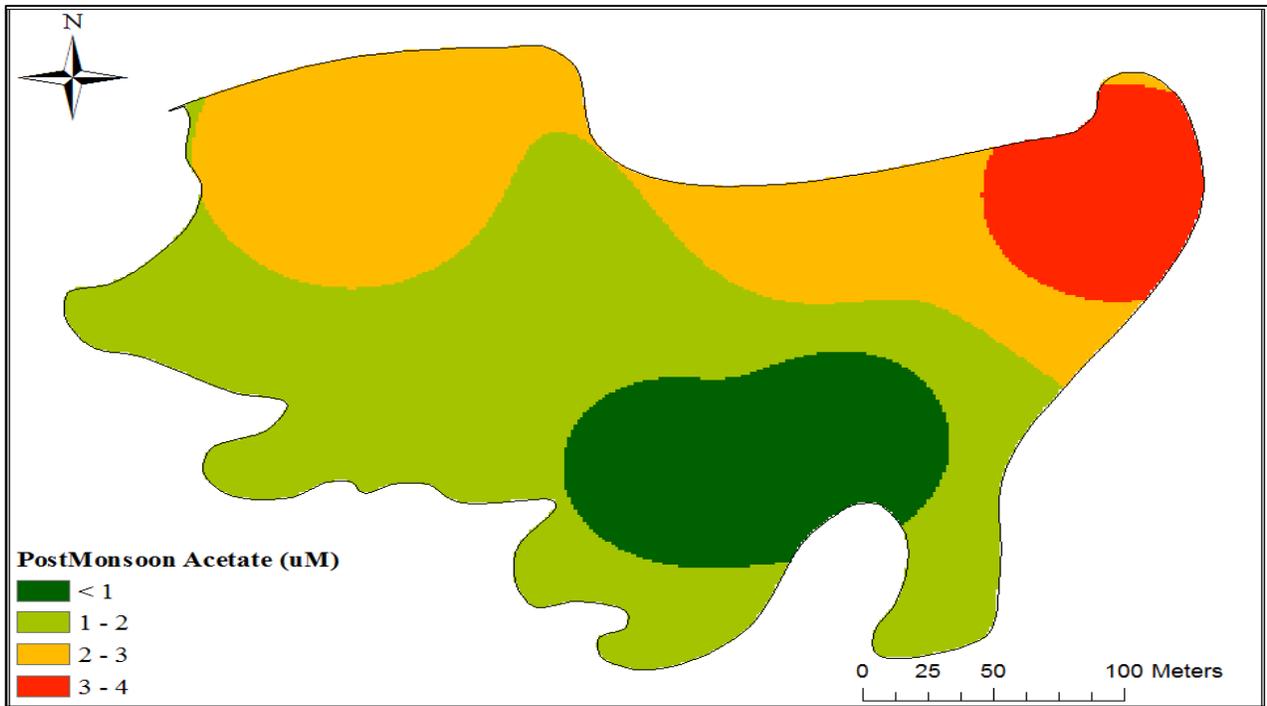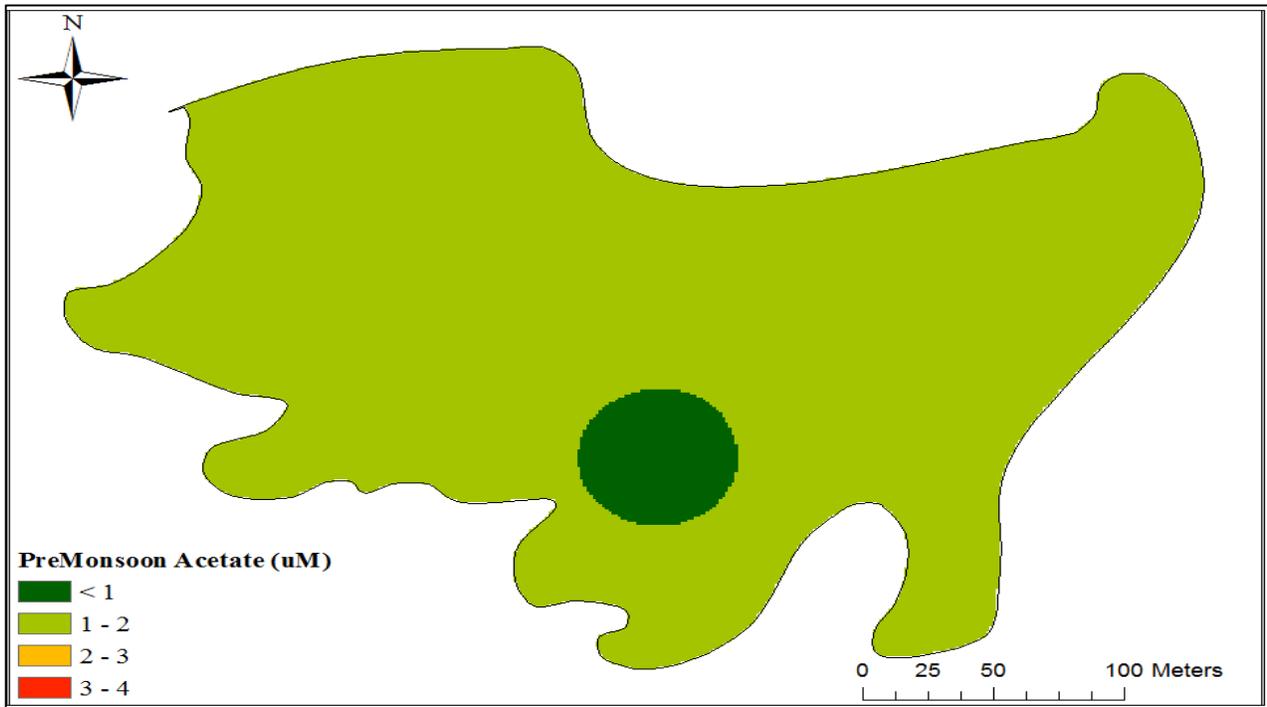
Figure A 20 Pre- and Post-Monsoon Acetate Concentrations at Bele
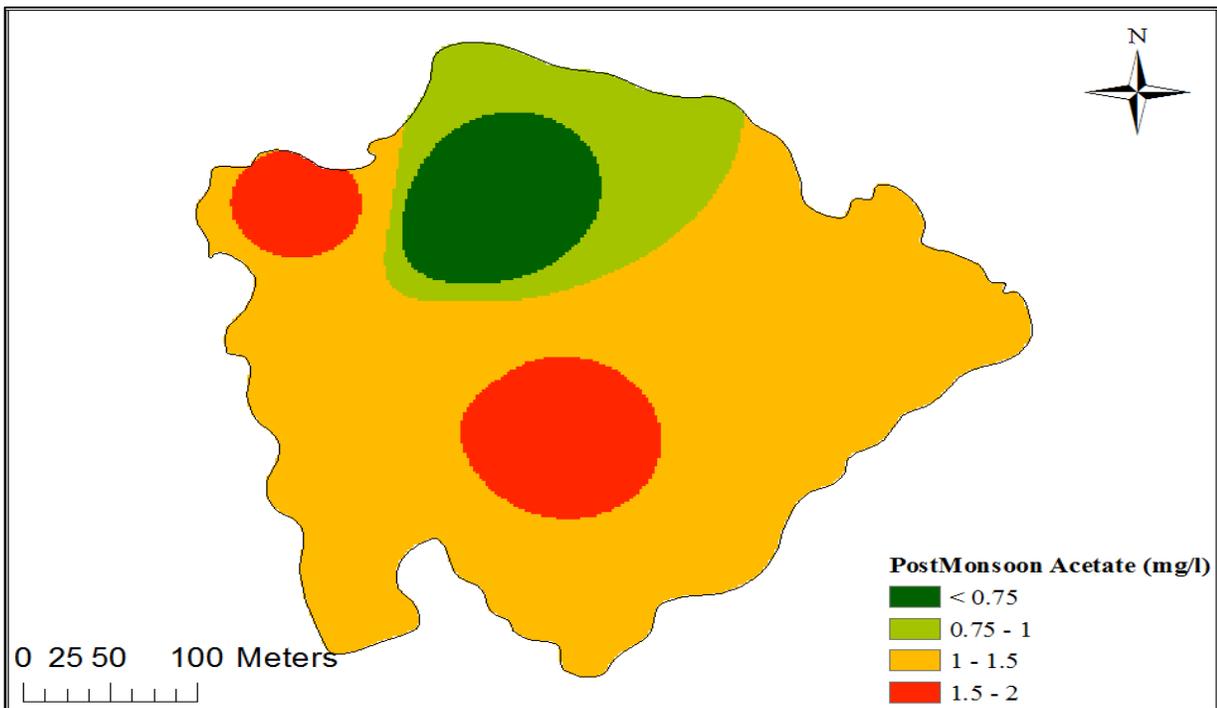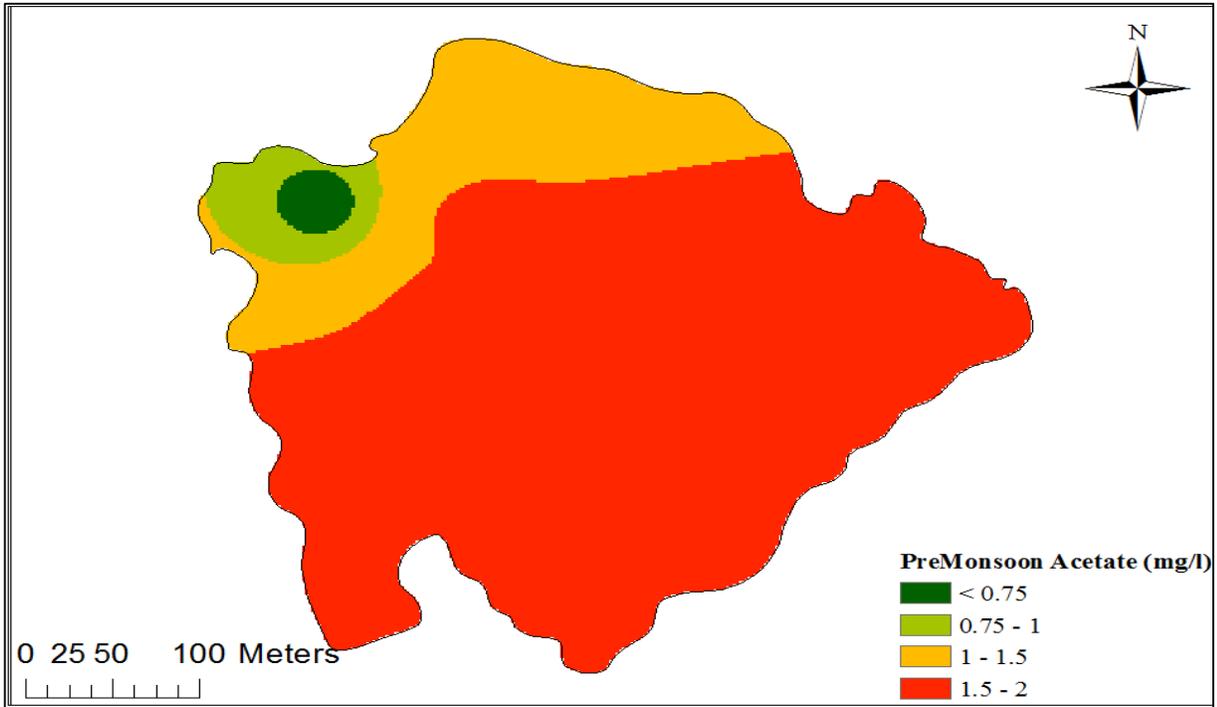
Figure A 21 Pre- and Post-Monsoon Acetate Concentrations at Radhanagar
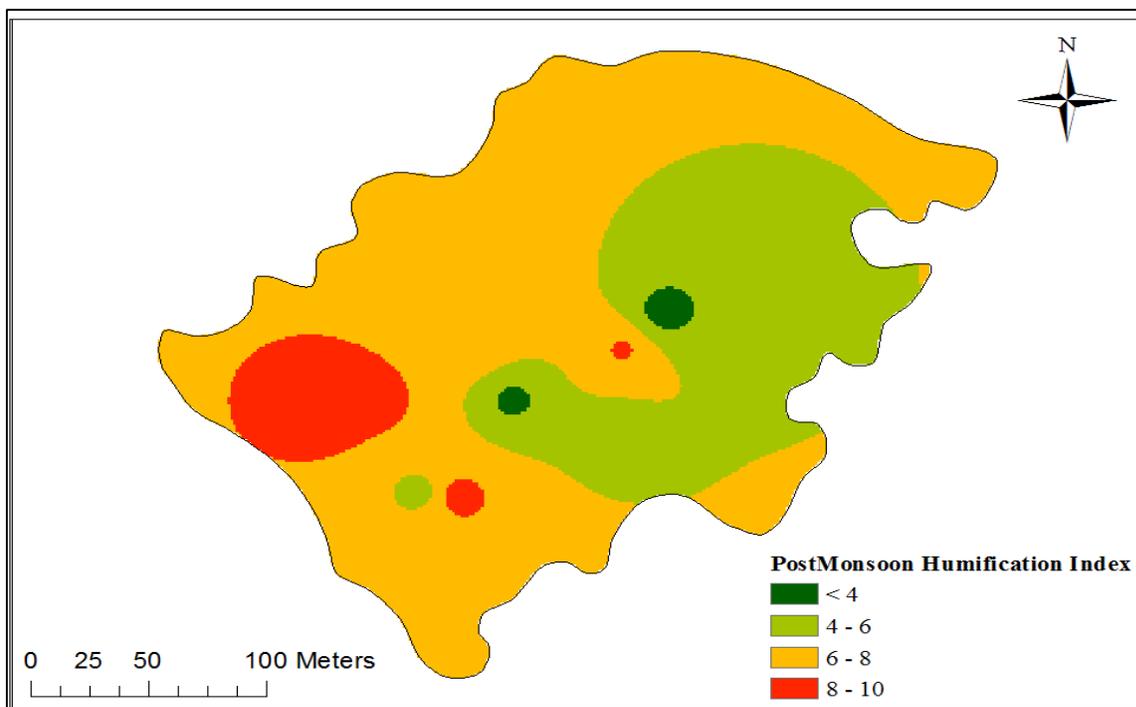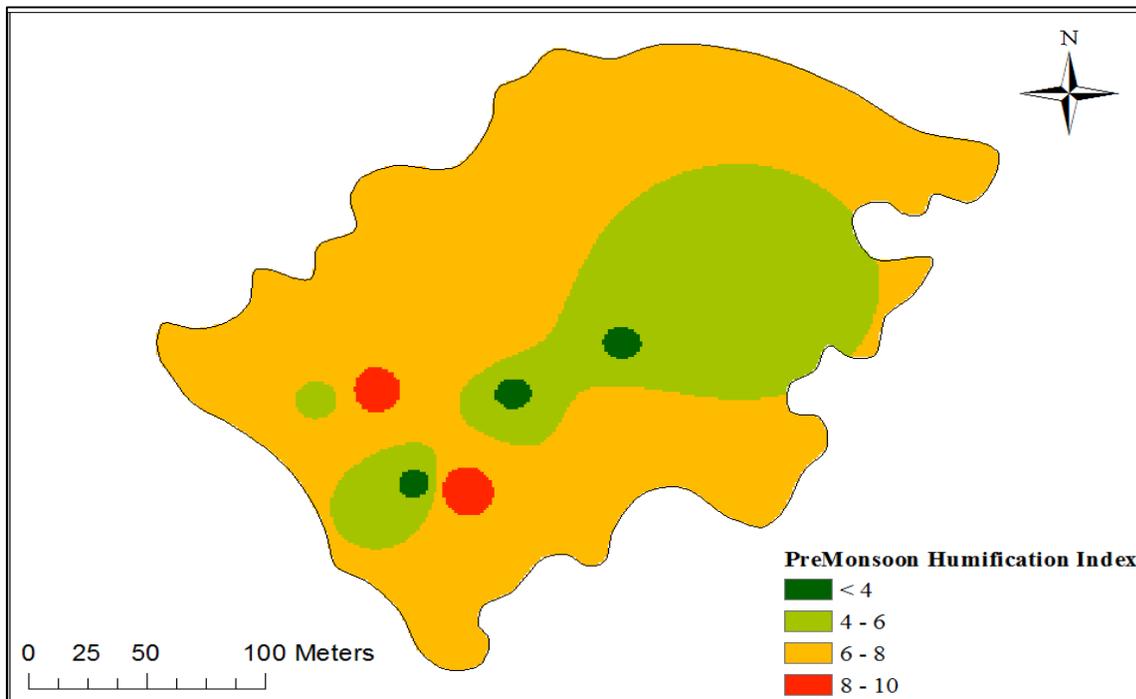
Figure A 22 Pre- and Post-Monsoon Humification Index (HIX) at Chakudanga
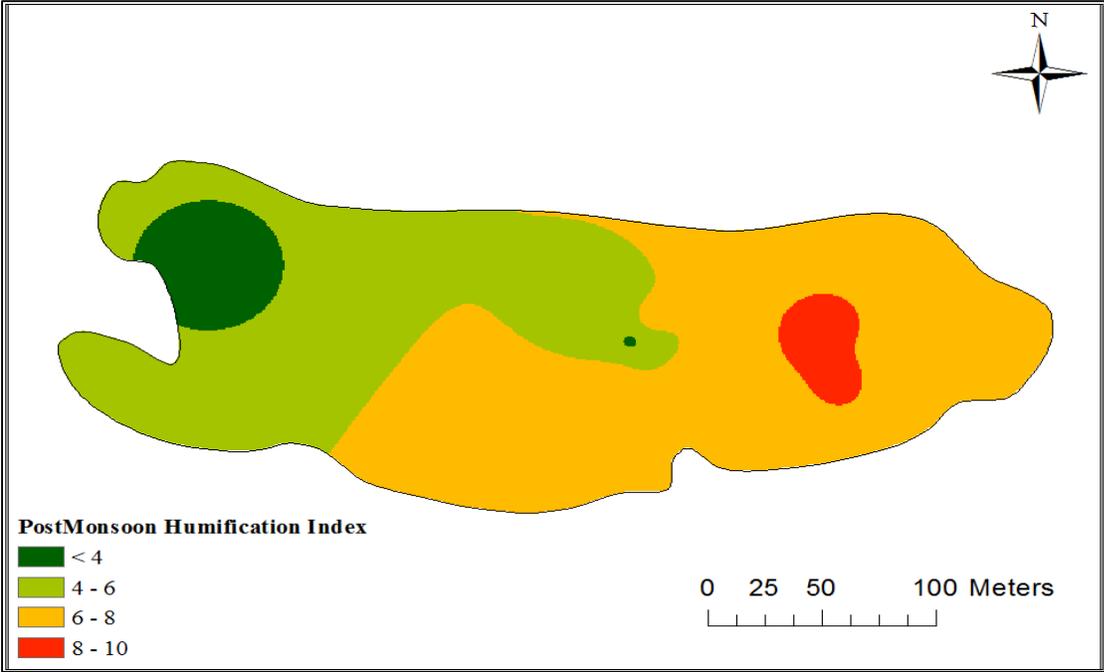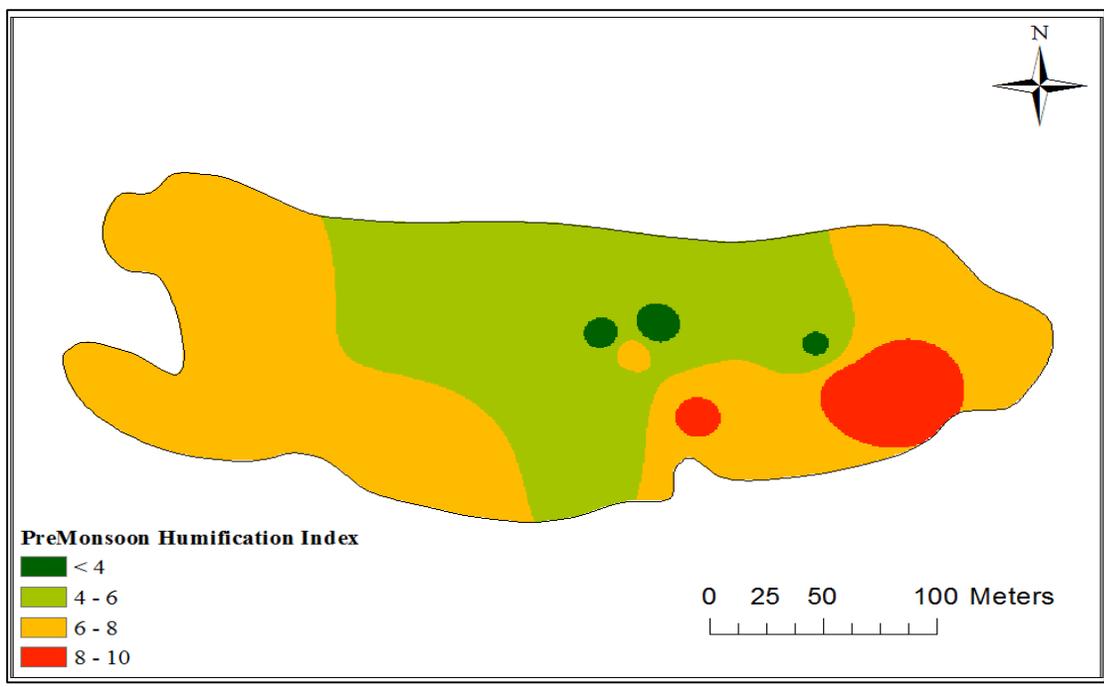
Figure A 23 Pre- and Post-Monsoon Humification Index (HIX) at Shahispur
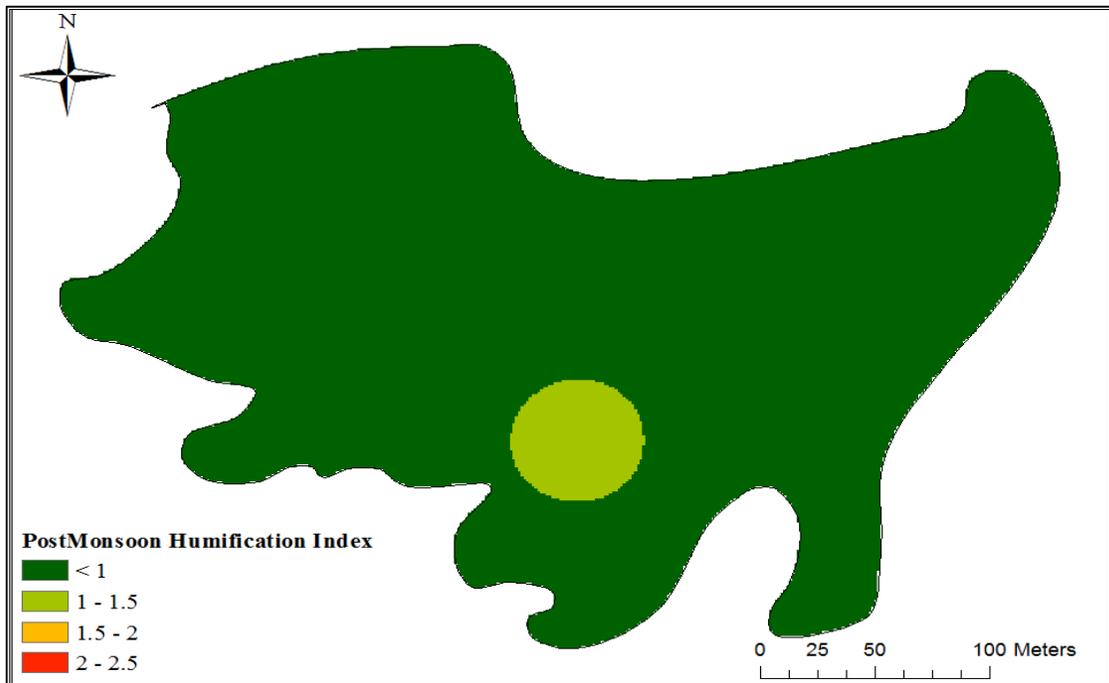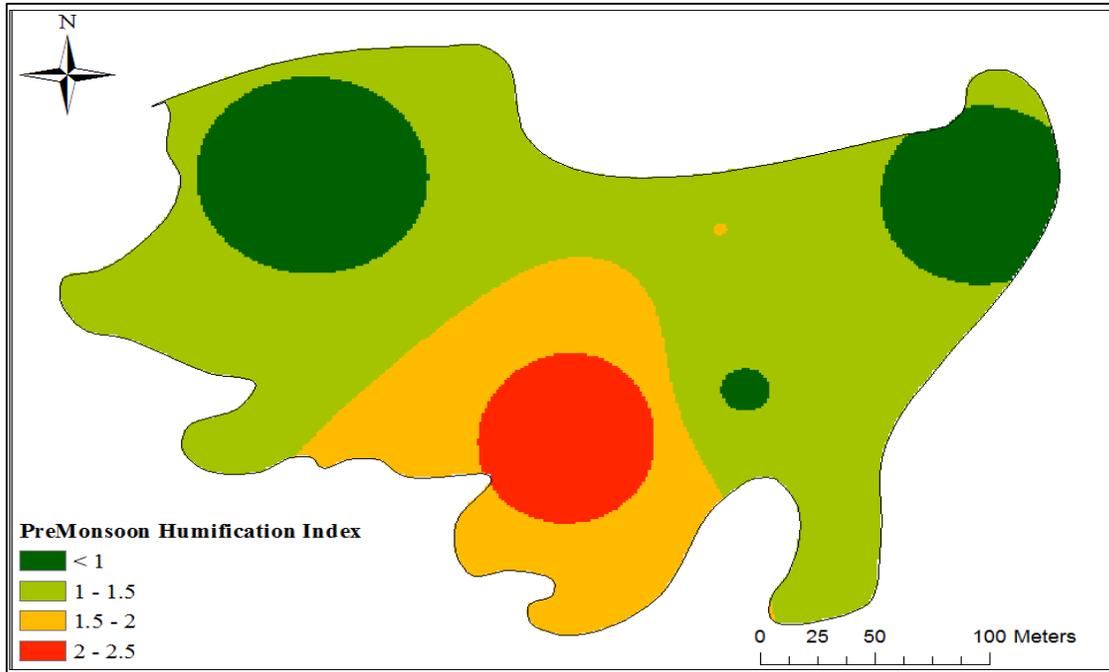
Figure A 24 Pre- and Post-Monsoon Humification Index (HIX) at Bele
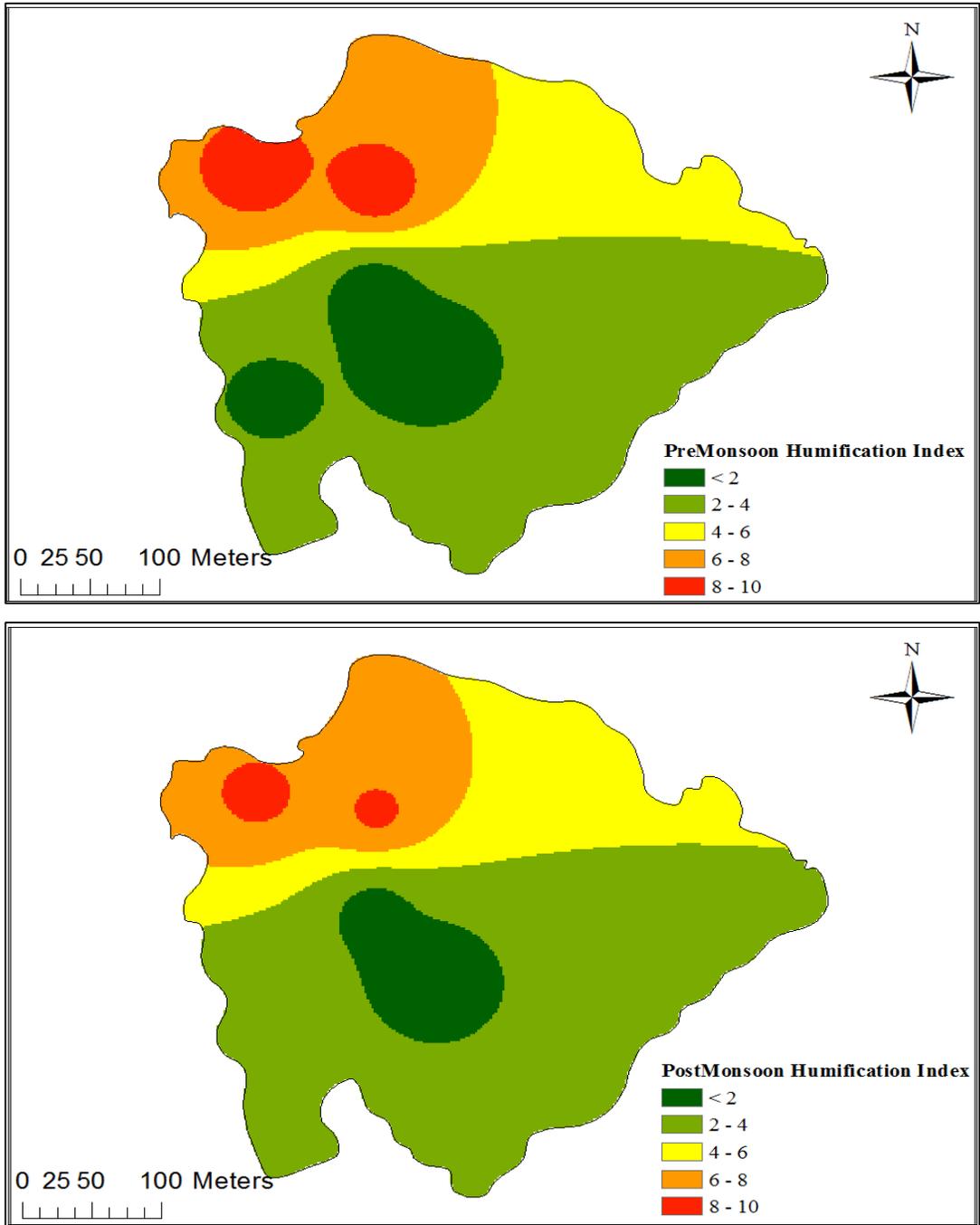
Figure A 25 Pre- and Post-Monsoon Humification Index (HIX) at Radhanagar
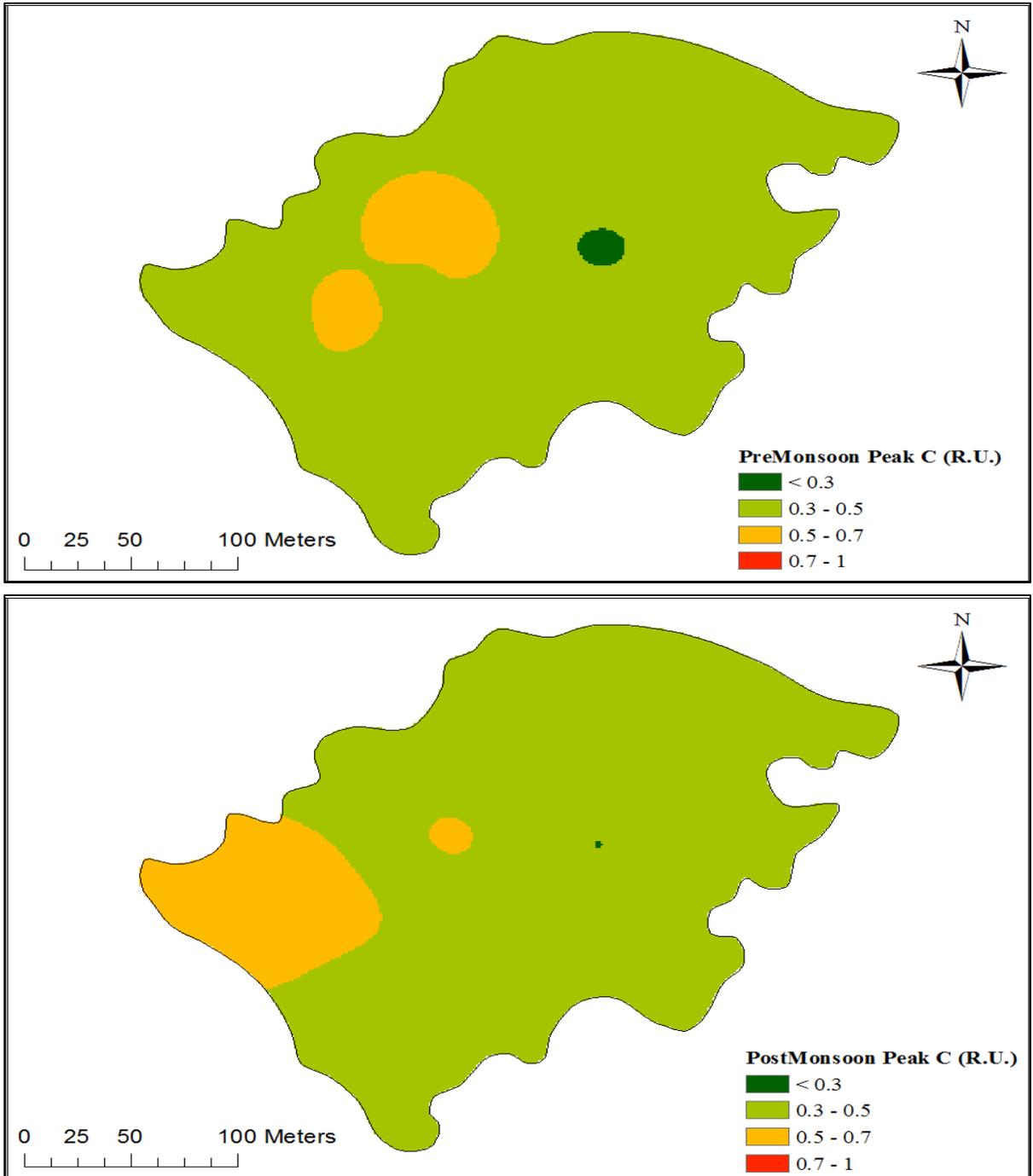
Figure A 26 Pre- and Post-Monsoon Peak C Intensity at Chakudanga
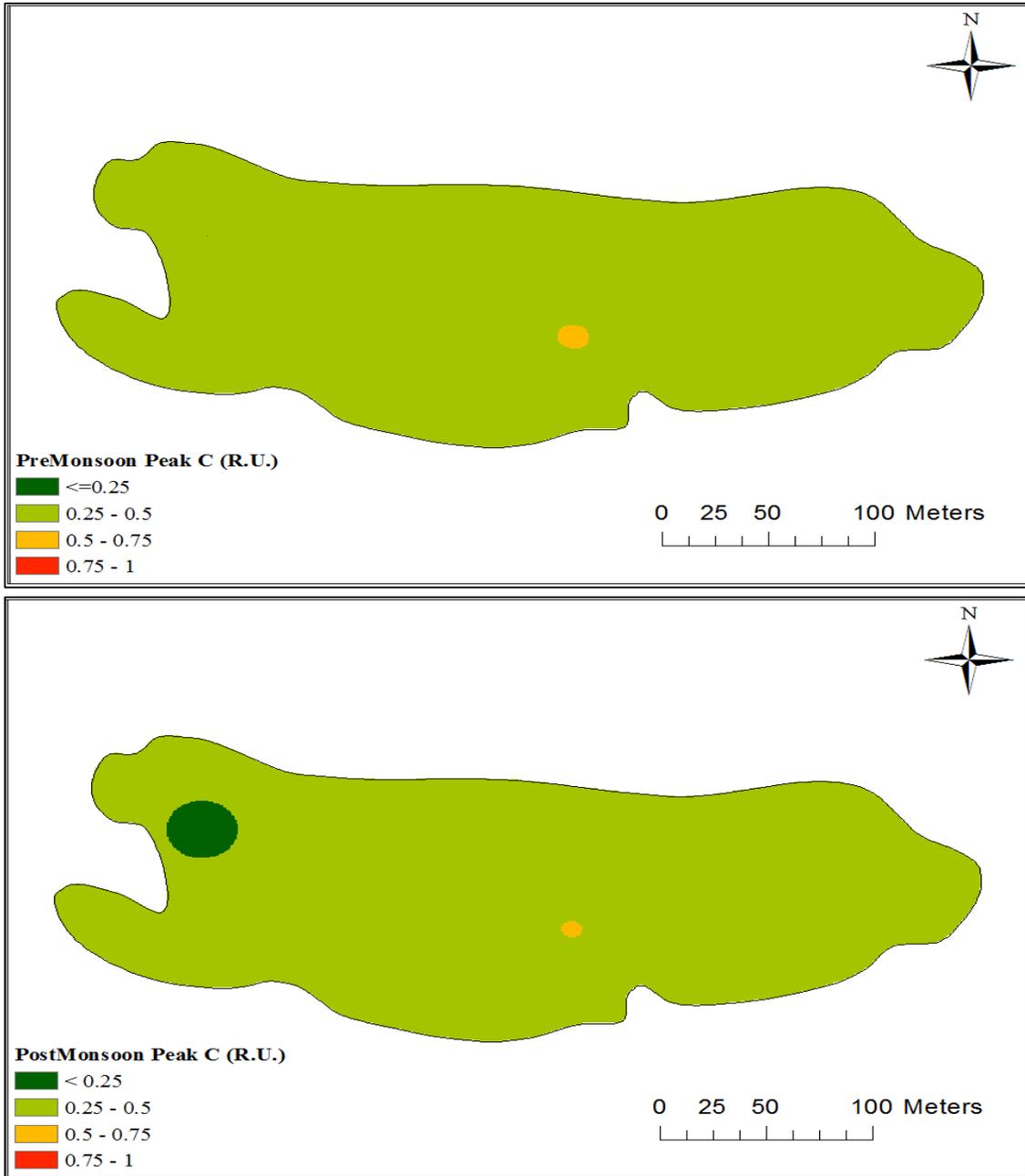
Figure A 27 Pre- and Post-Monsoon Peak C Intensity at Shahispur
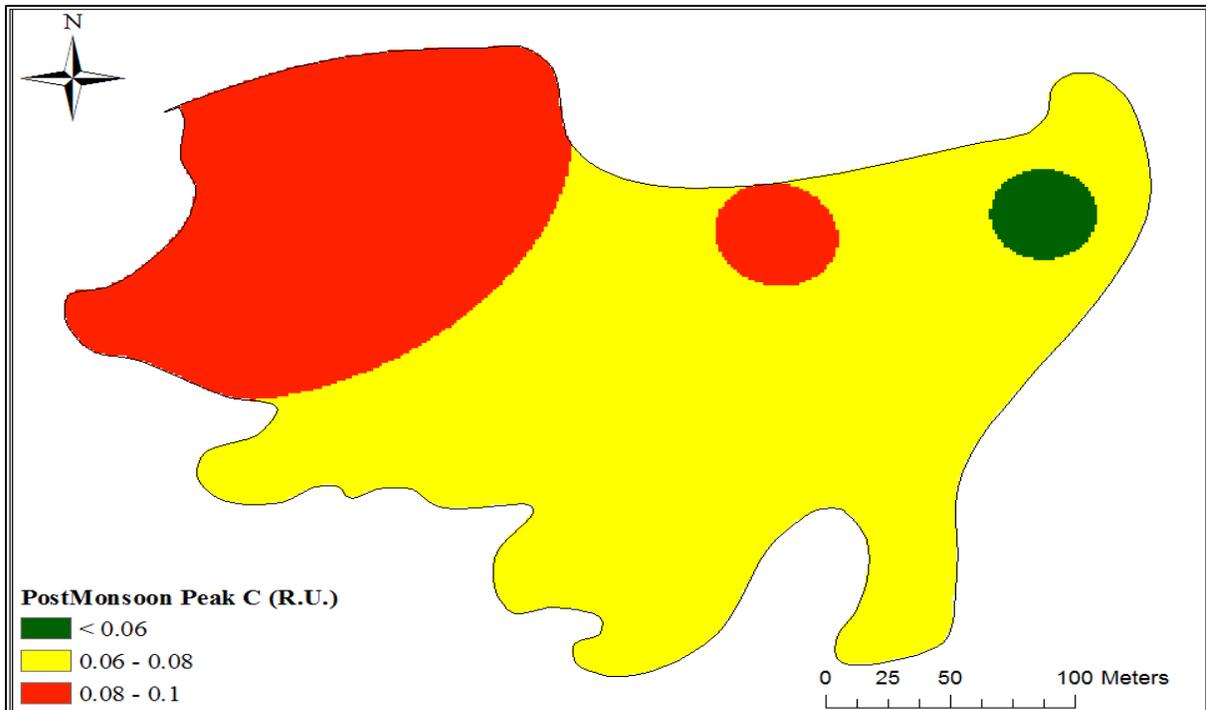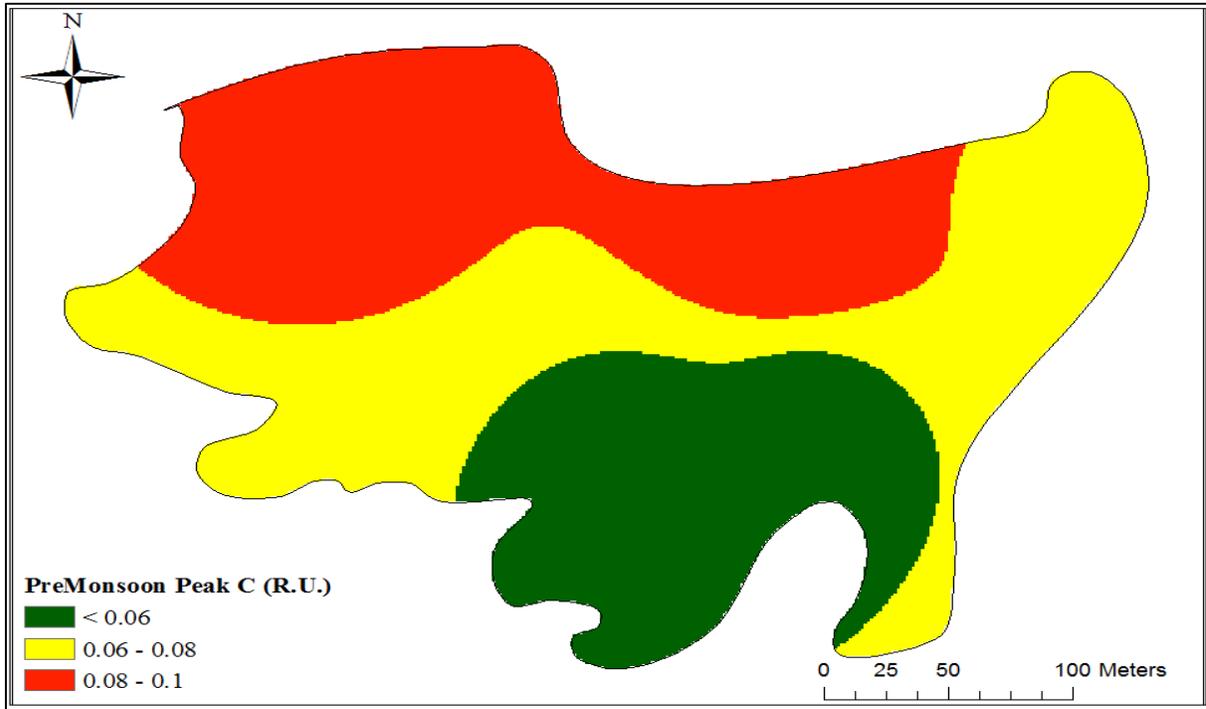
Figure A 28 Pre- and Post-Monsoon Peak C Intensity at Bele
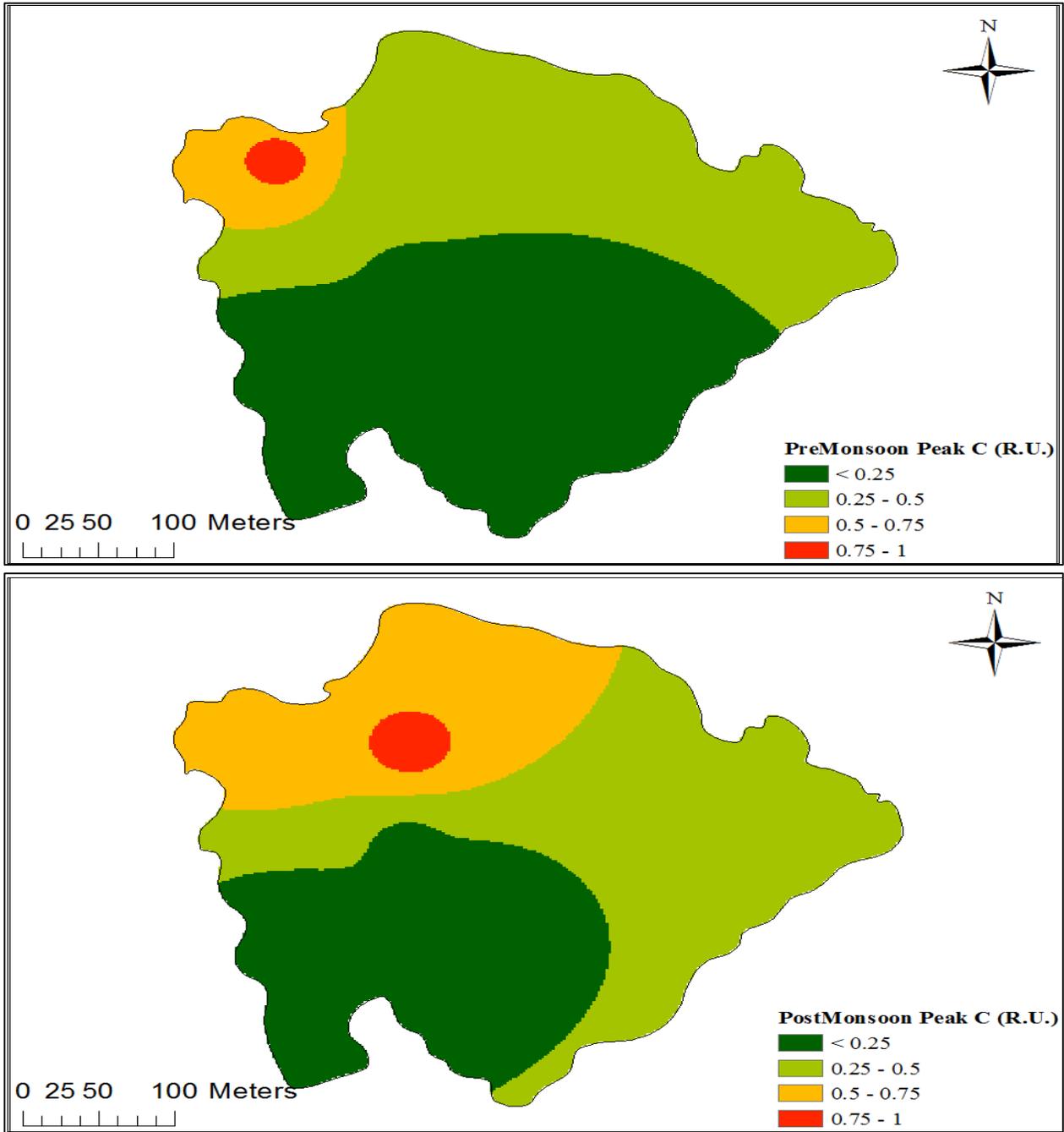
Figure A 29 Pre- and Post-Monsoon Peak C Intensity at Radhanagar
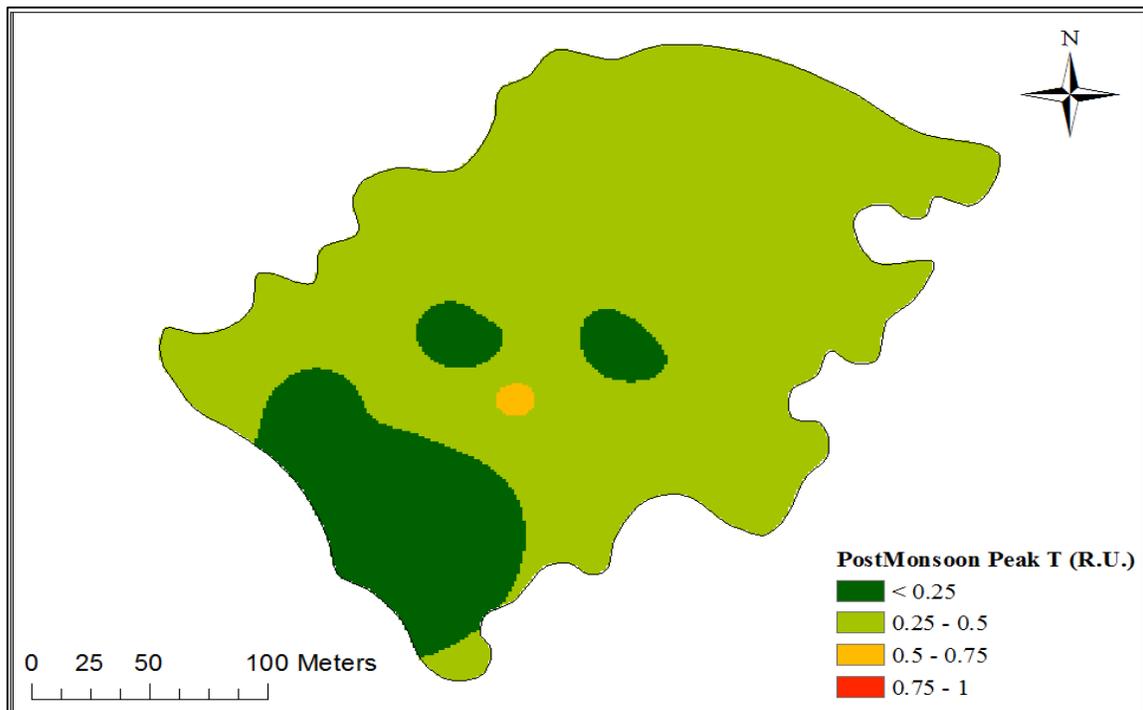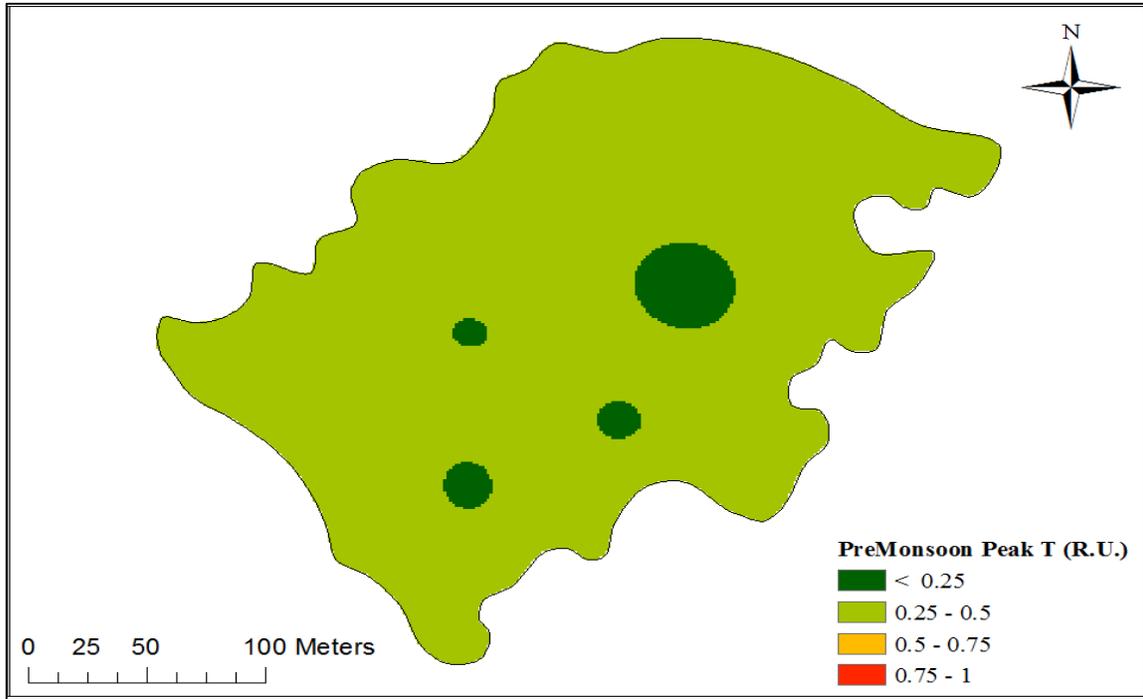
Figure A 30 Pre- and Post-Monsoon Peak T Intensity at Chakudanga
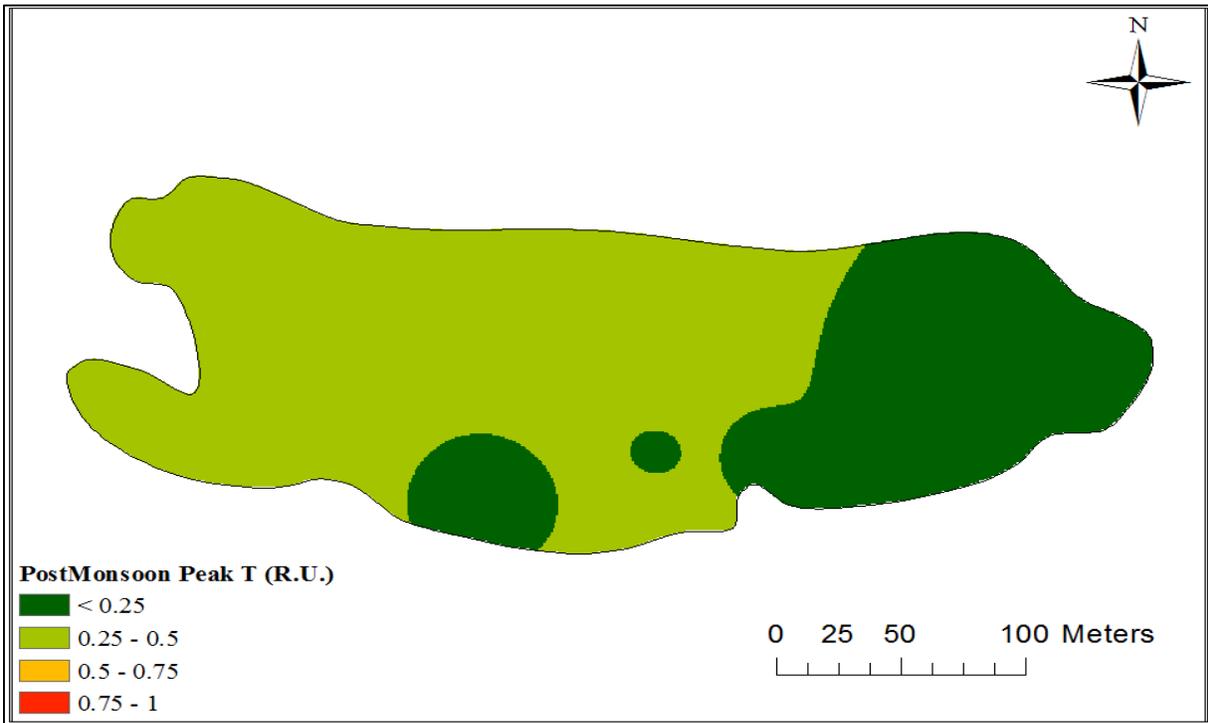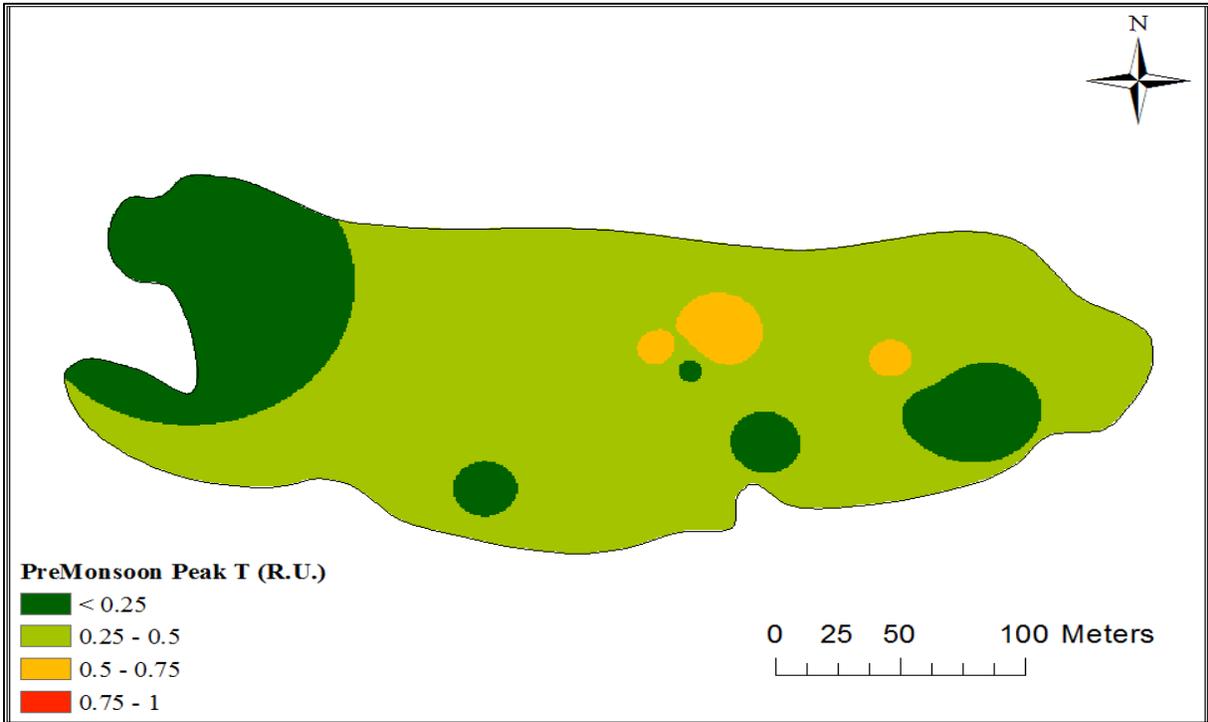
Figure A 31 Pre- and Post-Monsoon Peak T Intensity at Shahispur
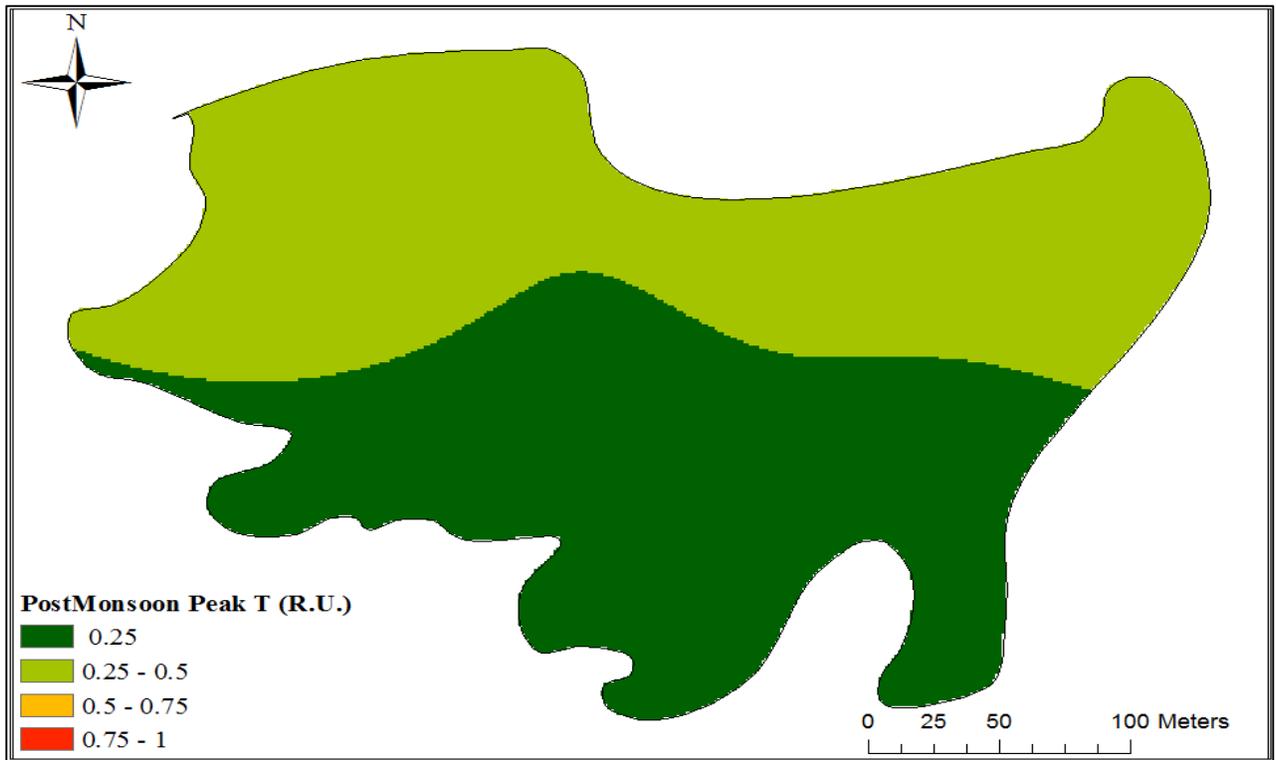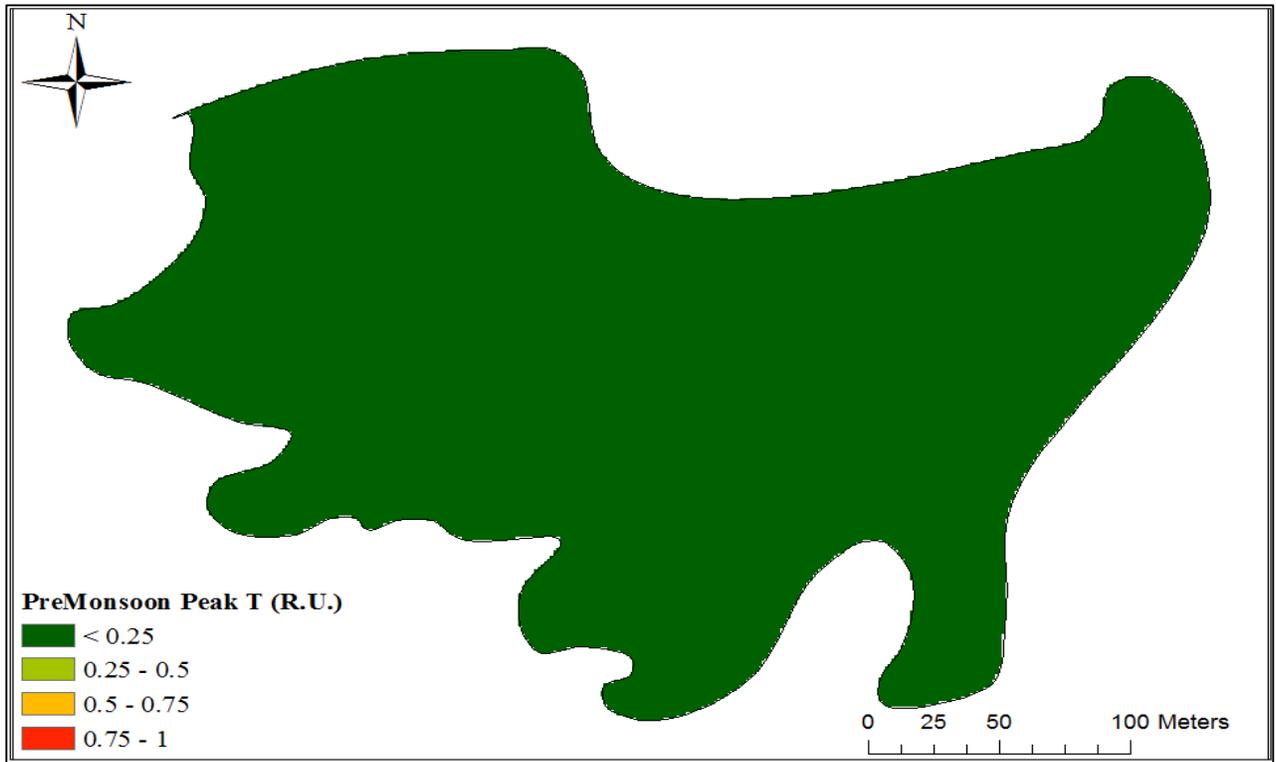
Figure A 32 Pre- and Post-Monsoon Peak T Intensity at Bele
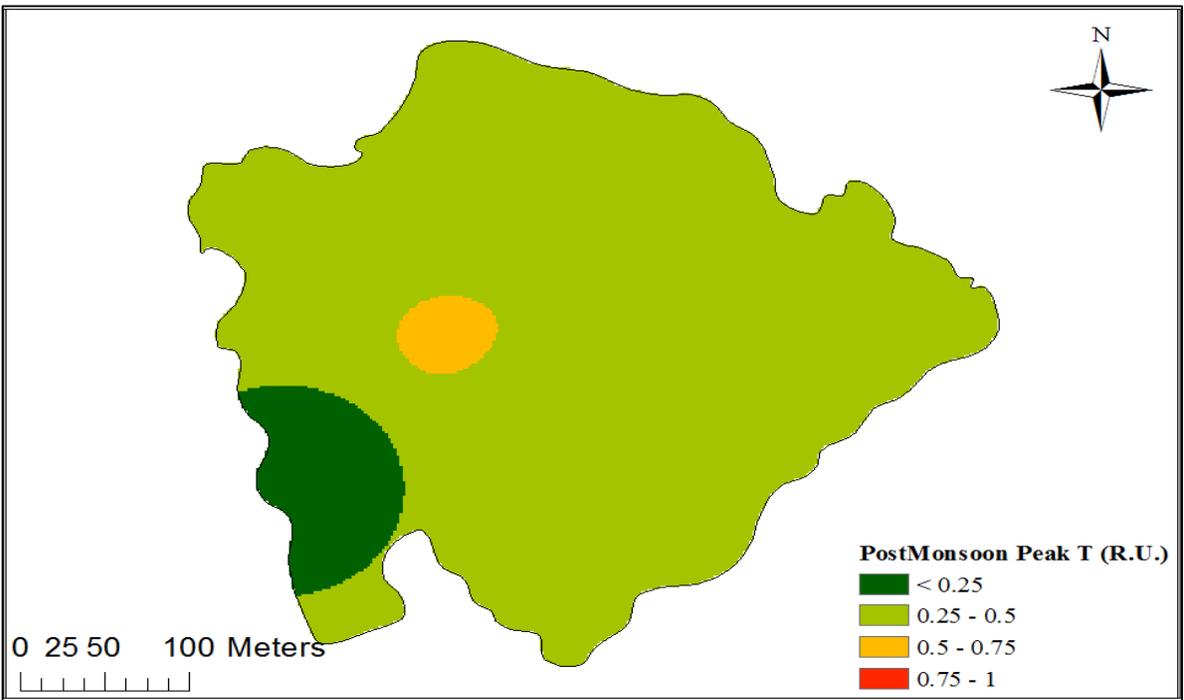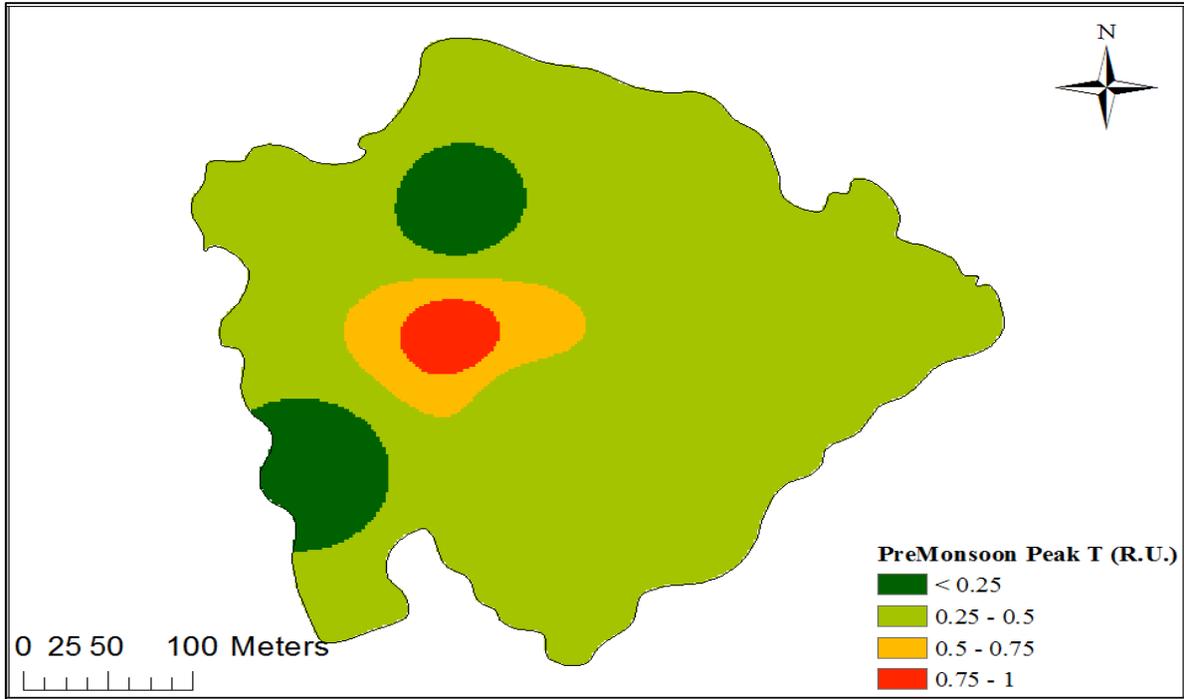
Figure A 33 Pre- and Post-Monsoon Peak T Intensity at Radhanagar

Appendix I - MATLAB code for correcting raw 3D-EEM data from Horiba Aqualog, computing fluorescence indices and preparing PARAFAC compatible files.

ProcessData.m

```
%Harshad Kulkarni / August 2016/
%This function is a main function that contains values for different
%variables, calls other functions to perform designated tasks.
function ProcessData(InputFolder)
%%%%%%%%%%%%%% Make Changes here if necessary %%%%%%%%%%%%%%%%
eminc = 2; %increment of emission wavelengths (nm)
exinc = 5; %increment of excitation wavelengths (nm)
em = 300:eminc:596; % emission wavelengths range
ex = 239:exinc:450; % excitation wavelengths range
%%%%%%%%%%%%%%Do not change anything here onwards%%%%%%%%%%%%%%%

RamanEnd = 450;
RamanBegin = 370;
RamanInc = 0.5;
%corrfact = 0.959242;
corrfact = 1;
emlen = length(em);
exlen = length(ex);
dfq = input('Is dilution Factor same for all samples? Enter \n 1 for YES \n 0 for NO \n =');
if (dfq == 1)
    df_same = input('Enter Dilution Factor = ');
    df_default = df_same;
else
    df_default = 1;
end
intq1 = input('For all samples,is Integration Time exactly SAME as Integration time used for raman? Enter \n 1 for
YES \n 0 for NO \n = ');
intq2 = input('Do all samples have exactly SAME integration time? Enter \n 1 for YES \n 0 for NO \n = ');
if(intq1 == 0)
    if(intq2 == 1)
        int_time_raman = input('Enter Integration Time used for Raman = ');
        intr = int_time_raman ;
        int_time_sample = input('Enter Integration Time used for Samples = ');
        ints = int_time_sample;
    else
        intr = 1;
        ints = 1;
    end
else
    intr = 1;
    ints = 1;
end
absq = input('Method for absorbance data extrapolation? Enter \n 0 for Linear \n 1 for Nonlinear (reccommended) \n
= ');
if (absq == 0)
    disp('You selected linear extrapolation');
elseif (absq == 1)
```

226

```matlab
        disp('You selected non-linear extrapolation');
end

disp('Sorting Raw Data Files');
%Calling function "SortData", sorting all .dat files into respective folders
SortData(InputFolder);
MainDirList = dir(InputFolder);
disp('Calculating Raman Area');
ramanfolderpath = '';
for a = 1:length(MainDirList)
    filename = MainDirList(a).name;
    if (strcmp(filename,'raman')==1)
        ramanfolderpath = [InputFolder filename '\'];
        % Calling function "raman", calculating Raman Area.
        raman(ramanfolderpath,corrfact,RamanEnd,RamanBegin,RamanInc);
        else
    end
end
close all;

disp('Processing Absorption Data');
absfolderpath =  [''];
for b = 1:length(MainDirList)
    filename = MainDirList(b).name;
    if(strcmp(filename,'Abs Spectra Graphs')==1)
        absfolderpath = [InputFolder filename '\'];
        % Calling function "ABS", processing absorption data, creating file to be used for inner filter correction.
        ABS(absfolderpath,eminc,exinc,em,ex,emlen,exlen,dfq,df_default,absq)
    else
    end
end

disp('Processing Blank Data');
blankfolderpath = [''];
for c = 1:length(MainDirList)

    filename = MainDirList(c).name;
    if(strcmp(filename,'Waterfall Plot Blank')==1)
        blankfolderpath = [InputFolder filename '\'];
        % Calling function "blank", processing blank data.
        blank(blankfolderpath,ramanfolderpath,absfolderpath,em,ex,ints,intr,intq1,intq2)
    else
    end
end

disp('Processing Sample Data');
samplefolderpath = [''];
for d = 1:length(MainDirList)
    filename = MainDirList(d).name;
    if(strcmp(filename,'Waterfall Plot Sample')==1)
        samplefolderpath = [InputFolder filename '\'];
        % Calling function "sample", processing sample data, corrections, saves final EEMs.

sample(InputFolder,samplefolderpath,blankfolderpath,ramanfolderpath,absfolderpath,ex,em,exinc,eminc,exlen,df_d
efault,dfq,ints,intr,intq1,intq2)
```

227

```
        else
        end

end
disp('Process Completed');
end
```

SortData.m

```
% Harshad Kulkarni / November 2015 / SDSU Mladenov Research Lab.
% This function sorts the .dat files according to the different types to be
% used later for calculations.
function val = SortData( FolderPath )
DirList = dir([FolderPath '*.dat']);
AllPatterns = {['raman'],['Abs Spectra Graphs'], ['Waterfall Plot Blank'],['Waterfall Plot
Sample'],['cuvette'],['Emission Spectrum Graph'],['Sample - Blank Waterfall Plot'],['Sample - Blank Contour
Plot'],['Processed Contour_ IFE_RM_NRM'],['Processed Graph_ IFE_RM_NRM'],['Processed Contour_
NRM'],['Processed Graph_ NRM'],['Processed Contour_ IFE'],['Processed Graph_ IFE']};
for i = 1:length(DirList)
    filename = DirList(i,1).name;
    Pat_Num = GetPattern( filename, AllPatterns );
    DestFolderPath = [FolderPath AllPatterns{1,Pat_Num}];
    %This creates a folder if it doesn't already exist.
    mkdir(DestFolderPath);
    warning('OFF');
    Inputfile = [FolderPath filename];
    movefile( Inputfile , DestFolderPath );
end
addpath(genpath(FolderPath));
end

function Pat_Num = GetPattern( filename , AllPatterns )

for PatternNum = 1: length( AllPatterns )
    value = strfind(filename,AllPatterns{1,PatternNum} );
    if( value ~= 0 )
        Pat_Num = PatternNum;
    end
end
end
```

raman.m

```
%Harshad Kulkarni / November 2015 / SDSU Mladenov Research Lab.
% This function calculates Raman Area from raw data.
function raman(ramanfolderpath,corrfact,RamanEnd,RamanBegin,RamanInc)
RamanDirList = dir([ramanfolderpath '*.dat']);
for j = 1:length(RamanDirList)
    [PathStr FileName Ext] = fileparts(RamanDirList(j).name);
    R = importdata(RamanDirList(j).name);
    R = R.data;
    plot(R(:,1),R(:,14));
    t = R(:,1);
    p = R(:,14);
    x = RamanBegin:RamanInc:RamanEnd;
```

```
    y = interp1(t,p,x,'spline');
    x = x';
    y = y';
    Rnew = [x,y];
    Rfind = find(Rnew == RamanBegin);
    Rfindend = find(Rnew == RamanEnd);
    Rlen = length(Rnew);
    Raman = Rnew(Rfind:Rfindend,2);
    %RamanC = Raman.*RC;
    RamanC = Raman*corrfact;
    y = RamanC;
    x = Rnew(Rfind:Rfindend,1);
    xlen = length(x) - 1;
    summation = 0;
    iteration=1;

for k=1:xlen
    y0 = y(k);
    y1 = y(k + 1);
    dx = x(k+1) - x(k);
    summation = summation + dx * (y0 + y1)/2;
    iteration = iteration+1;
end
BaseRect = (y(1)+y(xlen))/2*(x(xlen)-x(1));
RamanArea = summation - BaseRect;
RAOutputfile = [ramanfolderpath '\' FileName '.csv'];
%disp('Creating Raman Area File');
csvwrite(RAOutputfile,RamanArea);
end
end
```

blank.m

```
%Harshad Kulkarni / November 2015 / SDSU Mladenov Research Lab.
%This function imports, inner filter corrects and raman normalizes the raw
%blank data.
%This function uses inner filter correction file created in "ABS.m", raman area
%calculated in "raman.m"
function blank(blankfolderpath,ramanfolderpath,absfolderpath,em,ex,ints,intr,intq1,intq2)
BlankDirList = dir([blankfolderpath '*dat']);
for j = 1:length(BlankDirList)
    [PathStr BlankFileName Ext] = fileparts(BlankDirList(j).name);
    for k = 1:length(BlankFileName)
        if (BlankFileName(k)==')')
            N = k;
        else
        end
    end
    % Importing raw blank data
    Blankonlyname = BlankFileName(1:N);
    blankfilepath = [blankfolderpath BlankDirList(j).name];
    B = importdata(blankfilepath);
    [r,c] = size(B.data);
    FormatData = zeros(r,(c+1));
    FormatData(2:end,1) = str2double(B.rowheaders(2:end));
    FormatData(:,2:end) = B.data;
```

```matlab
B = FormatData;
[r,c] = size(B);
FormatData = zeros(size(B));
FormatData(:,1) = B(:,1);
count = 0;
for l = 2:c
FormatData(:,l) = B(:,c-count);
count = count+1;
end
B = FormatData;
[r,c] = size(B);
rows = B(:,1);
columns = B(1,:);
B1 = B(2:r,:);
[r,c] = size(B1);
%%%%%%%%%%%%%%%%%%%%%%%%%%%%%%%%%%%%%%%%%%%%%%%%%%%%%%%
%%%%%%%%%%%%%%%%%%%%
% Finding out "-ve" values and equaling to zeros.
 %for zr = 1:r
 %   for zc = 1:c

 %    if(B1(zr,zc)<0)
 %       B1(zr,zc)=0;
  % else
   % end

   %end
 %end
%%%%%%%%%%%%%%%%%%%%%%%%%%%%%%%%%%%%%%%%%%%%%%%%%%%%%%%
%%%%%%%%%%%%%%%%%%%%
 % Interpolating raw blank data to bring it in same range of excitation
 % and emission wavelengths as given in the "ProcessData.m"
 t = B1(:,1);
 p = B1(:,2:c);
 x =em';
 y = interp1(t,p,x,'spline');
 B1 = {x,[y]};
 B1 = cell2mat(B1);
 B1 = {columns',[B1]'};
 B1 = cell2mat(B1);
 [r,c] = size(B1);
 B1 = B1(2:r,:);

 t = B1(:,1);
 p = B1(:,2:c);
 x = ex';
 y = interp1(t,p,x,'spline');
 B1 = {x,[y]};
 B1 = cell2mat(B1);
 B1 = B1';
 emnew = {0 em};
 emnew = cell2mat(emnew);
 B1 = {emnew', [B1]};
 B1 = cell2mat(B1);
 B = B1;
```

230

```matlab
    [r,c] = size(B);
%%%%%%%%%%%%%%%%%%%%%%%%%%%%%%%%%%%%%%%%%%%%%%%%%%%%%%%
%%%%%%%%%%%%%%%%%%%
% Finding out "-ve" values and equaling to zeros.
  for m = 1:r
    for n = 1:c

      if(B(m,n)<0)
        B(m,n)=0;
      else
      end

    end
  end
%%%%%%%%%%%%%%%%%%%%%%%%%%%%%%%%%%%%%%%%%%%%%%%%%%%%%%
%%%%%%%%%%%%%%%%%%
B = B(2:r,2:c);
%%%%%%%%%%%%%%%%%%%%%%%%%%%%%%%%%%%%%%%%%%%%%%%%%%%%%%%
%%%%%%%%%%%%%%%%%%
%Applying inner filter correction to blank data.
Absdirlist = dir([absfolderpath '*.csv']);
IFCfile = zeros(r,c);
% Finding IFC file with matching name
for o = 1:length(Absdirlist)
    [PathStr IFCfilename Ext] = fileparts(Absdirlist(o).name);
  for p = 1:length(IFCfilename)
    if (IFCfilename(p)==')')
      N = p;
    else
    end
  end
    IFCfilename = IFCfilename(1:N);

  if (strcmp(IFCfilename, Blankonlyname)==1)
    %disp(IFCfilename);
    %disp(IFCfilename);
    openIFCfilename = [IFCfilename '.csv'];
    IFCfile = importdata(openIFCfilename);
  else
  end
end
    [r,c] = size(IFCfile);
    IFCfile = IFCfile(2:r,2:c);
    %Applying inner filter effect correction to blank file.
    Bci = B.*10.^(0.5*IFCfile);
%%%%%%%%%%%%%%%%%%%%%%%%%%%%%%%%%%%%%%%%%%%%%%%%%%%%%%%
%%%%%%%%%%%%%%%%%%
ramanareafilename =  dir([ramanfolderpath '*.csv']);
%Importing raman area calculated in "raman.m"
RamanArea = importdata(ramanareafilename.name);
disp('Current Sample is = ');
disp(Blankonlyname);
if (intq1 == 0)
   if(intq2 == 1)
     %int_time_raman = input('Enter Integration Time used for Raman = ');
```

```matlab
   %intr = int_time_raman ;
   %int_time_blank = input('Enter Integration Time used for Blank = ');
   %intb = int_time_blank;
   RamanArea = RamanArea*(ints/intr);
 else
   int_time_raman = input('Enter Integration Time used for Raman = ');
   intr = int_time_raman ;
   int_time_sample_individual = input('Enter Integration Time used for this Blank = ');
   ints1 = int_time_sample_individual;
   RamanArea = RamanArea*(ints1/intr);
 end
else
   RamanArea = RamanArea;
end
% Dividing blank file by raman area
Brc = Bci/RamanArea;
   Brc = {em',[Brc]};
   Brc = cell2mat(Brc);
   Brc = {[0 ex]',[Brc]'};
   Brc = cell2mat(Brc);
   Brc = Brc';
   BLOutputfilepath = [blankfolderpath  Blankonlyname '.csv'];
   csvwrite(BLOutputfilepath,Brc);
end
end
```

ABS.m

%Harshad Kulkarni / November 2015 / SDSU Mladenov Research Lab.
%This function creates inner filter correction file using raw absorbance
%data.
%This function also calls another function "suva" which calculates spectral
%properties for each sample and save it.

```matlab
function ABS(absfolderpath,eminc,exinc,em,ex,emlen,exlen,dfq,df_default,absq)
mkdir(absfolderpath,'Results');
ResultsPath = [absfolderpath 'Results' '\'];
resultsfile = [ResultsPath 'Results.txt'];
fid = fopen(resultsfile,'at');
fprintf(fid,'%s\t','"Sample Name"');
fprintf(fid,'%s\t','"abs254"');
fprintf(fid,'%s\t', '"S275_295"');
fprintf(fid,'%s\t', '"S350_400"');
fprintf(fid,'%s\n', '"Spectral Slope Ratio"');
AbsDirList = dir([absfolderpath '*.dat']);
mkdir(absfolderpath, 'Graphs');
FigureFolder = [absfolderpath 'Graphs' '\'];
for j = 1:length(AbsDirList)
   [PathStr, AbsFileName, Ext] = fileparts(AbsDirList(j).name);
for k = 1:length(AbsFileName)
     if (AbsFileName(k)==')')
        N = k;
     else
     end
end
   % Importing raw data into MATLAB.
```

232

```matlab
    Absonlyname = AbsFileName(1:N);
    disp('Current Sample is = ');
    disp(Absonlyname);
     if(dfq == 0)
       dilution_factor = input('Enter Dilution Factor = ');
       df = dilution_factor;
    else
       df = df_default;
     end
    filepath = [absfolderpath AbsDirList(j).name];
    abs = importdata(filepath);
    abs = [abs.data(:,1),abs.data(:,10)];
    abs = abs';
    [r,c] = size(abs);
    FormatData = zeros(size(abs));
    count = 0;
    for l = 1:c
    FormatData(:,l) = abs(:,c-count);
    count = count+1;
    end
    abs = FormatData';
  [rz,cz] = size(abs);
%%%%%%%%%%%%%%%%%%%%%%%%%%%%%%%%%%%%%%%%%%%%%%%%%%%%%%%
%%%%%%%%%%%%%%%%%%%%
% Finding out "-ve" values and equaling to zeros.
  for m = 1:rz
    for n = 1:cz

      if(abs(m,n)<0)
         abs(m,n)=NaN;
      else
      end

    end
  end
%%%%%%%%%%%%%%%%%%%%%%%%%%%%%%%%%%%%%%%%%%%%%%%%%%%%%%%
%%%%%%%%%%%%%%%%%%%%

%%%%%%%%%%%%%%%%%%%%%%%%%%%%%%%%%%%%%%%%%%%%%%%%%%%%%%%
%%%%%%%%%%%%%%%%%%%%
% Our instrument has 240:450 absorbance data for all previous samples, we
% need data upto 596 nm, so extrapolating the absorbance data linearly.

x = abs(:,1);
y = abs(:,2);
% if linear extrapolation is chosen during interactive questions.
if (absq == 0)
   disp(absq)
xev = ex(1):1:em(end);
ypred = interp1(x,y,xev,'linear','extrap');
xev = xev';
ypred = ypred';
abs = [xev,ypred];
```

```matlab
%%%%%%%%%%%%%%%%%%%%%%%%%%%%%%%%%%%%%%%%%%%%%%%%%%%%%%%
%%%%%%%%%%%%%%%%%%%
%intelegent extrapolation using shape learning modeling (slm) technique.
elseif (absq == 1)
    disp(absq)
[~,~,~,xev,ypred] = slmengine(x,y,'knots',[ex(1):50:em(end)],...
    'decreasing','on','concaveup','on','rightminvalue',0,'plot','on');
    xev = xev';
    ypred = ypred';

    xevnew = ex(1):1:em(end);
    yprednew = interp1(xev,ypred,xevnew,'spline');
    xevnew = xevnew';
    yprednew = yprednew';
    abs = [xevnew,df*yprednew];
end
%%%%%%%%%%%%%%%%%%%%%%%%%%%%%%%%%%%%%%%%%%%%%%%%%%%%%%%
%%%%%%%%%%%%%%%%%%%
% Calling function "suva" to calculate and save abs254, S275_295, S350_400 and SR for each sample.
suva(Absonlyname,resultsfile,abs);
%%%%%%%%%%%%%%%%%%%%%%%%%%%%%%%%%%%%%%%%%%%%%%%%%%%%%%%
%%%%%%%%%%%%%%%%%%%
% Plotting a graph of wavelength (X-axis) vs. absorabance (Y-axis) of
% actual data and modeled data using shape learning technique.
h = figure(j);
plot(xev,df*ypred,'r');
hold on
plot(x,y,'o');
%axis([200 600 0 0.01])
handle = gca;
set(handle,'fontsize',14);
ylabel('Absorbance');
xlabel('Wavelength');
title(Absonlyname);
FilePath = [FigureFolder AbsFileName];
saveas(h,FilePath,'png');
close(h);
%%%%%%%%%%%%%%%%%%%%%%%%%%%%%%%%%%%%%%%%%%%%%%%%%%%%%%%
%%%%%%%%%%%%%%%%%%%

waves = abs(:,1);
wave254 = find(waves == 254);
abs254 = abs(wave254,2);

exabsstart = find(waves == ex(1));
exabsend = find(waves == ex(exlen));

emabsstart = find(waves == em(1));
emabsend = find(waves == em(emlen));

uvlength = 1;
absint = abs(:,2)/uvlength;

ex_abs=absint(exabsstart:exinc:exabsend,:);
em_abs=absint(emabsstart:eminc:emabsend,:);
```

```
for p=1:length(em_abs)
    for q=1:length(ex_abs)
        % IFC is the file which is used for inner filter correction.
        IFC(p,q)=ex_abs(q)+em_abs(p);
    end
end
IFC = IFC(1:p,1:q);
IFC = IFC/df;
IFC = {em',[IFC]};
IFC = cell2mat(IFC);
IFC = IFC';
IFC = {[0 ex]',[IFC]};
IFC = cell2mat(IFC);
IFC = IFC';
UVOutputfilename = Absonlyname;
UVOutputfilepath = [absfolderpath  UVOutputfilename '.csv'];
csvwrite(UVOutputfilepath,IFC);
end
```

suva.m

```
%Harshad Kulkarni / November 2015 / SDSU Mladenov Research Lab.
% This function calculates spectral properties (%(Helms et al., 2008) for each sample and save it.
function suva(Absonlyname,resultsfile,abs)
    x = abs(:,1);
    y = abs(:,2);
    %Calculating absorbance coefficient
    abscoeff= y*2.303/0.01;
    %Calculating natural log of absorbance coefficient
    lnabscoeff = log(abscoeff);
    wave254 = find(x == 254);
    abs254 = abs(wave254,2);

    wave275 = find(x == 275);
    wave295 = find(x == 295);

    %Calculating slope between 275 nm and 295 nm
    line275_295 = x(wave275:wave295,1);
    Y275_295 = lnabscoeff(wave275:wave295,1);
    meanline275_295 = mean(line275_295);
    meanY275_295 = mean(Y275_295);
    num1 = (meanline275_295 - line275_295).*(meanY275_295 - Y275_295);
    den1 = (meanline275_295 - line275_295).^2;
    slope275_295 = (sum(num1))/(sum(den1));

    wave350 = find(x == 350);
    wave400 = find(x == 400);

    %Calculating slope between 350 nm and 400 nm
    line350_400 = x(wave350:wave400,1);
    Y350_400 = lnabscoeff(wave350:wave400,1);
    meanline350_400 = mean(line350_400);
    meanY350_400 = mean(Y350_400);
    num1 = (meanline350_400 - line350_400).*(meanY350_400 - Y350_400);
```

```matlab
    den1 = (meanline350_400 - line350_400).^2;
    slope350_400 = (sum(num1))/(sum(den1));

    %Calculating ratio of S275_295 and S350_400
    SR = slope275_295 / slope350_400;
    fid = fopen(resultsfile,'at');
    fprintf(fid,'%s\t',Absonlyname);
    fprintf(fid,'%f\t',abs254);
    fprintf(fid,'%f\t', slope275_295);
    fprintf(fid,'%f\t', slope350_400);
    fprintf(fid,'%f\n', SR);
end




% This is alternative code for the same purpose, however please use the above
% code.
% function suva(suvainput,df,suvaonlyname,Absonlyname,resultsfile)
% %DirList = dir([suvainput '*.dat']);
% %mkdir(suvainput,'Results');
% %ResultsPath = [suvainput 'Results' '\'];
% %resultsfile = [ResultsPath 'Results.txt'];
% %fid = fopen(resultsfile,'at');
% %fprintf(fid,'%s\t','"Sample Name"');
% %fprintf(fid,'%s\t','"abs254"');
% %fprintf(fid,'%s\t', '"S275_295"');
% %fprintf(fid,'%s\t', '"S350_400"');
% %fprintf(fid,'%s\n', '"Spectral Slope Ratio"');
% %for i = 1:length(DirList)
% %   [PathStr FileName Ext] = fileparts(DirList(i).name);
% %   for n = 1:length(FileName)
% %       if (FileName(n)=='-')
% %           N = n-1;
% %       else
% %       end
% %   end
% %   onlyname = FileName(1:N);
%     filepath = [suvainput suvaonlyname];
%     abs = importdata(filepath);
%     abs = [abs.data(:,1),abs.data(:,10)];
%     abs = abs';
%     [r,c] = size(abs);
%     FormatData = zeros(size(abs));
%     count = 0;
%     for j = 1:c
%     FormatData(:,j) = abs(:,c-count);
%     count = count+1;
%     end
%     abs = FormatData';
%
%%%%%%%%%%%%%%%%%%%%%%%%%%%%%%%%%%%%%%%%%%%%%%%%%%%
%%%%%%%%%%%%%%%%%%
% % The absorbance data associated with 3D EEM sample, is not compatible.
% % Hence interpolating it with increment of 1nm.
%     t = abs(:,1);
```

```
%    p = abs(:,2);
%    x = 240:1:600;
%    y = interp1(t,p,x,'linear','extrap');
%    x = x';
%    y = y';
%    abs = [x,y];
%    abs = [abs(:,1),df*abs(:,2)];
%    abscoeff= abs(:,2)*2.303/0.01;
%    lnabscoeff = log(abscoeff);
%    %plot(x,y);
%
%%%%%%%%%%%%%%%%%%%%%%%%%%%%%%%%%%%%%%%%%%%%%%%%%%%%%%%%%%%%%%%%%%%%%%%%%%%%%%%%%%
%    waves = abs(:,1);
%    wave254 = find(waves == 254);
%    abs254 = abs(wave254, 2);
%
%    wave275 = find(waves == 275);
%    wave295 = find(waves == 295);
%
%    line275_295 = x(wave275:wave295,1);
%    Y275_295 = lnabscoeff(wave275:wave295,1);
%    meanline275_295 = mean(line275_295);
%    meanY275_295 = mean(Y275_295);
%    num1 = (meanline275_295 - line275_295).*(meanY275_295 - Y275_295);
%    den1 = (meanline275_295 - line275_295).^2;
%    slope275_295 = (sum(num1))/(sum(den1));
%
%    wave350 = find(waves == 350);
%    wave400 = find(waves == 400);
%
%    line350_400 = x(wave350:wave400,1);
%    Y350_400 = lnabscoeff(wave350:wave400,1);
%    meanline350_400 = mean(line350_400);
%    meanY350_400 = mean(Y350_400);
%    num1 = (meanline350_400 - line350_400).*(meanY350_400 - Y350_400);
%    den1 = (meanline350_400 - line350_400).^2;
%    slope350_400 = (sum(num1))/(sum(den1));
%
%    SR = slope275_295 / slope350_400; %(Helms et al., 2008)
%
%    fid = fopen(resultsfile,'at');
%    fprintf(fid,'%s\t',Absonlyname);
%    fprintf(fid,'%f\t',abs254);
%    fprintf(fid,'%f\t', slope275_295);
%    fprintf(fid,'%f\t', slope350_400);
%    fprintf(fid,'%f\n', SR);
% end
```

sample.m

```
%Harshad Kulkarni / November 2015 / SDSU Mladenov Research Lab.
%This function imports, inner filter corrects, raman normalizes, blank
%subtracts and Rayleigh masks the raw sample data.
%This function calculates all fluorescence indices and peak intensities.
%This function refers to "raman.m", "ABS.m" and "blank.m" for raman area,
```

```matlab
%inner filter correction file and processed blank file respectively.
function
sample(InputFolder,samplefolderpath,blankfolderpath,ramanfolderpath,absfolderpath,ex,em,exinc,eminc,exlen,df_d
efault,dfq,ints,intr,intq1,intq2)
SampleDirList = dir([samplefolderpath '*dat']);
mkdir(InputFolder,'Results');
ResultsPath = [InputFolder 'Results' '\'];
resultsfile = [ResultsPath 'Results.txt'];
fid = fopen(resultsfile,'at');
fprintf(fid,'%s\t','"Sample Name"','"Fluroscence Index"','"Freshness Index"','"Humification
Index"','"Peak_A(ex260,maxem(380:460))"','"Peak_B(ex275,em310)"','"Peak_T(ex275,em340)"','"Peak_C(ex350,m
axem(420:480))"','"Peak_M(ex312,maxem(380:420))"','"CDOM(ex325,em470)"','"Tryptophan(ex285,em350)"');
fprintf(fid,'%s\n','"MaxEM@370nm"');

mkdir(ResultsPath, 'Data4Parafac');
ParafacDataPath = [ResultsPath 'Data4Parafac' '\'];

mkdir(ResultsPath, 'EEM Graphs');
mkdir(ResultsPath, 'Indices');
mkdir(ResultsPath, 'Peaks');
mkdir(ResultsPath, 'C3');
FigureFolder = [ResultsPath 'EEM Graphs' '\'];
FigureFolder2 = [ResultsPath 'Indices' '\'];
FigureFolder3 = [ResultsPath 'Peaks' '\'];
FigureFolder4 = [ResultsPath 'C3' '\'];
for j = 1:length(SampleDirList)
    [PathStr, SampleFileName, Ext] = fileparts(SampleDirList(j).name);
    for k = 1:length(SampleFileName)
        if (SampleFileName(k)==')')
            N = k;
        else
        end
    end
    % Importing raw sample data
    Sampleonlyname = SampleFileName(1:N);
    fprintf(fid,'%s\t',Sampleonlyname);
    filepath = [samplefolderpath SampleDirList(j).name];
    A = importdata(filepath);
    [r,c] = size(A.data);
    FormatData = zeros(r,(c+1));
    FormatData(2:end,1) = str2double(A.rowheaders(2:end));
    FormatData(:,2:end) = A.data;
    A = FormatData;
    [r,c] = size(A);
    FormatData = zeros(size(A));
    FormatData(:,1) = A(:,1);
    count = 0;
    for l = 2:c
    FormatData(:,l) = A(:,c-count);
    count = count+1;
    end
    A = FormatData;
    [r,c] = size(A);
    rows = A(:,1);
    columns = A(1,:);
```

```matlab
  A1 = A(2:r,:);% picture taken 1
  [r,c] = size(A1);


%%%%%%%%%%%%%%%%%%%%%%%%%%%%%%%%%%%%%%%%%%%%%%%%%%%%%%%%%
%%%%%%%%%%%%%%%%%%%%%
% Finding out "-ve" values and equaling to zeros.
 %for zr = 1:r
  %   for zc = 1:c

  %    if(A1(zr,zc)<0)
      %   A1(zr,zc)=0;
   %   else
    %  end

    %end
  %end
%%%%%%%%%%%%%%%%%%%%%%%%%%%%%%%%%%%%%%%%%%%%%%%%%%%%%%%%%
%%%%%%%%%%%%%%%%%%%
  % Interpolating raw sample data to bring it in same range of excitation
  % and emission wavelengths as given in the "ProcessData.m"
  t = A1(:,1);
  p = A1(:,2:c);
  x =em';
  y = interp1(t,p,x,'spline');
  A1 = {x,[y]};
  A1 = cell2mat(A1);
  A1 = {columns',[A1]'};
  A1 = cell2mat(A1);

  [r,c] = size(A1);
  A1 = A1(2:r,:);

  t = A1(:,1);
  p = A1(:,2:c);
  x = ex';
  y = interp1(t,p,x,'spline');
  A1 = {x,[y]};
  A1 = cell2mat(A1);
  A1 = A1';
  emnew = {0 em};
  emnew = cell2mat(emnew);
  A1 = {emnew', [A1]};
  A1 = cell2mat(A1);
  A = A1; % picture taken 2
  [rA,cA] = size(A);


%%%%%%%%%%%%%%%%%%%%%%%%%%%%%%%%%%%%%%%%%%%%%%%%%%%%%%%%%
%%%%%%%%%%%%%%%%%%%
% Finding out "-ve" values and equaling to zeros.
 for m = 1:rA
   for n = 1:cA

   if(A(m,n)<0)
       A(m,n)=0;
    else
```

```matlab
        end


      end
  end % picture taken 3
%%%%%%%%%%%%%%%%%%%%%%%%%%%%%%%%%%%%%%%%%%%%%%%%%%%%
%%%%%%%%%%%%%%%
   ROWS = A(1,2:cA);
   COLUMNS = A(2:rA,1);
   A = A(2:rA,2:cA);
%%%%%%%%%%%%%%%%%%%%%%%%%%%%%%%%%%%%%%%%%%%%%%%%%%%%
%%%%%%%%%%%%%%%%
%Applying inner filter correction to sample data.
   Absdirlist = dir([absfolderpath '*.csv']);
   IFCfile = zeros(rA,cA);
% Finding IFC file with matching name
for o = 1:length(Absdirlist)
    [PathStr, IFCfilename, Ext] = fileparts(Absdirlist(o).name);
   for p = 1:length(IFCfilename)
     if (IFCfilename(p)==')')
        N = p;
     else
     end
   end
   IFCfilename = IFCfilename(1:N);
   if (strncmp(IFCfilename, Sampleonlyname,N)==1)
    openIFCfile = [IFCfilename '.csv'];
    IFCfilepath = [absfolderpath openIFCfile];
    IFCfile = importdata(IFCfilepath);
   else
   end
end
  [r,c] = size(IFCfile);
%Applying inner filter effect correction to sample file.
  IFCfile = IFCfile(2:r,2:c);
  Aci = A.*10.^(0.5*IFCfile); % picture taken 4
%%%%%%%%%%%%%%%%%%%%%%%%%%%%%%%%%%%%%%%%%%%%%%%%%%%%
%%%%%%%%%%%%%%%%
   ramanareafilename =  dir([ramanfolderpath '*.csv']);
%Importing raman area calculated in "raman.m"
  RamanArea = importdata(ramanareafilename.name);
  disp('Current Sample is = ');
  disp(Sampleonlyname);
if (intq1 == 0)
   if(intq2 == 1)
      %int_time_raman = input('Enter Integration Time used for Raman = ');
      %intr = int_time_raman ;
      %int_time_sample = input('Enter Integration Time used for Samples = ');
      %ints = int_time_sample;
      RamanArea = RamanArea*(ints/intr);
   else
      disp('Current Sample is = ');
      disp(Sampleonlyname);
      int_time_raman = input('Enter Integration Time used for Raman = ');
      intr = int_time_raman ;
      int_time_sample_individual = input('Enter Integration Time used for this sample = ');
```

```matlab
        ints1 = int_time_sample_individual;
        RamanArea = RamanArea*(ints1/intr);
    end
else
    RamanArea = RamanArea;
end
    disp(RamanArea);
    % Dividing sample file by raman area
    Acir = Aci/RamanArea; % Picture taken 5
%%%%%%%%%%%%%%%%%%%%%%%%%%%%%%%%%%%%%%%%%%%%%%%%%
%%%%%%%%%%%%%%%%%%
% Finding processed blank file with matching name from "blank.m"
    bldirlist =  dir([blankfolderpath '*.csv']);
    for q = 1:length(bldirlist)
      [PathStr, blankfilename, Ext] = fileparts(bldirlist(q).name);
      for r = 1:length(blankfilename)
        if(blankfilename(r)==')')
          N =r;
        else
        end
      end
      blankfilename = blankfilename(1:N);
      if(strncmp(blankfilename,Sampleonlyname,N)==1)
        openblankfile = [blankfilename '.csv'];
        blankfilepath = [blankfolderpath openblankfile];
%Importing processed blank data from "blank.m"
        Blank = importdata(blankfilepath);
      else
      end
    end
    [r,c] = size(Blank);
    Blank = Blank(2:r,2:c);% picture taken 6
% Subtracting blank from the sample.
    Asub = Acir - Blank; % Picture taken 7
    if(dfq == 0)
      dilution_factor = input('Enter Dilution Factor = ');
      df = dilution_factor;
    else
      df = df_default;
    end
% Correction for dilution factor
    Adil = Asub*df;
    Adil2 =Adil;
    [rAdil2,cAdil2]=size(Adil2);
%%%%%%%%%%%%%%%%%
% Finding out "-ve" values and equaling to zeros.
  for m = 1:rAdil2
    for n = 1:cAdil2

    if(Adil2(m,n)<0)
       Adil2(m,n)=0;
     else
     end

    end
```

```matlab
  end % picture taken 3
%%%%%%%%%%%%%%%%%%%%%%%%%%%%%%%%%%%%%%%%%%%%%%%%%%%%%%%%
%%%%%%%%%%%%%%%
   % We do not use this part, but DO NOT DELETE.
   %ParafacDatafilepath = [ParafacDataPath Sampleonlyname '.csv'];
   %csvwrite(ParafacDatafilepath,Adil2);
   %Picture taken 8
%%%%%%%%%%%%%%%%%%%%%%%%%%%%%%%%%%%%%%%%%%%%%%%%%%%%%%%%
%%%%%%%%%%%%%%%%%
% Applying 1st and 2nd order Rayleigh masking to inner filter corrected,
% raman normalized and blank subtracted data.
   Slitwidth = 6;
   Acut = Adil;
   Acut = {ROWS',[Acut]'};
   Acut = cell2mat(Acut);
   Acut = Acut';
   emnew = {0,em};
   emnew = cell2mat(emnew);
   Acut = {emnew',Acut};
   Acut = cell2mat(Acut);
   %[r,c] = size(Acut);
   %t = Acut(:,1);
   %p = Acut(:,2:c);
   %x = exsample';
   %y = interp1(t,p,x,'spline');
   %Acut = y;
   %Acut = {exsample',[Acut]};
   %Acut = cell2mat(Acut);
   %Acut = Acut';
   %emsamplenew = {0,em};
   %emsamplenew = cell2mat(emsamplenew);
   %Acut = {emsamplenew',[Acut]};
   %Acut = cell2mat(Acut);
   [r,c] = size(Acut);
   Acut1 = Acut(2:r,2:c);
   Asize = size(Acut1);
   ylen = Asize(1);
   xlen = Asize(2);
   x = ex;
   y = em;
    xend = x(xlen);
   yend = y(ylen);
   [xi, yi] = meshgrid(x(1):1:xend,y(1):1:yend);
   %warning('OFF');
   zi = interp2(x, y, Adil, xi, yi, 'spline');
   exnew = xi(1,:);
   emnew1 = yi(:,1);
   exnewlen = length(exnew);

for s=1:exnewlen
   M = find(emnew1<(exnew(s)+Slitwidth*4));
   zi(M,s)=NaN;
end
for t=1:exnewlen
   N = find(emnew1>(exnew(t)*2-Slitwidth*4));
```

242

```matlab
    zi(N,t)=NaN;
end
%picture taken 9
Acut1 = zi;
%[rAcut1,cAcut1]=size(Acut1);
%%%%%%%%%%%%%%%%
% Finding out "-ve" values and equaling to zeros.
 %for m = 1:rAcut1
  %   for n = 1:cAcut1

   %   if(Acut1(m,n)<0)
     %     Acut1(m,n)=0;
    %   else
     %  end

     %end
  %end
%%%%%%%%%%%%%%
%Adil = Acut1;
%%%%%%%%%%%%%%%%%%
% Printing Emission-Excitation contour map and saving it to a file
h = figure(j);
%subplot(1,2,1);
contourf(exnew,emnew1,Acut1,30);
handle = gca;
set(handle,'fontsize', 28);
colormap(gray);
cmp = colormap;
cmp = flipud(cmp);
colormap(cmp);
% Comment the line 298 if you'd like to set the Y axis to a fixed intensity
% number, uncomment the lines 299 and 300, enter desired intensity number
% in line 299.
caxis([0, max(max(Acut1))]);
%caxis([0, 1]);
%caxis('manual');
H = colorbar('vert');
set(H,'fontsize',24);
ylabel('Em. (nm)','fontsize',28);
xlabel('Ex. (nm)','fontsize',28);
title(Sampleonlyname);
FilePath = [FigureFolder Sampleonlyname];
saveas(h,FilePath,'png');
close(h);
%%%%%%%%%%%%%%%%%
% Plotting emission intensities used to calculate FI, FrI and HIX in single
% graph.
h = figure(j);
% Plotting emission for FI
ex370 = find(exnew == 370);
plot(emnew1,Acut1(:,ex370),'black')
line370 = Acut1(:,ex370);
xmaxEm370=emnew1(Acut1(:,ex370) == max(Acut1(:,ex370)));
ymaxEm370=max(line370);
text(xmaxEm370,ymaxEm370,['370 (FI)'],...
```

```matlab
            'VerticalAlignment','bottom',...
            'HorizontalAlignment','center',...
            'FontSize',8);
hold on

% Plotting emission for FrI
ex310 = find(exnew == 310);
plot(emnew1,Acut1(:,ex310),'blue')
line310 = Acut1(:,ex310);
xmaxEm310=emnew1(Acut1(:,ex310) == max(Acut1(:,ex310)));
ymaxEm310=max(line310);
text(xmaxEm310,ymaxEm310,['310 (FrI)'],...
            'VerticalAlignment','bottom',...
            'HorizontalAlignment','center',...
            'FontSize',8);
hold on

% Plotting emission for HIX
ex254 = find(exnew == 254);
plot(emnew1,Acut1(:,ex254),'red')
line254 = Acut1(:,ex254);
xmaxEm254=emnew1(Acut1(:,ex254) == max(Acut1(:,ex254)));
ymaxEm254=max(line254);
text(xmaxEm254,ymaxEm254,['254 (HIX)'],...
            'VerticalAlignment','bottom',...
            'HorizontalAlignment','center',...
            'FontSize',8);
xlabel('Emission Wavelength, nm');
ylabel('Emission Intensity');
title(Sampleonlyname);
FilePath2 = [FigureFolder2 Sampleonlyname];
saveas(h,FilePath2,'png');
close(h);

%%%%%%%%%%%%%%%%
% Calculating and saving values of FI (Cory and McKnight,2005)
em470 = find(emnew1 == 470);
em520 = find(emnew1 == 520);
FI = Acut1(em470,ex370)./Acut1(em520,ex370);
if (FI>0)
fprintf(fid,'%f\t',FI);
else
    fprintf(fid,'%f\t',0);
end

% Calculating and saving values of FrI (Parlanti et al., 2000)
em380 = find(emnew1 == 380);
em420 = find(emnew1 == 420);
em435 = find(emnew1 == 435);
FrI = Acut1(em380,ex310)/max(Acut1(em420:em435,ex310));
if (FrI>0)
fprintf(fid,'%f\t',FrI);
else
    fprintf(fid,'%f\t',0);
end
```

```matlab
% Calculating and saving values of HIX (Zsolnay et al., 1999)
em435 = find(emnew1(:,1) == 435);
em480 = find(emnew1(:,1) == 480);
RedHum = line254(em435:em480,1);
for ir = 1:length(RedHum)
   if(RedHum(ir)<0)
     RedHum(ir)=0;
   else
    end
end
em300 = find(emnew1(:,1) == 300);
em345 = find(emnew1(:,1) == 345);
BlueHum = line254(em300:em345,1);
for ib = 1:length(BlueHum)
   if(BlueHum(ib)<0)
     BlueHum(ib)=0;
   else
    end
end
RedA = trapz(RedHum);
BlueA = trapz(BlueHum);
% Formulation by Zsolnay et al., 1999
HIX = RedA/BlueA;
% Formulation by Ohno, 2002
%HIX = RedA/(RedA+BlueA); %Ohno
if (HIX>0)
fprintf(fid,'%f\t',HIX);
else
   fprintf(fid,'%f\t',0);
end
%%%%%%%%%%%%%%%%%%
% Plotting emission intensities used to calculate Peaks A, B, T, C, and M
% in single graph.

h = figure(j);

% Plotting emission for Peak A
ex260 = find(exnew == 260);
plot(emnew1,Acut1(:,ex260),'black')
line260 = Acut1(:,ex260);
xmaxEm260=emnew1(Acut1(:,ex260) == max(Acut1(:,ex260)));
ymaxEm260=max(line260);
text(xmaxEm260,ymaxEm260,['260 (A)'],...
        'VerticalAlignment','bottom',...
        'HorizontalAlignment','center',...
        'FontSize',8);
hold on

% Plotting emission for Peaks B and T
ex275 = find(exnew == 275);
plot(emnew1,Acut1(:,ex275),'blue')
line275 = Acut1(:,ex275);
xmaxEm275=emnew1(Acut1(:,ex275) == max(Acut1(:,ex275)));
ymaxEm275=max(line275);
```

```
text(xmaxEm275,ymaxEm275,['275 (B&T)'],...
        'VerticalAlignment','bottom',...
        'HorizontalAlignment','center',...
        'FontSize',8);
hold on

% Plotting emission for Peak C
ex350 = find(exnew == 350);
plot(emnew1,Acut1(:,ex350),'red')
line350 = Acut1(:,ex350);
xmaxEm350=emnew1(Acut1(:,ex350) == max(Acut1(:,ex350)));
ymaxEm350=max(line350);
text(xmaxEm350,ymaxEm350,['350 (C)'],...
        'VerticalAlignment','bottom',...
        'HorizontalAlignment','center',...
        'FontSize',8);
hold on

% Plotting emission for Peak M
ex312 = find(exnew == 312);
plot(emnew1,Acut1(:,ex312),'black')
line312 = Acut1(:,ex312);
xmaxEm312=emnew1(Acut1(:,ex312) == max(Acut1(:,ex312)));
ymaxEm312=max(line312);
text(xmaxEm312,ymaxEm312,['312 (M)'],...
        'VerticalAlignment','bottom',...
        'HorizontalAlignment','center',...
        'FontSize',8);
hold on
%ex315 = find(exnew == 315);
%plot(emnew1,Acut1(:,ex315),'black')
%line315 = Acut1(:,ex315);
%xmaxEm315=emnew1(Acut1(:,ex315) == max(Acut1(:,ex315)));
%ymaxEm315=max(line315);
%text(xmaxEm315,ymaxEm315,['315 (X)'],...
%        'VerticalAlignment','bottom',...
%        'HorizontalAlignment','center',...
%        'FontSize',8);
%hold on
%ex355 = find(exnew == 355);
%plot(emnew1,Acut1(:,ex355),'black')
%line355 = Acut1(:,ex355);
%xmaxEm355=emnew1(Acut1(:,ex355) == max(Acut1(:,ex355)));
%ymaxEm355=max(line355);
%text(xmaxEm355,ymaxEm355,['355 (Cz)'],...
%        'VerticalAlignment','bottom',...
%        'HorizontalAlignment','center',...
%        'FontSize',8);
%hold on
%ex250 = find(exnew == 250);
%plot(emnew1,Acut1(:,ex250),'black')
%line250 = Acut1(:,ex250);
%xmaxEm250=emnew1(Acut1(:,ex250) == max(Acut1(:,ex250)));
%ymaxEm250=max(line250);
%text(xmaxEm250,ymaxEm250,['250 (Az)'],...
```

```matlab
%          'VerticalAlignment','bottom',...
%          'HorizontalAlignment','center',...
%          'FontSize',8);
xlabel('Emission Wavelength, nm');
ylabel('Emission Intensity');
title(Sampleonlyname);
FilePath3 = [FigureFolder3 Sampleonlyname];
saveas(h,FilePath3,'png');
close(h);
%%%%%%%%%%%%%%%%%
% Plotting emission intensities used to calculate Peaks CDOM and Tryp
% similar to those measured by C3 Submersible fluorometer
h = figure(j);

% Plotting emission for Peak CDOM
ex325 = find(exnew == 325);
plot(emnew1,Acut1(:,ex325),'black')
line325 = Acut1(:,ex325);
xmaxEm325=emnew1(Acut1(:,ex325) == max(Acut1(:,ex325)));
ymaxEm325=max(line325);
text(xmaxEm325,ymaxEm325,['325 (CDOM)'],...
          'VerticalAlignment','bottom',...
          'HorizontalAlignment','center',...
          'FontSize',8);
hold on

% Plotting emission for Peak Tryp
ex285 = find(exnew == 285);
plot(emnew1,Acut1(:,ex285),'black')
line285 = Acut1(:,ex285);
xmaxEm285=emnew1(Acut1(:,ex285) == max(Acut1(:,ex285)));
ymaxEm285=max(line285);
text(xmaxEm285,ymaxEm285,['285 (Tryp)'],...
          'VerticalAlignment','bottom',...
          'HorizontalAlignment','center',...
          'FontSize',8);
hold on
xlabel('Emission Wavelength, nm');
ylabel('Emission Intensity');
title(Sampleonlyname);
FilePath4 = [FigureFolder4 Sampleonlyname];
saveas(h,FilePath4,'png');
close(h);

%%%%%%%%%%%%%%%%%
% Calculating and saving values of Peak A (Coble, 1996)
em380 = find(emnew1 == 380);
em460 = find(emnew1 == 460);
Peak_A = max(Acut1(em380:em460,ex260));
if (Peak_A>0)
fprintf(fid,'%f\t',Peak_A);
else
   fprintf(fid,'%f\t',0);
end
```

```
% Calculating and saving values of Peak B (Coble, 1996)
em310 = find(emnew1 == 310);
Peak_B = Acut1(em310,ex275);
if (Peak_B>0)
fprintf(fid,'%f\t',Peak_B);
else
    fprintf(fid,'%f\t',0);
end

% Calculating and saving values of Peak T (Coble, 1996)
em340 = find(emnew1 == 340);
Peak_T = Acut1(em340,ex275);
if (Peak_T>0)
fprintf(fid,'%f\t',Peak_T);
else
    fprintf(fid,'%f\t',0);
end

% Calculating and saving values of Peak C (Coble, 1996)
em420 = find(emnew1 == 420);
em480 = find(emnew1 == 480);
Peak_C = max(Acut1(em420:em480,ex350));
if (Peak_C>0)
fprintf(fid,'%f\t',Peak_C);
else
    fprintf(fid,'%f\t',0);
end

% Calculating and saving values of Peak M (Coble, 1996)
em380 = find(emnew1 == 380);
em420 = find(emnew1 == 420);
Peak_M = max(Acut1(em380:em420,ex312));
if (Peak_M>0)
fprintf(fid,'%f\t',Peak_M);
else
    fprintf(fid,'%f\t',0);
end

% Calculating and saving values of Peak CDOM
em470 = find(emnew1 == 470);
CDOM = Acut1(em470,ex325);
if (CDOM>0)
fprintf(fid,'%f\t',CDOM);
else
    fprintf(fid,'%f\t',0);
end

% Calculating and saving values of Peak Tryp
em350 = find(emnew1 == 350);
Tryp = Acut1(em350,ex285);
if (Tryp>0)
fprintf(fid,'%f\t',Tryp);
else
    fprintf(fid,'%f\t',0);
end
```

248

```
fprintf(fid,'%f\n',xmaxEm370);
%ex315=find(exnew==315);
%em396=find(emnew1==396);
%Peak_X = Acut1(em396,ex315);
%if (Peak_X>0)
%fprintf(fid,'%f\t',Peak_X);
%else
%    fprintf(fid,'%f\t',0);
%end


%ex355=find(exnew==355);
%em473=find(emnew1==473);
%Peak_Cz = Acut1(em473,ex355);
%if (Peak_Cz>0)
%fprintf(fid,'%f\t',Peak_Cz);
%else
%    fprintf(fid,'%f\t',0);
%end


%ex250=find(exnew==250);
%em477=find(emnew1==477);
%Peak_Az = Acut1(em477,ex250);
%if (Peak_Az>0)
%fprintf(fid,'%f\n',Peak_Az);
%else
%    fprintf(fid,'%f\n',0);
%end


%%%%%%%%%%%%%%%%%%
% Add list of excitation wavelengths and emission wavelengths in 1st row
% and 1st column of the matrix.
A = Acut1;
A = {emnew1, A};
A = cell2mat(A);
A =  A';
exnew = {0,exnew};
exnew = cell2mat(exnew);
A = {exnew',A};
A = cell2mat(A);
A = A';
%%%%%%%%%%%%%%%%%
% Resetting the data format as required for PARAFAC model files.
   Ap = A';
   t = Ap(2:end,1);
   p = Ap(2:end,2:end);
   x =ex(1):exinc:ex(end);
   x = x';
   y = interp1(t,p,x,'spline');
   Ap = {x,[y]};
   Ap = cell2mat(Ap);
   Ap = Ap';
   emnew1 = emnew1';
   emnew1 = [0 emnew1];
```

```
  emnew1 = emnew1';
  Ap = [emnew1,Ap];

  t = Ap(2:end,1);
  p = Ap(2:end,2:end);
  x = em(1):eminc:em(end);
  x=x';
  y = interp1(t,p,x,'spline');
  Ap = {x,[y]};
  Ap = cell2mat(Ap);
  Ap = Ap';
  Apex = ex(1):exinc:ex(end);
  Apex = [0 Apex];
  Ap = [Apex',Ap];
  Ap = Ap';

  Slitwidth = 6;
  Apcut = Ap(2:end,2:end);
  Apsize = size(Apcut);
  ylen = Apsize(1);
  xlen = Apsize(2);
  x = ex(1):exinc:ex(end);
  y = em(1):eminc:em(end);
  xend = x(xlen);
  yend = y(ylen);
  [xi, yi] = meshgrid(x(1):exinc:xend,y(1):eminc:yend);
  %warning('OFF');
  zi = interp2(x, y, Apcut, xi, yi, 'spline');
  exnew = xi(1,:);
  emnew2 = yi(:,1);
  exnewlen = length(exnew);

for s=1:exnewlen
  M = find(emnew2<(exnew(s)+Slitwidth*4));
  zi(M,s)=NaN;
end
for t=1:exnewlen
  N = find(emnew2>(exnew(t)*2-Slitwidth*4));
  zi(N,t)=NaN;
end
%picture taken 9
Apcut1 = zi;

% Saving a file to be used in PARAFAC model.
ParafacDatafilepath = [ParafacDataPath Sampleonlyname '.csv'];
csvwrite(ParafacDatafilepath,Apcut1);
SampleOutputfilepath = [samplefolderpath  Sampleonlyname '.csv'];
csvwrite(SampleOutputfilepath,A);
end
disp('Total Number of Samples = ');
disp(j);
end
```

dataprep4pf.m

% Harshad Kulkarni / November 2015 / SDSU Mladenov Research Lab.

```matlab
% This function extracts data from all PARAFAC files created in "sample.m"
% and saves it in single .csv file.
function dataprep4pf(FolderPath)
%%%%%%%%%%%%%% Make Changes here if necessary %%%%%%%%%%%%%%%%
eminc = 2; %increment of emission wavelengths (nm)
exinc = 5; %increment of excitation wavelengths (nm)
em = 300:eminc:596; % emission wavelengths range
ex = 240:exinc:450; % excitation wavelengths range
%%%%%%%%%%%%%%Do not change anything here onwards%%%%%%%%%%%%%%%
DirList = dir([FolderPath '*.csv']);
mkdir(FolderPath, 'PF');
PFpath = [FolderPath 'PF' '\'];
MaxInt = [PFpath 'MaxInt.txt'];
fid = fopen(MaxInt,'at');
fprintf(fid,'%s\t','"Sample Name"');
fprintf(fid,'%s\n','"MaxInt"');
PFfilepath = [PFpath 'fl' '.csv'];
csvwrite(PFfilepath,zeros(149,43));
Exfilepath = [PFpath 'ex' '.csv'];
csvwrite(Exfilepath,zeros(43,1));
Emfilepath = [PFpath 'em' '.csv'];
csvwrite(Emfilepath,zeros(149,1));
normoption = input('Do you want to normalize the EEMs? Enter \n 1 for YES \n 0 for NO \n = ');
switch(normoption==1)
% Divides the EEM by the maximum intensity in that EEM to normalize each
% EEM to 1.
  case 1
     for i = 1:length(DirList)
 % [PathStr, FileName, Ext] = fileparts(DirList(i).name);
  fl1 = csvread(DirList(i).name);
  fprintf(fid,'%s\t',DirList(i).name);
 %sq = [fl1].^2;
 %Sum = sum(sq);
 %S = sum(Sum);
 %fl = fl1/S;

  mint = max(fl1);
  maxint = max(mint);
  fprintf(fid,'%f\n',maxint);
  fl = fl1/maxint;
  dlmwrite(PFfilepath, fl,'-append');
     end

  case 0
     for i = 1:length(DirList)
 % [PathStr, FileName, Ext] = fileparts(DirList(i).name);
  fl = csvread(DirList(i).name);
  dlmwrite(PFfilepath, fl,'-append');
     end
end
 fl = csvread(PFfilepath);
 fl = fl(150:end,:);
 dlmwrite(PFfilepath,fl,'roffset',1);
 dlmwrite(Exfilepath,ex','roffset',1);
 dlmwrite(Emfilepath,em','roffset',1);
```

end

loadpfdata.m

```
% Harshad Kulkarni / November 2015 / SDSU Mladenov Research Lab.
% This function compiles extracted data into a data structure
function loadpfdata(~)
%cd InputFolder;
clear;
clc;
% Reads excitation wavelengths
OriginalData.Ex = csvread('Ex.csv',1);
% Reads excitation wavelengths
OriginalData.Em = csvread('Em.csv',1);
% Reads fluorescence data
OriginalData.X= csvread('fl.csv',1);

%identifys the number of Excitation wavelengths
OriginalData.nEx=(size(OriginalData.Ex,1));
%identifys the number of Emission wavelengths
OriginalData.nEm=(size(OriginalData.Em,1));
%identifys the number of samples
OriginalData.nSample=(size(OriginalData.X,1)); OriginalData.nSample=OriginalData.nSample/OriginalData.nEm;

% Convert data into the data structure
OriginalData.X=(reshape(OriginalData.X',OriginalData.nEx,OriginalData.nEm,OriginalData.nSample));
OriginalData.X=permute(OriginalData.X,[3 2 1]);

%plots EEMs of the data with a 0.2s pause between plots.
%for i=(1:OriginalData.nSample), pause(0.2),
%contourf(OriginalData.Ex,OriginalData.Em,(reshape(OriginalData.X((i),:),OriginalData.nEm,OriginalData.nEx))),
colorbar
%title((i))
%xlabel('Ex. (nm)')
%ylabel('Em. (nm)')
%end
%deletes unwanted items from workspace
clear i;
%saves workspace
save pf.mat;
end
```